

**Synthesis and Complexation Studies of New Triazole Bridged-
Calix[4]arenes and Attempts to Synthesize a Modified
Homooxacalix[4]acenaphthene**

By

© Mahmood Aljabri

A thesis submitted to the School of Graduate Studies

In partial fulfillment of the requirements of the degree of

Master of Science in Chemistry

Department of Chemistry

Memorial University of Newfoundland

2014

St. John's

Newfoundland and Labrador

Dedication

To my Mother and Father

To my wife

And to my brother and sisters

Abstract

The possibility of synthesizing compounds capable of selective binding to metal ions has been extensively investigated. Such investigations mainly aim at making compounds available for metal ion testing. This work has been motivated by the fact that synthesizing proper receptors that can selectively and specifically interact with metal ions of interest is important for the development of supramolecular chemistry.

This thesis begins by providing a brief introduction to the main concept of supramolecular chemistry, often referred to as “Host-Guest Chemistry”. Chapter 1 also describes the forces that control supramolecular interactions between host and guest molecules. A thorough discussion about calixarenes, whose synthesis and complexation properties were one of the main objectives of this work, and the techniques used for the complexation studies are also presented in Chapter 1.

In Chapter 2, the syntheses of two new molecular receptors namely bis(naphthyl)methane-bridged macrocycles are described. These two receptors were subsequently characterized by ^1H - and ^{13}C -NMR spectroscopy and mass spectrometry. Chapter 2 also presents a study of the complexation properties of these receptors with different metal ions of interest which have been investigated using ^1H -NMR and fluorescence spectroscopy. Our results have shown that these two compounds are selective towards Fe^{3+} , Hg^{2+} and Cu^{2+} in a mixed 4:1 acetonitrile: chloroform solvent.

Chapter 3 presents the synthesis procedures that have been followed to develop fluorescent chemosensors based on acenaphthene-modified calix[4]arene-triazoles. The selectivity of these chemosensors towards metal ions has been studied using fluorescence and $^1\text{H-NMR}$ spectroscopy. The results obtained from these techniques which show their complexation properties are explained in detail in this chapter.

In Chapter 4, attempts made towards the modification of homooxacalix[4]-acenaphthene are presented. This modification has been performed with the hope that such a compound could selectively bind C_{70} fullerene, since the prototype compound was found to be selective towards C_{60} fullerene. Synthetic work towards the modification of homooxacalix[4]acenaphthene is on-going.

Acknowledgments

It is my deep pleasure to thank my supervisor, Professor Paris Georghiou, for his valuable guidance, important suggestions, great support, helpful discussions, constant encouragements, teaching, patience, efforts and help. Without these significant things this degree would never have been completed. I would like to extend my sincere admiration and thanks to him for affording me the opportunity to work in his laboratory and obtain a valuable experience from him.

I would like to express my deep appreciation to Dr. Shofiur Rahman for his kind help, suggestions, efforts, and helpful discussions. I am grateful also to Dr. Tayel AlHujran for his advice and suggestions, especially at the beginning of my master program. My deep thanks also to Mr. Abdullah Al Odhayb for his comments, edits, and discussions and to all members of the Georghiou group, both past and present.

I am grateful to Professors Graham Bodwell, Yuming Zhao, Sunil Pansare and Christina Bottaro for their teachings, discussions and comments. I would like to extend my thanks to the friendly staff in the Chemistry Department: Ms. Ebony Penney, Ms. Mary Flinn, Ms. Roslalind Collins and Ms. Gina Jackson, for their kind help and friendship. Thanks also to Ms. Linda Winsor for the training and support with mass spectrometry, Ms. Julie Collins for training and support with NMR spectroscopy and Mr. Tim Strange for his training and support with fluorescence spectroscopy.

My extreme deep appreciation extends to my mother, my father Dawod, my brother Muhammad, my sisters, my wife and my all friends in St. John's for their support, encouragements and patience.

Finally, I am grateful to Umm Al-Qura University for a scholarship, the Saudi culture bureau in Canada and the Ministry of Higher Education in Saudi Arabia for assistance and advice.

Table of contents

Title.....	i
Dedication.....	ii
Abstract.....	iii
Acknowledgments.....	v
Table of contents.....	vii
List of Figures.....	xiii
List of Schemes.....	xix
List of Tables.....	xxi
List of Abbreviations.....	xxii
List of Appendixes.....	xxv

Chapter 1 Introduction

1.1 Supramolecular chemistry	1
1.2 Non-covalent bonds	2
1.2.1 Electrostatic interactions	3
1.2.2 Hydrogen bonding.....	4
1.2.3 π -Interactions.....	6
1.2.4 Van der Waals interactions	8
1.2.5 Hydrophobic effects	9
1.3 Calixarenes.....	10
1.3.1 Conformations of calix[4]arenes.....	12
1.3.2 Distinction of the four conformations	14
1.3.3 Homooxalixarenes	15
1.4 Calixarene receptors.....	16
1.5 Characterization of complexation	22
1.5.1 Fluorescence spectroscopy.....	23
1.5.2 Nuclear magnetic resonance (NMR).....	24
1.5.3 Single-crystal X-ray diffraction	25
1.5.4 UV-visible spectroscopy	25

1.5.5 Mass spectrometry (MS)	25
1.5.6 Scanning probe microscopy (SPM).....	26
1.6 References.....	28

**Chapter 2 Synthesis and Complexation Properties of Triazole-bridged
Bisnaphthyl-Calix[4]arenes**

2.1 Introduction.....	32
2.1.1 Metal ions receptor.....	32
2.1.2 Triazole bridge-based calixarene chemosensors	34
2.2 Results and discussion	38
2.2.1 Design of bis(naphthyl)-bridged 1,2,3-triazole fluorescent receptors.....	38
2.2.2 Synthetic approach toward desired macrocycles	39
2.2.2.1 Synthesis of bis[3-(azidomethyl)-4-methoxy-1-naphthyl]methanes (9)	39
2.2.2.2 Synthesis of bis(<i>O</i> -propargyl)calix[4]arene derivatives 7 and 8	40
2.2.2.3 Synthesis of triazole-bridge bisnaphthyl-calix[4]arene macrocycles 5 and 6	42
2.2.3 Characterizations of the newly-synthesized compounds 5 and 6	43
2.3 Complexation studies.....	45
2.3.1 Complexation studies using fluorescence spectroscopy	45
2.3.1.1 Calculation of association constants.....	45

2.3.1.2 Fluorescence complexation survey with host 5 and 6	46
2.3.2 ¹ H-NMR complexation studies	54
2.3.2.1 Complexation of receptor 6 with Fe ³⁺	54
2.3.2.2 Complexation of receptor 5 with Fe ³⁺ ions	58
2.4 Conclusions.....	62
2.5 Experimental section.....	62
2.5.1 General experimental	62
2.5.2 Experimental	63
2.6 References.....	69

**Chapter 3 Synthesis and Complexation Properties of Triazole-bridged
Acenaphthene-Calix[4]arenes**

3.1 Introduction.....	72
3.1.1 Fluorescent metal ion chemosensors.....	72
3.2 Results and discussion	78
3.2.1 Design of acenaphthene-bridged 1,2,3-triazole fluorescent chemosensors	78
3.2.2 Synthesis approach toward desired macrocycles 12-12a	79
3.2.2.1 Synthesis of bis (azidomethyl) dialkoxyacenaphthene.....	79
3.2.2.2 Synthesis of macrocycles 12 and 12a	80

3.2.3 Characterizations of newly-synthesized compounds 12 and 12a	81
3.3 Complexation studies.....	83
3.3.1 Complexation studies using fluorescence spectroscopy	83
3.3.2 Complexation studies of 12 using ¹ H-NMR spectroscopy.....	90
3.4 Conclusions.....	94
3.5 Experimental section.....	94
3.5.1 Experimental	95
3.6 References.....	101
 Chapter 4 Attempts to Synthesize and Modify Homooxacalix[4]acenaphthene	
Derivatives	
4.1 Introduction.....	103
4.2 Synthesis of calixarene and homooxacalixarene	103
4.3 Results and discussion	110
4.3.1 Design of desired macrocycle 25	110
4.3.2 Synthesis of dibromoacenaphthenequinone (26)	111
4.3.3 Synthesis of dimethoxyacenaphthenequinone (30).....	112
4.3.4 Projected synthesis of desired macrocycle 25	114
4.4 Conclusions and future work	116

4.5 Experimental section.....	117
4.5.1 Experimental	117
4.6 References.....	119

List of Figures

Figure 1.1. (a) Formation of a host-guest system and (b) spontaneous self-assembly of aggregates of larger molecules formed by covalent synthesis of small molecules.....	2
Figure 1.2. Ion-dipole interaction in the sodium ion complex of [15]crown-5.	4
Figure 1.3. Dipole-dipole interaction in acetone.	4
Figure 1.4. Different types of hydrogen bonding.	5
Figure 1.5. A cation- π interaction and the quadrupole of benzene.....	7
Figure 1.6. Two types of π - π stacking interactions: face-to-face and edge-to-face.	8
Figure 1.7. The inclusion of toluene molecule by <i>p-tert</i> -butylcalix[4]arene as characterized by X-ray crystallography.	9
Figure 1.8. Left: <i>p-Tert</i> -butyl-calix[4]arene and Right: a Greek kalyx.	10
Figure 1.9. <i>p-Tert</i> -butylcalix[4]arene or 5,11,17,23-tetrabutylcalix[4]arene-25,26,27,28-tetrol.	11
Figure 1.10. Structure of <i>p-tert</i> -butylcalix[4]arene and its shape.	12
Figure 1.11. The four conformations of <i>p-tert</i> -butyl-calix[4]arene.	13
Figure 1.12. The anticipated signal patterns of the four conformations of calix[4]arene. .	15
Figure 1.13. Schematic representations of various types of homooxcalix[<i>n</i>]arenes.....	16
Figure 1.14. Structure of receptor 5 for cation detection.	18
Figure 1.15. Structures of fluorescence chemosensors.	19

Figure 1.16. Fluorescent chemosensor 8 which selectivity binds to Na ⁺	20
Figure 1.17. Structure of some anion receptors.	21
Figure 1.18. Structure of contact ion-pair receptor with selectivity to KCl.	22
Figure 2.1. Triazole-bridge based calixarenes 1a-c	35
Figure 2.2. Fluorescent receptor with two cationic binding sites.	35
Figure 2.3. Calixarene-binol-bis(1,2,3)-triazole receptor.	36
Figure 2.4. Changes of the observed fluorescence intensities upon addition to the 3 :Cu ²⁺ complex of each of the mandelic acid enantiomers shown.....	37
Figure 2.5. Structure of receptor 4 that selectively binds to Co ²⁺	38
Figure 2.6. <i>Left</i> : free ligands 5 and 6 ; and <i>right</i> : the geometry optimization (ball-and-stick) structure of 5 :Cu ²⁺ complex was fully optimized at the B3LYP level of DFT with the lanl2dz basis set in the gas phase Gaussian09 at 298 K.....	39
Figure 2.7. <i>Left</i> : Fluorescence spectra of 6 (16.4 μM) upon addition of Hg ²⁺ (0.2-3 equivalents) in acetonitrile/chloroform (v/v= 9:1) solutions. λ _{ex} = 282 nm	47
Figure 2.8. <i>Left</i> : Fluorescence spectra of 6 (16.4 μM) upon addition of Fe ³⁺ in acetonitrile/chloroform (v/v= 9:1) solutions. λ _{ex} = 282 nm.....	48
Figure 2.9. <i>Left</i> : Fluorescence spectra of 6 (16.4 μM) upon addition of Cu ²⁺ in acetonitrile/chloroform (v/v= 9:1) solutions. λ _{ex} = 282 nm.....	48

Figure 2.10. <i>Left</i> : Fluorescence spectra of 5 (34.6 μM) upon addition of Hg^{2+} in acetonitrile/chloroform (v/v= 9:1) solutions. $\lambda_{\text{ex}} = 284 \text{ nm}$	49
Figure 2.11. <i>Left</i> : Fluorescence spectra of 5 (34.6 μM) upon addition of Fe^{3+} in acetonitrile/chloroform (v/v= 9:1) solutions. $\lambda_{\text{ex}} = 284 \text{ nm}$	49
Figure 2.12. <i>Left</i> : Fluorescence spectra of 5 (34.6 μM) upon addition of Cu^{2+} in acetonitrile/chloroform (v/v= 9:1) solutions. $\lambda_{\text{ex}} = 284 \text{ nm}$	50
Figure 2.13. Job plot curves showing 1:1 complexation for 6 with Ni^{2+}	51
Figure 2.14. Job plot curves showing 1:1 complexation for 6 with Fe^{3+}	51
Figure 2.15. Job plot curves showing 1:1 complexation for 5 with Cu^{2+}	52
Figure 2.16. Job plot curves showing 1:1 complexation for 5 with Ni^{2+}	52
Figure 2.17. Histogram showing the fluorescence quenching of receptors 5 (red) and 6 (blue) with different metal ions.....	53
Figure 2.18. Histogram showing the association constants (K_{assoc}) values determined for receptors 5 (red) and 6 (blue) with different metal ions.	53
Figure 2.19. $^1\text{H-NMR}$ (500 MHz) titration spectra for the singlet proton signal of the triazole unit in 6 with increasing added amounts of $\text{Fe}(\text{ClO}_4)_3$	55
Figure 2.20. $^1\text{H-NMR}$ (500 MHz) titration spectra for the singlet proton signal of the bisnaphthyl-bridge ($-\text{CH}_2-$) in 6 with increasing added amounts of $\text{Fe}(\text{ClO}_4)_3$	55

Figure 2.21. ¹ H-NMR (500 MHz) titration spectra for the doublet equatorial proton signals of the calixarene bridging (–CH ₂ –) in 6 with increasing added amounts of Fe(ClO ₄) ₃	56
Figure 2.22. ¹ H-NMR (500 MHz) titration curves for the triazole, bisnaphthyl- and calixarene-methylene bridge (equatorial) signals in 6	57
Figure 2.23. ¹ H-NMR (500 MHz) titration spectra for the singlet proton signal of the triazole unit in 5 at δ 8.06 ppm and for the hydroxyl groups at δ 6.89 ppm with increasing added amounts of Fe(ClO ₄) ₃	58
Figure 2.24. ¹ H-NMR (500 MHz) titration spectra for the singlet proton signal of the bisnaphthyl-bridge (–CH ₂ –) in 5 with increasing added amounts of Fe(ClO ₄) ₃	59
Figure 2.25. ¹ H-NMR (500 MHz) titration spectra for the doublet equatorial proton signals of the calixarene bridging (–CH ₂ –) in 5 with increasing added amounts of Fe(ClO ₄) ₃	59
Figure 2.26. ¹ H-NMR (500 MHz) titration curves for the triazole, bisnaphthyl- and calixarene-methylene bridge (equatorial) signals in 5	61
Figure 3.1. Complexation of fluorescent chemosensor 1 with Cu ²⁺ ions.....	73
Figure 3.2. Fluorescent chemosensor based on a pyrazoline unit.....	74
Figure 3.3. Structures of calixarene-based fluorescent chemosensors with selectivity to Cu ²⁺ ions.....	75
Figure 3.4. Receptor based on calix[4]arene with aminoquinoline subunits.....	76

Figure 3.5. Variety of monomer and dimer macrocyclic receptors.	77
Figure 3.6. <i>Left</i> : free ligands 12 , 12a ; and <i>right</i> : the geometry optimization (ball-and-stick) structure of 12 :Cu ²⁺ complex was fully optimized at the B3LYP level of DFT with the lanl2dz basis set in the gas phase Gaussian09 at 298 K.....	78
Figure 3.7. <i>Left</i> : Fluorescence spectra of 12 (21.1 μM) upon addition of Cu ²⁺ in acetonitrile/chloroform (v/v= 9:1) solutions. λ _{ex} = 309 nm.....	84
Figure 3.8. <i>Left</i> : Fluorescence spectra of 12 (21.1 μM) upon addition of Fe ³⁺ in acetonitrile/chloroform (v/v= 9:1) solutions. λ _{ex} = 309 nm.....	85
Figure 3.9. <i>Left</i> : Fluorescence spectra of 12 (21.1 μM) upon addition of Hg ²⁺ in acetonitrile/chloroform (v/v= 9:1) solutions. λ _{ex} = 309 nm.....	85
Figure 3.10. <i>Left</i> : Fluorescence spectra of 12a (20.9 μM) upon addition of Cu ²⁺ in acetonitrile/chloroform (v/v= 9:1) solutions. λ _{ex} = 309 nm.....	86
Figure 3.11. <i>Left</i> : Fluorescence spectra of 12a (20.9 μM) upon addition of Hg ²⁺ in acetonitrile/chloroform (v/v= 9:1) solutions. λ _{ex} = 309 nm.....	86
Figure 3.12. <i>Left</i> : Fluorescence spectra of 12a (20.9 μM) upon addition of Fe ³⁺ in acetonitrile/chloroform (v/v= 9:1) solutions. λ _{ex} = 309 nm.....	87
Figure 3.13. Job plot curves showing 1:1 complexation for receptor 12 with Ni ²⁺	88
Figure 3.14. Job plot curves showing 1:1 complexation for 12a with Ni ²⁺	88

Figure 3.15. Histogram showing the fluorescence quenching of receptors 12 (blue) and 12a (red) with different metal ions.	89
Figure 3.16. Histogram showing the K_{assoc} values determined for receptors 12 (blue) and 12a (red) with different metal ions.	89
Figure 3.17. $^1\text{H-NMR}$ (500 MHz) titration spectra for the singlet proton signals of the triazole units in 12 with increasing added amounts of $\text{Fe}(\text{ClO}_4)_3$	91
Figure 3.18. $^1\text{H-NMR}$ (500 MHz) titration spectra for the singlet proton signal of ($-\text{CH}_2-$) acenaphthene-triazole bridge in 12 with increasing added amounts of $\text{Fe}(\text{ClO}_4)_3$	91
Figure 3.19. $^1\text{H-NMR}$ (500 MHz) titration spectra for the singlet proton signal of hydroxyl groups in 12 with increasing added amounts of $\text{Fe}(\text{ClO}_4)_3$	92
Figure 3.20. $^1\text{H-NMR}$ (500 MHz) titration curves for the triazole, acenaphthene-triazole ($-\text{CH}_2-$) bridge and the hydroxyl proton signals in 12	93
Figure 4.1. Structure of the hexadecakis-methylated homooxacalix[4]acenaphthene 25	110
Figure 4.2. Computer-generated image for the complex of the macrocycle 25 and C_{60} (<i>Left-</i> top view) and (<i>Right-</i> side view) where the arrows point to the methyl groups.....	111

List of Schemes

Scheme 1.1. Synthesis of Calix[4]arene.	11
Scheme 2.1. Synthetic route to bis[3-(azidomethyl)-4-methoxy-1-naphthyl]methane (9).	40
Scheme 2.2. Synthetic route used for the calixarene intermediates 7 and 8	41
Scheme 2.3. Synthesis of triazole-bridged bis(naphthyl)methyl-calix[4]arene 5 and 6 ...	42
Scheme 3.1. Synthesis of bis(azidomethyl)dimethoxyacenaphthene.....	80
Scheme 3.2. Synthesis of triazole-bridged acenaphthene-calix[4]arenes.....	81
Scheme 4.1. Synthesis of calix[4]naphthalenes.....	104
Scheme 4.2. Synthesis of <i>exo</i> -calix[4]naphthalene using [2+2] condensation.....	110
Scheme 4.3. Synthesis of calix[4]naphthalenes using [3+1] approach.....	105
Scheme 4.4. Synthesis of <i>endo</i> -calix[4]naphthalenes 10 and 10a	106
Scheme 4.5. Synthesis of homooxacalix[3]arene 12 and homooxacalix[4]arene 13	107
Scheme 4.6. Synthesis of homooxacalix[3]arene 16 and homooxacalix[4]arene 17	107
Scheme 4.7. Synthesis of homooxacalix[<i>n</i>]naphthalenes.	108
Scheme 4.8. Synthesis of homooxacalix[4]acenaphthene 22	109
Scheme 4.9. Synthesis of 5,6-dibromoacenaphthene-1,2-dione (26).	111
Scheme 4.10. Synthesis of 5,6-dimethoxyacenaphthene-1,2-dione (30).....	112

Scheme 4.11. Synthesis of dimethoxyacenaphthenequinone (30).....	114
Scheme 4.12. Synthesis of two intermediates 32 and 33	115
Scheme 4.13. Williamson ether synthetic approach to desired macrocycle 25	116

List of Tables

Table 1.1. Classification and properties of hydrogen bonds.....	6
Table 2.1. ¹ H-NMR (500 MHz) titration data for the triazole singlet and the bisnaphthyl singlet and the calixarene-bridge doublet signals of host 6	57
Table 2.2. ¹ H-NMR (500 MHz) titration data for the triazole singlet, the bisnaphthyl singlet and the calixarene-bridge doublet signals of host 5	60
Table 3.1. ¹ H-NMR (500 MHz) titration data for triazole singlet and singlet of the acenaphthene-bridge (–CH ₂ –) or methylene protons and the singlet proton of the hydroxyl groups of host 12	93
Table 4.1. Summary of attempts to obtain dimethoxyacenaphthenequinone (30) by oxidation 29 using CrO ₃	113

List of Abbreviations

Å	angstrom
APCI-MS	atmospheric pressure chemical ionization mass spectrometry
Bu	butyl
CAN	cerium ammonium nitrate
δ	chemical shift
d	day
DCM	dichloromethane
DMF	<i>N,N</i> -dimethylformamide
DNA	deoxyribonucleic acid
Et	ethyl
FS	fluorescence spectroscopy
Hz	hertz
h	hour
<i>J</i>	coupling constant (Hz)
<i>K_{assoc}</i>	association constant
kJ	kilojoule
LCMS	liquid chromatography mass spectrometry

m	multiplet (in $^1\text{H-NMR}$)
M	molar
M^+	molecular ion
Me	methyl
mp	melting point
MS	mass spectroscopy
NMR	nuclear magnetic resonance
NBS	<i>N</i> -bromosuccinimide
NR	no reaction
<i>p</i>	para
Ph	phenyl
ppm	parts per million
Pr	propyl
q	quartet (in $^1\text{H-NMR}$)
rt	room temperature
σ	sigma bond
s	singlet (in $^1\text{H-NMR}$)
t	triplet (in $^1\text{H-NMR}$)

<i>tert</i>	tertiary
THF	tetrahydrofuran
TMS	tetramethylsilane (in NMR)
TFA	trifluoroacetic acid

List of Appendixes

Appendix A: ^1H , ^{13}C -NMR spectra for compounds described in Chapter 2.....	121
Appendix B: Fluorescence titration experiments of receptors in Chapter 2.....	128
Appendix C: ^1H , ^{13}C -NMR spectra for compounds described in Chapter 3.....	143
Appendix D: Fluorescence titration experiments of receptors in Chapter 3.....	157
Appendix E: ^1H , ^{13}C -NMR spectra for compounds described in Chapter 4.....	166

Chapter 1

Introduction

1.1 Supramolecular chemistry

Jean-Marie Lehn, who was awarded the Chemistry Nobel Prize in 1987 along with Charles J. Pedersen and Donald J. Cram, defined supramolecular chemistry as “the chemistry of molecular assemblies and of the intermolecular bond”.¹ Supramolecular chemistry has been extensively studied due to its many potential applications in different fields such as chemistry, biology and physics.¹ In particular, supramolecular chemistry has gained considerable interest among the different disciplines of chemistry.² The interactions involved in the supramolecular assembly of molecular subunits or components depend on weak and reversible non-covalent interactions between the component molecules.³ Such interactions include hydrogen bonding, hydrophobic forces, van der Waals forces, π - π interactions and electrostatic effects.

The study of supramolecular chemistry is often categorized into:

- a. “Host-guest” chemistry, which is concerned with the study of the capability of large molecules to “host” smaller molecules via non-covalent interactions and as shown in Figure 1.1.
- b. “Self-assembly”, which is concerned with studies of the associations of two or more molecules reversibly via non-covalent interactions.⁴

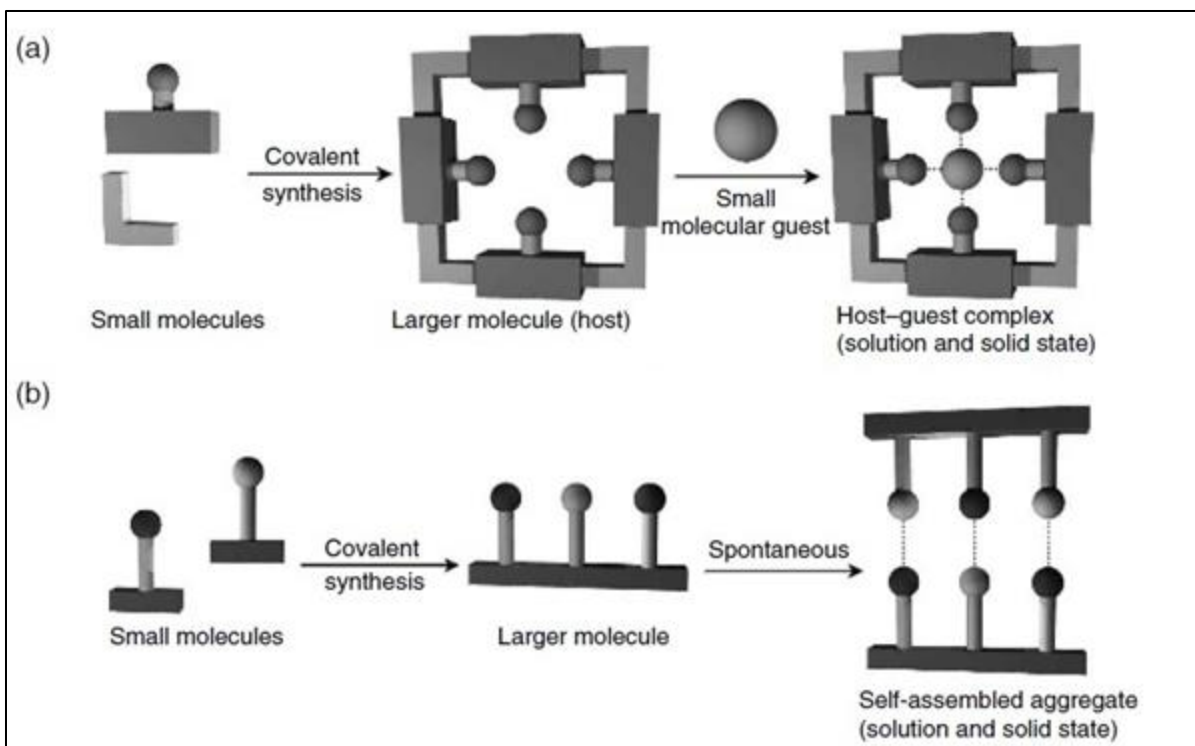


Figure 1.1. (a) Formation of a host-guest system and (b) spontaneous self-assembly of aggregates of larger molecules formed by covalent synthesis of small molecules. [used with permission from reference 4]⁴

It is noteworthy to mention that both host-guest systems and self-assembly encompass the interaction between two or more ionic or molecular chemical species. In host-guest systems the complementarity between the guest and the host is crucial whereas, in self-assembly between the species, complementarity might not be involved.²⁻⁴

1.2 Non-covalent bonds

Individual non-covalent interactions are weak bonds with dissociation energies typically in the range from 0.4 to $\sim 8.0 \text{ kJ mol}^{-1}$. Non-covalent bonds are substantially weaker and longer than covalent bonds (i.e. 0.36 nm vs 0.15 nm). Non-covalent interactions play a major role in biology: for example, the quaternary structure of

hemoglobin involves the non-covalent bonding between four component peptide chains and four heme units. There are several types of non-covalent bonds involved in host-guest interactions which can include ionic interactions and other types of electrostatic interactions such as hydrogen bonding, π - π interactions, van der Waals interactions and hydrophobic effects. A brief description of some of these types of interactions follows.²⁻⁵

1.2.1 Electrostatic interactions

Electrostatic interactions, in general, are due to the Coulombic interaction between two opposite formal or partial charges. Three types of electrostatic interactions of importance in supramolecular chemistry are described below:

a. Ion-ion interactions

Ion-ion interactions typically have bond strengths (100 - 350 kJ mol^{-1}) which are close to those of covalent bonds and exist due to the electrostatic interactions between oppositely charged ions.

b. Ion-dipole interactions

These are due to the binding between an ion and a polar molecule such as water, or other molecules which contain an oxygen or nitrogen atom, having lone pairs of electrons that can coordinate with positive ions. The bond energies for these types of interactions are around 50 - 200 kJ mol^{-1} . For example, the complexation between a crown ether, as host, and an alkali metal such as Na^+ , as guest, as shown in Figure 1.2.^{4,5}

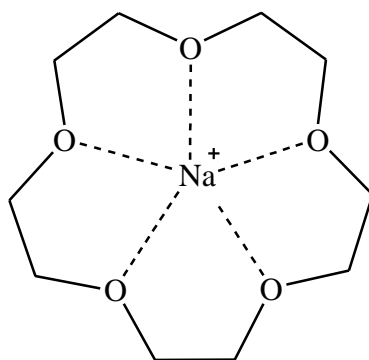


Figure 1.2. Ion-dipole interaction in the sodium ion complex of [15]crown-5.

c. Dipole-dipole interactions

Dipole-dipole interactions are weaker than the previous two interactions described and can exist between polar molecules that have permanent net dipoles. The bond energies in these types of interaction are approximately between 5-50 kJ mol⁻¹. (See Figure 1.3).

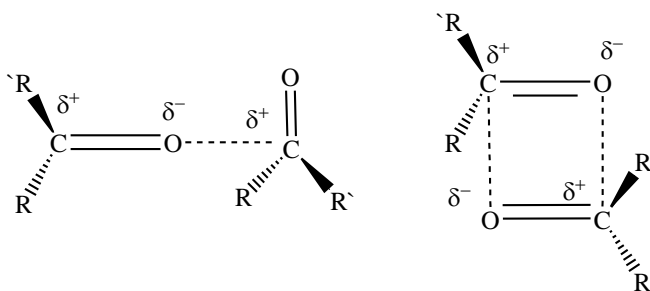


Figure 1.3. Dipole-dipole interaction in acetone.

1.2.2 Hydrogen bonding

The interaction of a hydrogen atom bound to an electronegative atom such as oxygen (O---H), with a dipolar bond in a neighboring molecule constitutes hydrogen bonding. This type of bonding is commonly represented as **D-H---A**, where **D** refers to a

donor atom and **A** is an acceptor atom. Both **D** and **A** can be electronegative atoms such as F and O. Figure 1.4 shows various types of hydrogen bonding geometries that depend on the angle of the interaction. The bond energies in hydrogen bonding, which are often stronger than dipole-dipole interactions, range from 4 to 120 kJ mol⁻¹.^{6,7} These types of hydrogen bonding have properties different from one other in terms of bond angle, length, and energy. These properties are listed in Table 1.1.

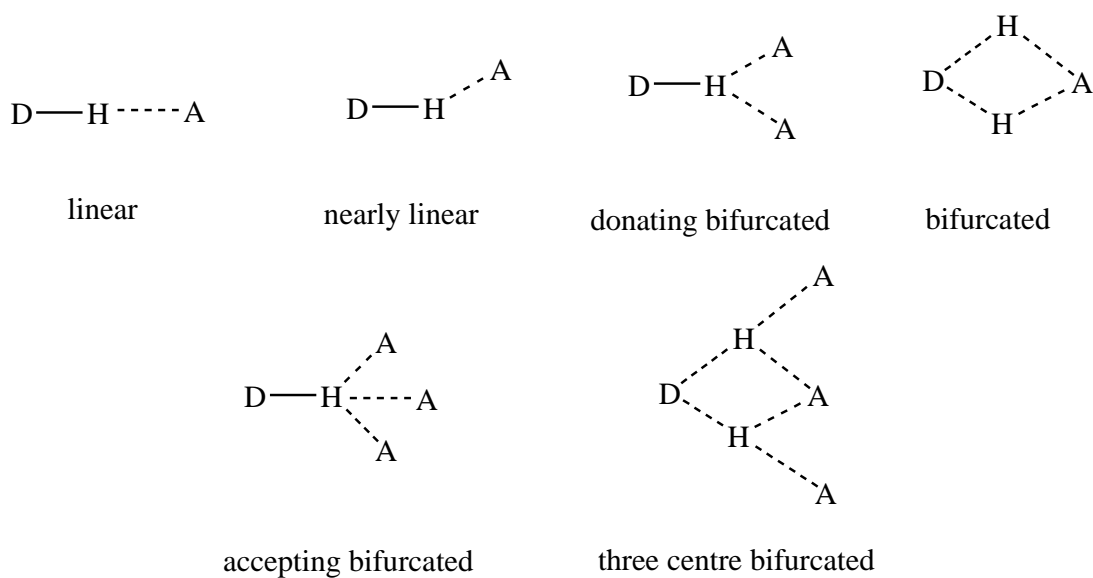


Figure 1.4. Different types of hydrogen bonding.

Table 1.1. Classification and properties of hydrogen bonds.⁴

Interaction	Strong	Moderate	Weak
D--H---A	Mainly covalent	Mainly electrostatic	Electrostatic
Bond energy (kJmol ⁻¹):	60–120	16–60	< 12
H--A Bond lengths (Å):	1.2–1.5	1.5–2.2	2.2–3.2
D--A Bond lengths (Å):	2.2–2.5	2.5–3.2	3.2–4.0
Bond angles:	175–180°	130–180°	90–150°
Examples:	HF complexes, H ₅ O ₂ ⁺	Acids, Alcohols DNA / RNA	C-H-----A D-H-----π

1.2.3 π -Interactions

π -Interactions are those interactions that occur between delocalized electrons or double bonds with other cations (alkaline and alkaline earth metal) or aromatic rings. Studies have shown that these types of interactions may be regarded as weak interactions (e.g. their bond energies are between 0 to 80 kJ mol⁻¹). π -interactions can be divided into two major types:

a. Cation- π interactions

These interactions, which are electrostatic in nature, are considered to be the strongest types of π -interactions.⁸ This is because they involve electrostatic forces, induced dipole and also charge-transfer. An example of a cation- π interaction was reported by Kebarle who observed that K⁺ ions are better stabilized by benzene

molecules than by water.⁹ Figure 1.5 demonstrates a cation- π interaction between benzene and a cation (e.g. K^+).

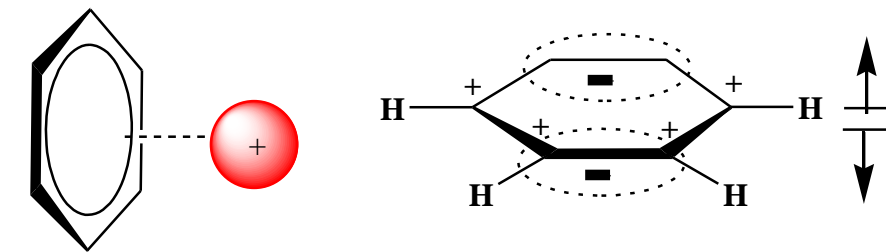


Figure 1.5. A cation- π interaction and the quadrupole of benzene.

b. π - π -stacking interactions

These interactions are weak interactions that take place between aromatic rings. They involve an electron-rich region interacting with an electron-poor one in two aromatic rings. These interactions can exist in two different types or shapes of π -stacking. The first one is called a “face-to-face” π - interaction, and is due to the attraction of the negatively charged π -electron cloud of the center of one aromatic ring with the partially-positive corner of an adjacent aromatic ring. The formation of the layered-structure graphite is a clear example of this face-to-face type.^{10,11} The second type of π -stacking interaction is called “face-to-edge” or “T-stacking”, which arise from the attraction between the negatively-charged central region of one aromatic ring with a hydrogen atom of the other ring where these two rings are perpendicular to each other (see Figure 1.6).

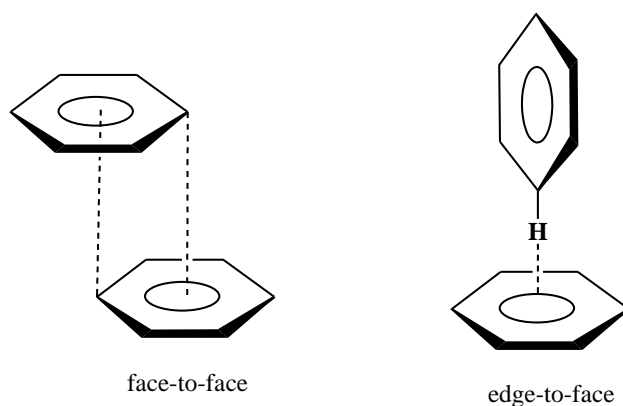


Figure 1.6. Two types of π - π stacking interactions: face-to-face and edge-to-face.

1.2.4 Van der Waals interactions

Van der Waals attractive forces between two or more molecules arises from one of three forces, namely permanent dipoles (Keesom forces), permanent induced-dipole (Debye forces), or instantaneous dipoles (London dispersion forces). The non-covalent bond energies for all three types are relatively weak (0 to 5 kJ mol⁻¹). One clear example of a Van der Waals interaction can be seen in the case where toluene is loosely incorporated within the cavity of *p*-*tert*-butylcalix[4]arene as shown in Figure 1.7.¹²

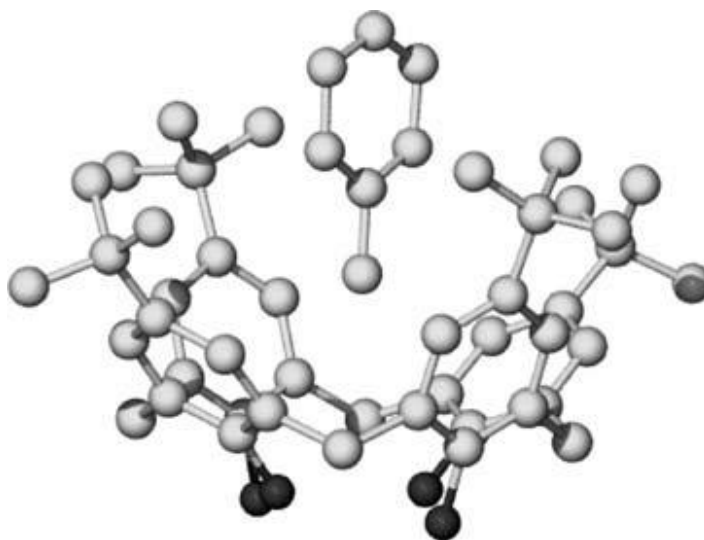


Figure 1.7. The inclusion of toluene molecule by *p-tert*-butylcalix[4]arene as characterized by X-ray crystallography.¹ [used with permission from reference 1].

1.2.5 Hydrophobic effects

These can be shown by the aggregation of non-polar substances in aqueous solution and by the exclusion of water molecules from large particles. Hydrophobic effects are important effects in supramolecular chemistry and in biology, as the formation of micelles.¹² This effect is also seen in the binding of host molecules such as cyclophanes and cyclodextrins with other organic guest molecules in water.⁴

1.3 Calixarenes

The term “calixarene” was first introduced in 1978 by C. D. Gutsche, who described the cyclic oligomers or macrocycles which were obtained from the condensation of *tert*-butylphenol and formaldehyde under refluxing conditions in the presence of a base such as NaOH or KOH (Scheme 1.1). The word calixarene is derived from a Greek word, “kalyx” or “calix” which is a type of vase, and “arene” refers to the aromatic building blocks, as shown in Figure 1.8. Calix molecules are therefore macrocycles which resemble a vase (or, a basket) in their shapes.^{14,15,17}

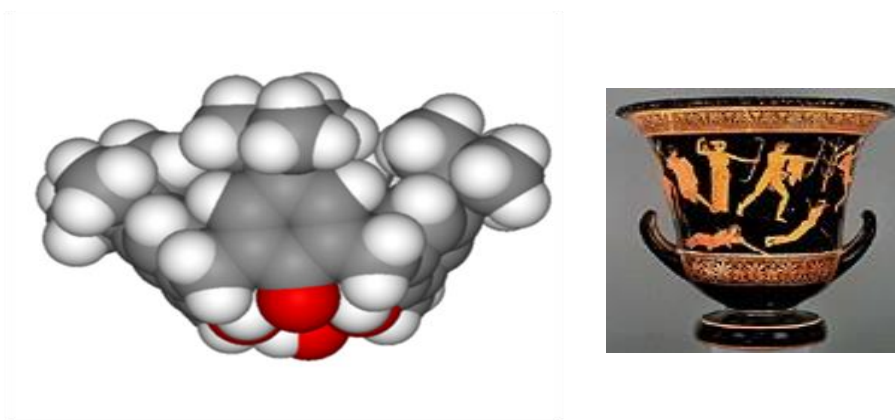
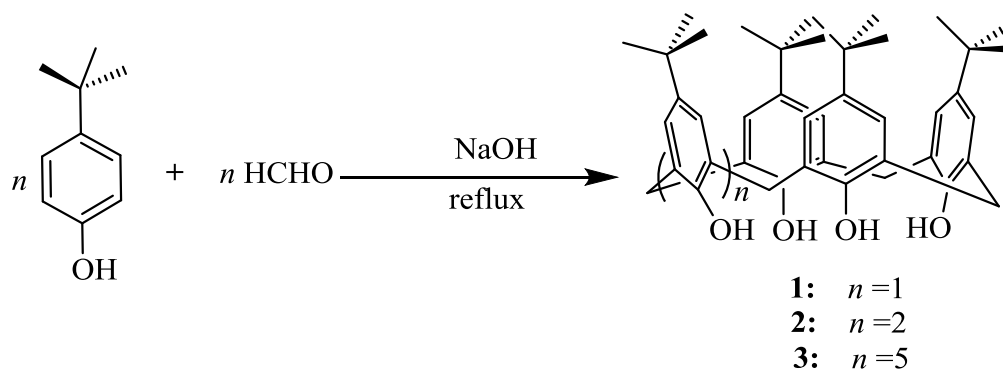


Figure 1.8. Left: *p*-*Tert*-butyl-calix[4]arene and Right: a Greek kalyx.¹⁵ [used with permission from reference 15].



Scheme 1.1. Synthesis of calix[4]arene.

Calixarenes have complicated systematic names, making their writing inconvenient. Gutsche therefore termed these macrocycles as *calixarenes* solely for the purpose of easier writing and communication. For instance, compound **4** which is 5,11,17,23-tetrabutylcalix[4]arene-25,26,27,28-tetrol (shown in Figure 1.9) was renamed by Gutsche as *p-tert*-butylcalix[4]arene both for its shape and for simplicity.¹⁶

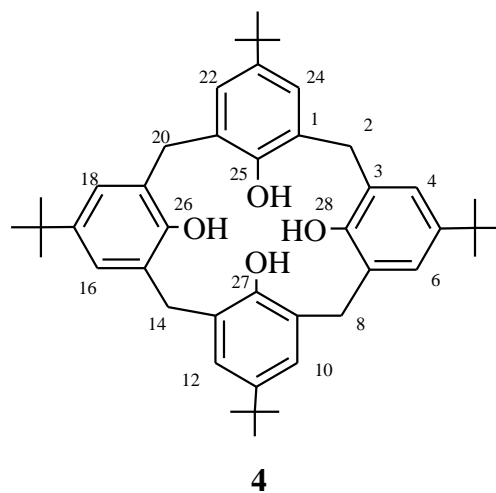


Figure 1.9. *p-Tert*-butylcalix[4]arene or 5,11,17,23-tetrabutylcalix[4]arene-25,26,27,28-tetrol.

1.3.1 Conformations of calix[4]arenes

Calix[4]arene has a basket-shaped conformation structure as shown in Figure 1.10. This conformation (*cone*) has two different rims. The “upper” or “wide” rim has, as shown in Figure 1.11, the *tert*-butyl groups. The second rim which carries the hydroxyl groups is called the “lower” rim or “narrow” rim which is due to hydrogen bonding between the hydroxyl groups. Both rims can be readily modified synthetically to bear different functional groups instead of the hydroxyl or *tert*-butyl groups. The lower rim for example, is often modified with binding sites which can be selective for specific guest ionic or molecular species.^{14,15,16}

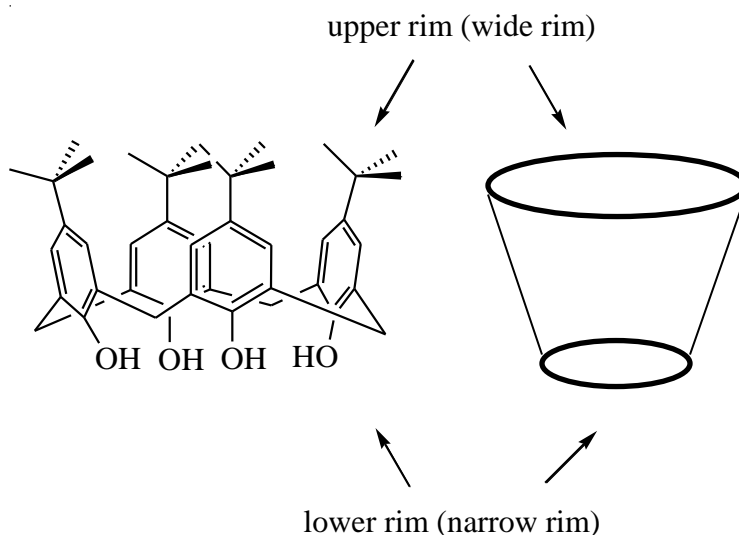


Figure 1.10. The structure of *p*-*tert*-butylcalix[4]arene and its shape.

The high flexibility of calix[4]arene can be controlled by suitable choices of substituents attached to the phenolic groups so that it can be synthesized into at least three other major conformations or atropisomers. This flexibility due to the rotation of the

phenolic units around the σ bonds of the methylene bridges, produces different conformations.^{14,18} Gutsche and Cornforth have given names for these conformations as follows: *cone* (u,u,u,u), *partial-cone* (u,u,u,d), *1,2-alternate* (u,u,d,d), and *1,3-alternate* (u,d,u,d), respectively, where “u” is the upward and “d” is the downward projection of the aryl group relative to an average plane defined by the methylene bridges.^{19,20} (See Figure 1.11).

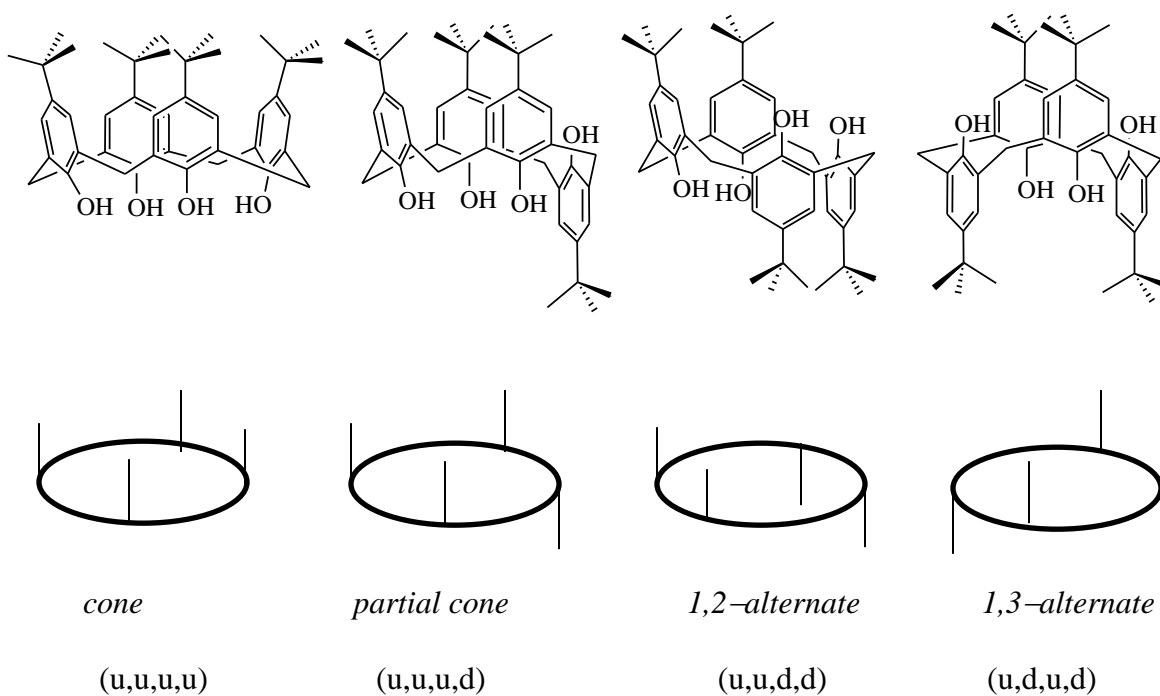


Figure 1.11. The four conformations of *p-tert-butyl-calix[4]arene*.

Among these four conformations, the *cone* conformation shows high stability due to the hydrogen-bond interactions of the hydroxyl groups in the lower-rim (narrow-rim). However, there are many factors that could affect the rotation and formation of these

conformations in calix[4]arenes such as temperature, solvent, the nature of the hydroxyl group and the *para* substituents.^{14,18,21}

1.3.2 Distinction of the four conformations

The four types of calix[4]arene conformations can be identified and distinguished using the ¹H-NMR and ¹³C-NMR chemical shifts for the methylene-bridges. The ¹H-NMR chemical shift patterns for the methylene-bridges are used to characterize the *cone* and *1,3-alternate* conformations. However, these chemical shifts cannot be used to characterize *partial-cone* and *1,2-alternate* conformations since they show similar patterns. De Mendoza and coworkers²³ however, have found that using ¹³C-NMR could effectively distinguish the four conformations of calix[4]arene. Their findings were based on the fact that the resonance arising from the methylene-bridge carbons is around 31 ppm when two adjacent aryl groups are in a *syn*-orientation. This signal is shifted to 37 ppm when the two adjacent aryl groups are in *anti*-orientation.²³ Figure 1.12 shows the possible signal patterns of the different conformations and are referred to as the “de Mendoza Rules”.¹⁶

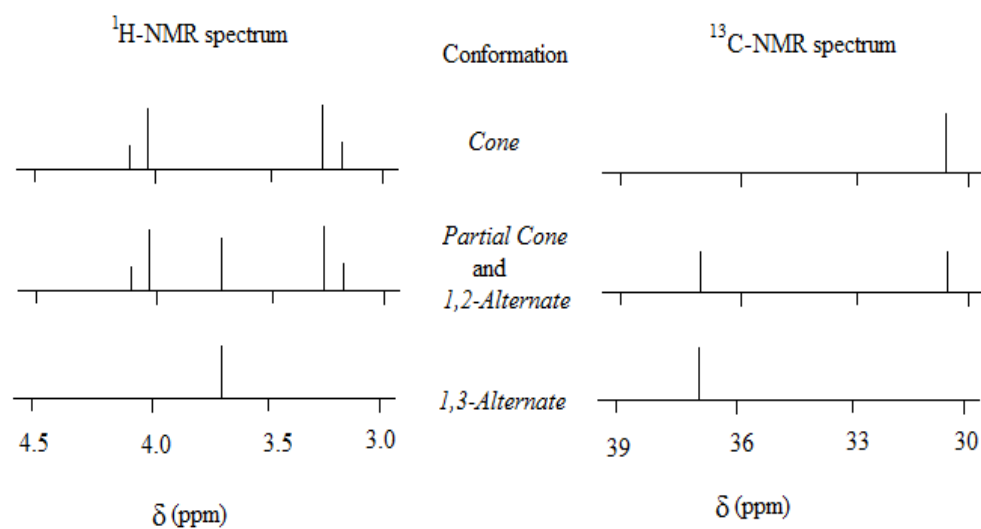


Figure 1.12. The anticipated signal patterns of the four conformations of calix[4]aene.¹⁶

1.3.3 Homooxacalixarenes

Calixarene structures are generally composed of phenol units that are connected together by methylene bridge linkages. Homooxacalixarenes (Figure 1.13) are calixarenes in which the $-\text{CH}_2-$ bridges are replaced by one or more $-\text{CH}_2\text{OCH}_2-$ groups.²⁴

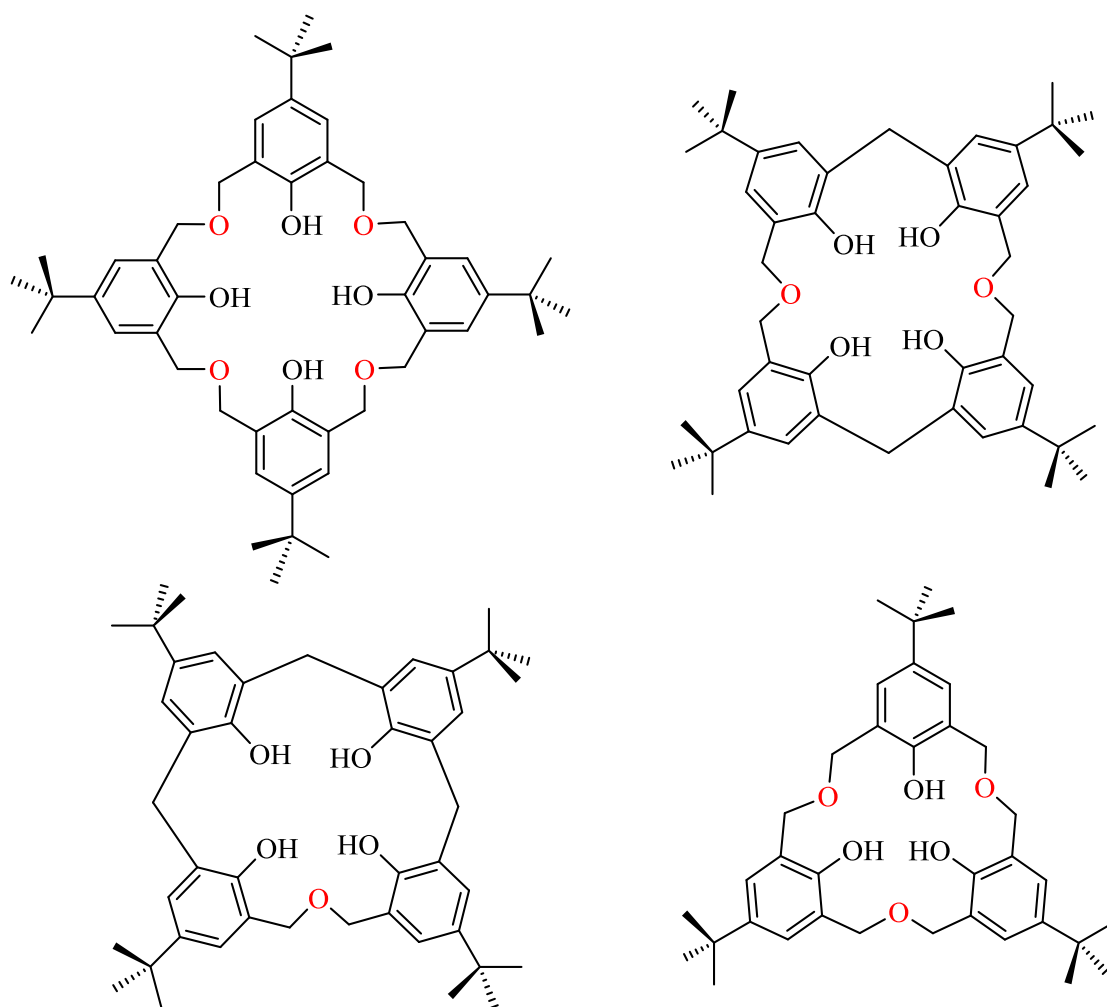


Figure 1.13. Schematic representations of various types of homooxcalix[*n*]arenes.

1.4 Calixarene receptors

Calixarenes have attracted substantial interest due to their appealing properties and their wide range of applications. Such applications include the design of catalysts, polymers, nanoparticles and superamolecular structures. One of the most valuable applications of calixarenes is using them as receptors capable of being functionalized

onto solid support surfaces. Calixarene derivatives can be used with ion-sensitive electrodes or sensors. The structural base of calix[4]arene is composed of four phenyl rings. These aromatic moieties make the calixarene cavity hydrophobic in nature and capable of binding to smaller molecules and ions. The structures of calixarenes can be further modified by fine-tuning the phenolic alkoxy substituents on the lower-rim of the structure making it capable of binding selectively to a variety of cations and anions (See Figure 1.10).^{13,25,26}

In 2007, Chang et al.²⁷ synthesized the calixarene derivative **5** having two triazole units in the lower rim (Figure 1.14) which acts as a chemosensor showing selectivity for Pb^{2+} and Ca^{2+} over a wide range of alkali, alkaline-earth and some transition metal ions. Different 1,2,3-triazoles containing calix[4]arenes can, in principle, be synthesized to selectivity complex with transition metal ions, alkali metal and alkaline-earth metal ions.

UV visible absorption spectroscopy studies were performed showing that only Pb^{2+} and Ca^{2+} was selectively recognized by the compound. The association constants for the complexes of **5** with Pb^{2+} and Ca^{2+} were determined using Benesi-Hildebrand²⁸ plots to give high association constants for 1:1 complexes of $8.57 \times 10^3 \text{ M}^{-1}$ and $7.06 \times 10^4 \text{ M}^{-1}$ respectively, confirming relatively efficient binding between the receptor and these two metal ions. ¹H-NMR and mass spectrometry studies were also used for further characterization of the complexation. It should be noted at the onset that the Benesi-Hildebrand method is outdated and inaccurate in most instances.^{28a} Modern computational advances permit relatively facile non-linear determinations.

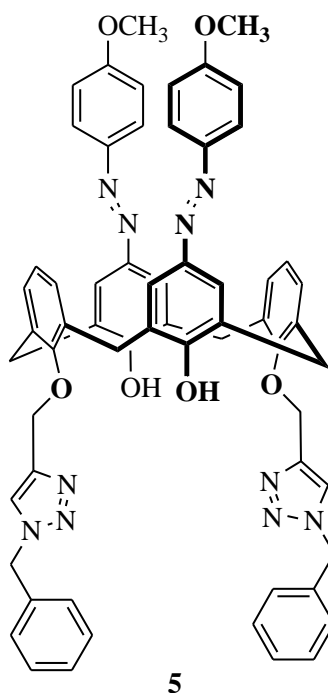


Figure 1.14. Structure of receptor **5** for cation detection.

In 2004, Kim's group²⁹ while working on developing calixarene-based fluorescent sensors concluded that amide groups work relatively well as substituents among the various functional groups studied. For instance, compound **6** has a calix[4]arene crown bearing two amide groups in the lower rim which is used to capture metal cations without any responses towards anions. Thus, they developed a calix[4]arene-based chemosensor, compound **7** (Figure 1.15), which can be used as a bifunctional host to capture both cations or anions. This calixarene-based sensor **7** was composed of a pyrene-appended calix[4]triazacrown-5 bearing four amide groups capable of binding anions or metal cations. This is due to the ability of the molecule to capture cations through the carbonyl oxygen atoms, and anions through hydrogen bonding between anions and the acidic

hydrogen atoms on the amide nitrogen atoms. These types of sensors are designed based on the photophysical changes which can be observed upon ion binding through photoinduced electron transfer (PET)³⁰ or photoinduced charge transfer (PCT).³¹

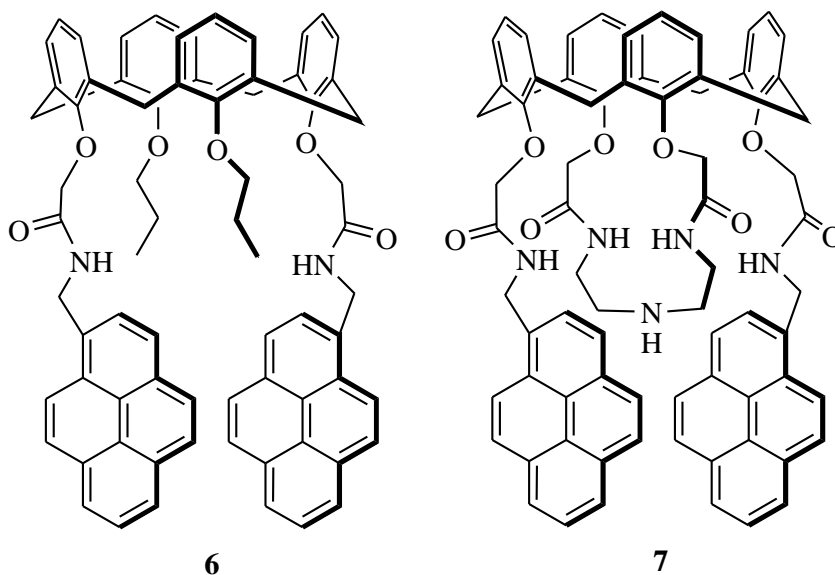


Figure 1.15. Structures of fluorescence chemosensors.

Since compound **7** can bind to both cations or anions, it can serve as an ion detector for F^- and also for heavy-metal ions such as Pb^{2+} and Co^{2+} . The fluorescence intensities that result from the binding of Pb^{2+} or Co^{2+} to receptor **7** are quenched because of the effect of reverse-PET, the presence of the heavy metal ion and conformational changes.²⁹ However, when F^- ions were added to compound **7**, the fluorescence intensity decreased due to the reverse-PET effect only. The complexation of Pb^{2+} with both pyreneamide and triazaamide were evaluated using both fluorescence and 1H -NMR titration experiments.

In 2009, KeRang³² and coworkers reported a new calixarene to be a fluorescent chemosensor having pyrene molecules in the upper rim as the fluorophore, and with tetraesters in the lower rim as the binding sites for guest ions.³² The fluorescence spectroscopy complexation studies showed that this receptor **8** is selective to sodium ions, versus other alkali and alkaline-earth metals, in a 1:1 host:guest ratio. During the study of the complexation, they observed that the excimer emission decreased while the monomer emission increased upon complexation with the sodium ions. Figure 1.16 shows the structure of chemosensor **8**.

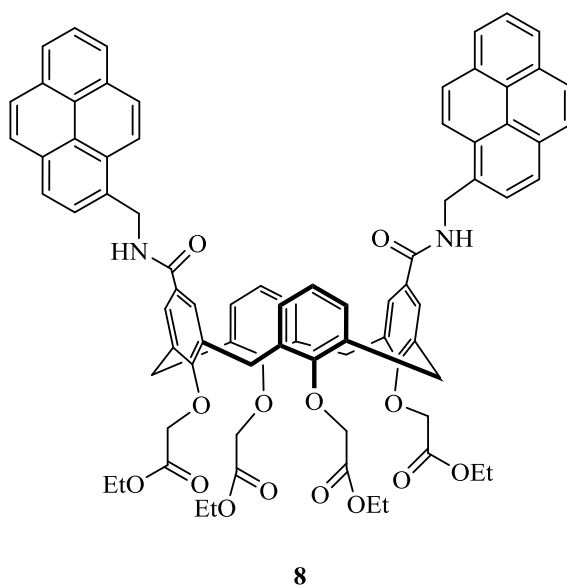


Figure 1.16. Fluorescent chemosensor **8** which selectivity binds to Na⁺.

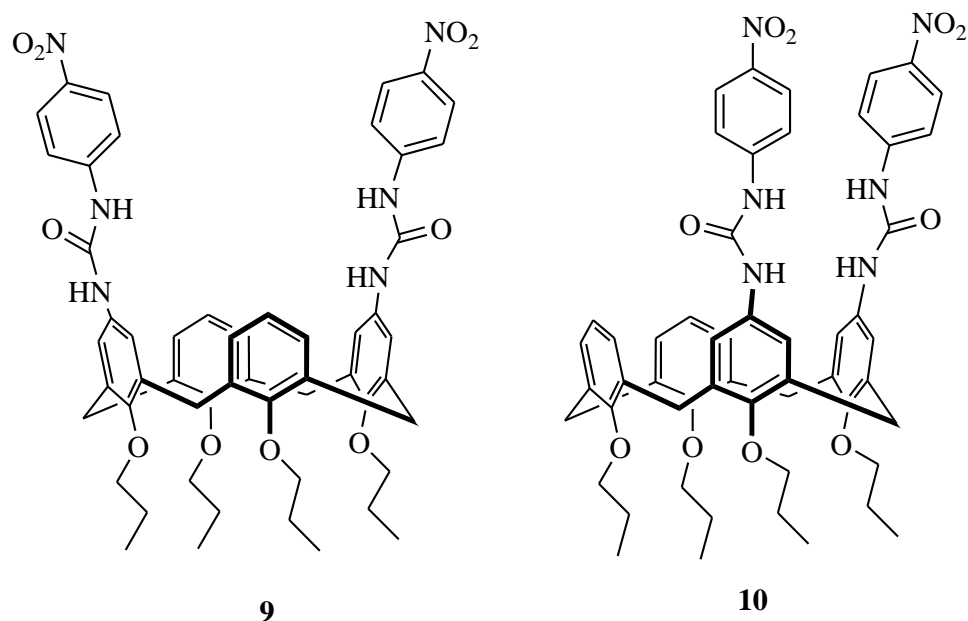


Figure 1.17. Structure of some anion receptors.

Lang et al.³³ proposed the new calix[4]arene-based bis-*p*-nitrophenylureas shown in Figure 1.17 as selective anion receptors. They functionalized the upper rim of the calixarene with urea derivatives to produce sites that have selective binding affinity toward halogens and carboxylates. As a result of the acidity of the hydrogen atoms on the urea entities, the binding between receptors and anions occur *via* hydrogen bonding, as clearly evidenced by the chemical shift changes in the ¹H-NMR spectra of the N-H hydrogens. They used ¹H-NMR and UV-vis spectroscopy to study the complexation between receptors **9** and **10** with various anions. Job plot analysis indicated the 1:1 complex stoichiometry in the case of the 1,4-functionalized receptor **9**, whereas 2:1 complex stoichiometry was observed in the case of the 1,2-functionalized receptor **10**.³³

In 2006, Beer and coworkers³⁴ reported a novel ditopic, or ion-pair, receptor that can bind both cations and anions at the same time. They synthesized **11**, a calix[4]diquinone attached to a isophthalamide motif in the lower rim. While cations coordinated to the diquinone, the isophthalamide amide groups bound to the anions ions *via* hydrogen-bonding with the hydrogen atoms in the amide units as observed in the ¹H-NMR titration studies. They observed a 1:1 complexation ratio using Job plot analysis. Figure 1.18 illustrates receptor **11** bound to the contact ion-pair, KCl.

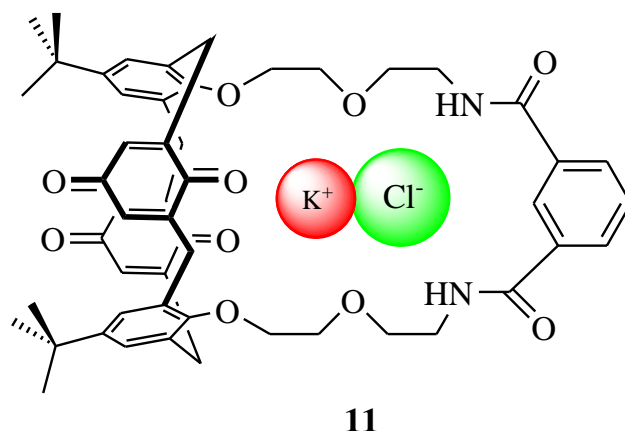


Figure 1.18. Structure of contact ion-pair receptor with KCl.

1.5 Characterization of complexation

There are several analytical techniques used to detect the complexation in host-guest systems in supramolecular chemistry. Some of these techniques, such as NMR, UV-vis and fluorescence spectroscopy can be used to measure the binding or association constants which are significant indicators of the strength of non-covalent bond interaction energies that occur between a host and a guest. Besides the bond energy, techniques such as NMR and single crystal X-ray diffraction can reveal the binding sites which

accommodate guest ions in the host molecules. Chemists have used different techniques to detect the host-guest complexation, depending on the host molecular properties. Some of these useful techniques will be briefly discussed below.

1.5.1 Fluorescence spectroscopy

Fluorescence spectroscopy (FS) is one of the most widely-used techniques for the effective detection of the host-guest complexation at low (e.g. 10^{-5} M) concentrations of the host molecule.³⁵ A receptor containing a fluorophore to be studied by FS is exposed to the light beam in a fluorometer, causing the excitation of electrons in the molecule which leads to the light emission. There are four types of mechanisms involved in fluorescence:

- a. **Photoinduced electron transfer (PET):** This is the most common mechanism. It is based upon a host molecule containing a fluorophore which is responsible for the absorption of light followed by emission of the fluorescence signal. The host molecule also has a receptor which is responsible for binding to a guest and is connected to the fluorophore by a spacer.^{35,36}
- b. **Photoinduced charge transfer (PCT):** This type of charge-transfer is also called “Intramolecular charge transfer” (ICT). It is similar to PET except that the receptor molecule is connected directly to the fluorophore. In this type of mechanism, the fluorescence emission signal that is emitted from the fluorophore is affected by the substituent groups on the receptor (recognition), causing a

change in the electron density of the fluorophore which changes the fluorescence emission.^{31,35}

- c. **Excimer:** An excimer according to the IUPAC Gold Book of definitions is “an electronically excited dimer, 'non-bonding' in the ground state. For example, a complex formed by the interaction of an excited molecular entity with a ground state partner of the same structure”.³⁷ Besides the interaction with the receptor as described above, fluorophores can also interact with each other. The distance between these two fluorophores is important for the formation for the excimer.³⁵
- d. **Fluorescence resonance energy transfer (FRET):** This is the fourth type of fluorescence mechanism. In this mechanism, there are two fluorophores on the same receptor molecule, one acting as a donor and one as an acceptor. The donor provides the energy from its excited states to the acceptor which will thus produce the fluorescence emission.^{35,38}

1.5.2 Nuclear magnetic resonance (NMR)

The use of ¹H-NMR spectroscopy enables one to explore the host-guest complexation in supramolecular chemistry involving organic molecules. NMR can be used to determine the binding site of a host molecule through the changing in the chemical shifts of the protons in the host molecule whether they become shielded or deshielded by the local environmental change in the host arising from the non-covalent bond formed between the host and guest molecules. In addition, this chemical shift allows the evaluation of the binding constant between the host and guest molecules. However, ¹H-NMR has lower sensitivity as compared with fluorescence spectroscopy

and thus requires higher concentrations (typically $\sim 10^{-3}$ M) of the host molecules which may have limited solubility in the NMR solvents.³⁹

1.5.3 Single-crystal X-ray diffraction

Single-crystal X-ray diffraction is an important analytical technique for the analysis of a host-guest complex in the solid state. The X-ray diffraction structure can provide precise information about the binding site and which atoms are involved in the complexation. X-ray diffraction has the drawback in that the binding constant cannot be determined and of course only provides the solid-state information.³⁹

1.5.4 UV-visible spectroscopy

Ultraviolet-visible spectroscopy is a highly sensitive technique used for the detection of host-guest complexation. In comparison with NMR spectroscopy, UV-visible spectroscopy allows the use of lower concentrations ($\sim 10^{-6}$ M) of the host than NMR does, however, UV-visible spectroscopy is less helpful than NMR for studying the actual binding sites of a host molecule.³⁹

1.5.5 Mass spectrometry (MS)

Mass spectrometry, in particular with electrospray ionization, can also be used as an additional tool for the characterization of host-guest complexation in gas-phase supramolecular systems.

1.5.6 Scanning probe microscopy (SPM)

SPM techniques such as scanning tunneling microscopy (STM) and atomic force microscopy (AFM) are also employed in the characterization of guest-host supramolecular systems. These techniques can provide valuable information about self-assembly onto a solid surface. Such information can be used, for example, to investigate the orientation of molecules on a solid surface.⁴⁰

Objectives and results

The objectives of the work described in this thesis include the synthesis and the characterization of some new triazole-bridged calix[4]arenes and calix[4]acenaphthenes and some of their supramolecular complexation properties.

In Chapter 2, a description of the synthesis of two new receptors, namely bis(naphthyl)methane-bridged macrocycles using Yamato's⁴¹ methodology will be provided. This chapter also includes also the characterization of these macrocycles using ¹H- and ¹³C-NMR spectroscopy and mass spectroscopy. Also presented are the complexation studies of these receptors with different metal ions using fluorescence spectroscopy and the investigation of the binding constant for the complexes. ¹H-NMR results which were used to determine which protons are involved in complex formation will also be presented.

The synthesis of a new fluorescent chemosensor based on acenaphthene-modified calix[4]arene-triazoles is described in Chapter 3. This chapter will also include complexation studies of these new receptors with a variety of metal ions, which were

conducted by using techniques such as fluorescence and $^1\text{H-NMR}$ spectroscopy, to investigate the affinity between metal ions and these acenaphthene-containing receptors.

Chapter 4 of this thesis will highlight attempts to modify homooxacalix[4]acenaphthene, whose synthesis and characterization has been previously reported by AlHujran et al.⁴² This compound was found to be a selective receptor for C_{60} fullerene due to its size. Molecular modeling showing that a new wide rim-modified homooxacalix[4]acenaphthene, which was targeted for synthesis, could be an important new receptor for larger fullerene guest molecules such as C_{70} .

1.6 References

1. Steed, J. W.; Atwood, J. L. *Supramolecular Chemistry*, John Wiley & Sons Ltd, England, 2000.
2. Schneider, H. *Application of Supramolecular Chemistry*, Taylor and Francis Group, 2012.
3. Doziuk, H. *Introduction to Supramolecular Chemistry*, Kluwer Academic Publishers, 2002.
4. Steed, J. W.; Turner, D. R.; Wallace, K. J. *Core Concepts in Supramolecular Chemistry and Nanochemistry*, John Willy & Sons Ltd, England, 2007.
5. Anslyn, E. V.; Dougherty, D. A. *Modern Physical Organic Chemistry*, University Science Books, Sausalito, CA, USA, 2006.
6. Jeffery, G. A. *An Introduction to Hydrogen Bonding*, Oxford University Press, Oxford, UK, 1997.
7. Steiner, T. *Chem. Commun.* **1997**, 727-734.
8. Ma, J. C.; Dougherty, D. A. *Chem. Rev.* **1997**, 97, 1303–1324.
9. Mecozzi, S.; West, A. P.; Dougherty, D. A. *J. Am. Chem. Soc.* **1996**, 118, 2307-2308.
10. Sinnokrot, M. O.; Valeev, E. F.; Sherril, C. D. *J. Am. Chem. Soc.* **2002**, 124, 10887-10893.
11. Rashkin, M. J.; Waters, M. L. *J. Am. Chem. Soc.* **2002**, 124, 1860-1861.
12. Enright, G. D.; Brouwer, E. B.; Udachin, K. A.; Ratcliffe, C. I.; Ripmeester, J. A. *Acta. Cryst.* **2002**, 58, 1032-1035.

13. Ulman, A. *Chem. Rev.* **1996**, *96*, 1533–1554.
14. Gutsche, C. D. *Calixarenes Revisited*, Royal Society of Chemistry, Cambridge, 1998.
15. Gutsche, C. D. *Calixarene an Introduction*, Royal Society of Chemistry, Cambridge, 2008.
16. Mandolini, L.; Ungaro, R. *Calixarenes in Action*, Imperial College Press, London, 2000.
17. Gutsche, C. D.; Dhawan, B.; No, K. H.; Muthukrishnan, R. *J. Am. Chem. Soc.* **1981**, *103*, 3782.
18. Iwamoto, K.; Araki, K.; Shinkai, S. *J. Org. Chem.* **1991**, *56*, 4955–4962.
19. Gutsche, C. D.; Dhawan, B.; Levine, J. A.; No, K. H.; Bauer, L. J. *Tetrahedron*, **1983**, *39*, 409-426.
20. Cornforth, J. W.; Morgan, E. D.; Potts, K. T.; Rees, R. J. W. *Tetrahedron*, **1973**, *29*, 1659.
21. (a) Gutsche, C. D. *Acc. Chem. Res.* **1983**, *16*, 161-165. (b) Van Hoorn, W. P., Van Veggel, F. C. *J. Org. Chem.* **1996**, *61*, 7180
22. Vicens, J.; Bohmer, V. *Calixarenes a Versatile Class of Macrocyclic Compounds*, Kluwer Academic Publishers, Cambridge, 1990.
23. Jaime, C.; Mendoza, J. D.; Prados, P.; Nieto, P. M.; Sanchez, C. *J. Org. Chem.* **1991**, *56*, 3372-3376.
24. Asfari, Z.; Bohmer, V.; Harrowfield, J.; Vicens, J. *Calixarenes 2001*, Kluwer Academic Publisher, Dordrecht The Netherlands, 2001.

25. Vicens, J.; Harrowfield, J. *Calixarenes in the Nanoworld*, Springer, Dordrecht, Holland, 2007.
26. Georghiou, P. E.; Rahman, S.; Valluru, G.; Dawe, L. N.; Rahman, S. M.; Alodhayb, A. N.; Beaulieu, L. Y. *New J. Chem.* **2013**, *37*, 1298-1301.
27. Chang, K. C.; Su, I. H.; Lee, G. H.; Chung, W. S. *Tetrahedron Lett.* **2007**, *48*, 7274-7278.
28. Benesi, H. A.; Hildebrand, J. H. *J. Am. Chem. Soc.* **1949**, *71*, 2703-2707. (a)
Thordarson, P. *Chem. Soc. Rev.* **2011**, *40*, 1305–1323.
29. Lee, J. Y.; Kim, S. K.; Jung, J. H.; Kim, J. S. *J. Org. Chem.* **2005**, *70*, 1463-1466.
30. Joyce, L. A.; Shabbir, S. H.; Anslyn, E. V. *Chem. Soc. Rev.* **2010**, *39*, 3621–3632.
31. Baruah, M.; Qin, W.; Vallee, R. A. L.; Beljonne, D.; Rohand, T.; Dehaen, W.;
Boens, N. *Org. Lett.* **2005**, *7*, 4377-4380.
32. KeRang, W.; DongSheng, G.; BangPing, J.; Yu, L. *Sci. China. Ser. B-Chem.* **2009**, *52*, 513- 517.
33. Lang, K.; Curinova, P.; Dudic, M.; Proskova, P.; Stibor, I.; Stastny, V.; Lhotakb, P.
Tetrahedron **2005**, *46*, 4469-4472.
34. Lankshear, M. D.; Cowley, A. R.; Beer, P. D. *Chem. Commun.* **2006**, *6*, 612-614.
35. Lakowics, J. R. *Principles of Fluorescence Spectroscopy*, Springer, Maryland, USA, 2006.
36. Silva, P. A.; Moodyb, T. S.; Wright, G. D. *Analyst.* **2009**, *134*, 2385-2393.
37. Nic, M.; Jirat, J.; Kosata, B. *IUPAC Gold Book*, International Union of Pure and Applied Chemistry, Prague, 2005.

38. Yuan, M.; Zhou, W.; Liu, X.; Zhu, M.; Li, J.; Yin, X.; Zheng, H.; Zuo, Z.; Ouyang, C.; Liu, H.; Li, Y.; Zhu, D. *J. Org. Chem.* **2008**, *73*, 5008-5014.
39. Schneider, H. J.; Yatsimirsky, A. K. *Principles and Methods in Supramolecular Chemistry*, John Wiley & Sons Ltd, Chichester, 2000.
40. Pan, G.; Bu, J.; Wang, D.; Liu, J.; Wan, L.; Zheng, Q.; Bai, C. *J. Phys. Chem. B.* **2003**, *107*, 13111-13116.
41. Jin, C. C.; Kinoshita, T.; Cong, H.; Ni, X.-L. Zeng, X.; Hughes, D. L.; Redshaw, C.; Yamato, T. *New J. Chem.* **2012**, *36*, 2580-2586.
42. AlHujran, T.; Dawe, L. N.; Georghiou, P. E. *Org. Lett.* **2012**, *14*, 3530-3533.

Chapter 2

Synthesis and Complexation Properties of Trizole-bridged Bisnaphthyl-Calix[4]arenes

2.1 Introduction

In this chapter, a description will be provided of the synthesis of two new molecular receptors namely, bis(naphthyl)methane-bridged macrocycles, using Yamato's¹ methodology. The experimental section in this chapter includes the characterization of these macrocycles using ¹H- and ¹³C-NMR spectroscopy and mass spectrometry. Also presented are the complexation studies of these receptors with different metal ions using fluorescence spectroscopy (FS) and the determination of the binding constants for the metal complexes formed. The results which were obtained from ¹H-NMR titration studies were also used to determine which protons are involved in the complex formation and will also be presented.

2.1.1 Metal ion receptors

The design and synthesis of new receptors for metal ions is of current ongoing interest in supramolecular chemistry. This is because of the role that metal ions play in many fields, especially in biology, chemical processes and in the environment.^{2,3} Iron ions are a clear example of the important roles that some metal ions play in the human body and in other organisms.² Biologically, iron is the most essential transition-metal since it plays an essential role in carrying oxygen in the heme molecule. It acts also as a

cofactor in enzymatic reactions of the mitochondrial respiratory chain.³ Iron is a redox-active metal, and thus besides its significant roles in essential cellular processes it can also be a harmful catalyst for Fenton or Haber–Weiss type reactions causing oxidative stress by producing destructive hydroxyl radicals.^{4,5} Either a deficiency, or an excess of (Fe^{3+}) can cause a variety of diseases such as anemia, liver and kidney damage, diabetes, heart disease and cancer.^{2,4} Fluorescent chemosensors that can selectively detect iron ions are rare and due to the importance of discrimination between Fe^{3+} and Fe^{2+} in the regulation of their biological function, the design of a fluorescent chemosensor capable of binding selectivity to Fe^{3+} ions is an important challenge.^{6,7} Besides the toxicity of copper and iron, mercury is regarded as one of the most prevalent toxic metals of all of the heavy metals.⁸ Mercury can be found naturally in the ocean and the Earth's crust, arising from volcanic eruptions. In addition, mercury could cause poisoning particularly for workers who work in mining and mineral processing. Mercury ions (Hg^{2+}) have harmful effects on human health as they accumulate in living tissues where they have a high affinity to bind with sulfhydryl groups in proteins which can block their function.^{8a,9} Methyl mercury is a particular toxic form which is more easily bioaccumulated than inorganic mercury. Several studies indicate that methylmercury is linked to subtle developmental deficits in children exposed *in-utero* such as decreased performance in tests of language skills, memory function and attention deficits.^{8b} The toxicity is related to the fact that biological ligands such as proteins, DNA, and enzymes all have sulfhydryl groups which can coordinate with the mercury ions. Consequently, toxic levels of mercury (Hg^{2+}) leads to significant damage to the brain, kidney, stomach, and central nervous system.⁹

Therefore, chemists have recently focused on the design of highly sensitive receptors that can bind selectively to Hg^{2+} and other transition metal ions.¹⁰

2.1.2 Triazole bridge-based calixarene chemosensors

Fluorescent metal ion sensors have been designed using a variety of molecules such as crown ethers, porphyrins, calixarenes and other types of molecules.¹¹ However, because of the unique relatively robust framework of the calixarenes which incorporate a wide and naturally hydrophobic cavity, and upper- and lower-rims which can be selectively functionalized with suitable podand groups, calixarene molecules have provided an important framework for many fluorescent chemosensors. Recently, calixarenes as chemosensors which incorporate 1,2,3-triazole units as fluorophores, have been reported.^{12,13} The 1,2,3-triazole units are stable functional groups which have been shown to be good binding sites for cations and especially transition metal ions, to form selective supramolecular complexes.¹⁴ “Click Chemistry” (the term was first introduced by K. Barry Sharpless¹⁵ in 2001) has been extensively used to generate triazole units. One of the most useful synthetic methods commonly referred to as “Cu(I)-catalyzed azide-alkyne cycloaddition” (or “CuAAC”) reactions is widely used for the cyclization of an azide with a terminal alkyne. This is because these reactions possess several useful features, including the possible use of a variety of solvents and functional groups, the simplicity in performance, the potential of high yields under mild reaction conditions and high reaction rate.^{16,17} This method has been adopted in a wide range of applications in the biological, materials, and medicinal chemistry areas.¹⁸

In 2005, Ryu and Zhao¹⁷ were the first to use the CuAAC synthetic method in a calixarene moiety, to produce the 1,2,3-triazole-based calixarene **1**, as shown in Figure 2.1. They used the lower-rim terminal alkyne-bearing calixarene as a scaffold upon which to generate the 1,2,3-triazole functional group which could bind to different metal cations *via* non-covalent interactions.

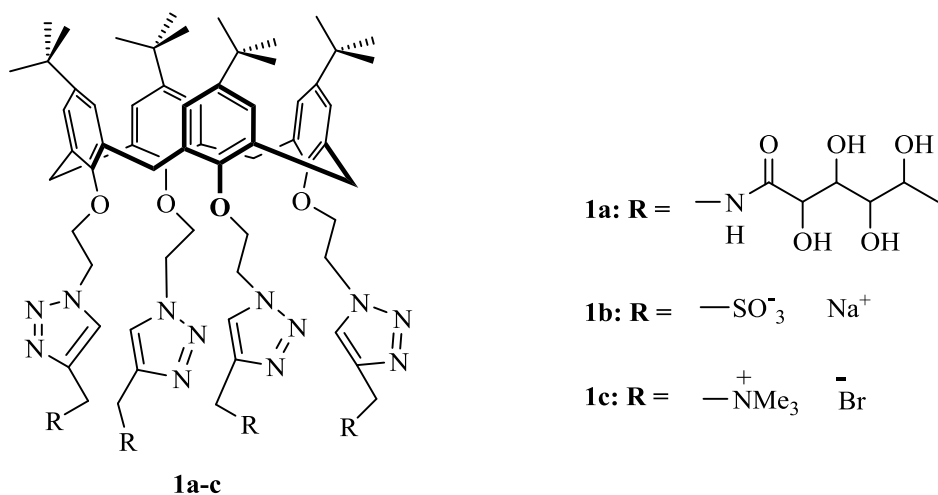


Figure 2.1. Triazole-bridge based calixarenes **1a-c**.

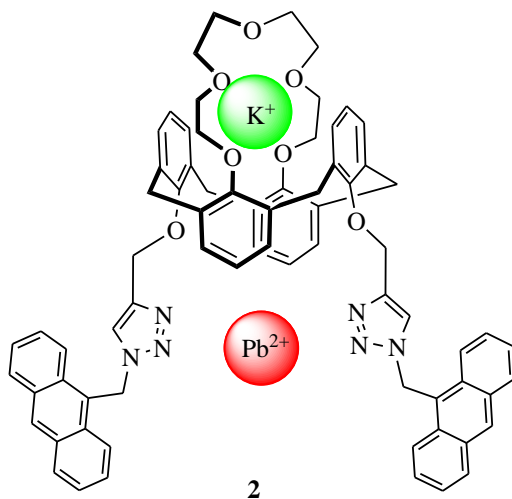


Figure 2.2. Fluorescent receptor with two cationic binding sites.

In 2007, Chung et al.²⁰ reported a novel *1,3-alternate* calix[4]crown-5 fluorescent receptor **2** (Figure 2.2) that has the ability to bind two different cationic guests which could attach to the two binding sites, namely the triazole units on the upper rim and the crown-5 unit on the lower rim. Using fluorescence and ¹H-NMR titration studies in CH₃CN/CHCl₃ (1000:4) and (3:1) respectively, they showed that receptor **2** formed 1:1 complexes and exhibited selective binding to Hg²⁺, Cr²⁺, Pd²⁺ and Cu²⁺ ions through the triazole units. The fluorescence intensity of chemosensor **2** was quenched due to the reverse-PET and the heavy metal effect once bound to these metal ions. As a result of having crown-5 in the lower rim as another binding site, **2** also detected K⁺ ions and showed slight enhancement in the emission intensity of fluorescence.

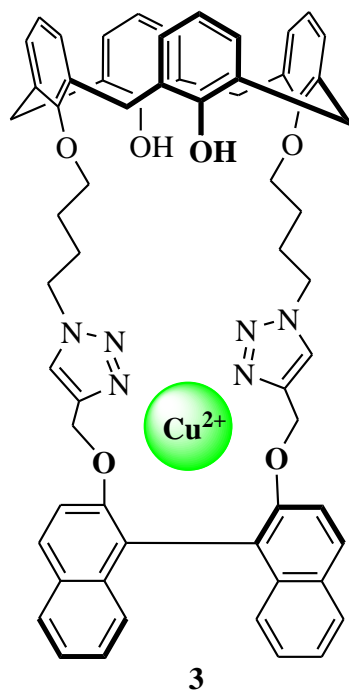


Figure 2.3. Calixarene-binol-bis(1,2,3)-triazole receptor.

The fluorescent calixarene receptor **3** (Figure 2.3) that was introduced by Li and coworkers²¹ in 2012 is an example of a chiral chemosensor. They used CuAAC in order to synthesize **3** which incorporated a chiral 1,1'-bi-2-naphthol (“binol”) that bridged the distally-disubstituted 1,2,3-triazole-functionalized calixarene. Fluorescence complexation studies were conducted for **3** which showed high selectivity towards sensing Cu²⁺ ions over other tested transition metal, alkaline-earth metal or alkali metal ions. A unique advantage of **3**:Cu(II) complexation is its capacity for chiral recognition, for example, to distinguish mandelic acid enantiomers. Figure 2.4 shows the difference in fluorescence intensities resulting from adding the respective mandelic acid epimers to the **3**:Cu(II) complex.

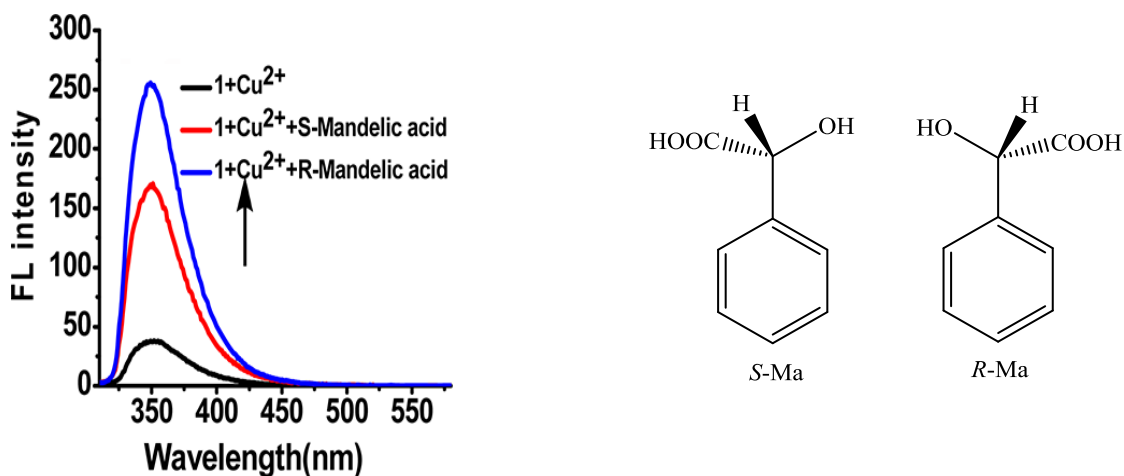


Figure 2.4. Changes of the observed fluorescence intensities upon addition to the **3**:Cu²⁺ complex of each of the mandelic acid enantiomers shown.

Rao et al.²² synthesized a new 1,3-disubstituted calix[4]arene chemosensor **4** in which the two 1,3-triazole groups were linked to anthracene groups. This receptor, **4**, was found to be capable of selective 1:1 binding with Co^{2+} ions is shown in Figure 2.5. They synthesized the desired chemosensor *via* a CuAAC methodology.

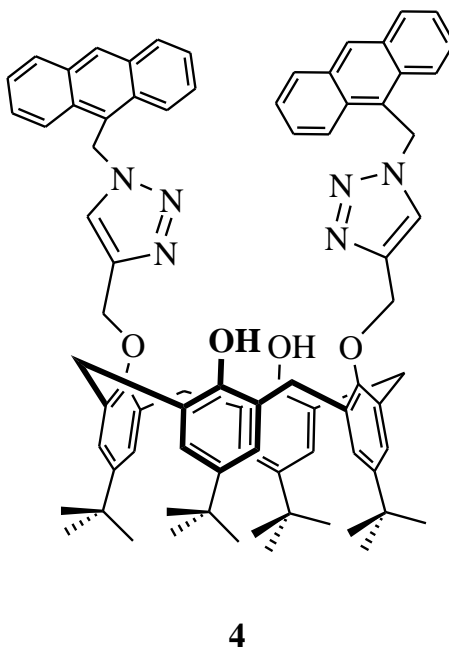


Figure 2.5. Structure of receptor **4** that selectively binds to Co^{2+} .

2.2 Results and discussion

2.2.1 Design of bis(naphthyl)-bridged 1,2,3-triazole fluorescent receptors

A gas-phase Gaussian09²⁴-generated DFT, B3LYP/lanl2dz-geometry-optimized structure, suggested that a bis(naphthyl)-bridged 1,2,3-triazole receptor such as **5** as shown in Figure 2.6, could be a potential viable transition metal ion receptor²³, e.g. Cu^{2+} or Fe^{3+} .

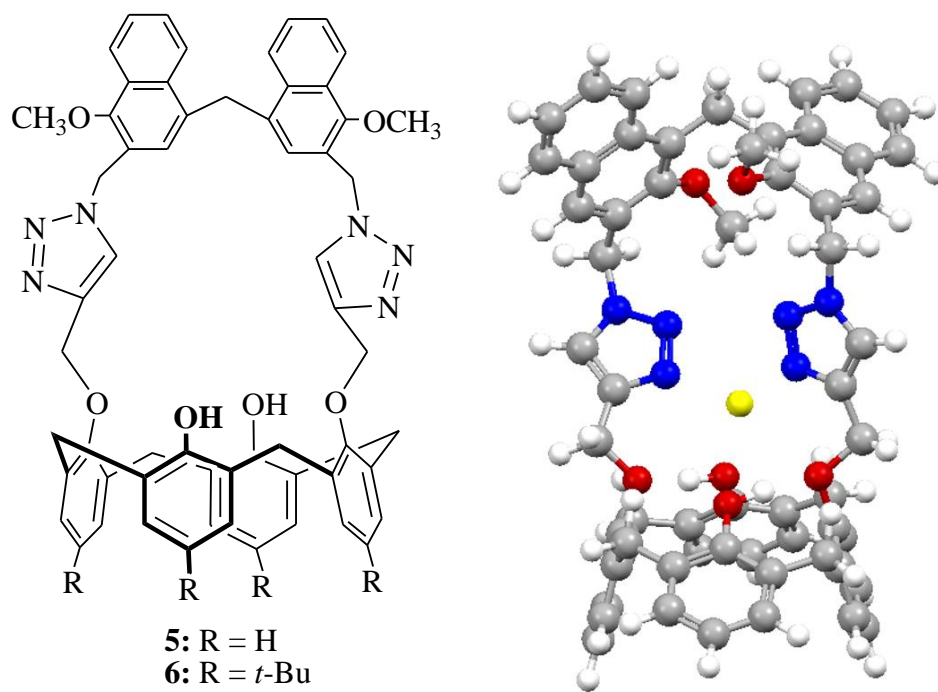


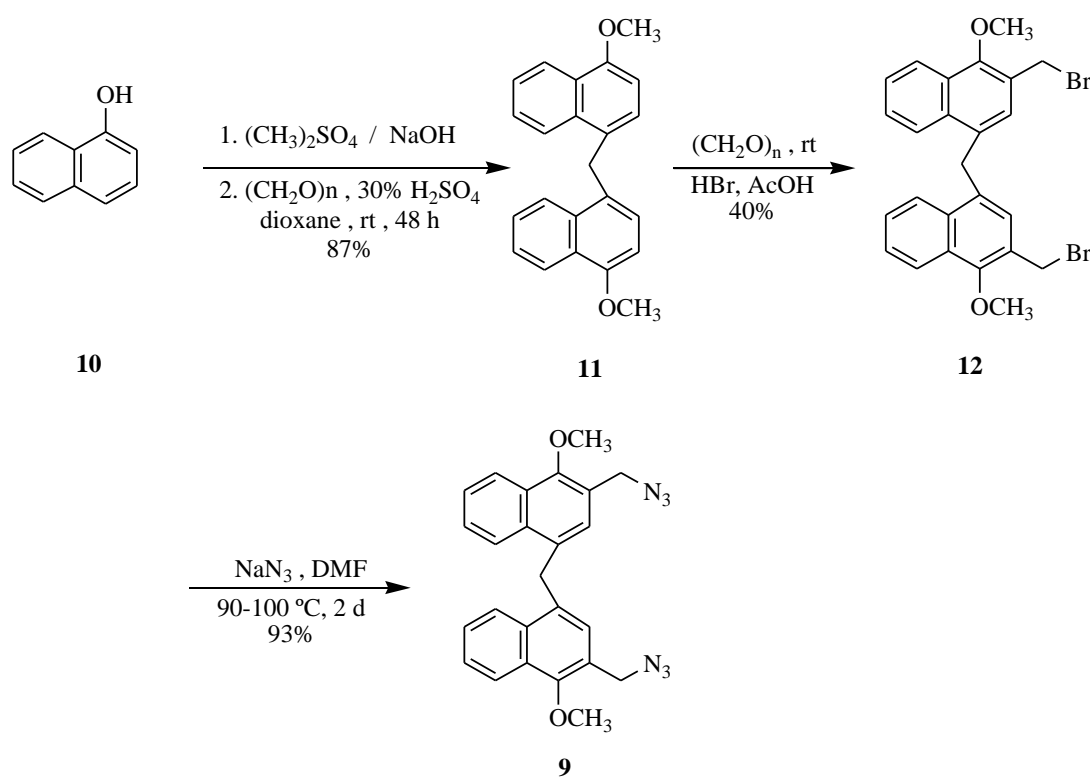
Figure 2.6. *Left:* free ligands **5** and **6**; *right:* the geometry-optimized (ball-and-stick) structure of **5**:Cu²⁺ complex was fully optimized with the B3LYP level of DFT and the lan12dz basis set in the gas phase Gaussian 09²⁴ at 298 K. Colour code: Cu²⁺ = yellow, triazole nitrogen = blue, hydrogen = white and oxygen atom = red.

2.2.2 Synthetic approach toward desired macrocycles

2.2.2.1 Synthesis of bis[3-(azidomethyl)-4-methoxy-1-naphthyl]methanes (**9**)

The desired de-*tert*-butyl bis(naphthyl) triazole-bridged calixarene targets, **5** and its *tert*-butyl calixarene analogue **6**, were achieved applying the CuAAC coupling methodology to intermediates **7** and **8**, respectively, with **9** (Scheme 2.3). The synthesis of **9** (Scheme 2.1) starts from 1-hydroxynaphthalene **10** which was reacted with dimethyl sulfate in the presence of NaOH to produce 1-methoxynaphthalene, followed by an acid-catalyzed reaction with paraformaldehyde in dioxane solvent for 48 h at room temperature. An 84% yield of bis(4-methoxy-1-naphthyl)methane (**11**)²⁵ was obtained.

Reaction of **11** with HBr and paraformaldehyde in acetic acid at room temperature formed bis[3-(bromomethyl)-4-methoxy-1-naphthyl]methane (**12**) in 40% yield, as reported previously by Georghiou and Ashram.²⁶ In the next step, bis[3-(azidomethyl)-4-methoxy-1-naphthyl]methane (**9**), was obtained by reacting **12** with sodium azide in dimethylformamide at 90 °C for 48 h. This intermediate was obtained in an excellent yield (93%).

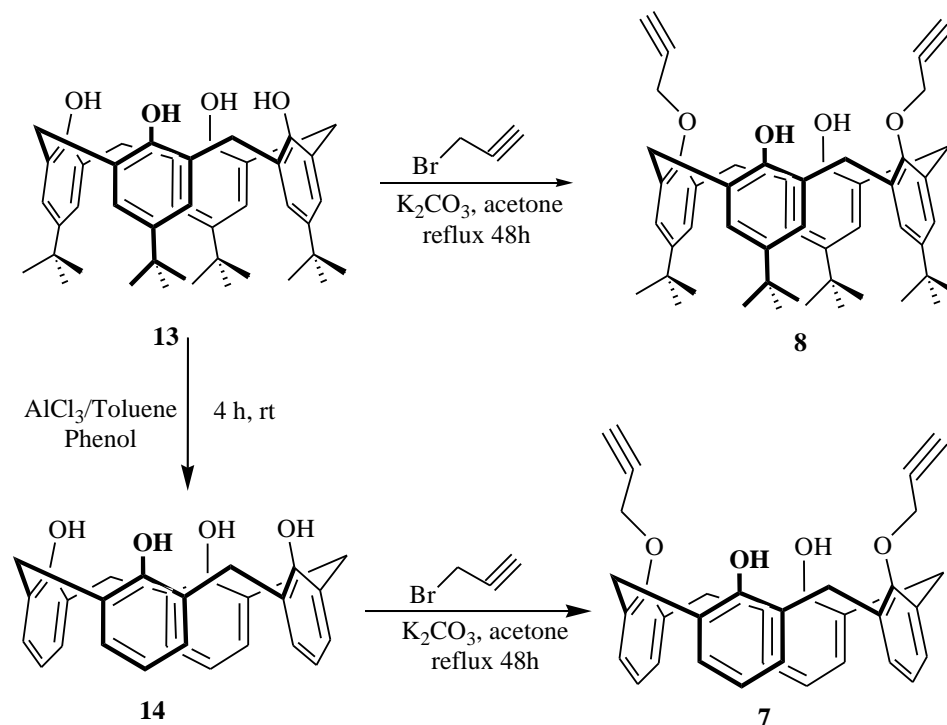


Scheme 2.1. Synthetic route to bis[3-(azidomethyl)-4-methoxy-1-naphthyl]methane (**9**).

2.2.2.2 Synthesis of bis(*O*-propargyl)calix[4]arene derivatives **7** and **8**

The other intermediate calixarenes **7** and **8** which were required for the target macrocycles **5** and **6**, respectively, were synthesized successfully as outlined in Scheme 2.2. The synthesis of the calixarene **8** started from the well-known calixarene, tetra-*p*-

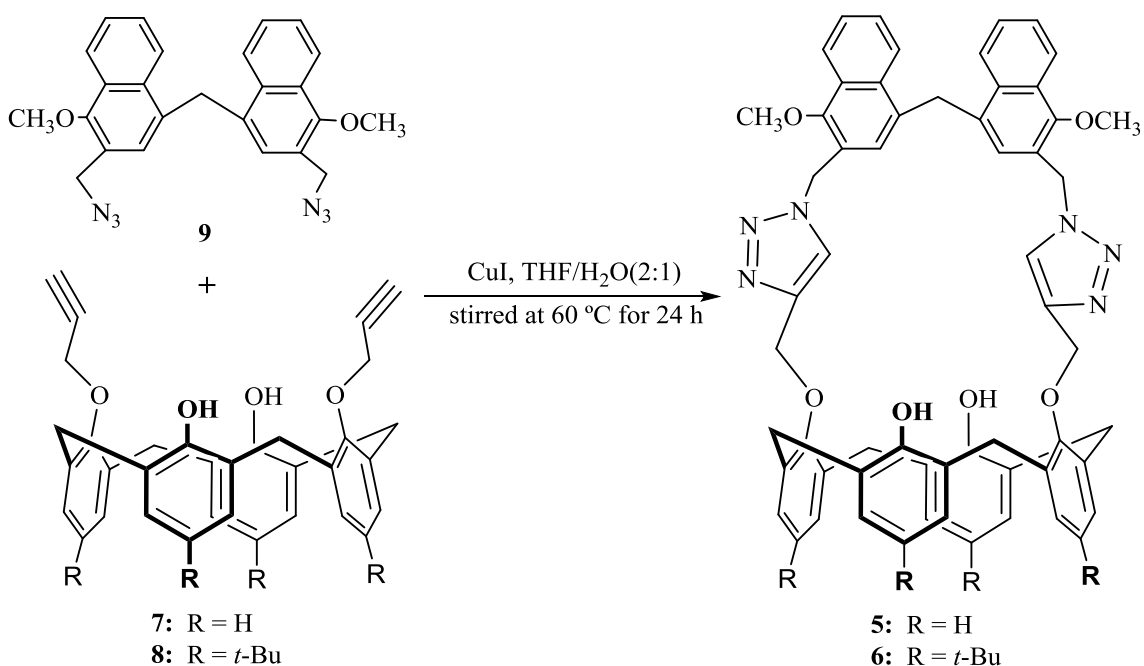
tert-butylcalix[4]arene (**13**) via alkylation with propargyl bromide in the presence of potassium carbonate in acetone for 48 h under reflux conditions.²⁷ The other calixarene intermediate **7**, was obtained by treating **13** with aluminum trichloride in toluene at room temperature to afford the *de-tert*-butyl calixarene **14**. Alkylation of **14** employing the reported conditions with propargyl bromide in the presence of potassium carbonate in acetone at room temperature, however, did not produce **7**.²⁸ The conditions were modified by using the same reagents but heating to reflux for 48 h, as was needed with **13**, to afford **7** successfully in 60% yield. The corresponding *tert*-butylated **8** could be synthesized in the same way, to afford **8** in 78 % yield.



Scheme 2.2. Synthetic route used for the calixarene intermediates **7** and **8**.

2.2.2.3 Synthesis of triazole-bridge bisnaphthyl-calix[4]arene macrocycles **5** and **6**

Cyclization of azide **9** with calix[4]arene **7**, and with **8** was achieved by using copper (CuI) catalyst in 2:1 THF/H₂O. These reactions are essentially 1,3-dipolar cycloadditions between the terminal alkyl groups of **7** or **8**, with the azide units of **9** to generate the 1,2,3-triazole-bridged macrocycles **5** and **6**. It is noteworthy that these types of cyclizations were first reported by Huisgen²⁹ in 1960. The desired macrocycles **5** and **6** were produced in 30% and 25% yields, respectively. Scheme 2.3 below illustrates the synthesis of the two macrocycles.



Scheme 2.3. Synthesis of triazole-bridged bis(naphthyl)methyl-calix[4]arene **5** and **6**.

2.2.3 Characterizations of the newly-synthesized compounds **5** and **6**

All of the newly-synthesized compounds were characterized using ^1H - and ^{13}C -NMR spectroscopy and mass spectrometry. Macrocycles **5** and **6** have almost similar structures with the only difference being that *t*-Bu groups are attached to the *para*-position of the calix[4]arene moiety in macrocycle **6**. The ^1H -NMR spectra revealed new proton singlet signals at δ 8.01 and 7.99 ppm for macrocycles **5** and **6** respectively in CDCl_3 . These peaks are related to the triazole units of the macrocycles formed from the CuAAC reactions and are expected to appear in these regions. Two other proton singlet signals were affected by the triazole units and were observed at δ 5.22 and 5.81 ppm for macrocycle **5** and at δ 5.14 and 5.74 ppm for **6**. These signals refer to the two bridge protons which are attached to the triazole units. The ^1H -NMR spectrum shows two sets of AX doublets at δ 3.08-3.12 and 4.04-4.09 ppm for **5**, and shows peaks at δ 3.17-3.21 ppm and δ 4.14-4.18 ppm for **6**. All of the aforementioned AX signals are related to the calixarene bridge ($-\text{CH}_2-$). Two sharp singlet signals appeared at δ 4.06 and 4.18 ppm for **5**, and at δ 4.04 and 4.48 ppm for **6**, due to the methoxy groups and the bisnaphthyl bridge ($-\text{CH}_2-$) respectively. The other two singlet signals appearing at δ 0.95 and 1.25 ppm are related to the *t*-Bu groups in macrocycle **6**. Also, the ^1H -NMR shows eight downfield signals for **6**: four of which appear as singlets at δ 6.76 and 6.95 ppm, corresponding to the calixarene moiety. The signal at δ 6.88 ppm is due to the hydroxyl groups, that at δ 7.07 ppm corresponds to the bisnaphthyl moiety, the two doublets at δ 7.88-7.91 and 8.20-8.23 ppm are related to the bisnaphthyl moiety, and the last two

signals are triplets which are also related to the bisnaphthyl moiety, appear at δ 7.47-7.51 and 7.55-7.60 ppm. Moreover, the $^1\text{H-NMR}$ spectrum for macrocycle **5** also shows eight downfield signals: two triplet signals are at δ 6.54-6.59 and 6.68-6.73 ppm, one doublet signal is at δ 6.80-6.82 ppm. These three signals correspond to the calixarene moiety. Two singlet signals are observed at δ 6.88 and 7.62 ppm and are related to the hydroxyl groups and the bisnaphthyl unit, respectively. Two signals were doublet signals appearing at δ 7.83-7.85 and 8.21-8.24 ppm and are related to the bisnaphthyl unit. The last signal appearing as a multiplet at δ 7.47-7.59 is also due to the bisnaphthyl unit.

The $^{13}\text{C-NMR}$ spectra for macrocycles **5** and **6** are simpler and consisted of twenty signals between δ 122.85 to 152.84 ppm (downfield signals). These can be explained as follows: a) eight signals are related to the calixarene moieties; b) two signals are due to the triazole units; c) ten signals are linked to the bisnaphthyl moieties. In addition, macrocycle **6** has eight up-field signals between δ 31.01 and 70.00 ppm. Four signals located between δ 30.96 and 33.90 ppm and are due to the *tert*-Bu groups. One signal located within these four signals is related to the calixarene methylene bridges. The next signal at δ 48.68 ppm is assigned to the methoxy groups, and the other signal at δ 63.07 ppm, results from overlapping between the bisnaphthyl ($-\text{CH}_2-$) bridge and the signal of the triazole-bisnaphthyl bridges ($-\text{CH}_2-$). The last signal at δ 70.00 ppm and is due to the calixarene ($-\text{O}-\text{CH}_2-$) triazole. Macrocycle **5** showed only four signals between δ 31.66 to 70.33 ppm. The most up-field signal at δ 31.66 ppm is due to the calixarene methylene ($-\text{CH}_2-$) bridges. The next signal due to the methoxy groups was

found at δ 48.45 ppm. The signal at δ 63.27 ppm is overlapped between the bisnaphthyl ($-\text{CH}_2-$) bridge and the signal of the triazole-bisnaphthyl bridges ($-\text{CH}_2-$). The signal at δ 70.33 ppm is due to the calixarene-triazole ($-\text{O}-\text{CH}_2-$). LCMS was also used to confirm these macrocycles and showed clearly signals at m/z 938.3 $[\text{M}^+]$ and 1163.3 $[\text{M}^+]$ for **5** and **6**, respectively.

2.3 Complexation studies

Complexation studies of these two macrocyclic receptors **5** and **6** were conducted using $^1\text{H-NMR}$ and fluorescence spectroscopy. Fluorescence spectroscopy is more sensitive than $^1\text{H-NMR}$ spectroscopy and so was chosen to investigate the complexation phenomena with various alkali metal, alkaline-earth metal and transition metal ions.

2.3.1 Complexation studies using fluorescence spectroscopy

2.3.1.1 Calculation of association constants

The association constants (K) determined for the complexation between hosts **5** and **6** and the metal ions examined were based on the fluorescence data and were calculated employing a modified Bensi-Hildebrand^{30a} method using equations 1 and 2:

$$\frac{1}{(F_o - F)} = \frac{1}{(F_o - F_{fc})} + \frac{1}{K(F_o - F_{fc})[M]} \quad (1)$$

$$\frac{1}{(F_o - F)} = \frac{1}{(F_o - F_{fc})} + \frac{1}{K(F_o - F_{fc})[M]^{1/2}} \quad (2)$$

In these equations, K is the association constant, F_o is the fluorescence intensity of the free host, F is the observed fluorescence intensity of the host-guest complex, and F_{fc} is the fluorescence intensity upon saturation. $[M]$ is the concentration of the guest ion in mol L⁻¹. According to these equations, a plot of $1/(F_o-F)$ vs $1/[M]$ giving a straight line indicates 1:1 stoichiometry between the host and metal ions. A plot $1/(F_o-F)$ vs $1/[M]^{1/2}$ giving a straight line, indicates 1:2 stoichiometry between the host and metal ions.^{30b-c} In the titrations conducted during the present study, all of the plots showed clear linear relationships using equation (1), with correlation coefficients > 0.993. The 1:1 binding constants were obtained from equation (3):

$$K = (\text{y-intercept})/(\text{slope}) \quad (3)$$

Note: $[M]$ have in the B-H approach assumes that it is $[M] + [M]_{\text{complex}}$.

2.3.1.2 Fluorescence complexation survey studies with host 5 and 6

Since fluorescence spectroscopy is a sensitive technique, dilute $\sim 10^{-5}$ M stock solutions of **5** and **6** (3.46×10^{-5} M) and (1.64×10^{-5} M) respectively, were prepared in a 9:1 CH₃CN:CHCl₃ mixed solvent. Both **5** and **6** displayed monomer emissions at 331 nm and 343 nm at the 282-nm excitation wavelength. The fluorescence emissions were quenched upon adding the metal ions as a result of complexation occurring between the host and the guest. The affinities of the receptors to various cationic guests were evaluated in order to investigate the selectivity of these compounds toward these metal ions. The cationic guests that were surveyed were: Na⁺, K⁺, Ca²⁺, Ba²⁺, Mg²⁺, Sr²⁺, Ag⁺, Co²⁺, Cd²⁺, Fe²⁺, Fe³⁺, Cu²⁺, Hg²⁺, Pd²⁺, Zn²⁺, Ni²⁺ and Mn²⁺ ions, all of which were used

as their respective perchlorate salts in aqueous solution. Fluorescence spectroscopy studies were performed showing that Fe^{3+} ions were selectively recognized by **6** and **5**. Association constants were calculated using the Benesi-Hildebrand equations for these cationic guests and gave the highest values namely, $2.21 \times 10^5 \text{ M}^{-1}$ for the **5**: Fe^{3+} and $3.32 \times 10^4 \text{ M}^{-1}$ for the **6**: Fe^{3+} complexes. Figures 2.7 to 2.12 show the FS titration experiments conducted for the receptors **5** and **6** with different metal ions. These figures also display the association constants calculated for the complexes with the metal ions, at 343 nm and 330 for receptor **5**, and at 331 nm and 343 nm wavelengths for receptor **6**. The highest association constant values with the macrocycles were obtained with Fe^{3+} , Cu^{2+} and Hg^{2+} .

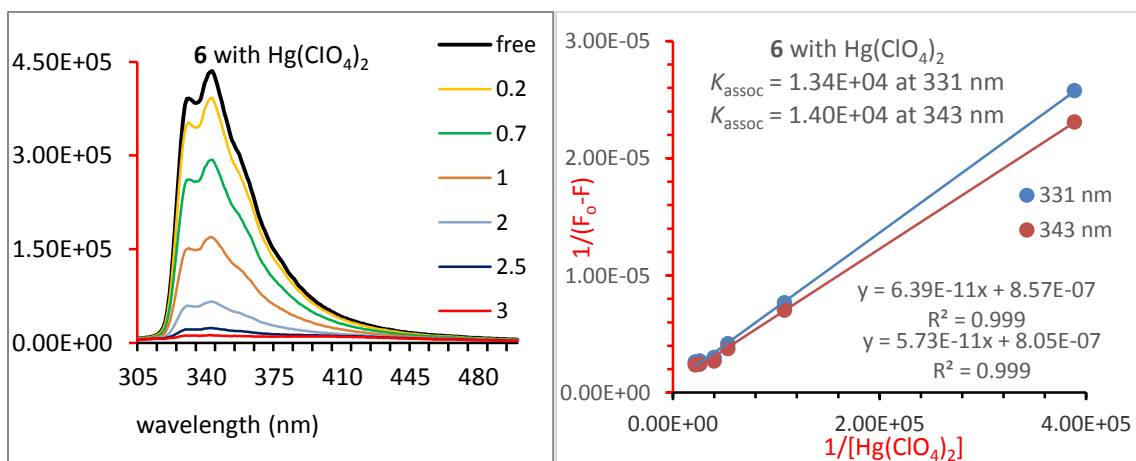


Figure 2.7. *Left:* Fluorescence spectra of **6** (16.4 μM) upon addition of Hg^{2+} (0.2-3 equivalents) in acetonitrile/chloroform (v/v= 9:1) solutions. $\lambda_{\text{ex}} = 282 \text{ nm}$. *Right:* Benesi-Hildebrand plots of $1/(F_o - F)$ versus $1/[\text{Hg}(\text{ClO}_4)_2]$ for **6** upon titration with Hg^{2+} . The linear fits showed 1:1 complexation for **6** and Hg^{2+} . The association constants were calculated for the changes at the 331 nm and the 343 nm wavelengths.

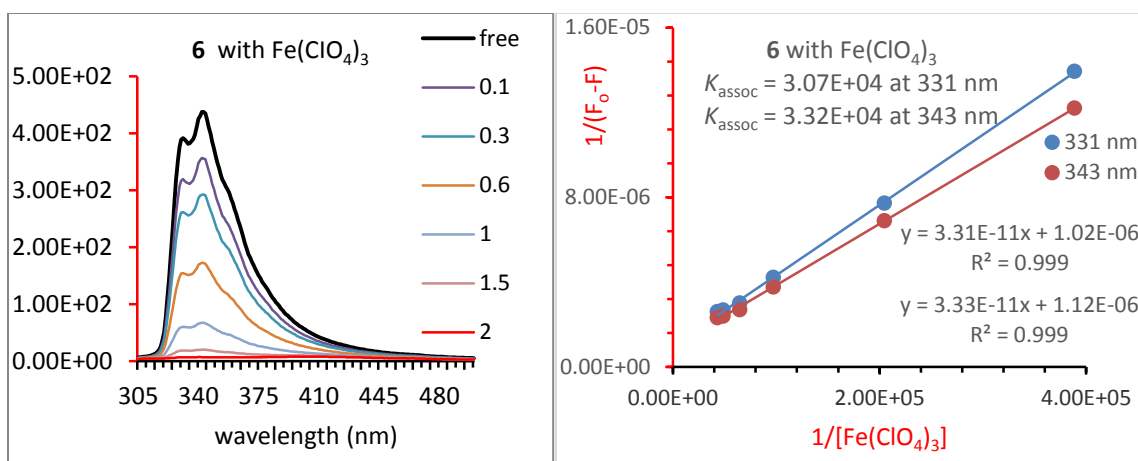


Figure 2.8. *Left:* Fluorescence spectra of **6** (16.4 μM) upon addition of Fe^{3+} in acetonitrile/chloroform (v/v= 9:1) solutions. $\lambda_{\text{ex}} = 282 \text{ nm}$. *Right:* Benesi-Hildebrand plots of $1/(F_o-F)$ versus $1/[\text{Fe}(\text{ClO}_4)_3]$ for **6** upon titration with Fe^{3+} (1-2 equivalents). The linear fits showed 1:1 complexation for **6** and Fe^{3+} . The association constants were calculated for the changes at the 331 nm and the 343 nm wavelengths.

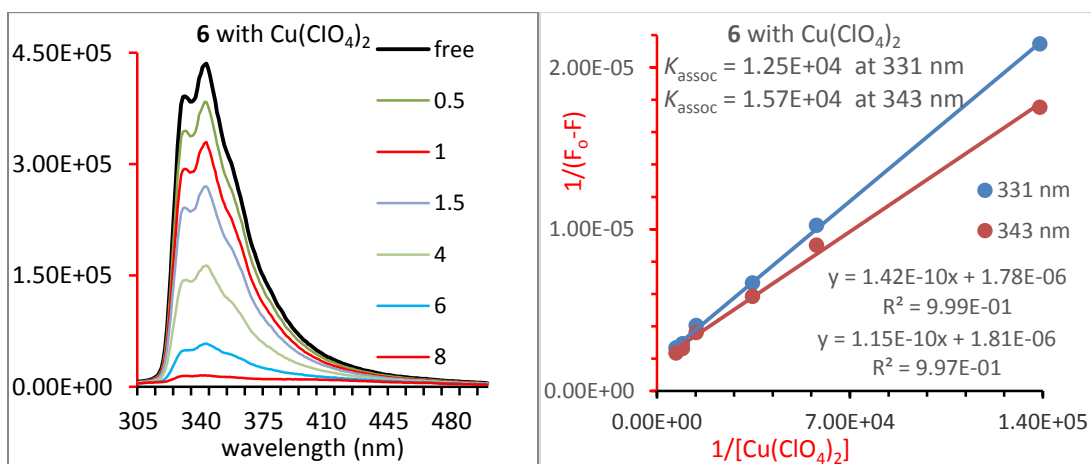


Figure 2.9. *Left:* Fluorescence spectra of **6** (16.4 μM) upon addition of Cu^{2+} in acetonitrile/chloroform (v/v= 9:1) solutions. $\lambda_{\text{ex}} = 282 \text{ nm}$. *Right:* Benesi-Hildebrand plots of $1/(F_o-F)$ versus $1/[\text{Cu}(\text{ClO}_4)_2]$ for **6** upon titration with Cu^{2+} (0.5-8 equivalents). The linear fits showed 1:1 complexation between **6** and Cu^{2+} . The association constants were calculated for the changes at the 331 nm and the 343 nm wavelengths.

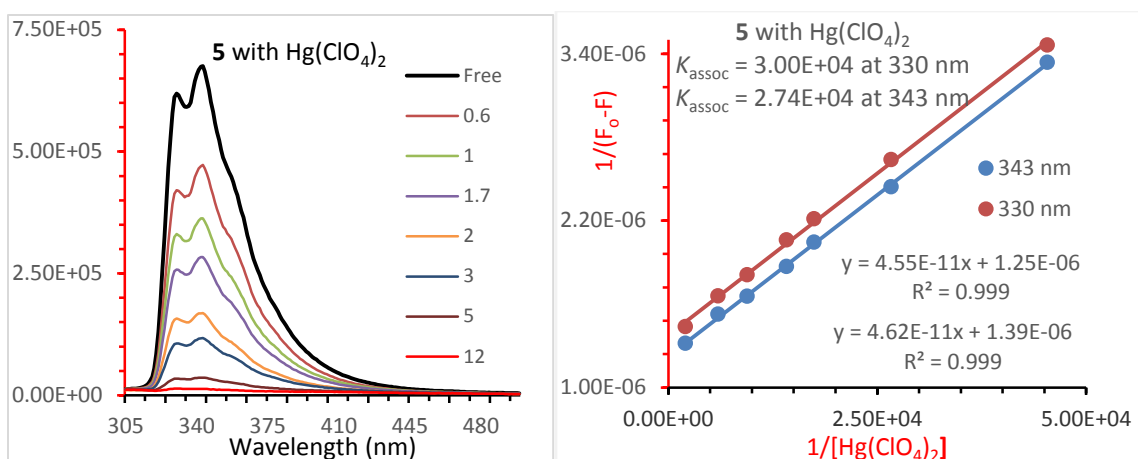


Figure 2.10. *Left:* Fluorescence spectra of **5** (34.6 μ M) upon addition of Hg²⁺ in acetonitrile/chloroform (v/v= 9:1) solutions. λ_{ex} = 284 nm. *Right:* Benesi-Hildebrand plots of $1/(F_o-F)$ versus $1/[\text{Hg}(\text{ClO}_4)_2]$ for **5** upon titration with Hg²⁺ (0.6-12 equivalents). The linear fits showed 1:1 complexation between **5** and Hg²⁺. The association constants were calculated for the changes at the 330 nm and the 343 nm wavelengths.

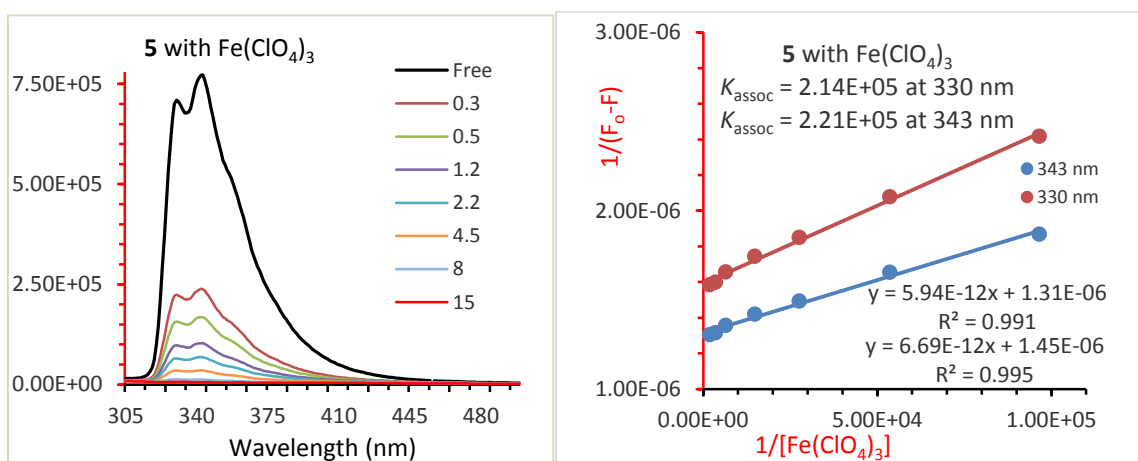


Figure 2.11. *Left:* Fluorescence spectra of **5** (34.6 μ M) upon addition of Fe³⁺ in acetonitrile/chloroform (v/v= 9:1) solutions. λ_{ex} = 284 nm. *Right:* Benesi-Hildebrand plots of $1/(F_o-F)$ versus $1/[\text{Fe}(\text{ClO}_4)_3]$ for **5** upon titration with Fe³⁺ (0.3-15 equivalents). The linear fits showed 1:1 complexation between **5** and Fe³⁺. The association constants were calculated for the changes at the 330 nm and the 343 nm wavelengths.

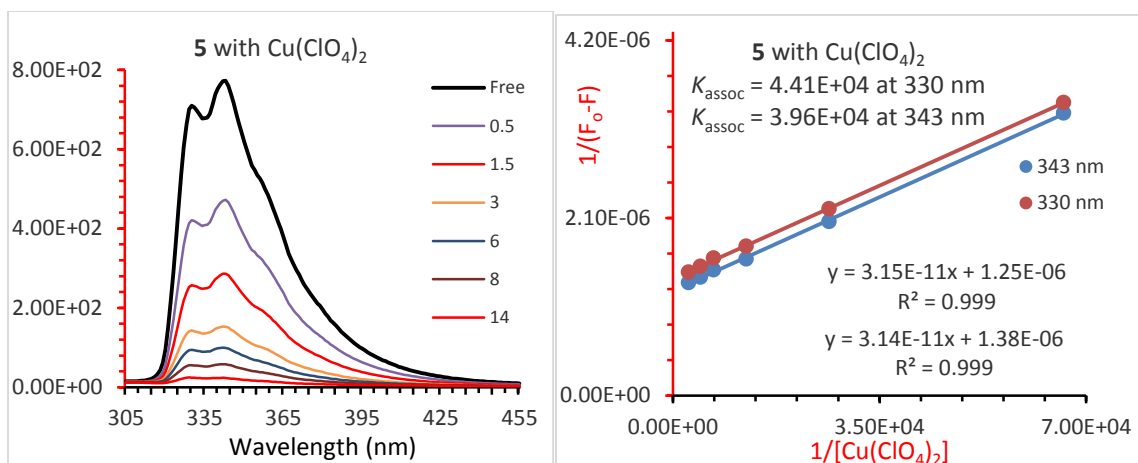


Figure 2.12. *Left:* Fluorescence spectra of **5** (34.6 μM) upon addition of Cu^{2+} in acetonitrile/chloroform (v/v= 9:1) solutions. $\lambda_{\text{ex}} = 284$ nm. *Right:* Benesi-Hildebrand plots of $1/(F_o-F)$ versus $1/[\text{CuClO}_4)_2]$ for **5** upon titration with Cu^{2+} (0.5-14 equivalents). The linear fits showed 1:1 complexation between **5** and Cu^{2+} . The association constants were calculated for the changes at the 330 nm and the 343 nm wavelengths

The titration data showed that 1:1 host-guest complexes were formed as did the Job plot analysis which was performed for Cu^{2+} and Ni^{2+} ions with **5**, and for host **6** with Fe^{3+} and Ni^{2+} . Figures 2.13-2.16 show these Job plots.

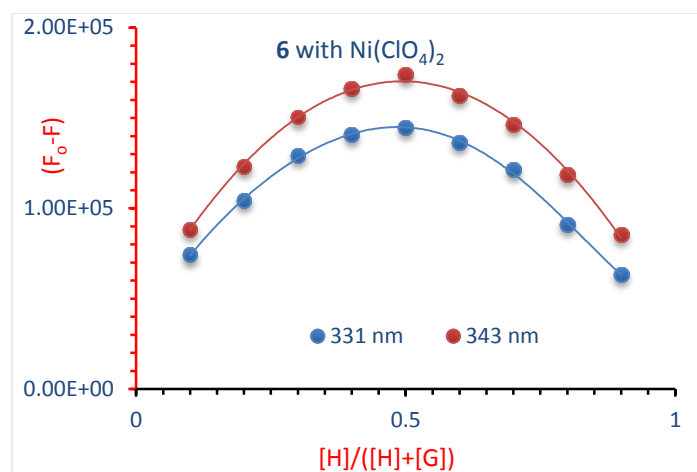


Figure 2.13. Job plot curves showing 1:1 complexation for **6** with Ni²⁺.

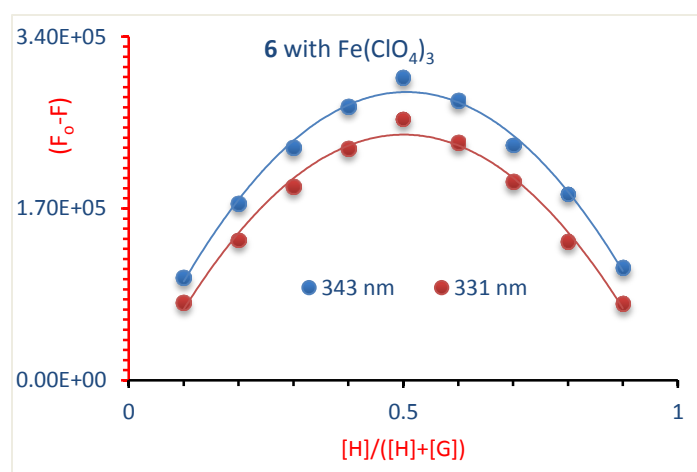


Figure 2.14. Job plot curves showing 1:1 complexation for **6** with Fe³⁺.

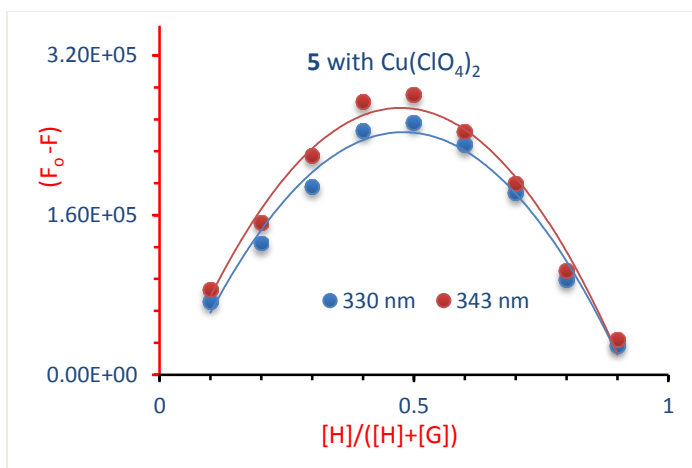


Figure 2.15. Job plot curves showing 1:1 complexation for **5** with Cu^{2+} .

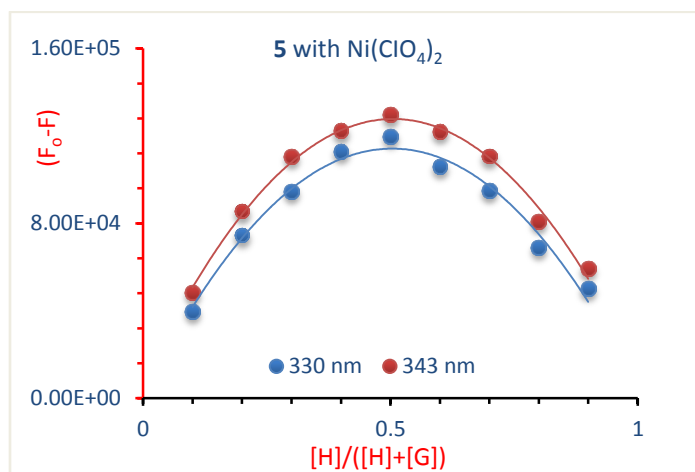


Figure 2.16. Job plot curves showing 1:1 complexation for **5** with Ni^{2+} .

A comparison of the fluorescence quenching observed when each of the receptors **5** and **6** were titrated with the 17 different metal ions tested is shown in Figure 2.17. As can be seen in this figure, the greatest degree of quenching is found with Fe^{3+} , Hg^{2+} and Cu^{2+} .

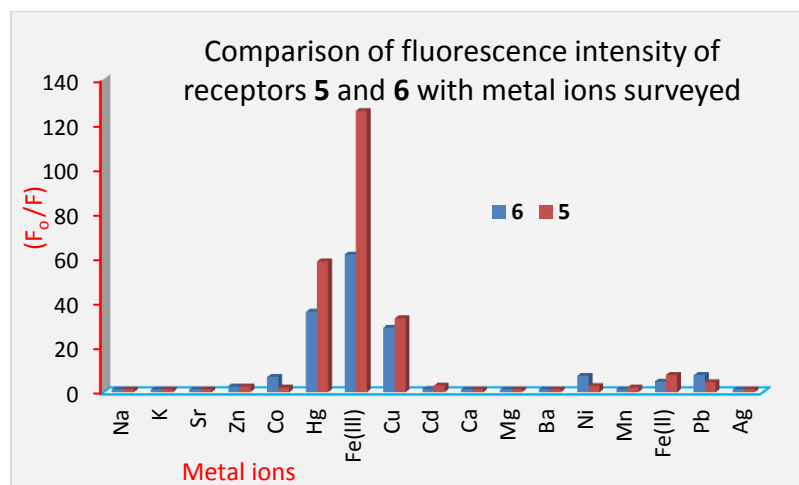


Figure 2.17. Histogram showing the fluorescence quenching of receptors **5** (red) and **6** (blue) with different metal ions.

Figure 2.18 shows the association constants determined for all of the complexes and it is clearly evident that the complexation between **5** and Fe³⁺ ions shows the largest K value of $\sim 2.35 \times 10^5$ upon the changing in fluorescent intensity.

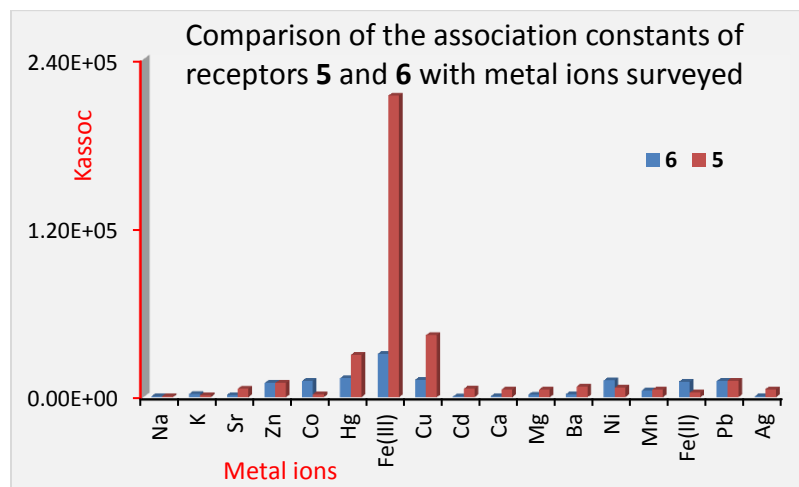


Figure 2.18. Histogram showing the association constants (K_{assoc}) values determined for receptors **5** (red) and **6** (blue) with different metal ions.

2.3.2 ¹H-NMR complexation studies

¹H-NMR spectroscopy was chosen as the other technique in the complexation study since it is more capable of determining the binding sites of the host molecules in the complexes. Stock solutions of the host molecules **5** (2.84×10^{-3} M) and **6** (2.58×10^{-3} M), were respectively prepared in a 4:1 CDCl₃:CD₃CN solvent mixture previously found to be suitable for the complexes.

2.3.2.1 Complexation of receptor **6** with Fe³⁺

Since the FS studies previously revealed that **6** was highly sensitive to Fe³⁺, this was the metal ion of choice for conducting a follow-up ¹H-NMR spectroscopic titration complexation study with, **6**. Strong chemical shift changes of several protons of the host molecule could be observed in the titration experiments in which aliquots of Fe(ClO₄)₃ were added to **6**: (a) The aromatic singlet proton signal of the triazole unit broadened and shifted from δ 8.12 ppm to 8.32 ppm as shown in Figure 2.19; (b) the singlet proton signal due the methylene bridge of the bisnaphthyl group shifted from δ 4.45 ppm to 4.64 ppm, as shown in Figure 2.20; and (c) the doublet proton signals of the calixarene bridging methylene (–CH₂–) groups' equatorial protons shifted from δ 3.17 ppm to 3.30 ppm (See Figure 2.21).

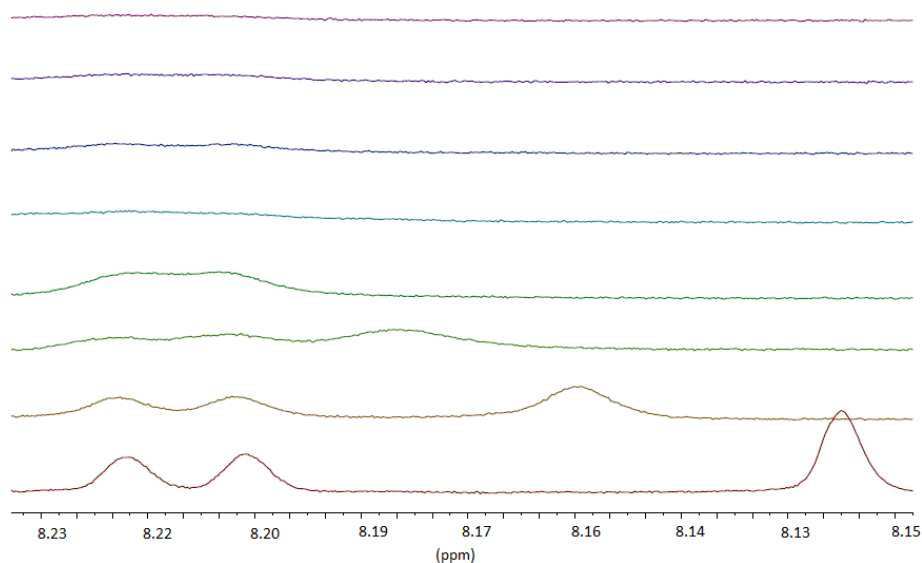


Figure 2.19. $^1\text{H-NMR}$ (500 MHz) titration spectra in 4:1 CDCl_3 ; CD_3CN for the singlet proton signal of the triazole unit in **6** with increasing added amounts of $\text{Fe}(\text{ClO}_4)_3$. From bottom to top $[\text{Fe}(\text{ClO}_4)_3] = 0.0$; 7.5×10^{-4} ; 1.5×10^{-3} ; 2.9×10^{-3} ; 5.6×10^{-3} ; 1.0×10^{-2} ; 1.5×10^{-2} ; 2.0×10^{-2} M.

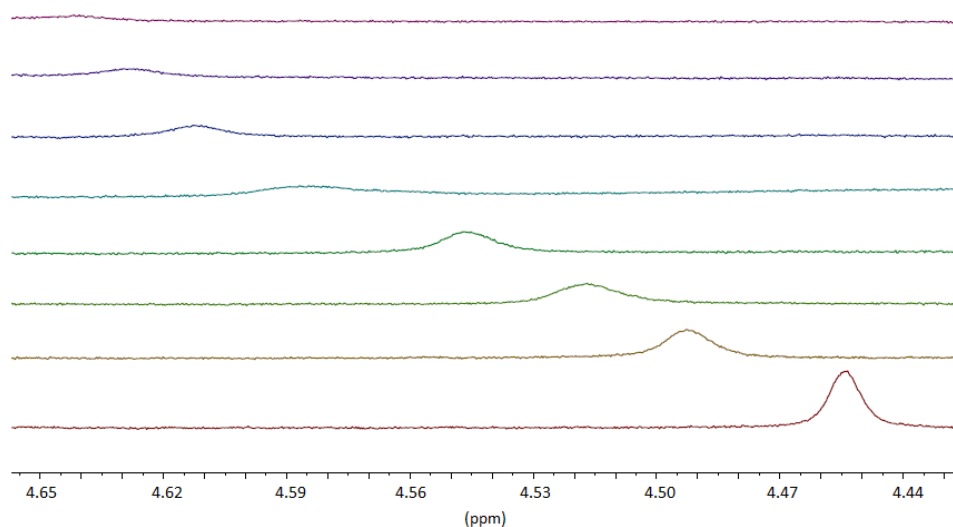


Figure 2.20. $^1\text{H-NMR}$ (500 MHz) titration spectra in 4:1 CDCl_3 ; CD_3CN for the singlet proton signal of the bisnaphthyl-bridge ($-\text{CH}_2-$) in **6** with increasing added amounts of $\text{Fe}(\text{ClO}_4)_3$. From bottom to top $[\text{Fe}(\text{ClO}_4)_3] = 0.0$; 7.5×10^{-4} ; 1.5×10^{-3} ; 2.9×10^{-3} ; 5.6×10^{-3} ; 1.0×10^{-2} ; 1.5×10^{-2} ; 2.0×10^{-2} M.

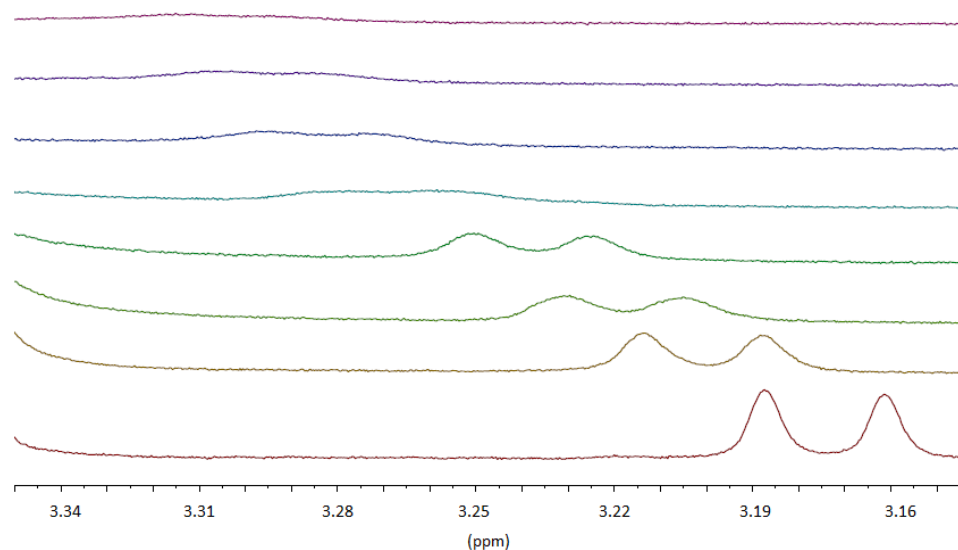


Figure 2.21. $^1\text{H-NMR}$ (500 MHz) titration spectra in 4:1 CDCl_3 ; CD_3CN for the doublet equatorial proton signals of the calixarene bridging ($-\text{CH}_2-$) in **6** with increasing added amounts of $\text{Fe}(\text{ClO}_4)_3$. From bottom to top $[\text{Fe}(\text{ClO}_4)_3] = 0.0$; 7.5×10^{-4} ; 1.5×10^{-3} ; 2.9×10^{-3} ; 5.6×10^{-3} ; 1.0×10^{-2} ; 1.5×10^{-2} ; 2.0×10^{-2} M.

The association constants were calculated using the 1:1 binding isotherm according to Connors³¹ and using the “Origin6” Program,³² and were based on the chemically-induced shifts in the $^1\text{H-NMR}$ (500 MHz) spectra of the host macrocycles from the titration experiments. The K_{assoc} values were calculated for the three most significant chemical shifts observed and gave values of $198 \pm 10 \text{ M}^{-1}$ based on the triazole signal, $309 \pm 10 \text{ M}^{-1}$ based on the bisnaphthyl-bridge signals; and $269 \pm 13 \text{ M}^{-1}$ based on the calixarene bridging ($-\text{CH}_2-$) equatorial signals (Figure 2.22).

Table 2.1. ¹H-NMR (500 MHz) titration data for the triazole singlet and the bisnaphthyl singlet and the calixarene-bridge doublet signals of host **6**.

Sample	[G]/[H]	Triazole δ	$\Delta\delta$ Hz	Bisnaphthyl δ	$\Delta\delta$ Hz	Doublet δ	$\Delta\delta$ Hz
Free Host		8.123		4.454		3.174	
1	0.29	8.160	18.5	4.494	20.0	3.200	13.0
2	0.58	8.183	30.0	4.521	33.5	3.217	21.5
3	1.1	8.208	42.5	4.548	47.0	3.239	32.5
4	2.2	8.257	67.0	4.582	64.0	3.259	42.5
5	4.0	8.294	85.5	4.612	79.0	3.283	54.5
6	5.7	8.315	96.0	4.625	85.5	3.292	59.0
7	7.7	8.328	102.5	4.640	93.0	3.302	64.0

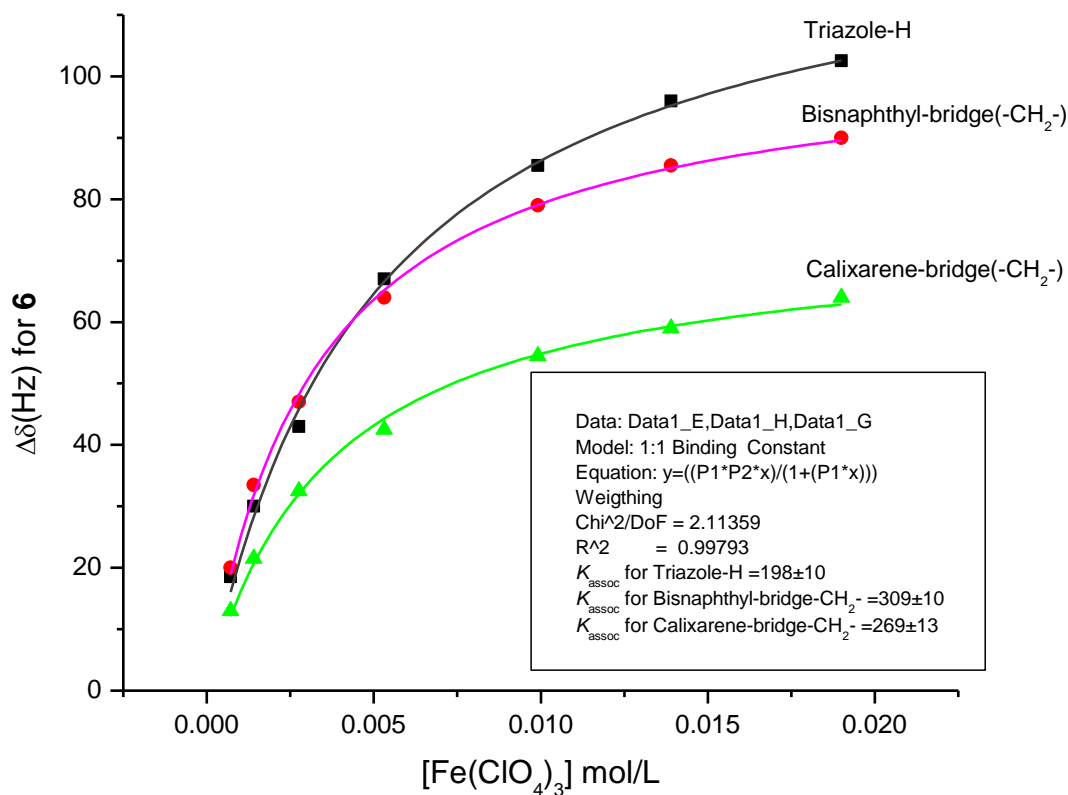


Figure 2.22. ¹H-NMR (500 MHz) titration curves for the triazole, bisnaphthyl- and calixarene-methylene bridge (equatorial) signals in **6**.

2.3.2.2 Complexation of receptor **5** with Fe³⁺ ions

In the titration experiment with receptor **5** with Fe(ClO₄)₃, significant changes in chemical shift were observed which were similar to those which occurred for receptor **6**: (a) The aromatic singlet of the triazole unit shifted from δ 8.06 ppm to 8.34 ppm (Figure 2.23); (b) the singlet due to the methylene bridge of the bisnaphthyl group shifted from δ 4.45 ppm to 4.64 ppm (Figure 2.24); and (c) the doublet signals of the calixarene methylene (-CH₂-) groups' equatorial protons shifted from δ 3.11 ppm to 3.28 ppm, as shown in Figure 2.25.

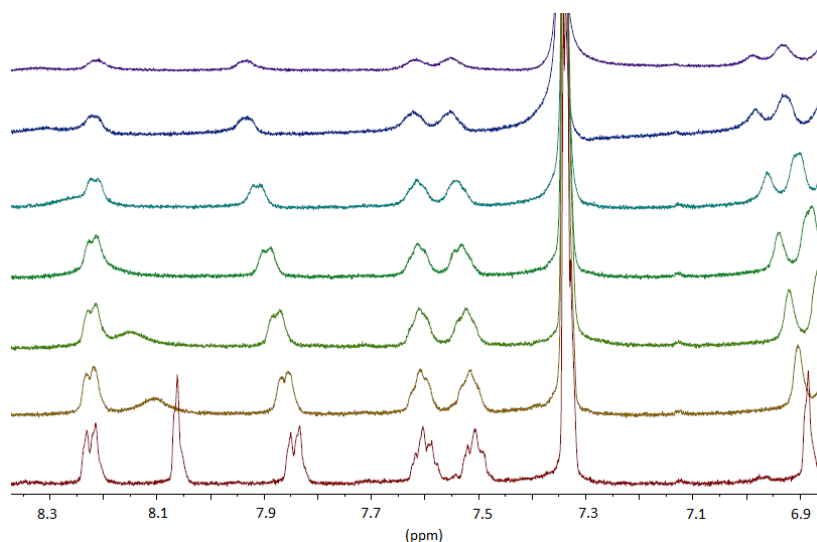


Figure 2.23. ¹H-NMR (500 MHz) titration spectra in 4:1 CDCl₃; CD₃CN for the singlet proton signal of the triazole unit in **5** at δ 8.06 ppm and for the hydroxyl groups at δ 6.89 ppm with increasing added amounts of Fe(ClO₄)₃. From bottom to top [Fe(ClO₄)₃] = 0.0; 7.1×10⁻⁴; 1.4×10⁻³; 2.7×10⁻³; 5.3×10⁻³; 9.9×10⁻³; 1.4×10⁻²; 1.9×10⁻² M.

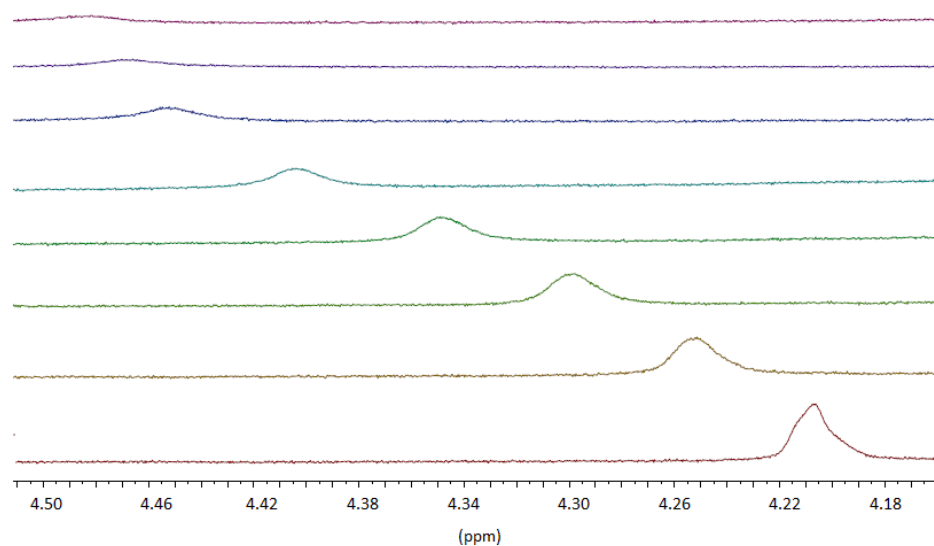


Figure 2.24. $^1\text{H-NMR}$ (500 MHz) titration spectra in 4:1 CDCl_3 ; CD_3CN for the singlet proton signal of the bisnaphthyl-bridge ($-\text{CH}_2-$) in **5** with increasing added amounts of $\text{Fe}(\text{ClO}_4)_3$. From bottom to top $[\text{Fe}(\text{ClO}_4)_3] = 0.0$; 7.1×10^{-4} ; 1.4×10^{-3} ; 2.7×10^{-3} ; 5.3×10^{-3} ; 9.9×10^{-3} ; 1.4×10^{-2} ; 1.9×10^{-2} M.

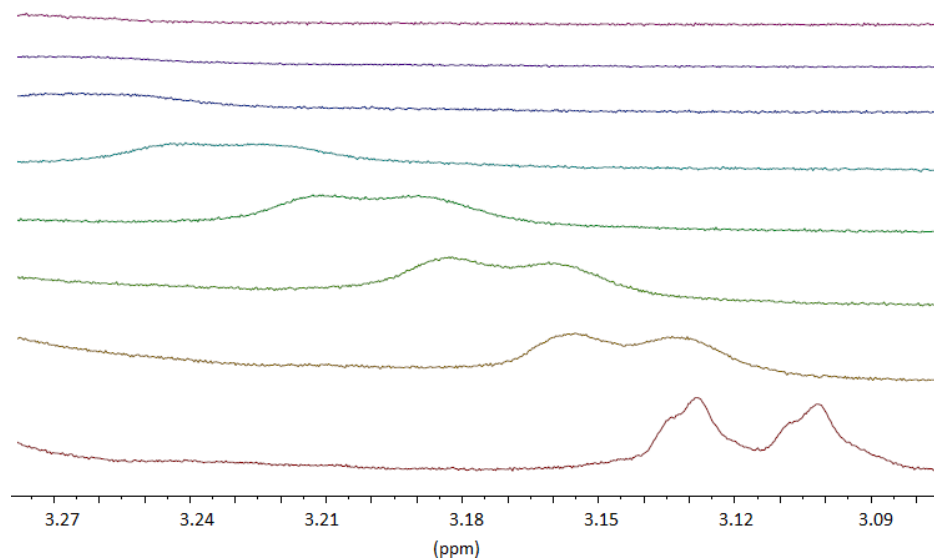


Figure 2.25. $^1\text{H-NMR}$ (500 MHz) titration spectra in 4:1 CDCl_3 ; CD_3CN for the doublet equatorial proton signals of the calixarene bridging ($-\text{CH}_2-$) in **5** with increasing added amounts of $\text{Fe}(\text{ClO}_4)_3$. From bottom to top $[\text{Fe}(\text{ClO}_4)_3] = 0.0$; 7.1×10^{-4} ; 1.4×10^{-3} ; 2.7×10^{-3} ; 5.3×10^{-3} ; 9.9×10^{-3} ; 1.4×10^{-2} ; 1.9×10^{-2} M.

The K_{assoc} values were also calculated as before, for the **5**:Fe³⁺ complexation based on the three significant chemical shifts in the macrocycle **5** using the 1:1 binding isotherm according to Connors.³¹ The K_{assoc} values were calculated to be $280 \pm 8 \text{ M}^{-1}$ and $253 \pm 7 \text{ M}^{-1}$, based upon the chemical shift changes for the bisnaphthyl bridge and triazole signals respectively, and $247 \pm 12 \text{ M}^{-1}$, based on the calixarene-bridging methylene groups' equatorial signals (Figure 2.26).

Table 2.2. ¹H-NMR (500 MHz) titration data for the triazole singlet, the bisnaphthyl singlet and the calixarene-bridge doublet signals of host **5**.

Sample	[G]/[H]	Triazole δ	$\Delta\delta$ Hz	Bisnaphthyle δ	$\Delta\delta$ Hz	Doublet δ	$\Delta\delta$ Hz
Free Host		8.062		4.206		3.115	
1	0.25	8.115	26.5	4.255	24.5	3.145	15.0
2	0.50	8.155	46.5	4.294	44.0	3.168	26.5
3	0.97	8.210	74.0	4.350	72.0	3.200	42.5
4	1.9	8.261	99.5	4.404	99.0	3.231	58.0
5	3.5	8.306	122	4.453	124	3.267	76.0
6	4.9	8.326	132	4.472	133	3.273	79.0
7	6.7	8.342	140	4.489	142	3.285	85.0

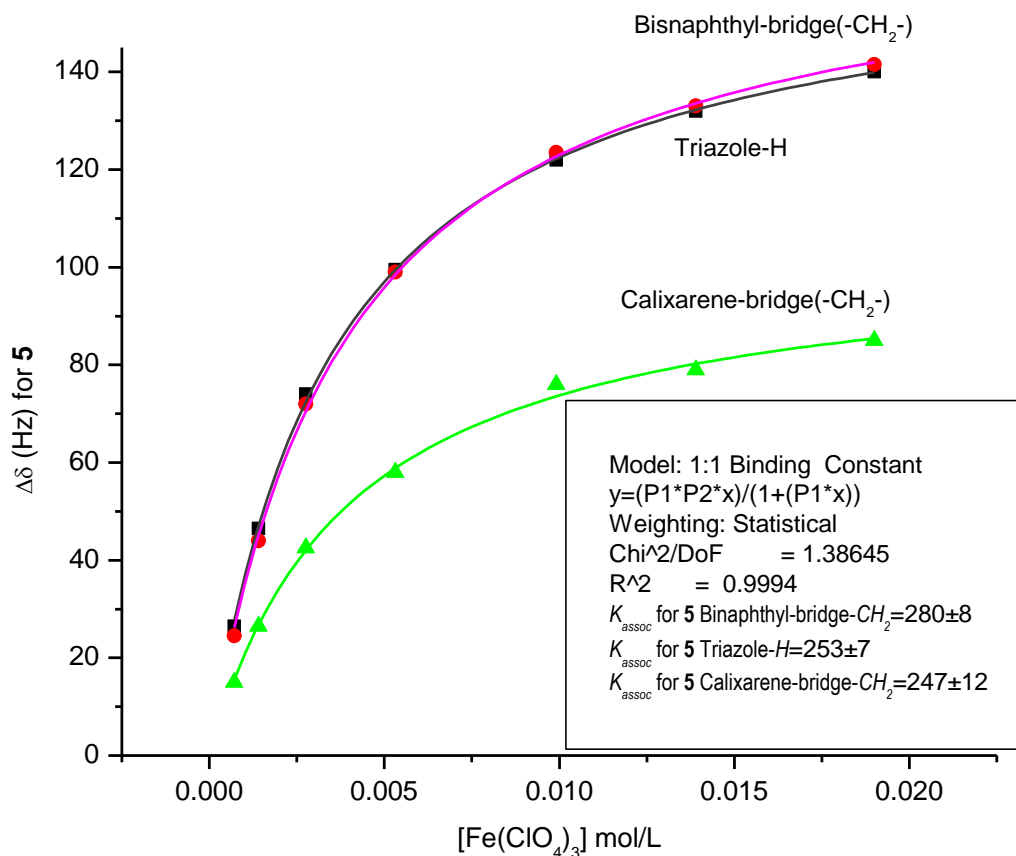


Figure 2.26. ¹H-NMR (500 MHz) titration curves for the triazole, bisnaphthyl- and calixarene-methylene bridge (equatorial) signals in **5**.

The ¹H NMR titration experiments clearly revealed significant chemical shift changes for the signal of the triazole protons and also slight shifts for the hydroxyl protons. Thus the most likely site for the binding of the Fe³⁺ in both **5** and **6** is, as depicted in Figure 2.26 for the **5**:Fe³⁺ complex, between the two triazole moieties and above the free hydroxyl groups.

2.4 Conclusions

The two new receptors namely, bis(naphthyl)methane-bridged macrocycles **5** and **6**, were successfully synthesised and characterized. Their complexation properties with various metal ions were also investigated using both fluorescence spectroscopy and ^1H -NMR spectroscopy. The fluorescence studies proved that **5** and **6** possess high binding selectivities for Fe^{3+} , Hg^{2+} and Cu^{2+} ions as indicated by the significant fluorescence quenching in their titration spectra. These were formed as 1:1 complexes which was confirmed by ^1H -NMR spectroscopy titrations which also revealed the most likely binding sites of the metal ions with the macrocycles. The triazole proton signals showed the greatest chemical shift changes during the titration experiments indicating that the triazole units are the binding sites in the supramolecular complexes formed by the metal ions with macrocycles **5** and **6**.

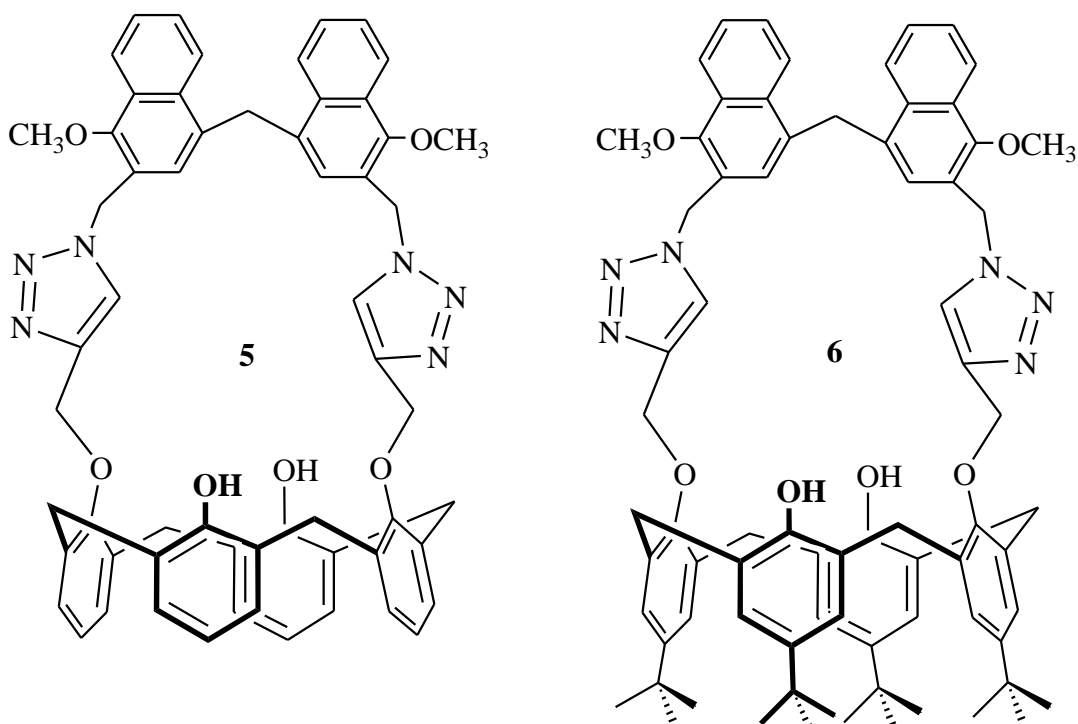
2.5 Experimental section

2.5.1 General experimental

All the metal ion salts were received from Sigma Aldrich in >99 % purity. High-purity spectral grade CHCl_3 and CH_3CN were supplied by as sigma Aldrich and used as received. The instruments which were used to characterize the newly-synthesized compounds were including NMR and LCMS. ^1H -NMR and ^{13}C -NMR were recorded on a Bruker Avance 500 and 300 MHz spectrometers respectively in which using deuterium solvents containing SiMe_4 as an internal standard at δ 0.00 ppm. [MestrelNova](#) software

was used for plotting the $^1\text{H-NMR}$ and $^{13}\text{C-NMR}$ spectra. LCMS was employed to measure the mass of the newly-synthesized compounds.

2.5.2 Experimental



25,27-Dihydroxy-26,28-bis(1,2,3-triazol-1-methylnaphthalene)calix[4]arene (5)

Copper (I) iodide (35 mg) was added to a mixture of **9** (188 mg, 0.376 mmol) and **14** (150 mg, 0.342 mmol) in 30 mL of THF and water (2:1). The mixture was stirred and heated at 65 °C for 24 h under N_2 . The reaction mixture was cooled to room temperature followed by addition of chloroform (100 mL) and water (40 mL). The organic layer was separated and dried over anhydrous MgSO_4 and the solvent was removed using a rotavap. The residue was purified by simple column chromatography (silica gel), eluting with

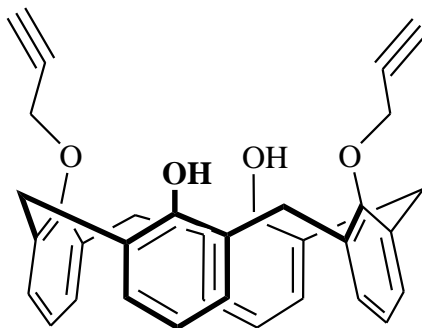
DCM:methanol (90:10) to give a colorless solid (85 mg, 30%, m.p.129.1 °C). ¹H NMR (CDCl₃, 300 MHz): δ = 3.10 (d, *J* = 12 Hz, 4H), 4.07 (d, *J* = 15 Hz, 4H), 4.06 (s, 6H), 4.18 (s, 2H), 5.22 (s, 4H), 5.81 (s, 4H), 6.57 (t, *J* = 6 Hz, 2H) 6.70 (t, *J* = 6 Hz, 2H), 6.81 (d, *J* = 6 Hz, 8H), 6.88 (s, 2H), 7.53 (m, 4H), 7.62 (s, 2H), 7.84 (d, *J* = 6 Hz, 2H), 8.01 (s, 2H), 8.22 (d, *J* = 9 Hz, 2H). ¹³C NMR (CDCl₃, 75.46 MHz): δ = 31.7, 48.5, 63.3, 70.3, 119.3, 123.0, 123.1, 123.9, 124.4, 125.6, 126.3, 126.9, 127.4, 127.9, 128.1, 128.4, 129.1, 132.9, 133.2, 133.3, 144.2, 152.5, 152.7, 152.8. APCI (+) MS (*m/z*): 938.3 (M⁺).

5,11,17,23-Tetra-*tert*-butyl-25,27-dihydroxy-26,28-bis(1,2,3-triazol-1-methyl naphthalene)calix[4]arene (6)

Copper (I) iodide (35 mg) was added to a mixture of **9** (218 mg, 0.301 mmol) and **8** (120 mg, 0.273 mmol) in 24 mL of THF and water (2:1). The mixture was stirred and heated at 65 °C for 24 h under N₂. The reaction mixture was cooled to room temperature followed by addition of chloroform (100 mL) and water (40 mL). The organic layer was separated and dried over anhydrous MgSO₄ and the solvent was removed using a rotavap. The residue was purified by simple column chromatography (silica gel), eluting with DCM:methanol (90:10) to give a colorless solid (80 mg, 25%, m.p. 174.5 °C). ¹H NMR (CDCl₃, 300 MHz): δ = 0.95 (s, 18H), 1.25 (s, 18H), 3.19 (d, *J* = 12 Hz, 4H), 4.04 (s, 6H), 4.16 (d, *J* = 12 Hz, 4H), 4.47 (s, 2H), 5.15 (s, 4H), 5.75 (s, 4H), 6.76 (s, 4H), 6.88 (s, 2H), 6.95 (s, 4H), 7.07 (s, 2H), 7.49 (t, *J* = 9 Hz, 2H), 7.58 (t, *J* = 9 Hz, 2H) 7.89 (d, *J* = 9 Hz, 2H), 7.99 (s, 2H), 8.22 (d, *J* = 9 Hz, 2H). ¹³C-NMR (CDCl₃, 75.46 MHz): δ = 31.0, 31.6, 32.0, 33.8, 33.9, 48.7, 63.1, 70.0, 122.9, 123.1, 123.9, 124.29, 125.1, 125.8,

126.3, 127.0, 127.4, 128.0, 128.1, 132.6, 132.9, 133.4, 141.9, 144.4, 147.4, 150.1, 150.6, 152.9). APCI (+) MS (m/z): 1163.3 (M^+).

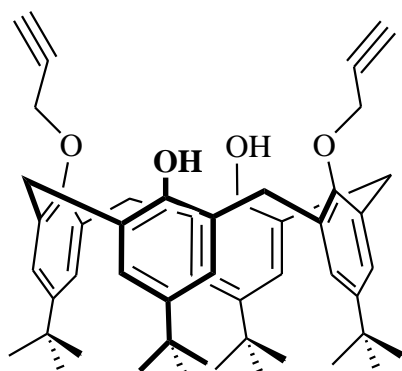
25,27-Dihydroxy-26,28-bis(*O*-propargyl)calix[4]arene (7)



A mixture of potassium carbonate (885 mg, 5.89 mmol) and calix[4]arene **14** (1.00 g, 2.35 mmol) in dry acetone (25 mL) was stirred at room temperature for 1 h. A solution of propargyl bromide (980 mg, 8.24 mmol) in dry acetone (5 mL) was added dropwise into the above stirred mixture over a period of 5 min. The reaction mixture was heated at reflux for 2 days and was then allowed to cool to room temperature. The reaction mixture was filtered over Celite[®] to remove insoluble particles, and the filtrate was concentrated using a rotavap. The residue was taken up in dichloromethane (20 mL) and was acidified with aqueous 1.0 M HCl, and the product was extracted with dichloromethane (3×50 mL). The combined organic extract was successively washed with water and brine (50 mL), dried over anhydrous Na₂SO₄, filtered, and the solvent was removed on a rotavap. The residue was purified by crystallized from CH₂Cl₂/CH₃OH to afford **7** as a light yellow solid (660 mg, 55% yield). ¹H NMR (CDCl₃, 300 MHz): δ = 2.57 (t, J = 3.0 Hz, 2H), 3.41 (d, J = 12 Hz, 4H), 4.41 (d, J = 12 Hz, 4H), 4.79 (d, J = 3

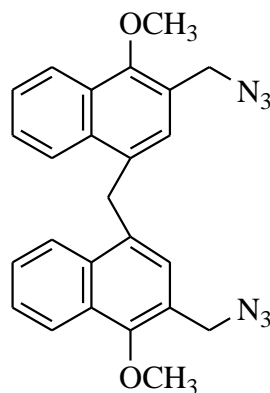
Hz, 4H), 6.72 (m, 4H), 7.07 (d, $J = 9$ Hz, 4H), (d, $J = 9$ Hz, 4H). ^{13}C -NMR (CDCl_3 , 75.46 MHz): $\delta = 31.8, 63.4, 78.3, 119.2, 125.7, 128.2, 128.5, 128.9, 133.4, 151.4, 152.9$. APCI (+) MS (m/z): 500 (M^+).

5,11,17,23-Tetra-*tert*-butyl-25,27-dihydroxy-26,28-bis(*O*-propargyl)calix[4]arene (8)



5,11,17,23-Tetra-*tert*-butyl-25,27-dihydroxy-26,28-bis(*O*-propargyl)calix[4]arene (**8**) was prepared as described by Pathak et al.²⁷

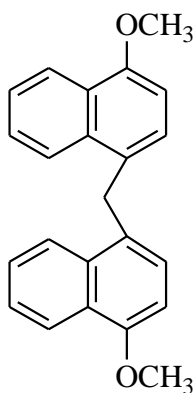
Bis[3-(azidomethyl)-4-methoxy-1-naphthyl]methane (9)



To a mixture of **12** (0.98 g, 1.9 mmol) and sodium azide (2.00 g, 30.8 mmol), was added 20 mL of dimethylformamide. The mixture was stirred at 90 °C under N_2 for 48 h. After cooling to room temperature, the reaction mixture was poured into water (100 mL) and extracted with ethyl acetate (2×100 mL). The combined organic layers were washed

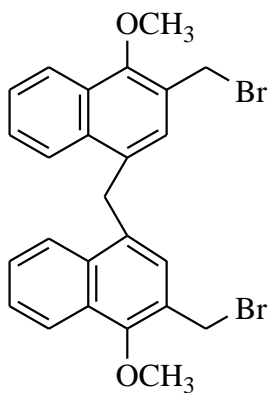
with brine solution (50 mL). The organic layer was then dried over anhydrous MgSO_4 and the solvent was removed using a rotavap. The residue was purified by simple column chromatography (silica gel), eluting with hexane:ethyl acetate (80:20) to give a colorless solid (0.78 g, 93%, m.p. 23.2 °C). ^1H NMR (CDCl_3 , 300 MHz): δ = 4.01 (s, 6H), 4.44 (s, 4H), 4.80 (s, 2H), 7.02 (s, 2H), 7.57 (m, 4H), 8.03 (d, J = 6, 2H), 8.21 (d, J = 9, 2H). ^{13}C -NMR (CDCl_3 , 75.46 MHz): δ = 49.4, 63.3, 123.2, 123.3, 124.4, 126.2, 126.9, 128.2, 128.3, 132.5, 133.5, 153.8.

Bis(4-methoxy-1-naphthyl)methane (**11**)



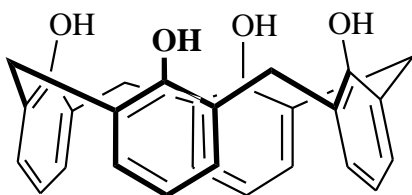
Bis(4-methoxy-1-naphthyl)methane (**11**) was prepared as described by Schreiber and Kennedy.²⁵

Bis[3-(bromomethyl)-4-methoxy-1-naphthyl]methane (**12**)



Bis[3-(bromomethyl)-4-methoxy-1-naphthyl]methane (**12**) was prepared as described by Ashram et al.²⁶

25,26,27,28-Tetrahydroxy-calix[4]arene (14)



25,26,27,28-Tetrahydroxy-calix[4]arene (**14**) was

prepared as describe by Chawla and Santra.³³

2.6 References

1. Jin, C. C.; Kinoshita, T.; Cong, H.; Ni, X.-L. Zeng, X.; Hughes, D. L.; Redshaw, C.; Yamato, T. *New J. Chem.* **2012**, *36*, 2580-2586.
2. Farina, M.; Avila, D. S.; Rocha, J. B.; Aschner, M. *Neurochemistry International*, **2013**, *62*, 575-594
3. Chio, Y. W.; Park, G. H.; Na, Y. J.; Jo, H. Y.; Lee, S. A.; You, G. R.; Kim, C. *Sensors and Actuators B.* **2014**, *193*, 343-352.
4. Touati, D. *Archives of Biochemistry and Biophysics*, **2000**, *373*, 1-6.
5. Boveris, A.; Sebio, R.; Ferrarotti, N.; Magrina, C.; Torti, H.; Massot, F.; Repetto, M. *Journal of Inorganic Biochemistry*, **2013**, *116*, 63-69.
6. Pathak, R. K.; Dissingou, J.; Hinge, V. K.; Thawari, A. G.; Basu, S. K.; Rao, C. P. *Anal. Chem.* **2013**, *85*, 3707-3714.
7. Hu, S.; Wu, G.; Xu, C.; Dong, J.; Gao, Q. *Journal of Photochemistry and Photobiology A: Chemistry*, **2013**, *270*, 37-42.
8. (a) Renzoni, A.; Zino, F.; Franchi, E. *Environmental Research*, **1998**, *77*, 68-72. (b) Rice, D. C.; Schoeny, R.; Mahaffey, K. *Risk Anal.* **2003**, *23* (1) 107-115.
9. Zahir, F.; Rizwi, S. J.; Haq, S. K.; Khan, R. H. *Environmental Toxicology and Pharmacology*, **2005**, *20*, 351-360.
10. Xue, X.; Wang, F.; Liu, X. *J. Am. Chem. Soc.* **2008**, *130*, 3244-3245.
11. Kim, J. S.; Quang, T. D. *Chem. Rev.* **2007**, *107*, 3780-3799.
12. Sahin, O.; Yilmaz, M. *Tetrahedron*, **2011**, *67*, 3501-3509.

13. Mandolini, L.; Ungaro, R. *Calixarenes in Action*, Imperial College Press, London, 2000.
14. Lau, Y. H.; Rutledge, P. J.; Watkinson, M.; Todd, M. H. *Chem. Soc. Rev.* **2011**, *40*, 2848-2866.
15. Kold, H. C.; Finn, M. G.; Sharpless, K. B. *Angew. Chem. Int. Ed.* **2001**, *40*, 2004-2021.
16. El-Sagheer, A. F.; Brown, T. *Chem. Soc. Rev.* **2010**, *39*, 1388-1405.
17. Ryu, E.; Zhao, Y. *Org. Lett.* **2005**, *7*, 1035-1037.
18. Chu, C.; Liu, R. *Chem. Soc. Rev.* **2011**, *40*, 2177-2188.
19. Moses, J. E.; Moorhouse, A. D. *Chem. Soc. Rev.* **2007**, *36*, 1249-1262.
20. Chang, K.; Su, I.; Senthilvelan, A.; Chung, W. *Org. Lett.* **2007**, *9*, 3363-3366.
21. Miao, F.; Zhou, J.; Tian, D.; Li, H. *Org. Lett.* **2012**, *14*, 3572-3575.
22. Mummdivarapu, V. S.; Hinge, V. K.; Tabbasum, K.; Gonnade, R. G.; Rao, C. P. *J. Org. Chem.* **2012**, *78*, 3570-3575.
23. Lakowics, J. R. *Principles of Fluorescence Spectroscopy*, Springer, Maryland, USA, 2006.
24. Gaussian 09, Revision C.01, Frisch, M. J.; Trucks, G. W.; Schlegel, H. B.; Scuseria, G. E.; Robb, M. A.; Cheeseman, J. R.; Scalmani, G.; Barone, V.; Mennucci, B.; Petersson, G. A.; Nakatsuji, H.; Caricato, M.; Li, X.; Hratchian, H. P.; Izmaylov, A. F.; Bloino, J.; Zheng, G.; Sonnenberg, J. L.; Hada, M.; Ehara, M.; Toyota, K.; Fukuda, R.; Hasegawa, J.; Ishida, M.; Nakajima, T.; Honda, Y.; Kitao, O.; Nakai, H.; Vreven, T.; Montgomery, Jr. J. A.; Peralta, J. E.; Ogliaro, F.; Bearpark, M.;

Heyd, J. J.; Brothers, E.; Kudin, K. N.; Staroverov, V. N.; Keith, T.; Kobayashi, R.; Normand, J.; Raghavachari, K.; Rendell, A.; Burant, J. C.; Iyengar, S. S.; Tomasi, J.; Cossi, M.; Rega, N.; Millam, J. M.; Klene, M.; Knox, J. E.; Cross, J. B.; Bakken, V.; Adamo, C.; Jaramillo, J.; Gomperts, R.; Stratmann, R. E.; Yazyev, O.; Austin, A. J.; Cammi, R.; Pomelli, C.; Ochterski, J. W.; Martin, R. L.; Morokuma, K.; Zakrzewski, V. G.; Voth, G. A.; Salvador, P.; Dannenberg, J. J.; Dapprich, S.; Daniels, A. D.; Farkas, O.; Foresman, J. B.; Ortiz, J. V.; Cioslowski, J.; Fox, D. J. Gaussian, Inc., Wallingford CT, 2010.

25. Schreiber, K. C.; Kennedy, M. C. *J. Org. Chem.* **1956**, *21*, 1310-1311.
26. Ashram, M. Ph.D. Dissertation, Memorial University of Newfoundland, 1997.
27. R. K. Pathak, V. K. Hinge, M. Mondal, C. P. Rao, *J. Org. Chem.* **2011**, *76*, 10039–10049.
28. Xu, W.; Vittal, J. J.; Puddephatt, R. J. *Can. J. Chem.* **1996**, *74*, 766- 774.
29. Huisgen, R. *Angew. Chem. Int. Ed.* **1963**, *75*, 604-637.
30. (a) Benesi, H. A.; Hildebrand, J. H. *J. Am. Chem. Soc.* **1949**, *71*, 2703-2707. (b) Jisha, V. S.; Thomas, A. J.; Ramaiah, D. *J. Org. Chem.* **2009**, *74*, 6667–6673. (c) Bano, S.; Mohd, A.; Khan, A.; Siddiqi, K. S. *J. Chem. Eng. Data.* **2010**, *55*, 5759-5765.
31. Connors, K. A. *Binding Constants*, Wiley, New York, 1987.
32. Association constants were calculated using a nonlinear curve fitting program, using the program ORIGINPro 6 from OriginLab Corporation.
33. Chawla, H. M.; Santra, A. *Synth. Commun.* **2001**, *31*, 2605-2611.

Chapter 3

Synthesis and Complexation Properties of Triazole-bridged

Acenaphthene-Calix[4]arenes

3.1 Introduction

The syntheses of two new fluorescent chemosensors based on acenaphthene-modified calix[4]arene-triazoles are described in this chapter. The complexation studies of these new receptors were conducted using fluorescence and $^1\text{H-NMR}$ spectroscopy, with a variety of metal ions and the results are presented herein. The complexation studies of these new receptors demonstrate that they possess a selective response toward Cu^{2+} ions by fluorescence-quenching. Only minimal fluorescence quenching was found with the other metal ions which were tested with these receptors.

3.1.1 Fluorescent metal ion chemosensors

During the last decade, many different fluorescent chemosensors have been developed for the detection of metal ions in biological applications and in supramolecular chemistry.¹ The high sensitivity of using fluorescence spectroscopy along with the possibility of using a low concentration of host molecules are some of its advantageous features. Metals such as Cu^{2+} , Pb^{2+} and Fe^{3+} are of concern due to their toxicity to humans and in the environment. Such concerns result from the fact that heavy metals in general can undergo bioaccumulation and formation of complexes with proteins.^{2a} While some of these metal ions such as Fe^{3+} and Cu^{2+} ions in low concentration are essential for the

proper functioning of the human body, other heavy metals such as Pb^{2+} ions are hazardous, even at low concentrations. The toxicological effects of these metal ions depend on their concentration, their interaction with other species in the ecosystem, as well as their chemical properties. In particular, copper ions which play a substantial role in biological systems can form complexes with proteins, producing electron-transfer functions in the organism's cells, generating vital energy.^{2b} However, an excess of copper ions in the organism's cells can disrupt the biological system, causing diseases such as Wilson's and Alzheimers. One of the harmful effects of copper ions is that they are utilized as catalysts in the Fenton reaction, to produce hydroxyl radicals which cause oxidative stress.^{1,2}

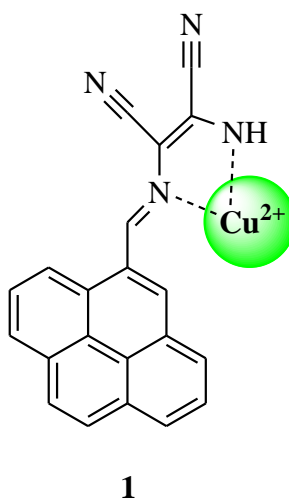


Figure 3.1. Complexation of fluorescent chemosensor **1** with Cu^{2+} ions.

In 2010, Wu et al.³ reported a new fluorescent chemosensor that has a pyrene unit as the fluorophore and diaminomaleonitrile as the metal binding site, as shown in Figure 3.1. They used fluorescence spectroscopy in order to investigate the affinity of receptor **1**

to different metal ions. Cu^{2+} ions in particular showed highly-enhanced fluorescence emission for the receptor while only minimal changes were observed with other tested metal ions in (1:1) acetonitrile:water. Enhancement of the fluorescence emission was raised by the complexation of receptor **1** with Cu^{2+} ions, causing the photoinduced electron-transfer mechanism to be deactivated. The association constant (K_{assoc}) of the complexation of receptor **1** with Cu^{2+} was calculated using Benesi-Hildebrand plots and reported to be $5.55 \times 10^3 \text{ M}^{-1}$, in a 1:1 stoichiometry as confirmed by a Job plot analysis.

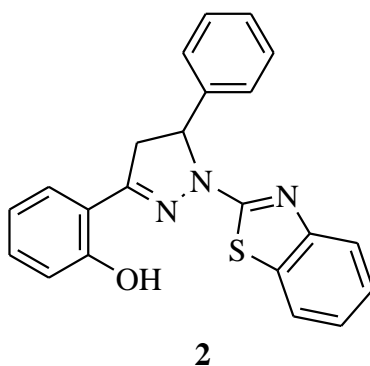


Figure 3.2. Fluorescent chemosensor based on a pyrazoline unit.

A new receptor based on a pyrazoline unit has been synthesized by Hu et al.⁴ They evaluated the selectivity of compound **2** (Figure 3.2) to a number of metal ions using fluorescence spectroscopy and UV-vis spectroscopy for titration experiments. Single-crystal X-ray diffraction was also utilized by them to further confirm the geometry of the complex. Receptor **2** showed remarkable quenching of the fluorescence spectra upon adding Cu^{2+} to the receptor, compared with other tested metal ions. Consequently, it was determined that receptor **2** has high affinity to bind selectively to Cu^{2+} . Photoinduced energy-transfer (PET) was the mechanism involved in the quenching of the fluorescence

spectra of **2** upon binding with the metal ions. Using Benesi-Hildebrand plots, a high association constant (i.e. $9.3 \times 10^4 \text{ M}^{-1}$) was observed for the 1:1 complexation between the receptor and Cu^{2+} .

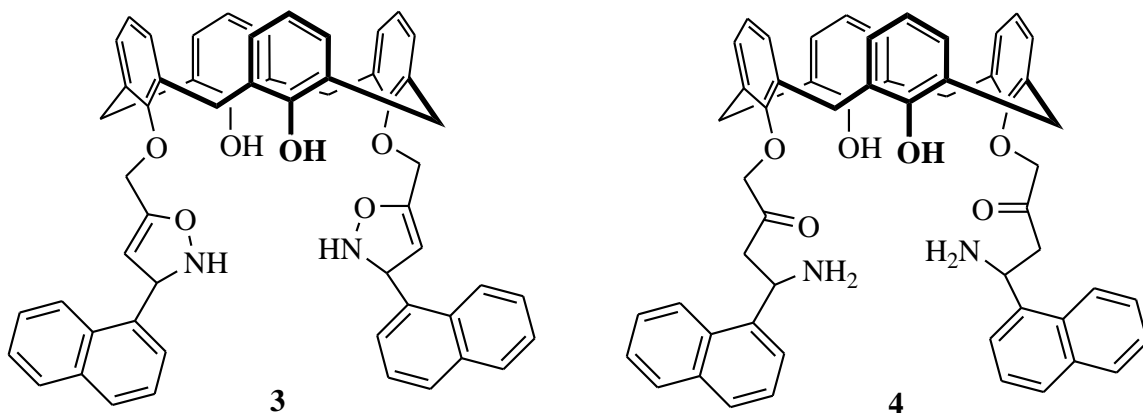


Figure 3.3. Structures of calixarene-based fluorescent chemosensors with selectivity to Cu^{2+} ions.

In 2009, Chung and coworkers⁵ synthesized two new fluorescent chemosensors **3** and **4** (Figure 3.3) based on calix[4]arene scaffolds bearing naphthalene moieties with different binding sites for each receptor. An investigation of the ability of **3** and **4** to bind cations and anions was conducted using fluorescence and Uv-vis spectroscopies. High selectivity of the receptors **3** and **4** toward Cu^{2+} ions with different responses in fluorescence spectra was observed. Once receptor **3** is bound to Cu^{2+} ions, the fluorescence emission was quenched due to the reverse-PET and the heavy metal ion effect. On the other hand, enhancement of fluorescent spectra was achieved when receptor **4** is bound to the Cu^{2+} ions due to the overlap between the two naphthalene moieties and MLCT (i.e. metal-to-ligand charge-transfer). MLCT occurred between the phenolic group and Cu^{2+} ions resulting in a **4**: Cu^+ complex. The **4**: Cu^+ complex shows a

ditopic receptor cooperative feature as a result of the enhancement of the fluorescence emission after adding carboxylate or fluoride ions to the complex. However, there was no change in the fluorescence emission when adding the same anions to the receptor **4** alone.

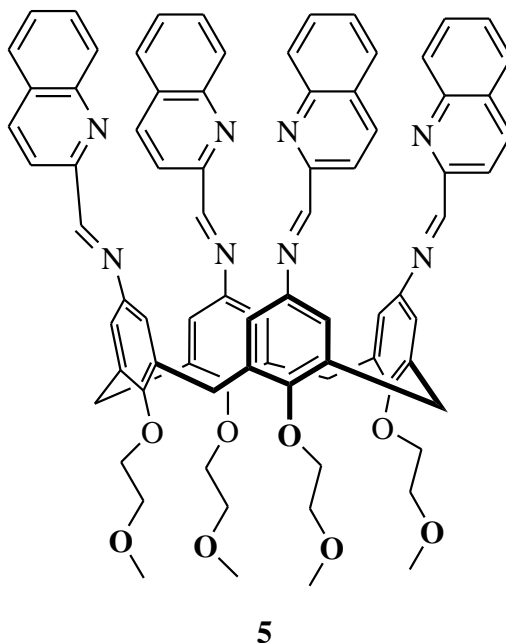


Figure 3.4. Receptor based on calix[4]arene with aminoquinoline subunits.

Li et al.⁶ reported a new calix[4]arene-based receptor **5** (Figure 3.4) having four aminoquinoline units, to obtain a fluorescent chemosensor which would be selective toward metal ions. This receptor also exhibited a high affinity and selectivity to coordinate with Cu^{2+} ions. Fluorescence emission was gradually enhanced upon adding Cu^{2+} ions to the receptor **5** in acetonitrile due to the blocking of PET and the conformational restriction of the aminoquinoline units. The K_{assoc} values which were obtained were: $3.67 \times 10^7 \text{ M}^{-1}$ and $1.75 \times 10^3 \text{ M}^{-1}$ for the complexes with Cu^{2+} and Zn^{2+} ions respectively 1:1 host-guest complexes.

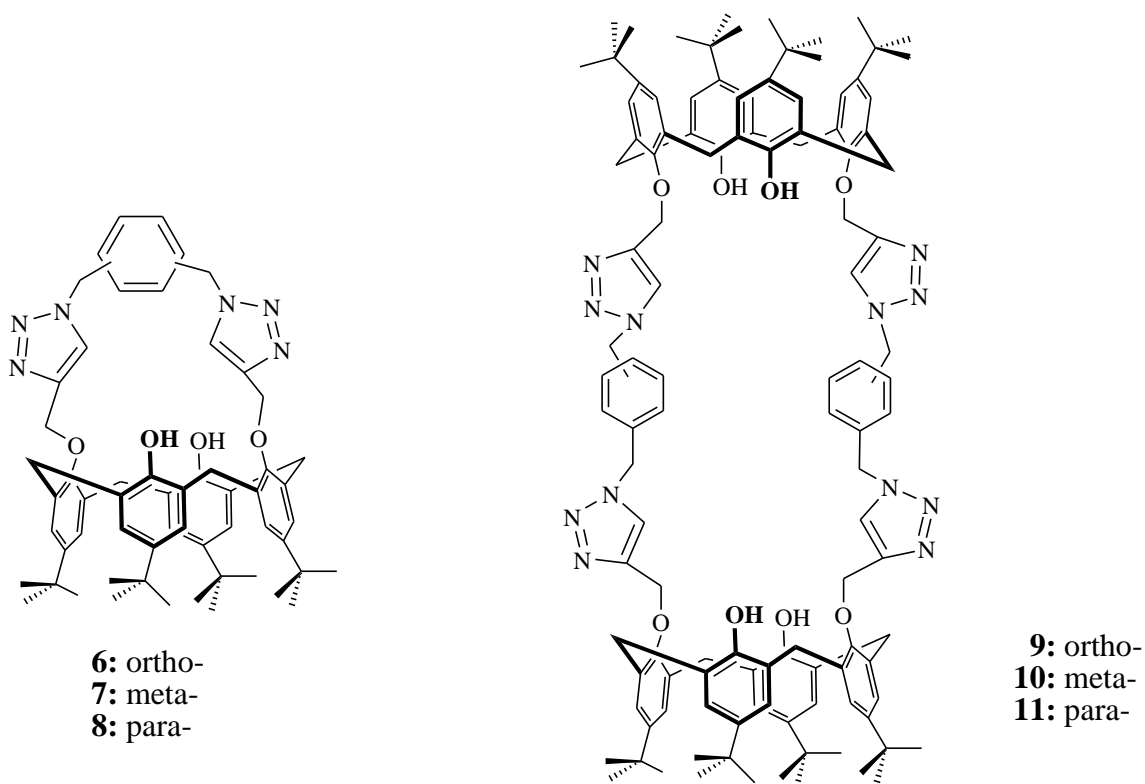


Figure 3.5. Variety of monomer and dimer macrocyclic receptors.

Sanfrutos et al.⁷ reported the synthesis of several other macrocyclic receptors based on a calix[4]arene platform. They functionalized the lower-rim of the calix[4]arene with two triazole units producing new fluorescent chemosensors that could potentially act as host molecules. CuAAC methodology was employed to obtain these macrocycles by reacting terminal alkynes with azides in order to produce the desired macrocycles, **6-11** as seen in Figure 3.5. Monomer macrocycles **6-8** were the major products in moderate yields while dimer macrocycles **9-11** were obtained as minor products.

3.2 Results and discussion

3.2.1 Design of acenaphthene-bridged 1,2,3-triazole fluorescent chemosensors

Two new fluorescent chemosensors, **12** and **12a** for Cu^{2+} ions, which consist of calix[4]arenes attached to an acenaphthene moiety by two triazole units were synthesized as appealing new hosts, for transition metal ions. Gas-phase Gaussian09⁸-generated DFT, B3LYP/lanl2dz-geometry-optimized structures obtained by Dr. Shofiur Rahman and Professor Georghiou predicted that Cu^{2+} would be an appropriate guest ion for the chemosensors **12** and **12a** (e.g. Figure 3.6). Synthesis of these fluorescent sensors, therefore, has been the main objective described in this chapter, followed by an investigation of their complexation properties towards metal ions of interest.

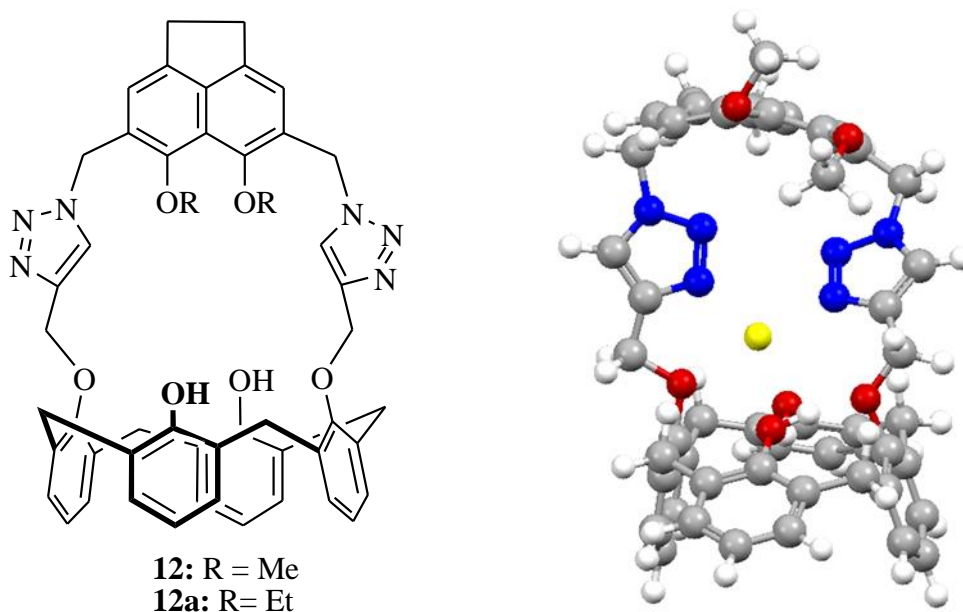
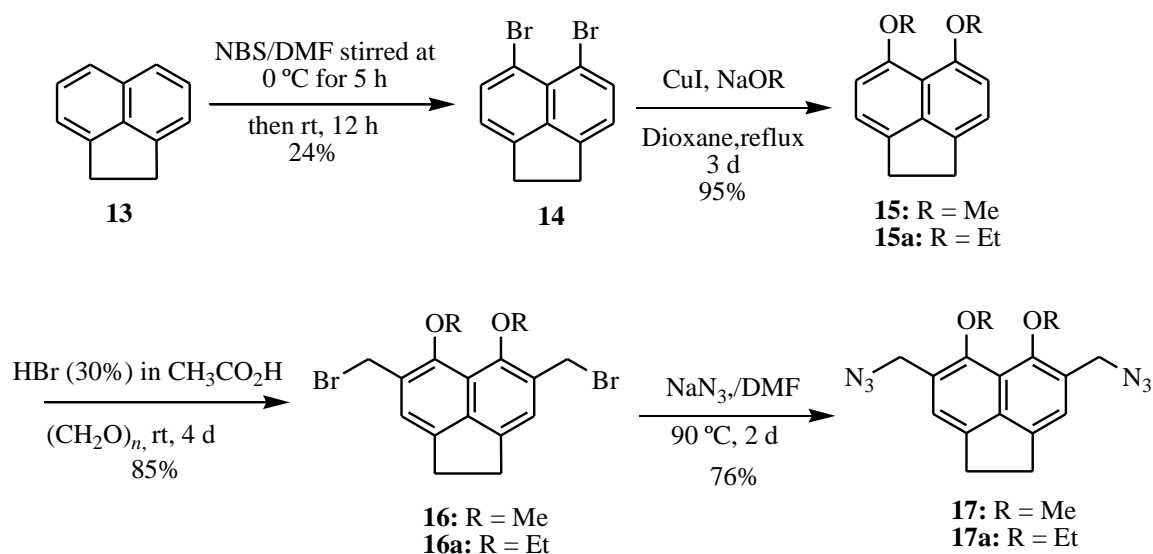


Figure 3.6. *Left:* free ligands **12** and **12a**; and *right:* the geometry-optimized (ball-and-stick) structure of **12:Cu²⁺** complex was fully optimized with the B3LYP level of DFT and the lanl2dz basis set in the gas phase Gaussian 09⁸ at 298 K. Colour code: Cu^{2+} = yellow, triazole nitrogen = blue, hydrogen = white and oxygen atom = red.

3.2.2 Synthesis approach toward desired macrocycles 12-12a

3.2.2.1 Synthesis of bis (azidomethyl) dialkoxyacenaphthene

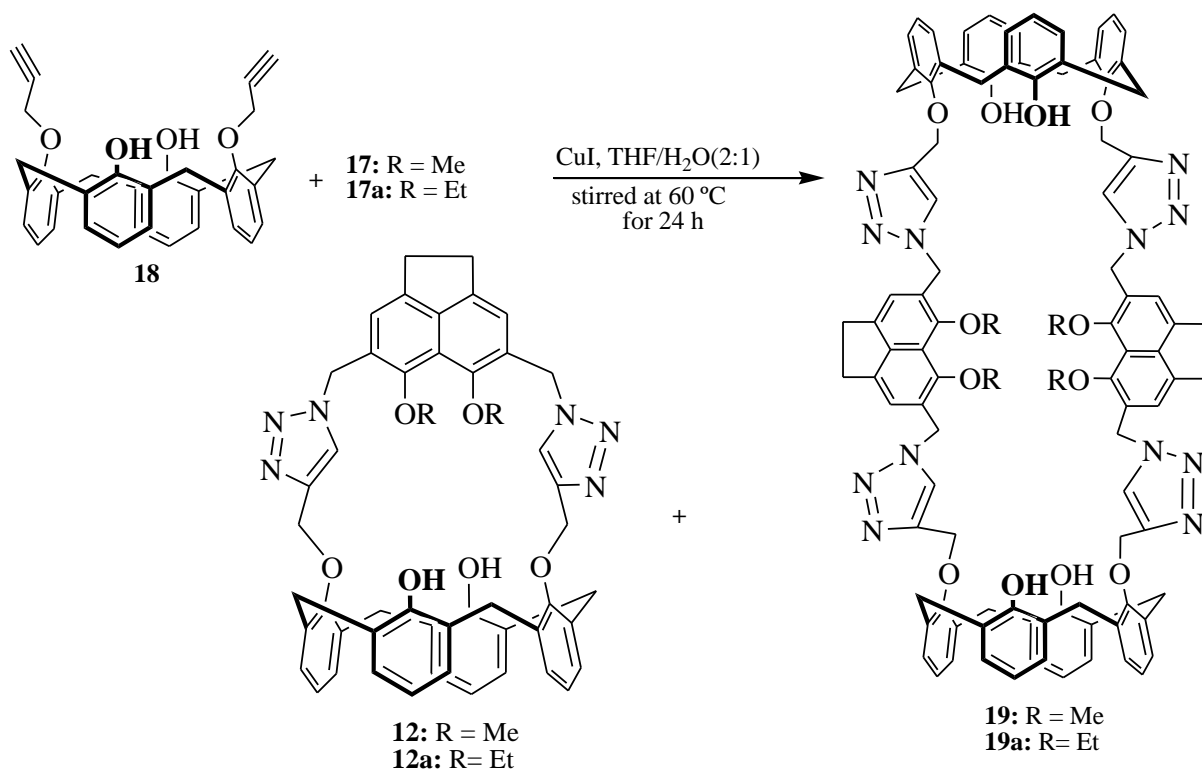
The synthesis of **12** and **12a** started from the bromination of acenaphthene **13** using a procedure initiated by Tanaka et al.⁹ and developed by Neudorff.¹⁰ The procedure starts by adding *N*-bromosuccinimide (NBS) to a solution of acenaphthene in DMF at 0 °C, then stirring at room temperature for 12 h, producing 5,6-dibromoacenaphthene **14** in 24% yield. Reaction of Cu(I) iodide with **14** in the presence of the freshly-prepared sodium methoxide, or ethoxide in 1,4-dioxane with heating at reflux for three days, after which, the corresponding dialkoxyacenaphthenes **15** or **15a** were obtained in excellent yields (93%). This procedure was developed by AlHujran and Georghiou¹¹ using a modified-Ulmann methodology.¹² Compounds **15** or **15a** were reacted with HBr (30%) by mass in glacial acetic acid and paraformaldehyde for four days at room temperature in order to produce the corresponding 4,7-bisbromomethyl-5,6-dialkoxyacenaphthenes **16** and **16a** respectively, in yields of 85%. Sodium azide was reacted with **16** or **16a** in dimethylformamide at 90 °C for two days, producing 4,7-bis(azidomethyl)-5,6-dialkoxyacenaphthenes (**17**) and (**17a**) respectively in 76% yields. The synthetic approach is shown in Scheme 3.1.



Scheme 3.1. Synthesis of bis(azidomethyl)dimethoxyacenaphthene.

3.2.2.2 Synthesis of macrocycles **12** and **12a**

CuAAC reactions were involved in the last step of the synthesis to produce the desired macrocycles employing Yamato's methodology,¹³ in which cyclization of the terminal alkyne **18** with terminal azide **17** or **17a** in the presence of CuI in 2:1 THF/H₂O was performed. The mixture was stirred at 60 °C for 24 h to produce the corresponding 1,2,3-triazole-bridged acenaphthene-calix[4]arenes **12** or **12a** in 40% and 20% yields, respectively, as the major products of the respective reactions, while dimer **19** or **19a**, the corresponding by-products, were also formed. Scheme 3.2 illustrates the synthesis of macrocycles.



Scheme 3.2. Synthesis of triazole-bridged acenaphthene-calix[4]arenes.

3.2.3 Characterizations of newly-synthesized compounds **12** and **12a**

^1H - and ^{13}C -NMR and LCMS spectroscopy were employed to characterize the newly-synthesized macrocycles. The ^1H -NMR spectra of macrocycles **12** and **12a** in CDCl_3 display one new singlet signal at δ 8.06 and 7.98 ppm, respectively, due to the formation of the triazole moieties. The two singlet proton signals of the bridges attached to the triazole moieties were affected by the formation of the triazole units and appeared at δ 5.16 and 5.68 ppm for **12**, and at δ 5.15 and 5.73 ppm for **12a**. In addition, the ^1H -NMR spectrum of **12** shows four up-field signals as follows: two singlets are at δ 3.14 and 3.74 ppm indicating the acenaphthene bridge ($-\text{CH}_2-$) and the methoxy groups

respectively, and two doublets appear at δ 3.14-3.18 and 4.10-4.14 ppm, corresponding to the calixarene bridge ($-\text{CH}_2-$). However, for macrocycle **12a**, five up-field signals were observed: a triplet at δ 1.38-1.42 ppm and a quartet at δ 3.92-3.99 ppm, both are due to the ethoxy groups. Two doublet signals are at δ 3.13-3.17 and 4.10-4.14 ppm and are related to the calixarene bridge ($-\text{CH}_2-$), and one singlet at δ 3.13 ppm related to the acenaphthene bridge ($-\text{CH}_2-$). The ^1H -NMR spectra of **12** and **12a** show other five downfield signals for each macrocycle as follows: one multiplet shows at the same place for both macrocycles at δ 6.56-6.61 ppm, two doublets at δ 6.75-6.77 and 6.76-6.78 ppm for **12** and **12a** respectively, with both corresponding to the calixarene moieties. The last two singlets are at δ 7.13 and 7.67 ppm for **12**, and at δ 7.09 and 7.61 ppm for **12a** and are due to the hydroxyl groups and the acenaphthene units, respectively.

The ^{13}C -NMR spectra of **12** and **12a** show the two signals related to the triazole units which appear downfield between δ 119 to 152 ppm, and eight signals which are due to the calix[4]arene moieties. Six signals are due to the acenaphthene. Macrocycle **12** showed five signals from δ 30.05 to 69.99 ppm, one is due to the methoxy groups, two are due to the acenaphthene ($-\text{CH}_2-\text{CH}_2-$) bridge and the calixarene bridges. The remaining two are due to the triazole bridges ($-\text{CH}_2-$). However macrocycle **12a** showed one extra signal appearing at δ 15 ppm, indicating the presence of the ethoxy group instead of the methoxy groups. The “dimeric” or [2+2] macrocycles **19** and **19a** showed similar ^1H - and ^{13}C -NMR spectra to those of the corresponding monomers. However

LCMS was employed to distinguish these macrocycles and provided signals that clearly indicate the mass of the newly-synthesized macrocycles.

3.3 Complexation studies

Fluorescence spectroscopy (FS) and $^1\text{H-NMR}$ spectroscopy were used in order to probe the potential complexation of the macrocycles **12** and **12a** toward various metal ions. The metal ions that were tested are Cu^{2+} , Hg^{2+} , Fe^{3+} , Fe^{2+} , Pb^{2+} , Ni^{2+} , Zn^{2+} , Ag^{2+} , Ca^{2+} , Co^{2+} , Cd^{2+} and all of these metals were used as their perchlorate salts.

3.3.1 Complexation studies using fluorescence spectroscopy

FS was the technique first used to evaluate the selectivity of the receptors **12** and **12a** toward the metal ions. Stock solutions of the host macrocycles **12** and **12a** (2.11×10^{-5} M) and (2.09×10^{-5} M) respectively, were prepared in a 9:1 $\text{CH}_3\text{CN}:\text{CHCl}_3$ solvent mixture. Both receptors **12** and **12a** exhibit a monomer emission at 360 nm at the 309 nm excitation wavelength. Only one fluorescence emission appeared in these macrocycles, indicating the rigidity of the receptors. In contrast, the bisnaphthyl derivatives receptors which were reported in the previous chapter were more flexible due to the methylene-bridge, thus revealing two monomer fluorescence emissions. The fluorescence spectra of both fluorescent sensors **12** and **12a** were quenched once the metal ions were added to the solutions of the receptors as a result of the complexation. Considerable quenching in the fluorescence spectra upon the addition of Cu^{2+} , Hg^{2+} and Fe^{3+} , respectively, was observed. However, there were only slight changes observed in the fluorescence emissions when the other metal ions such as Ag^+ and Cd^{2+} were tested. The association

constants of the complexes were calculated by employing the Bensi-Hildebrand equation, and the highest values were obtained for the complexes of **12** and **12a** with Cu^{2+} , giving $1.73 \times 10^4 \text{ M}^{-1}$ and $6.66 \times 10^3 \text{ M}^{-1}$, respectively.^{14,15} Job plot analysis indicated 1:1 host-guest complex formation for both receptors. Figures 3.7 to 3.12 show the titration experiments for the complexation with the three metal ions that showed the highest selectivity to the receptors, as evidenced by their K_{assoc} values.

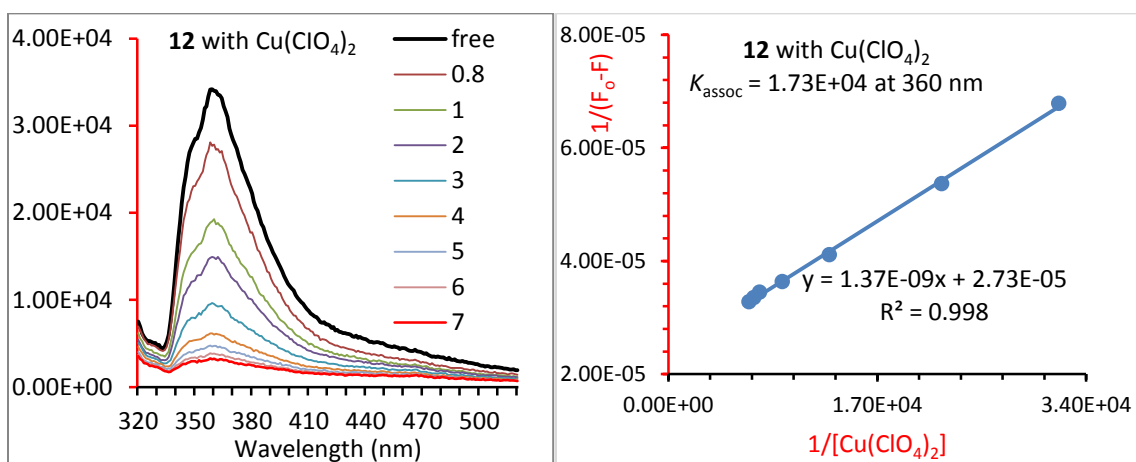


Figure 3.7. *Left:* Fluorescence spectra of **12** (21.1 μM) upon addition of Cu^{2+} in acetonitrile/chloroform (v/v= 9:1) solutions. $\lambda_{\text{ex}} = 309 \text{ nm}$. *Right:* Benesi-Hildebrand plot of $1/(F_0 - F)$ versus $1/[\text{Cu}(\text{ClO}_4)_2]$ for **12** upon titration with Cu^{2+} (0.8-7 equivalents). The linear fit showed a 1:1 complexation of **12** and Cu^{2+} . The association constants were calculated for the changes at the 360 nm wavelength.

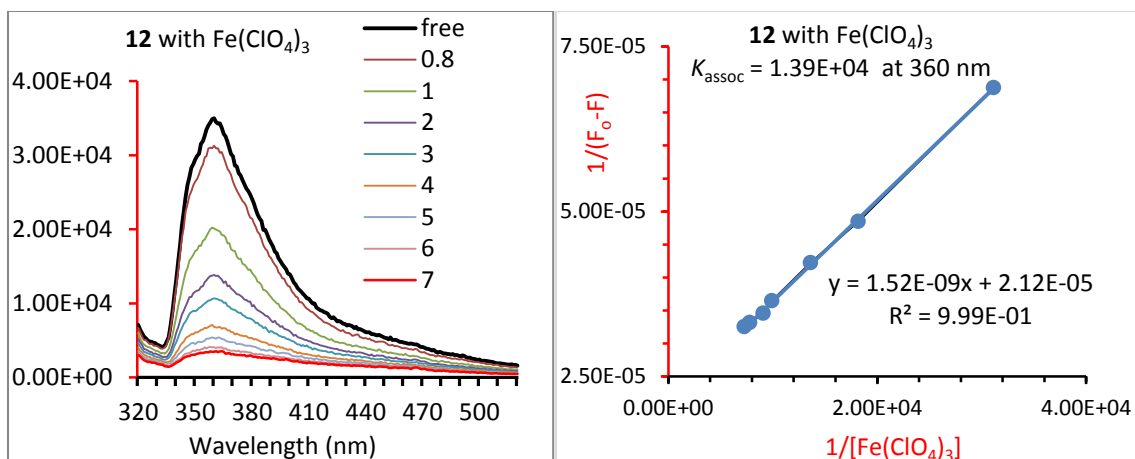


Figure 3.8. *Left:* Fluorescence spectra of **12** (21.1 μM) upon addition of Fe^{3+} in acetonitrile/chloroform ($v/v=9:1$) solutions. $\lambda_{\text{ex}} = 309 \text{ nm}$. *Right:* Benesi-Hildebrand plot of $1/(F_0-F)$ versus $1/[\text{Fe}(\text{ClO}_4)_3]$ for **12** upon titration with Fe^{3+} (0.8-7 equivalents). The linear fit showed a 1:1 complexation of **12** with Fe^{3+} . The association constants were calculated for the changes at the 360 nm wavelength.

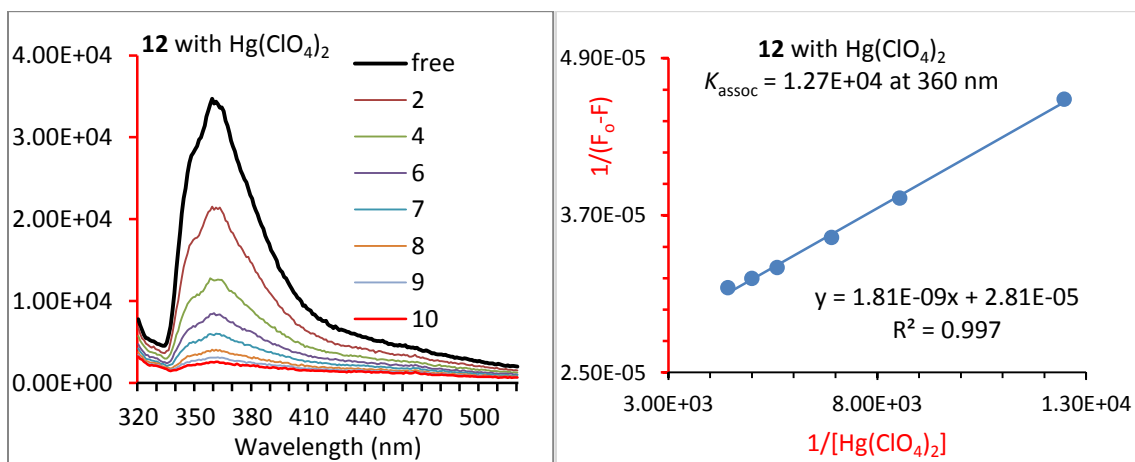


Figure 3.9. *Left:* Fluorescence spectra of **12** (21.1 μM) upon addition of Hg^{2+} in acetonitrile/chloroform ($v/v=9:1$) solutions. $\lambda_{\text{ex}} = 309 \text{ nm}$. *Right:* Benesi-Hildebrand plot of $1/(F_0-F)$ versus $1/[\text{Hg}(\text{ClO}_4)_2]$ for **12** upon titration with Hg^{2+} (2-10 equivalents). The linear fit showed a 1:1 complexation of **12** with Hg^{2+} . The association constants were calculated for the changes at the 360 nm wavelength.

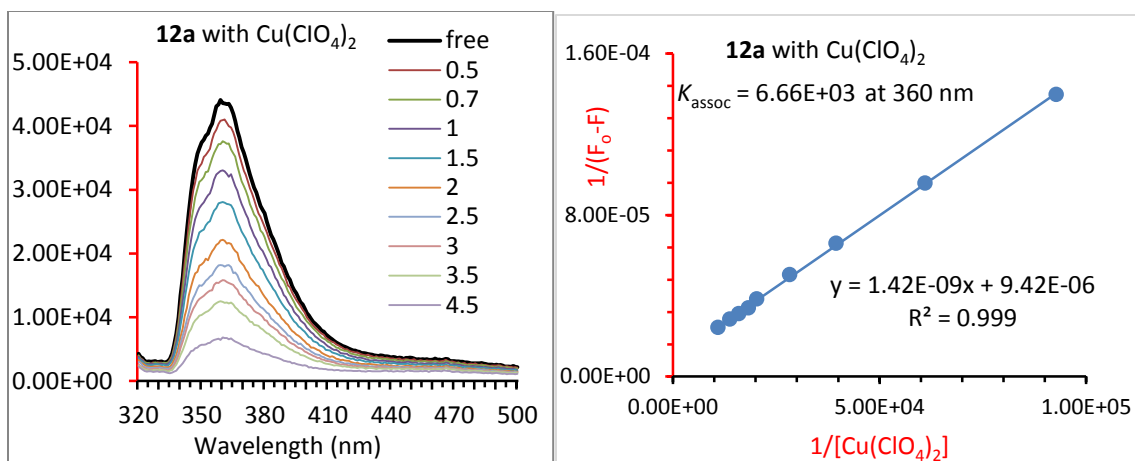


Figure 3.10. *Left:* Fluorescence spectra of **12a** (20.9 μM) upon addition of Cu^{2+} in acetonitrile/chloroform ($v/v=9:1$) solutions. $\lambda_{\text{ex}} = 309$ nm. *Right:* Benesi-Hildebrand plot of $1/(F_0-F)$ versus $1/[\text{Cu}(\text{ClO}_4)_2]$ for **12a** upon titration with Cu^{2+} (0.5-4.5 equivalents). The linear fit showed a 1:1 complexation of **12a** with Cu^{2+} . The association constants were calculated for the changes at the 360 nm wavelength.

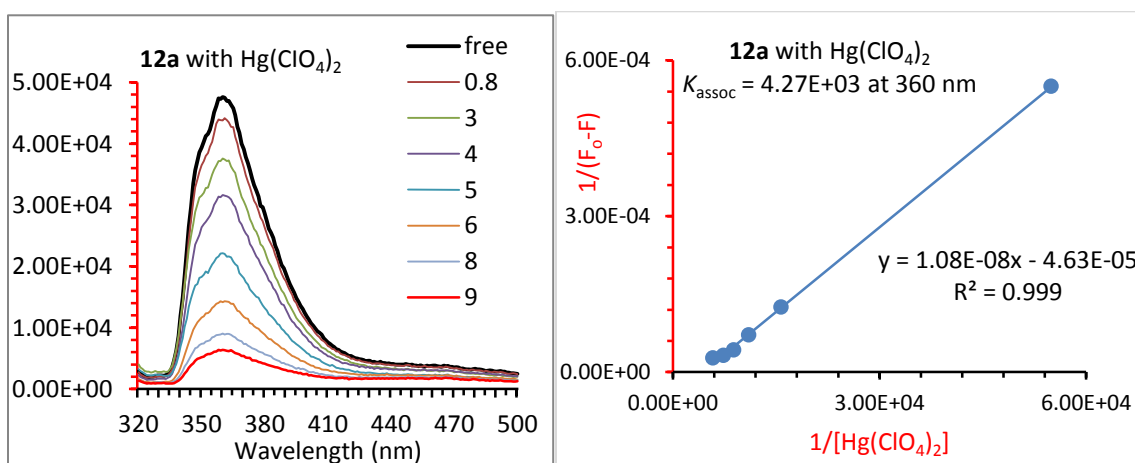


Figure 3.11. *Left:* Fluorescence spectra of **12a** (20.9 μM) upon addition of Hg^{2+} in acetonitrile/chloroform ($v/v=9:1$) solutions. $\lambda_{\text{ex}} = 309$ nm. *Right:* Benesi-Hildebrand plot of $1/(F_0-F)$ versus $1/[\text{Hg}(\text{ClO}_4)_2]$ for **12a** upon titration with Hg^{2+} (0.8-9 equivalents). The linear fit showed a 1:1 complexation of **12a** with Hg^{2+} . The association constants were calculated for the changes at the 360 nm wavelength.

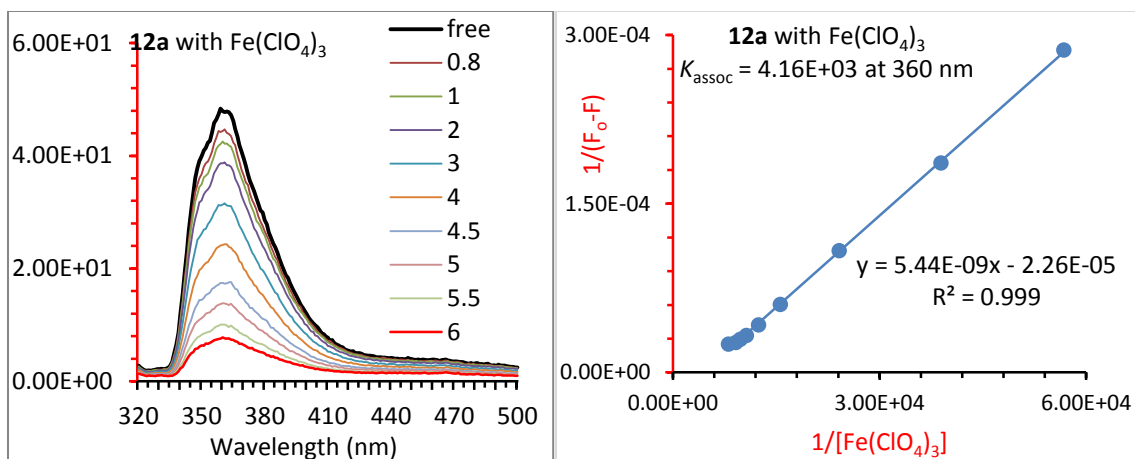


Figure 3.12. *Left:* Fluorescence spectra of **12a** (20.9 μM) upon addition of Fe^{3+} in acetonitrile/chloroform (v/v= 9:1) solutions. $\lambda_{\text{ex}} = 309 \text{ nm}$. *Right:* Benesi-Hildebrand plot of $1/(F_o-F)$ versus $1/[\text{Fe}(\text{ClO}_4)_3]$ for **12a** upon titration with Fe^{3+} (0.8-6 equivalents). The linear fit showed a 1:1 complexation of **12a** with Fe^{3+} . The association constants were calculated for the changes at the 360 nm wavelength.

The complexations were shown to be 1:1 host-guest complexes as found by representative Job plot analysis which were performed for the receptors **12** and **12a** with Ni^{2+} ions. Figures 3.13 and 3.14 show the Job plots corresponding to the 1:1 ratios of the complexes between the hosts and Ni^{2+} .

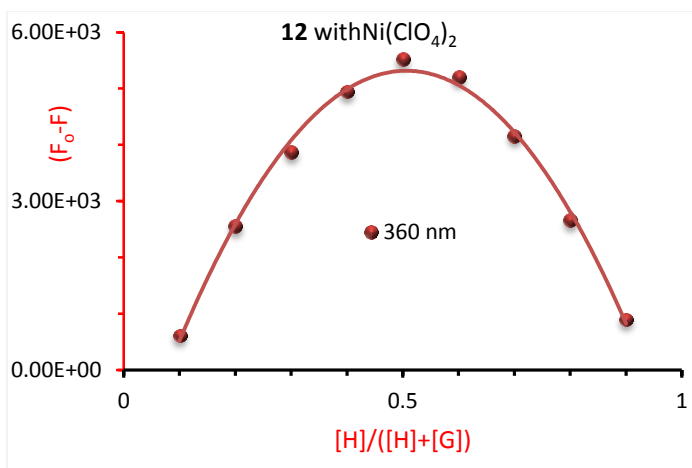


Figure 3.13. Job plot curves showing 1:1 complexation for receptor **12** with Ni²⁺.

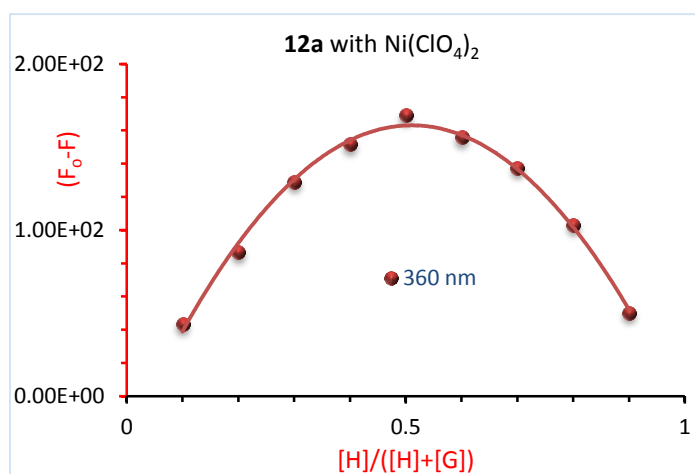


Figure 3.14. Job plot curves showing 1:1 complexation for **12a** with Ni²⁺.

The selectivity of the receptors for the tested metal ions was evaluated in terms of the fluorescence intensities and the K_{assoc} values from the FS analysis. The receptors **12** and **12a** showed the greatest selectivity to Cu²⁺ and afforded the highest K_{assoc} values $\sim 1.73 \times 10^4 \text{ M}^{-1}$ for complex formation with **12** and **12a** (Figures 3.15 and 3.16). However,

relatively high K_{assoc} values for Hg^{2+} and Fe^{3+} were observed as well, so the selectivity was not as great as with the receptors described in Chapter 2.

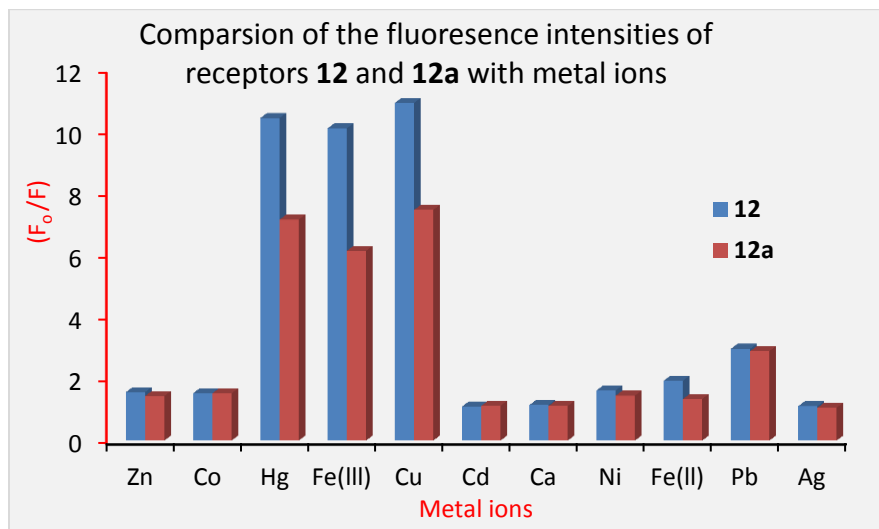


Figure 3.15. Histogram showing the fluorescence quenching of receptors **12** (blue) and **12a** (red) with different metal ions.

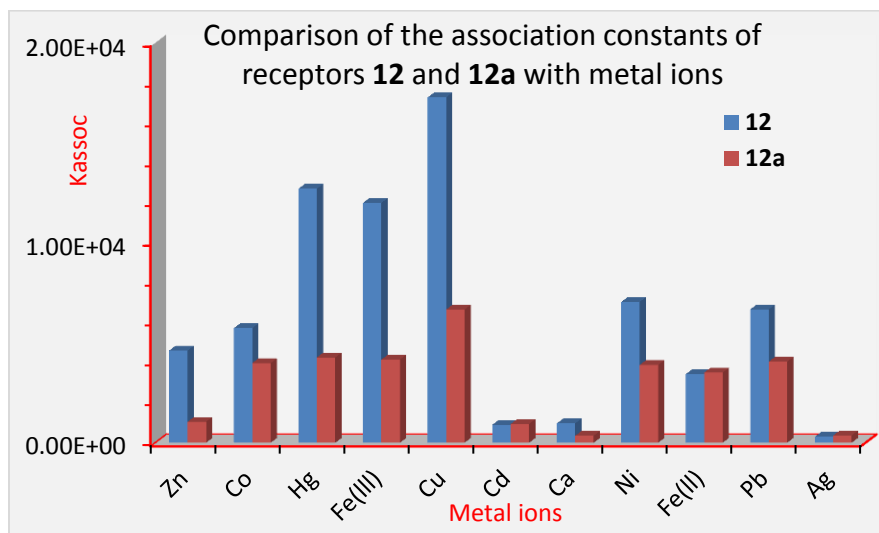


Figure 3.16. Histogram showing the K_{assoc} values determined for receptors **12** (blue) and **12a** (red) with different metal ions.

3.3.2 Complexation studies of **12** using $^1\text{H-NMR}$ spectroscopy

A stock solution of macrocycle **12** (4.37×10^{-3} M in 4:1 $\text{CDCl}_3:\text{CD}_3\text{CN}$) was found to be suitable for the complexation studies using $^1\text{H-NMR}$ spectroscopy. The titration experiments were carried out between macrocycle **12** and Fe^{3+} ions in order to observe the changes of the chemical shifts of the macrocycle affected by the binding with the metal ions. The titration experiments showed that: (a) The highest shift was observed for the singlet proton of the triazole units, which shifted from δ 8.037 ppm to 8.085 ppm, as shown in Figure 3.17. (b) The acenaphthene-triazole ($-\text{CH}_2-$) bridge protons' signal was also shifted downfield from δ 5.707 ppm to 5.745 ppm (Figure 3.18). (c) The slight shifts in hydroxyl groups signals ($-\text{OH}$) from δ 7.151 ppm to 7.161 ppm. (Figure 3.19).

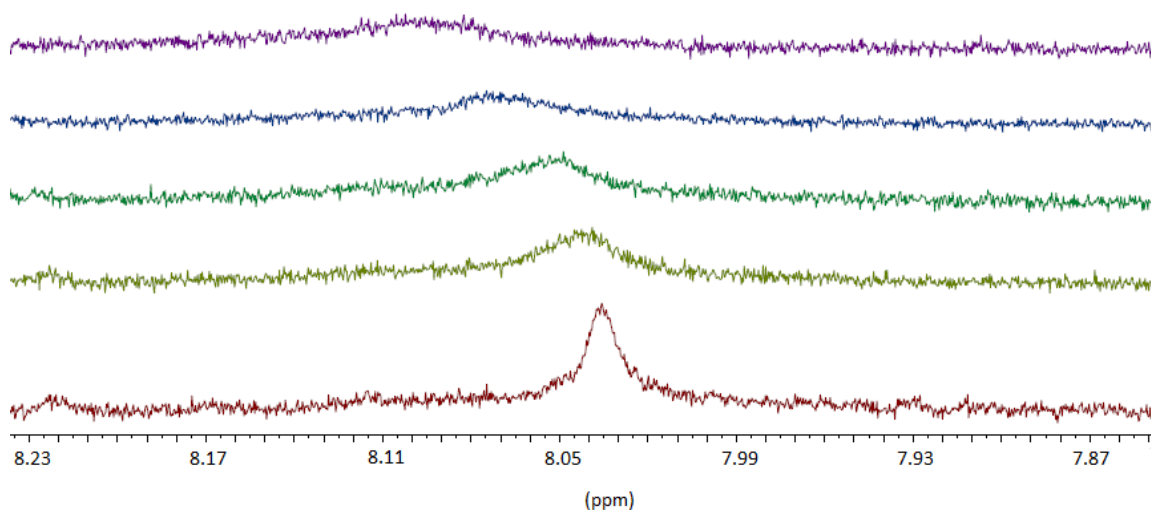


Figure 3.17. $^1\text{H-NMR}$ (500 MHz) titration spectra in 4:1 $\text{CDCl}_3:\text{CD}_3\text{CN}$ for the singlet proton signals of the triazole units in **12** with increasing added amounts of $\text{Fe}(\text{ClO}_4)_3$. From bottom to top $[\text{Fe}(\text{ClO}_4)_3] = 0.0; 7.1 \times 10^{-4}; 1.4 \times 10^{-3}; 2.8 \times 10^{-3}; 5.3 \times 10^{-3}$ M.

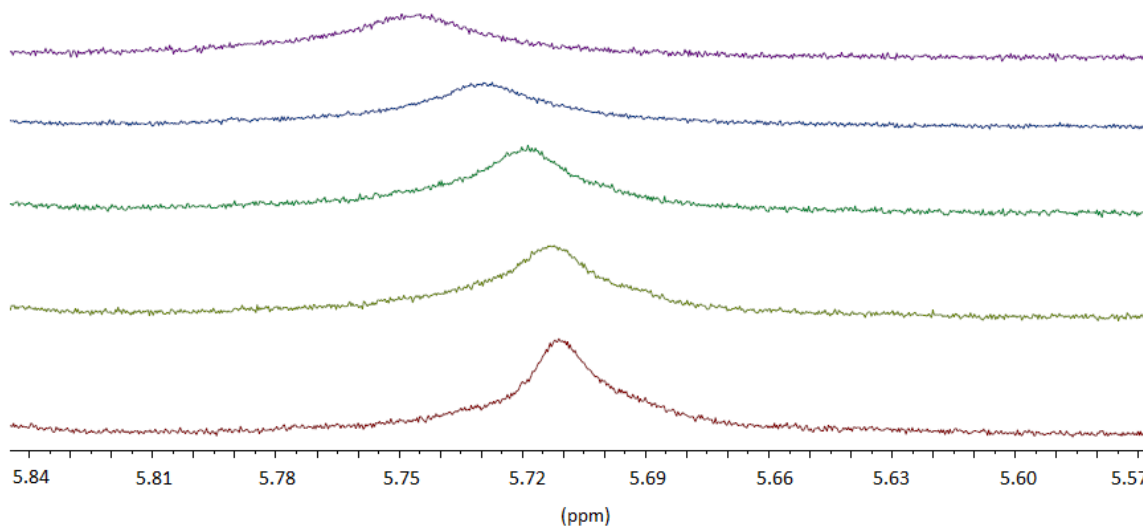


Figure 3.18. $^1\text{H-NMR}$ (500 MHz) titration spectra in 4:1 $\text{CDCl}_3:\text{CD}_3\text{CN}$ for the singlet proton signal of $(-\text{CH}_2-)$ acenaphthene-triazole bridge in **12** with increasing added amounts of $\text{Fe}(\text{ClO}_4)_3$. From bottom to top $[\text{Fe}(\text{ClO}_4)_3] = 0.0; 7.1 \times 10^{-4}; 1.4 \times 10^{-3}; 2.8 \times 10^{-3}; 5.3 \times 10^{-3}$ M.

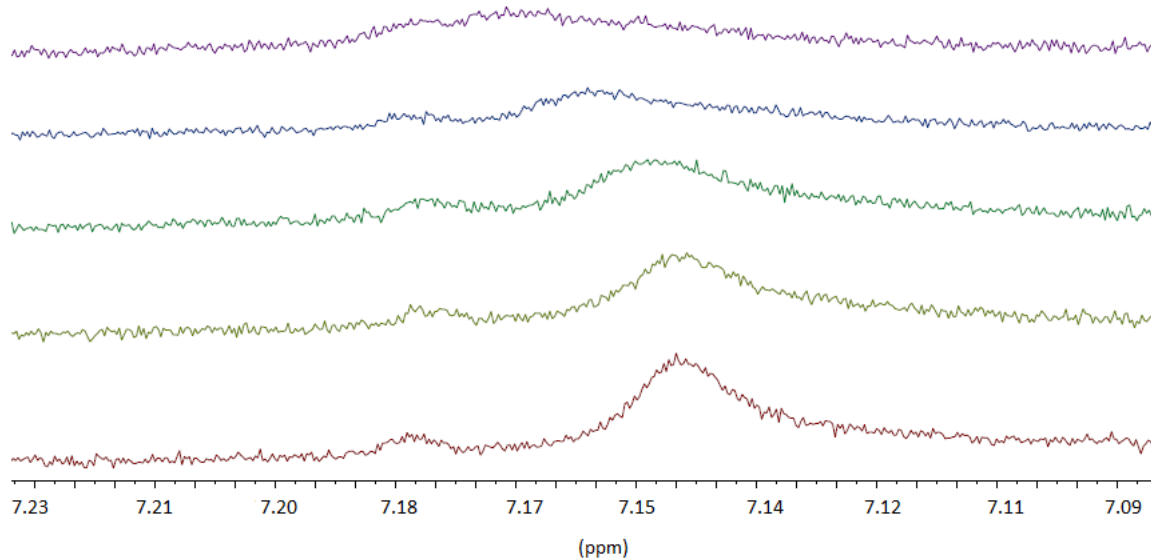


Figure 3.19. $^1\text{H-NMR}$ (500 MHz) titration spectra in 4:1 $\text{CDCl}_3:\text{CD}_3\text{CN}$ for the singlet proton signal of hydroxyl groups in **12** with increasing added amounts of $\text{Fe}(\text{ClO}_4)_3$. From bottom to top $[\text{Fe}(\text{ClO}_4)_3] = 0.0$; 7.1×10^{-4} ; 1.4×10^{-3} ; 2.8×10^{-3} ; 5.3×10^{-3} M.

The K_{assoc} values were calculated employing a non-linear 1:1 binding isotherm for the three significant proton signals which were shifted, as seen in Table 3.1. The Origin6¹⁶ program was used to plot the concentration of the guest ($[\text{Guest}]$) against the observed chemical shift changes ($\Delta\delta$) in Hz in order to calculate the association constants. The measured K_{assoc} values found were $119 \pm 11 \text{ M}^{-1}$ and $180 \pm 46 \text{ M}^{-1}$ based on the triazole signals and the hydroxyl group signals respectively, and $101 \pm 13 \text{ M}^{-1}$ based on the ($-\text{CH}_2-$) acenaphthene-triazole bridge proton signals (Figure 3.20).

Table 3.1. $^1\text{H-NMR}$ (500 MHz) titration data for triazole singlet and singlet of the acenaphthene-bridge ($-\text{CH}_2-$) or methylene protons and the singlet proton of the hydroxyl groups of host **12**.

Sample	[G]/[H]	Triazole δ	$\Delta\delta$ Hz	CH_2 -bridged δ	$\Delta\delta$ Hz	OH δ	$\Delta\delta$ Hz
Free Host		8.037		5.707		7.151	
1	0.24	8.047	5.0	5.714	3.5	7.153	1.2
2	0.48	8.155	9.0	5.721	6.8	7.157	3.1
3	0.95	8.167	15	5.731	12	7.161	5.0
4	1.8	8.085	24	5.745	19	7.165	7.0

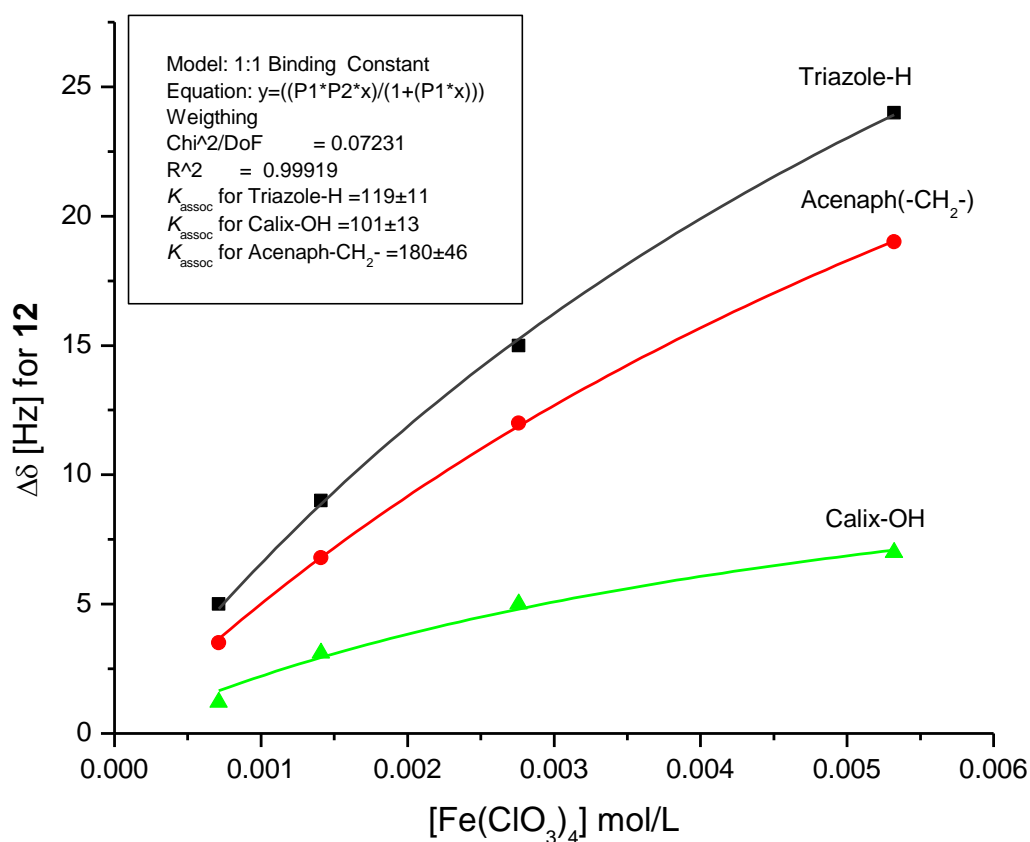


Figure 3.20. $^1\text{H-NMR}$ (500 MHz) titration curves for the triazole, acenaphthene-triazole ($-\text{CH}_2-$) bridge and the hydroxyl proton signals in **12**.

3.4 Conclusions

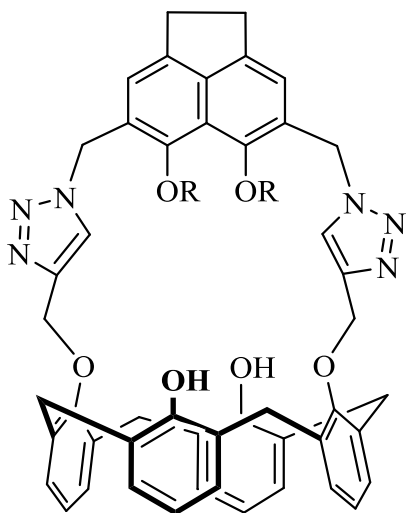
Two new acenaphthene-calix[4]arene macrocycles **12,12a** and **19,19a** were synthesized using the CuAAC methodology and were characterized successfully. Complexation studies were also conducted with receptors **12** and **12a** using fluorescence and $^1\text{H-NMR}$ spectroscopy. The results based on these studies showed that these macrocycles have high affinity to bind selectively as 1:1 host-guest complexes with Cu^{2+} ions, as compared to the other metal ions tested. The fluorescence spectra of the macrocycles demonstrate significant quenching upon the addition of Cu^{2+} ions. The triazole units are defined as the binding sites of the macrocycles as found from the clear changes of the triazole unit's proton signals which resulted from the $^1\text{H-NMR}$ titration experiments.

3.5 Experimental section

The $^1\text{H-NMR}$ and $^{13}\text{C-NMR}$, fluorescence spectroscopy and mass spectrometry used in the characterization of the newly-synthesized compounds were described in the experimental section of Chapter 2.

3.5.1 Experimental

25,27-Dihydroxy-26,28-bridge[4,7-bis-methyl-5,6-dimethoxy-(1,2,3-triazolacenaphthalene)]calix[4]arene (**12**)



12: R = Me

12a: R = Et

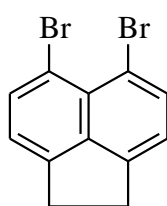
Copper (I) iodide (25 mg) was added to a mixture of **17** (100 mg, 0.310 mmol) and **18** (154 mg, 0.310 mmol) in 20 mL of THF and water (2:1). The mixture was stirred and heated at 65 °C for 24 h under N₂. The reaction mixture was cooled to room temperature followed by addition of DCM (100 mL) and water (40 mL). The organic layer was separated and dried over anhydrous MgSO₄ and the solvent was removed using a rotavap. The residue was purified by

simple column chromatography (silica gel), eluting with DCM:methanol (96:4) to give **12** as a colorless solid (100 mg, 40%, m.p.162 °C). ¹H NMR (CDCl₃, 300 MHz): δ = 3.14 (s, 4H), 3.16 (d, *J* = 12, 4H), 3.74 (s, 6H), 4.12 (d, *J* = 12 Hz, 4H), 5.16 (s, 4H), 5.68 (s, 4H), 6.58 (m, 4H), 6.76 (d, *J* = 6 Hz, 4H), 6.91 (d, *J* = 9 Hz, 4H), 7.13 (s, 2H), 7.67 (s, 2H), 8.06 (s, 2H). ¹³C NMR (CDCl₃, 75.46 MHz): δ = 30.1, 31.4, 49.2, 63.2, 70.0, 119.3, 120.0, 121.3, 123.9, 125.7, 126.9, 127.9, 128.4, 129.0, 133.3, 142.7, 143.3, 144.1, 150.5, 151.2, 152.9. APCI (+) MS (*m/z*): 825.3 (M⁺).

25,27-Dihydroxy-26,28-bridge[4,7-bis-methyl-5,6-diethoxy-(1,2,3-triazolacenaphthalene)]calix[4]arene **12a**

Copper (I) iodide (25 mg) was added to a mixture of **17a** (103 mg, 0.290 mmol) and **18** (146 mg, 0.290 mmol) in 20 mL of THF and water (2:1). The mixture was stirred and heated at 65 °C for 24 h under N₂. The reaction mixture was cooled to room temperature followed by addition of chloroform (100 mL) and water (40 mL). The organic layer was separated and dried over anhydrous MgSO₄ and the solvent was removed using a rotavap. The residue was purified by simple column chromatography (silica gel), eluting with DCM:methanol (96:4) to give **12a** as a colorless solid as the major product (50 mg, 20%, m.p.185 °C). ¹H NMR (CDCl₃, 300 MHz): δ = 1.40 (t, *J* = 9 Hz, 6H), 3.13 (s, 4H), 3.15 (d, *J* = 12 Hz, 4H), 3.96 (q, *J* = 6, 4H), 4.12 (d, *J* = 12 Hz, 4H), 5.15 (s, 4H), 5.73 (s, 4H), 6.59 (m, 4H), 6.77 (d, *J* = 6 Hz, 4H), 6.91 (d, *J* = 9 Hz, 4H), 7.09 (s, 2H), 7.61 (s, 2H), 7.98 (s, 2H). ¹³C-NMR (75.46 MHz, CDCl₃): δ = 15.6, 30.0, 31.4, 49.5, 69.9, 72.2, 119.2, 120.4, 120.9, 123.9, 125.7, 127.1, 127.9, 128.4, 128.9, 133.3, 142.6, 143.1, 143.1, 149.5, 151.3, 152.9. APCI (+) MS (*m/z*): 853.3 (M⁺).

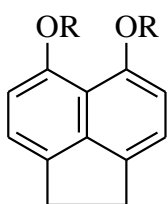
5,6-Dibromoacenaphthene (**14**)



5,6-Dibromoacenaphthene (**14**) was prepared as described by Tanaka.^{9,10}

Tanaka and Kasai.^{9,10}

5,6-Dialkoxyacenaphthene (**15**) and (**15a**)

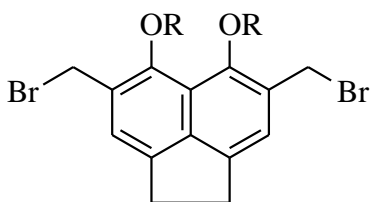


5,6-Dialkoxyacenaphthenes (**15**) and (**15a**) was prepared as described by

AlHujran et al.¹¹

15: R = Me
15a: R = Et

4,7-Bis(bromomethyl)-5,6-dialkoxyacenaphthene (**16**) and (**16a**)



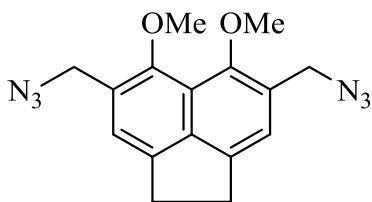
16: R = Me

16a: R = Et

4,7-Bis(bromomethyl)-5,6-dialkoxyacenaphthenes (**16**)

and (**16a**) was prepared as described by AlHujran et al.¹¹

4,7-Bis(azidomethyl)-5,6-dimethoxyacenaphthene (**17**)

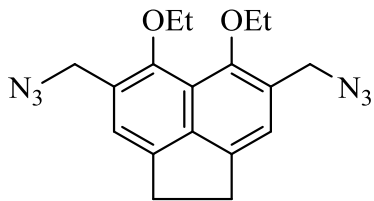


To a mixture of **16** (950 mg, 2.38 mmol) and sodium azide (2,00 g, 30.8 mmol), was added 30 mL of dimethylformamide. The mixture was stirred at 90 °C under N₂ for 48 h. The reaction mixture was cooled to

room temperature followed by addition of ethyl acetate (100 mL) and water (40 mL).

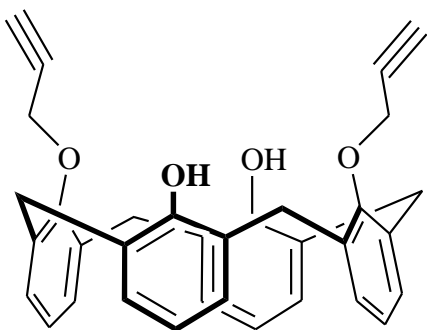
The organic layer was separated and dried over anhydrous MgSO₄ and the solvent was removed using a rotavap. The residue was purified by simple column chromatography (silica gel), eluting with hexane:ethyl acetate (90:10) to give a yellow solid (580 mg, 76%, m.p.126 °C). ¹H NMR (CDCl₃, 300 MHz): δ = 3.37 (s, 4H), 3.91(s, 6H), 4.56 (s, 4H), 7.24 (s, 2H). ¹³C NMR (CDCl₃, 75.46 MHz): δ = 30.2, 50.1, 63.3, 119.9, 121.6, 127.1, 142.3, 143.2, 150.9.

4,7-Bis(azidomethyl)-5,6-diethoxyacenaphthene (17a)



To a mixture of **16a** (1.20 g, 2.80 mmol) and sodium azide (2.35 g, 33.8 mmol), was added 20 mL of dimethylformamide. The mixture was stirred at 90 °C under N₂ for 48 h. After cooling to room temperature, the reaction was worked-up by adding water (50 mL) followed by addition of ethyl acetate (100 mL) and then brine solution (50 mL). The organic layer was separated and dried over anhydrous MgSO₄ and filtered. The solvent was removed on a rotavap. The crude product was purified by simple column chromatography, eluting with hexane:ethyl acetate (90:10), to obtain a colorless solid (700 mg, 71%, m.p.74.4 °C). ¹H NMR (CDCl₃, 300 MHz): δ = 1.46 (t, *J* = 9 Hz, 6H), 3.36 (s, 4H), 4.03 (q, *J* = 6 Hz, 4H), 4.56 (s, 4H), 7.24 (s, 2H). ¹³C-NMR (75.46 MHz, CDCl₃): δ = 15.6, 30.2, 50.3, 72.0, 120.4, 121.3, 127.3, 142.1, 143.2, 150.0.

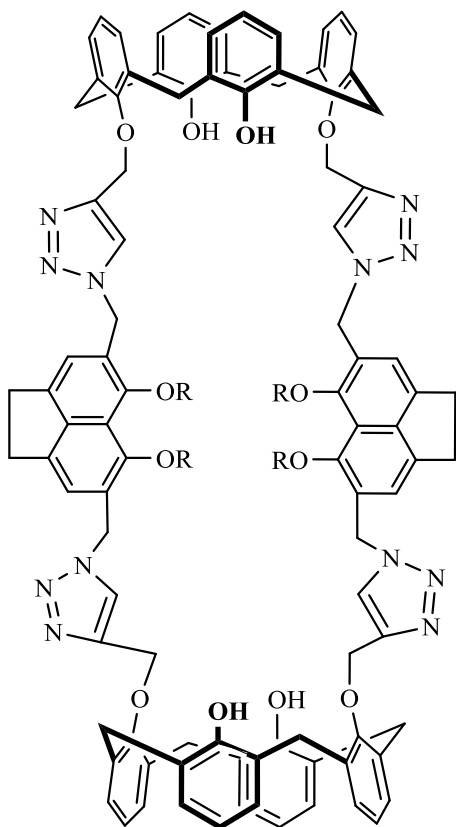
25,27-Dihydroxy-26,28-bis(*O*-propargyl)calix[4]arene (18)



25,27-Dihydroxy-26,28-bis(*O*-propargyl)calix[4]arene (**18**)

was prepared as described in Chapter 2.

**25,27-Dihydroxy-26,28-bridge[4,7-bis-methyl-5,6-dimethoxy-(1,2,3-triazolacena-
thalene)]calix[4]arene (Dimer) (19)**



19: R = Me
19a: R = Et

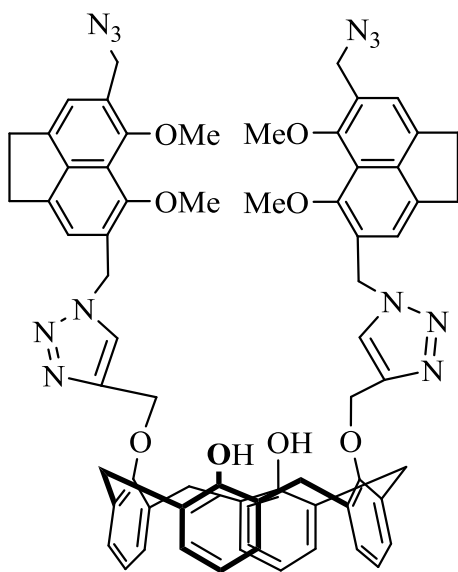
The minor product from CuAAC reaction of **18** with **17** was purified by simple column chromatography (silica gel), eluting with DCM:methanol (96:4) to give **19** as a yellow solid (20 mg, 10%, m.p.184.30 °C). ¹H NMR (CDCl₃, 300 MHz): δ = 3.14 (d, *J* =12 Hz, 8H), 3.18 (s, 8H), 3.72 (s, 12H), 4.11 (d, *J* = 12 Hz, 8H), 5.11 (s, 8H), 5.70 (s, 8H), 6.59 (t, *J* = 9 Hz, 4H), 6.68 (t, *J* = 9 Hz, 4H), 6.76 (d,

J = 9 Hz, 8H), 6.89 (d, *J* = 6 Hz, 8H), 7.06 (s, 4H), 7.31 (s, 4H), 7.91 (s, 4H). ¹³C NMR (CDCl₃, 75.46 MHz): δ = 28.2, 30.1, 31.4, 63.2, 69.5, 119.1, 121.1, 123.7, 125.5, 126.9, 127.9, 128.4, 128.9, 133.1, 142.7, 143.2, 143.8, 149.4, 150.4, 151.5, 152.9. APCI (+) MS (*m/z*): 1650.3 (M⁺).

**25,27-Dihydroxy-26,28-bridge[4,7-bis-methyl-5,6-diethoxy-(1,2,3-triazolacena-
thalene)]calix[4]arene (Dimer) (19a)**

The minor product from the reaction of **18** with **17a** was purified by simple column chromatography (silica gel), eluting with DCM:methanol (96:4) to give **19a** as a yellow solid (10 mg, 6%, m.p.204.30 °C). ¹H NMR (CDCl₃, 300 MHz): δ = 1.35 (t, *J* = 9 Hz, 12H), 3.14 (s, 8H), 3.15 (d, *J* = 12 Hz, 8H), 3.88 (q, *J* = 6, 8H), 4.10 (d, *J* = 12, 8H) 5.06 (s, 8H), 5.69 (s, 8H), 6.59 (t, *J* = 6, 4H), 6.88 (t, *J* = 6, 4H) 6.77 (d, *J* = 9, 8H), 6.89 (d, *J* = 9, 8H), 6.95 (s, 4H), 7.31 (s, 4H), 7.84 (s, 4H). APCI (+) MS (*m/z*): 1706.3 (M⁺).

25,27-Dihydroxy-26,28-bridge-bis[4,7-bis-methyl-5,6-dimethoxy-(1,2,3-triazol
acenaphthalene)]calix[4]arene (20)



The dimer intermediate **20** was purified by simple column chromatography (silica gel), eluting with DCM:methanol (96:4) to give **20** as a colorless solid (15 mg, 10%, m.p.184.30 °C). ¹H NMR (CDCl₃, 300 MHz): δ = 3.17 (s, 4H), 3.21 (s, 4H), 3.26 (d, *J* = 9, 4H), 3.69 (s, 6H), 3.91 (s, 6H), 4.14 (d, *J* = 15, 4H), 4.51 (s, 4H), 5.18 (s, 4H), 5.70 (s, 4H), 6.60 (t, *J* = 6, 4H), 6.69 (t, *J* = 6 Hz, 4H), 6.81 (d, *J* = 6, 4H), 6.92 (d, *J* = 9, 4H), 7.16 (s, 2H), 7.23 (s, 2H),

7.71 (s, 2H), 8.13 (s, 2H). ¹³C NMR (CDCl₃, 75.46 MHz): δ = 30.1, 30.1, 31.4, 43.8, 49.4, 50.0, 63.2, 63.3, 119.3, 119.9, 121.1, 121.8, 121.8, 123.9, 125.7, 126.7, 127.3, 127.9, 128.4, 129.0, 133.3, 142.4, 142.7, 143.3, 144.2, 150.5, 150.8, 151.2, 151.3, 152.9. APCI (+) MS (*m/z*): 1150.3 (M⁺).

3.6 References

1. Zhao, Y.; Zhang, X. B.; Han, Z. X.; Qiao, L.; Li, C. Y.; Jian, L. X.; Shen, G. L.; Yu, R. Q. *Anal. Chem.* **2009**, *81*, 7022- 7030.
2. (a) Duruibe, J. O.; Ogwuegbu, M. O.; Egwurugwu, J. N. *Int. J. Phys. Sci.* **2007**, *2*, 112- 118. (b) Kozłowski, H.; Klos, A. J.; Brasun, J.; Gaggelli, E.; Valensin, D.; Valensin, G. *Coordination Chemistry Reviews*, **2009**, *253*, 2665-2685.
3. Wu, S. P.; Wang, T. H.; Liu, S. R. *Tetrahedron*, **2010**, *66*, 9655-9658.
4. Hu, S.; Zhang, S.; Hu, Y.; Tao, Q.; Wu, A. *Dyes and Pigments*, **2013**, *96*, 509-515.
5. Ho, L. T.; Chang, K. C.; Lee, G. H.; Liu, Y. H.; Chung, W. S. *Chem. Eur. J.* **2009**, *16*, 6152- 6160.
6. Li, G. K.; Xu, Z. X.; Chen, C. F.; Huang, Z. T. *Chem. Commun.* **2008**, *15*, 1774- 1775.
7. Sanfrutos, J. M.; Munoz, M. O.; Jaramillon, J. L.; Mateo, F. H.; Gonzalez, F. S.; *J. Org. Chem.* **2008**, *73*, 7768-7771.
8. Gaussian 09, Revision C.01, Frisch, M. J.; Trucks, G. W.; Schlegel, H. B.; Scuseria, G. E.; Robb, M. A.; Cheeseman, J. R.; Scalmani, G.; Barone, V.; Mennucci, B.; Petersson, G. A.; Nakatsuji, H.; Caricato, M.; Li, X.; Hratchian, H. P.; Izmaylov, A. F.; Bloino, J.; Zheng, G.; Sonnenberg, J. L.; Hada, M.; Ehara, M.; Toyota, K.; Fukuda, R.; Hasegawa, J.; Ishida, M.; Nakajima, T.; Honda, Y.; Kitao, O.; Nakai, H.; Vreven, T.; Montgomery, Jr. J. A.; Peralta, J. E.; Ogliaro, F.; Bearpark, M.; Heyd, J. J.; Brothers, E.; Kudin, K. N.; Staroverov, V. N.; Keith, T.; Kobayashi, R.; Normand, J.; Raghavachari, K.; Rendell, A.; Burant, J. C.; Iyengar, S. S.; Tomasi, J.;

Cossi, M.; Rega, N.; Millam, J. M.; Klene, M.; Knox, J. E.; Cross, J. B.; Bakken, V.; Adamo, C.; Jaramillo, J.; Gomperts, R.; Stratmann, R. E.; Yazyev, O.; Austin, A. J.; Cammi, R.; Pomelli, C.; Ochterski, J. W.; Martin, R. L.; Morokuma, K.; Zakrzewski, V. G.; Voth, G. A.; Salvador, P.; Dannenberg, J. J.; Dapprich, S.; Daniels, A. D.; Farkas, O.; Foresman, J. B.; Ortiz, J. V.; Cioslowski, J.; Fox, D. J. Gaussian, Inc., Wallingford CT, 2010.

9. Tanaka, N.; Kasai, T. *Bull. Chem. Soc. Jpn.* **1981**, *54*, 3020-3025.
10. Neudorff, W. D.; Lentz, D.; Anibarro, M.; Schluter, A. D. *Chem. Eur. J.* **2003**, *9*, 2745-2757.
11. AlHujran, T.; Dawe, L. N.; Georghiou, P. E. *Org. Lett.* **2012**, *14*, 3530-3533.
12. (a) Ulmann, F. *Chem. Ber.* **1904**, *37*, 853-854. (b) Lindley, J. *Tetrahedron*, **1984**, *40*, 1433-1456.
13. Jin, C. C.; Kinoshita, T.; Cong, H.; Ni, X.-L. Zeng, X.; Hughes, D. L.; Redshaw, C.; Yamato, T. *New J. Chem.* **2012**, *36*, 2580-2586.
14. Bano, S.; Mohd, A.; Khan, A.; Siddiqi, K. S. *J. Chem. Eng. Data.* **2010**, *55*, 5759-5765.
15. Benesi, H. A.; Hildebrand, J. H. *J. Am. Chem. Soc.* **1949**, *71*, 2703-2707.
16. Association constants were calculated using a nonlinear curve fitting program, using the program ORIGINPro 6.1 from OriginLab Corporation.

Chapter 4

Attempts to Synthesize and Modify Homooxacalix[4]acenaphthene Derivatives

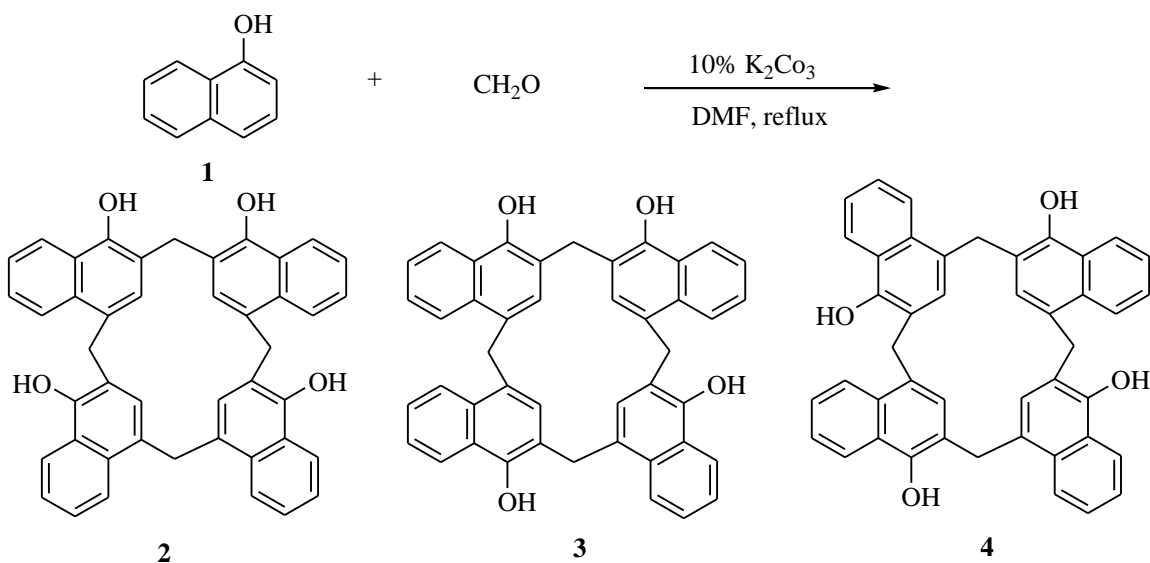
4.1 Introduction

In this chapter, attempts to modify homooxacalix[4]acenaphthene, whose synthesis and characterization has been previously reported by AlHujran et al.,¹ will be presented. This compound was found to be a receptor for fullerene C₆₀ and molecular modeling suggested that an appropriately modified homooxacalix[4]acenaphthene could lead to a new receptor for the larger fullerene, C₇₀.

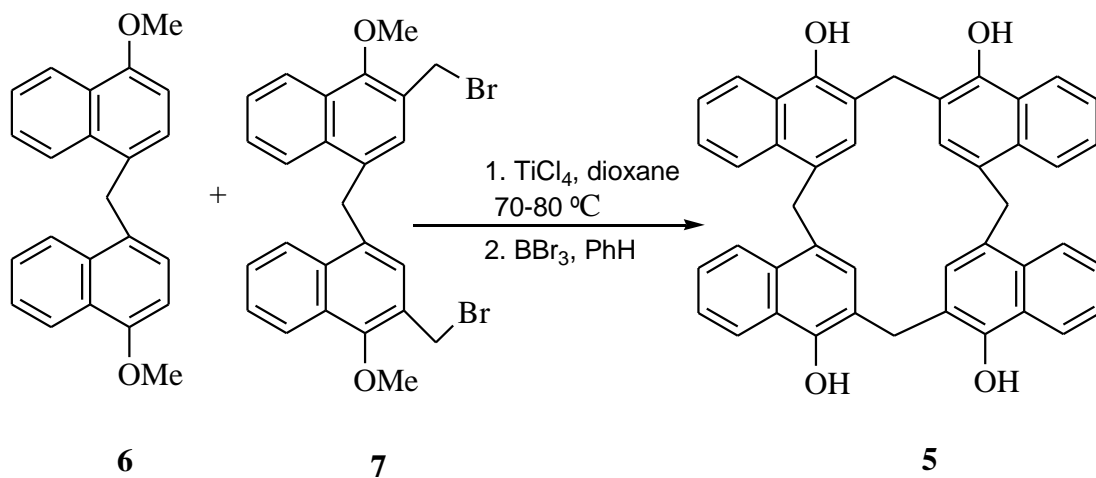
4.2 Synthesis of calixarene and homooxacalixarene

In 1993, Georghiou and Li² reported the synthesis of a new class of macrocyclic compounds which they named calix[4]naphthalenes which were derived from 1-naphthol. They synthesized three different regioisomeric *exo*-calix[4]naphthalenes out of four possible isomers by the direct base-mediated condensation of 1-naphthol with paraformaldehyde in DMF, at reflux. The calix[4]naphthalenes were produced in relatively low yields, as shown in Scheme 4.1.³ The synthesis of the fourth regioisomer *exo*-calix[4]naphthalene **5**, was achieved by a [2+2] cycloaddition approach and was reported later by Ashram and Georghiou et al.⁴ The condensation of bis(4-methoxy-1-naphthyl)methane **6** with bis[3-(bromomethyl)-4-methoxy-1-naphthyl]-methane **7** using

TiCl₄ as catalyst was performed in dioxane solvent, and the product was then demethylated using BBr₃ to produce **5**. (Scheme 4.2).

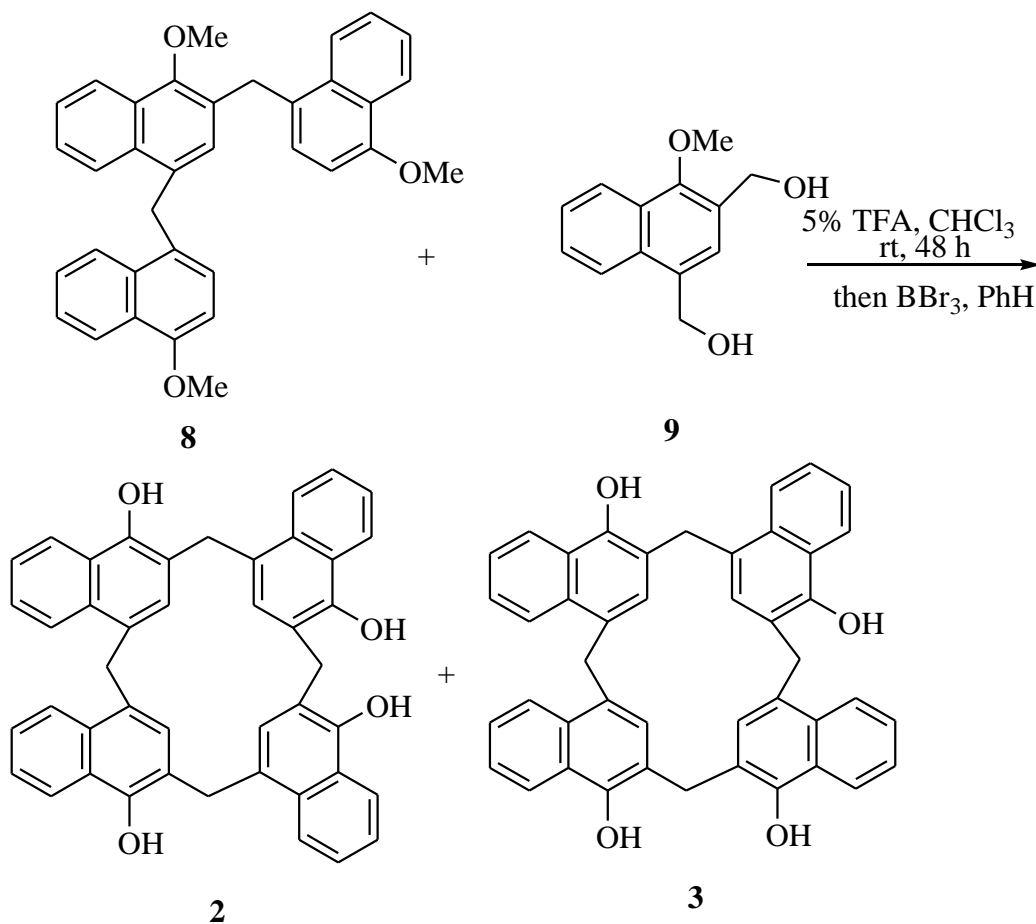


Scheme 4.1. Synthesis of calix[4]naphthalenes.



Scheme 4.2. Synthesis of *exo*-calix[4]naphthalene using [2+2] condensation.

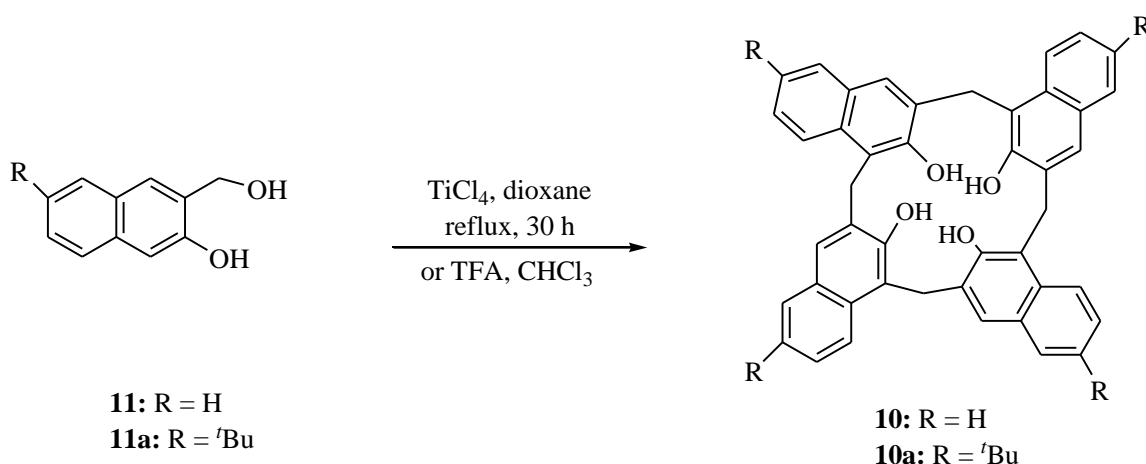
These authors also used a [3+1] approach in order to synthesize two of the calix[4]naphthalenes⁴ namely **2** and **3** (Scheme 4.3). Condensation of trimer(methoxynaphthalene) **8** with bis(hydroxymethyl)naphthalene (**9**) using 5% of trifluoroacetic acid (TFA) in chloroform at room temperature for 48 h, followed by demethylation using BBr₃, afforded a mixture of calix[4]naphthalenes **2** and **3**.



Scheme 4.3. Synthesis of calix[4]naphthalenes using [3+1] approach.

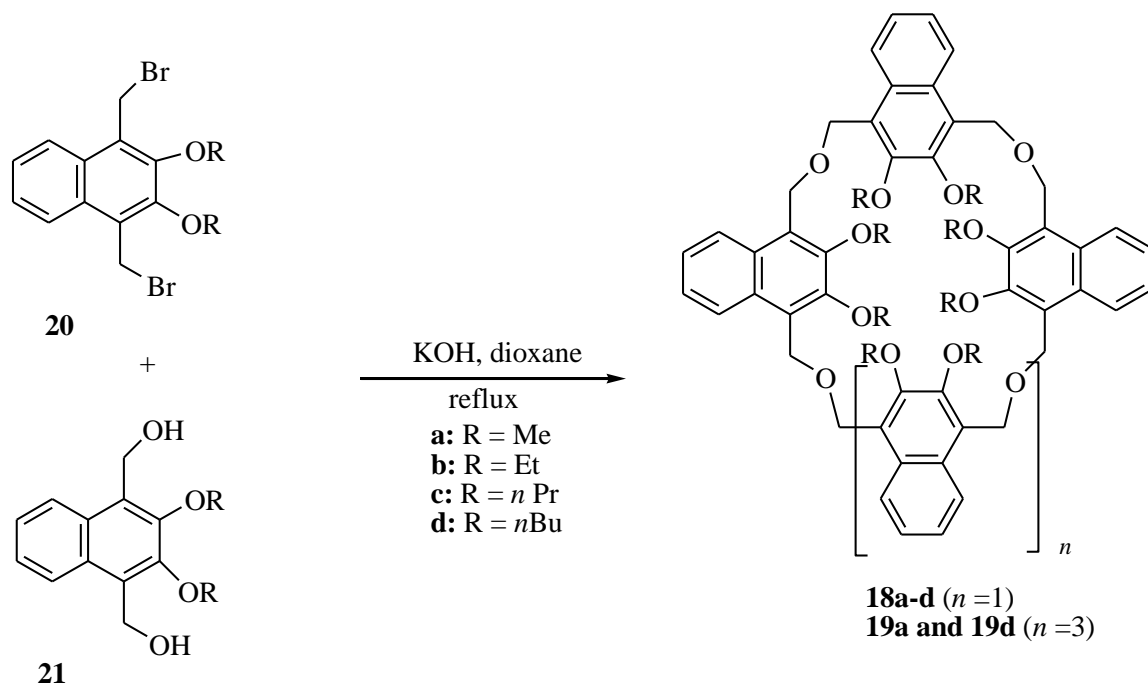
In 1993, Andreetti et al.⁶ reported a synthesis of *endo*-calix[4]naphthalene **10** from **11** which has a deep- and electron-rich cavity. The Georgiou group was able to

show that the *t*-butylated analogue **10a** could bind the electron-deficient C₆₀ fullerene. Self-condensation of 3-hydroxymethyl-2-naphthol (**11**) using TiCl₄ in dioxane solvent at reflux was the approach used to synthesize compound **10a** in low yield. However Georghiou and coworkers³ have modified the procedure to improve the yields, and they synthesized the *tert*-butyl *endo*-calix[4]naphthalene **10a** via the self-condensation of **11a** involving a modification of Andereetti's original procedure, as shown in Scheme 4.4.⁷



Scheme 4.4. Synthesis of *endo*-calix[4]naphthalenes **10** and **10a**.

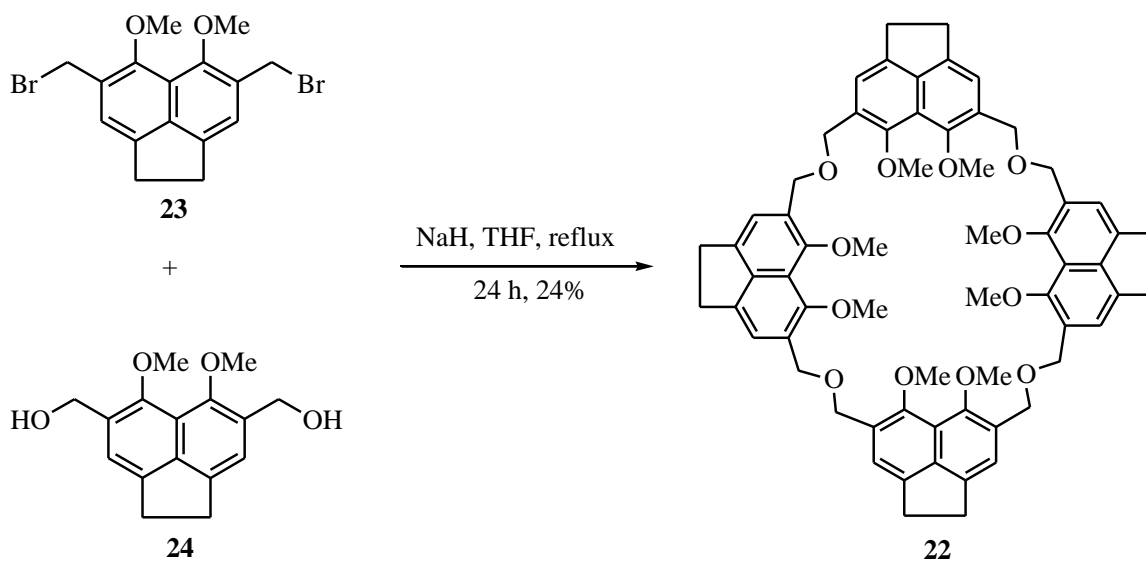
Georghiou et al.⁸ investigated the supramolecular complexation between the *endo*-calix[4]naphthalenes **10** and **10a** with C₆₀ fullerene using spectrophotometric methods. The complexation studies showed that relatively strong complexes were formed between the receptors and C₆₀ fullerene in carbon disulfide via most likely π - π interactions. Benesi-Hildebrand equations were employed at the time to determine the association constants of the 1:1 complexes formed and were found to be 3.4×10^3 and $0.1 \times 10^3 \text{ M}^{-1}$, respectively.⁸



Scheme 4.7. Synthesis of homooxacalix[*n*]naphthalenes.

In 2005, Georghiou and coworkers¹⁰ reported the synthesis of a series of homooxacalix[4]naphthalenes **18a-d** and homooxacalix[6]naphthalenes **19a** and **19d** in relatively moderate yields. They used a Williamson ether coupling reaction (Scheme 4.7) between compounds **20** and **21** using potassium hydroxide in dioxane to generate the homooxacalix[4]naphthalenes macrocycles **18a-d** in ~ 18% yields, and to also generate two homooxacalix[6]naphthalenes, **19a** and **19d**, in low yields (i.e. 3%). ¹H-NMR spectroscopy and UV-vis spectroscopy were employed to study the complexes formed between **18a-d** and other electron-deficient guests such as C₆₀ fullerene. However, the complexation studies failed to show any complex formation between C₆₀ fullerene and

these macrocycles. On the other hand, macrocycles **18a** and **18b** were shown to have the ability to bind tetramethylammonium (TMA) ions in a 1:1 host-guest complex.



Scheme 4.8. Synthesis of homooxalix[4]acenaphthene **22**.

AlHujran et al.¹ reported the first member of a new class of homooxalix[4]arene (**22**) based on linking acenaphthene units.¹¹ The precursor compounds **23** and **24** were first synthesized from acenaphthene itself *via* a modified Ullmann coupling methodology, followed by reaction with HBr and paraformaldehyde in glacial acetic acid to obtain **23**, which was then treated with calcium carbonate to produce **24**. The previous methodology used to produce **18a-d** was involved here (i.e. Williamson ether coupling reaction) in order to synthesize **22** in moderate yield, from the reaction of **23** with **24**, using sodium hydride in THF solvent at reflux for 24 h. The new macrocycle **22** was characterized by NMR and single crystal X-ray analysis. The complexation properties between the new macrocycle **22** and C₆₀ fullerene were investigated using ¹H-NMR spectroscopy. The

complexation studies showed that **22** has a suitable cavity to bind C₆₀ fullerene in toluene-*d*₈ and formed a 1:1 complex. The binding constant was also calculated and found to be 620 ± 100 M⁻¹.

4.3 Results and discussion

4.3.1 Design of desired macrocycle **25**

Homooxacalix[4]acenaphthene **22** has a sufficiently large cavity to bind to C₆₀ fullerene. Molecular modeling suggested an attractive new modified homooxacalix[4]-acenaphthene **25**.¹² The presence of the 16 methyl groups on the periphery of the annulus could favour stronger C₆₀ and C₇₀ binding with **25** (Figure 4.1 and 4.2) due to the additional π–methyl interactions possible. The synthesis of **25** is the main objective described in this chapter, but at the time of writing, the work is still ongoing.

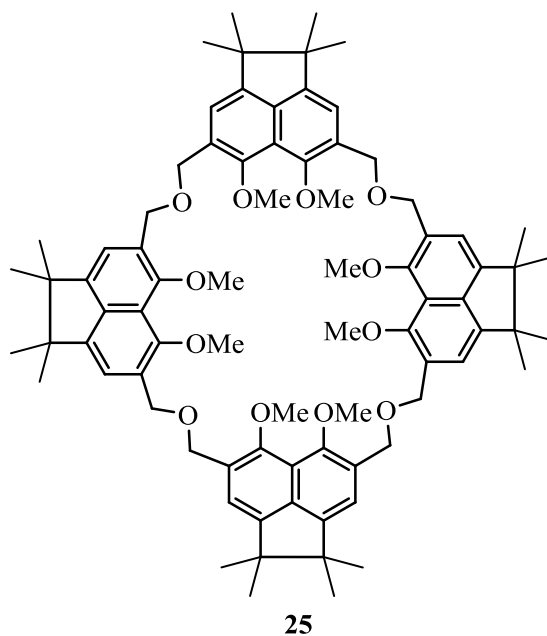


Figure 4.1. Structure of the hexadecakis-methylated homooxacalix[4]acenaphthene **25**.

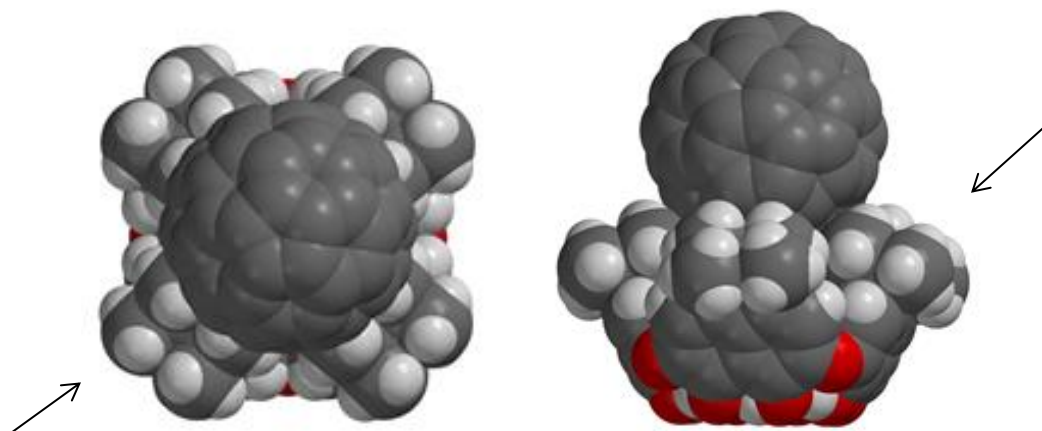
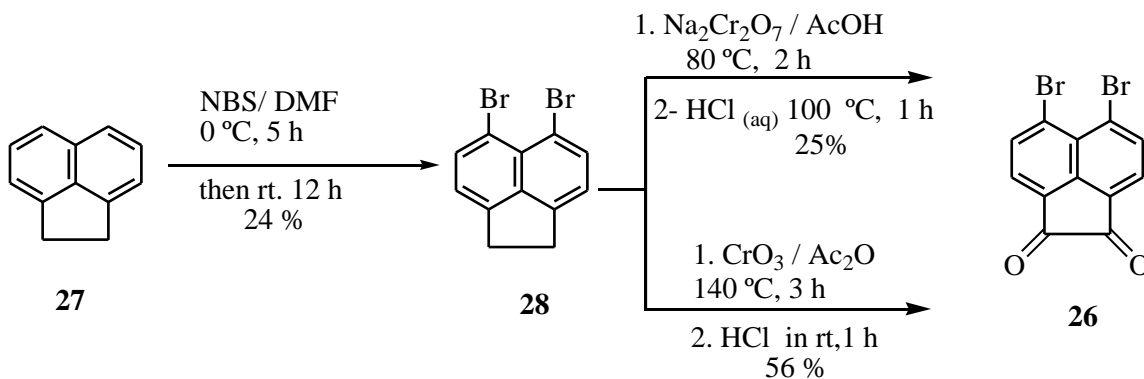


Figure 4.2. Computer-generated image for the complex of the macrocycle **25** and C_{60} (*Left- top view*) and (*Right- side view*) where the arrows point to the methyl groups.

4.3.2 Synthesis of dibromoacenaphthenequinone (**26**)

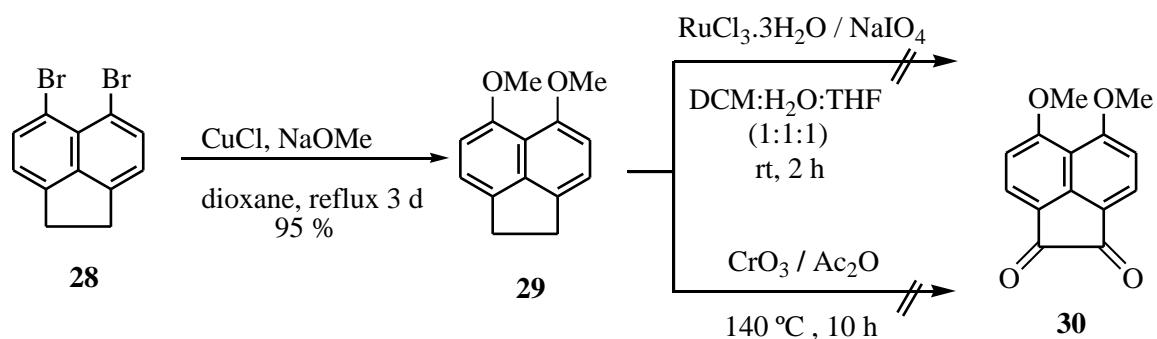


Scheme 4.9. Synthesis of 5,6-dibromoacenaphthene-1,2-dione (**26**).

Synthesis of diketone **26** was one of our target preparing starting materials needed toward the synthesis of macrocycle **25**. Bromination of acenaphthene **27** using NBS in DMF lead to dibromoacenaphthene **28** which was previously reported by Tanaka.¹³ Oxidation of the ethylene bridge of acenaphthene was performed using two different procedures. Mallory et al.¹⁴ reported a procedure to produce **26** by treatment of **28** with

sodium dichromate in acetic acid for 2 h at 80 °C. The precipitate was then added to boiling aqueous sodium carbonate, then the mixture was dissolved in chlorobenzene at 55 °C. This was followed by the addition of aqueous sodium bisulfite to the mixture which was then stirred for 1 h. The resulting mixture was treated then with 25 mL of 1.0 M of hydrochloric acid then the solid residue was recrystallized from chlorobenzene to obtain dibromoacenaphthenequinone (**26**) as yellow crystals in 25% yield. However, the other reported procedure which was used to obtain **26** was that of Tasmer and coworkers.¹⁵ In their procedure, chromium trioxide was added in portions to a solution of dibromacenaphthene (**28**) in acetic anhydride. The solution then was stirred at 140 °C for 3 h, then allowed to cool to 0 °C followed by adding 1.0 M hydrochloric acid to the resulting mixture. After work-up, the resulting crude mixture was recrystallized from glacial acetic acid to afford **26** in 56% yields, which was higher than those obtained by the Mallory procedure.

4.3.3 Synthesis of dimethoxyacenaphthenequinone (**30**)



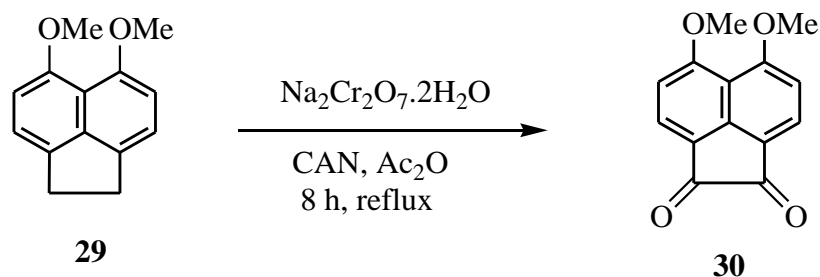
Scheme 4.10. Synthesis of 5,6-dimethoxyacenaphthene-1,2-dione (**30**).

Dimethoxyacenaphthene (**29**) was synthesized using a modified Ulman coupling reaction as described by AlHujran et al.¹ Several attempts were undertaken to produce dimethoxyacenaphthenequinone (**30**): Treatment of **29** at room temperature with sodium periodate using ruthenium chloride hydrate in a mixture of solvents consisting of DCM, THF and water in a 1:1:1 ratio, was the first failed attempt to produce **30**.¹⁶ Although chromium trioxide could oxidize dibromoacenaphthene successfully to obtain **27**, when the same reagent was also employed to try to produce **30** from **29** using various conditions with different solvents and catalysts, none of the desired product was obtained. Table 4.1 is a summary of the failed attempts to form **30** using chromium trioxide.¹⁵

Table 4.1. Summary of attempts to obtain dimethoxyacenaphthenequinone (**30**) by oxidation of **29** using CrO₃.

Entry	Time (h)	Condition	Solvent	Catalyst	Product 30
1	8	reflux	Ac ₂ O	CAN	nr
2	24	reflux	Ac ₂ O	–	nr
3	8	reflux	AcOH	CAN	nr
4	24	reflux	AcOH	–	nr
5	24	reflux	CH ₃ CN	CAN	nr

CAN: ceric ammonium nitrate, nr: no reaction.

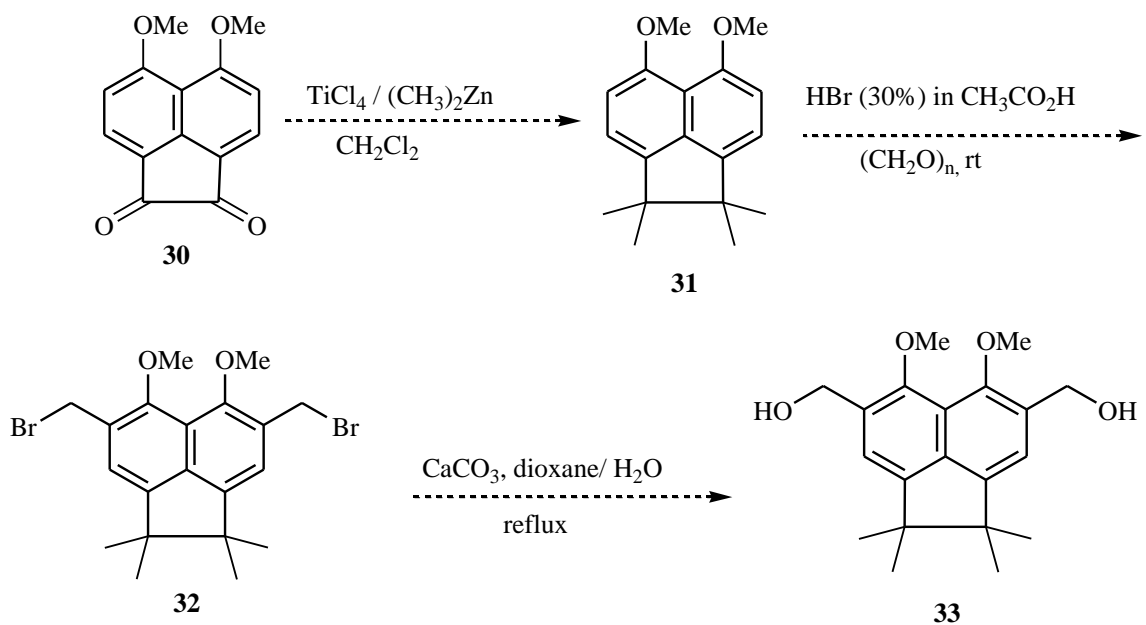


Scheme 4.11. Synthesis of dimethoxyacenaphthenequinone (**30**).

Oxidation of **29** to form dimethoxyacenaphthenequinone (**30**) finally was successfully achieved using a modification of a reported procedure.¹⁷ Sodium dichromate dihydrate in acetic acid anhydride was found to be an efficient oxidant that was used in the reported procedure to oxidize the ethylene bridge of the acenaphthene moiety. Treatment of **29** with sodium dichromate dihydrate in acetic acid anhydride for 8 h at reflux, using ceric ammonium nitrate (CAN), successfully produced **30** in yields of 50%.

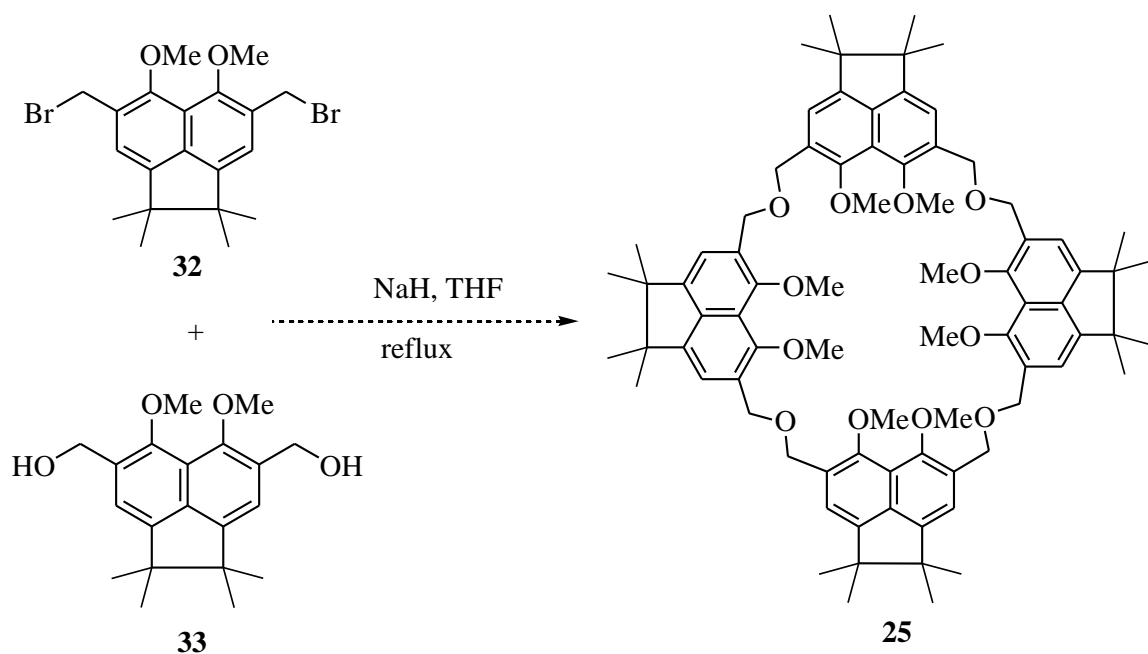
4.3.4 Projected synthesis of desired macrocycle **25**

The next step proposed for the synthesis of **25**, requires the *gem* dimethylation of **30** via a Rietz reaction¹⁸ using titanium tetrachloride and dimethylzinc in dichloromethane to produce **31**. Subsequently, **31** should easily undergo di-bromomethylation with paraformaldehyde and 30% by mass HBr in acetic acid at room temperature to afford bis(bromomethyl)acenaphthenequinone (**32**). Reaction of **32** with calcium carbonate in dioxane and water, at reflux, should produce the corresponding bishydroxymethyl **33**. (Scheme 4.12).



Scheme 4.12. Synthesis of two intermediates **32** and **33**.

The last step to the desired macrocycle **25** requires a Williamson ether coupling reaction between **32** and **33** as has been used in the previous syntheses to produce the previously described homooxacalixarene.^{1,10} (Scheme 4.13). Work in this project was suspended, as dimethoxyacenaphthene **29** was diverted in order to produce the triazole-bridged macrocycles described in Chapter 3.



Scheme 4.13. Williamson ether synthetic approach to desired macrocycle **25**.

4.4 Conclusions and future work

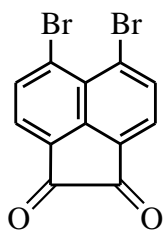
The attempts at the synthesis of the target macrocycle **25** are still ongoing. However, the important oxidation of 5,6-dimethoxyacenaphthene (**29**) to produce the corresponding diketone **30** has been achieved. The synthetic step for the *gem* demethylation of the acenaphthenequinone is still under investigation at the time of the writing of this thesis.

4.5 Experimental section

General experimental conditions are described in Chapter 2.

4.5.1 Experimental

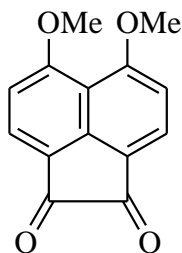
5,6-Dibromoacenaphthene-1,2-dione (**26**)



26

5,6-dibromoacenaphthene-1,2-dione (**26**) was prepared and described by Mallory et al.¹⁴

5,6-Dimethoxyacenaphthene-1,2-dione (**30**)



30

Ceric ammonium nitrate (CAN) (100 mg) was added to a mixture of **29** (100 mg, 0.467 mmol) and sodium dichromate dihydrate (800 mg, 2.80 mmol) in 20 mL of acetic anhydride. The mixture was stirred at reflux for 8 h under N₂. The reaction mixture was cooled to room temperature, followed by addition of ethyl acetate (100 mL) and water (50 mL). The organic layer was separated and washed with aqueous 40% by mass NaCO₃. After the organic extract was dried over anhydrous MgSO₄ and filtered, the

solvent was removed using a rotavap. The residue was purified by simple column chromatography (silica gel), eluting with ethyl acetate:hexane (60:40) to give a colorless solid (55 mg, 50%, m.p. 324.2 °C). ^1H NMR (CDCl_3 , 300 MHz): δ = 4.11 (s, 6H), 7.08 (d, J = 9 Hz, 4H), 8.59 (d, J = 9, 4H). ^{13}C NMR (CDCl_3 , 75.46 MHz): δ = 56.7, 99.9, 106.8, 110.2, 110.4, 136.4, 161.2, 164.4. APCI (+) MS (m/z): 243.1 (M^+).

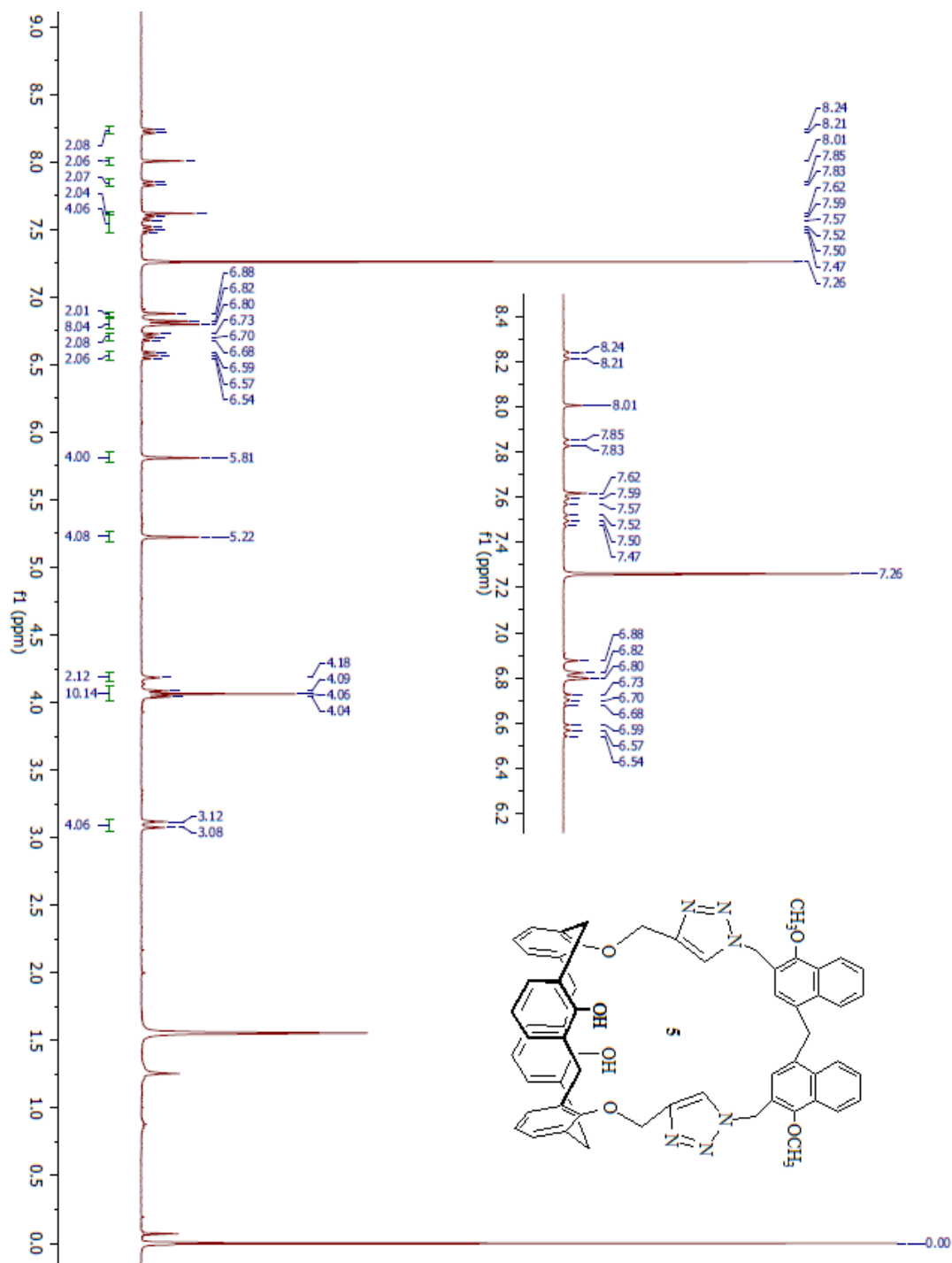
4.6 References

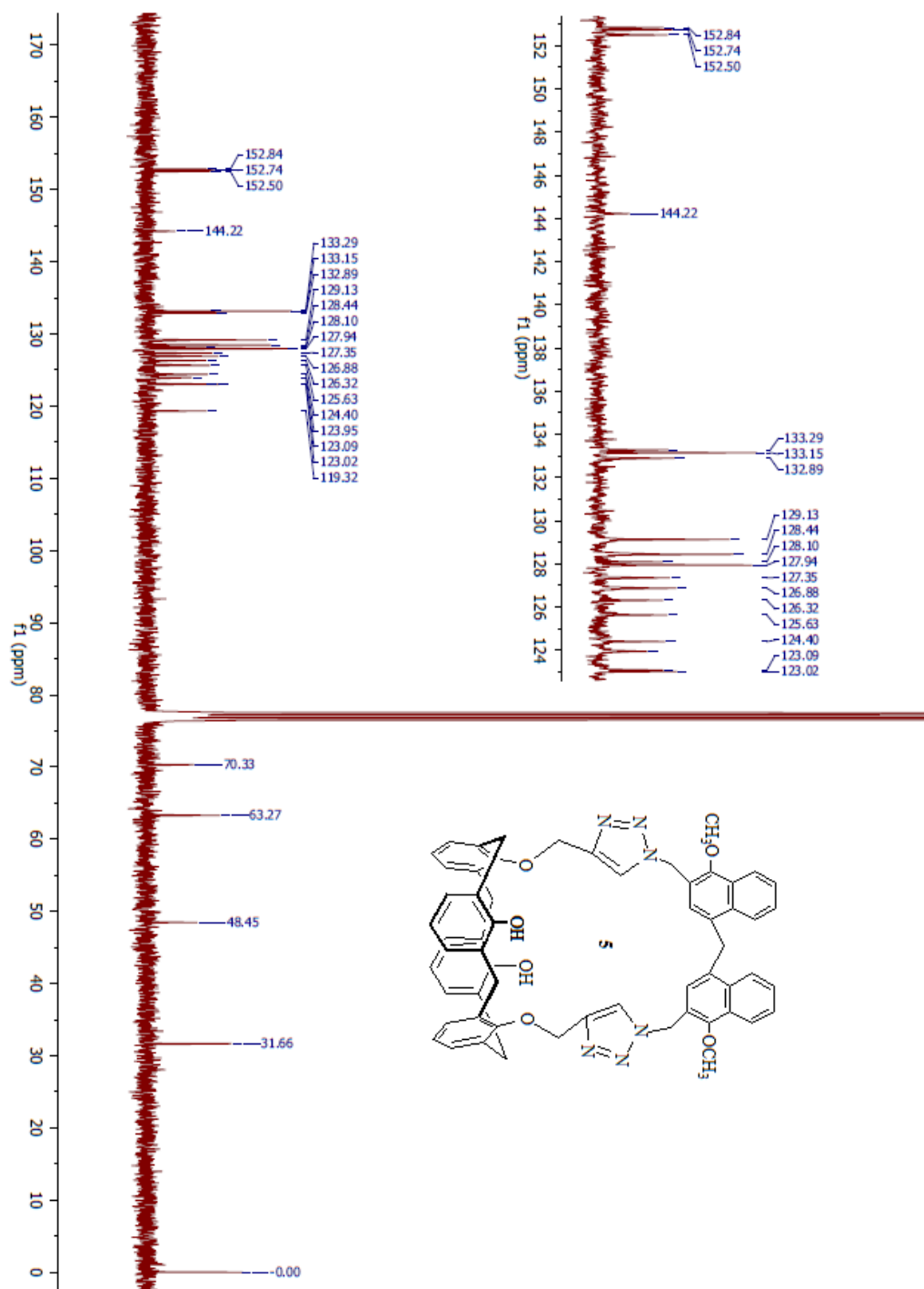
1. AlHujran, T.; Dawe, L. N.; Georghiou, P. E. *Org. Lett.* **2012**, *14*, 3530-3533.
2. (a) Georghiou, P. E.; Li, Z. *Tetrahedron Lett.* **1993**, *34*, 2887-2890. (b) Georghiou, P. E.; Li, Z. *J. Incl. Phenom. Mol. Recogni. Chem.* **1994**, *19*, 55-60.
3. Li, Z. Ph. D. Dissertation, Memorial University of Newfoundland, 1996.
4. Ashram, M. Ph.D. Dissertation, Memorial University of Newfoundland, 1997.
5. Georghiou, P. E.; Ashram, M.; Li, Z.; Chaulk, S. G. *J. Org. Chem.* **1995**, *60*, 7284-7289.
6. Andreetti, G. D.; Bohmer, V.; Jordan, G.; Tabatabai, M.; Ugozzoil, F.; Vogt, W.; Wolff, A. *J. Org. Chem.* **1993**, *58*, 4023-4032.
7. Georghiou, P. E.; Ashram, M.; Clase, H. J.; Bridson, J. N. *J. Org. Chem.* **1998**, *63*, 1819-1826.
8. Georghiou, P. E.; Mizyed, S.; Chowdhury, S. *Tetrahedron Lett.* **1999**, *40*, 611-614.
9. Komastu, N. *Tetrahedron Lett.* **2001**, *42*, 1733-1736.
10. Tran, A. H.; Miller, D. O.; Georghiou, P. E. *J. Org. Chem.* **2005**, *70*, 1115-1211.
11. AlHujran, T. Ph.D. Dissertation, Memorial University of Newfoundland, 2012.
12. Molecular modeling was conducted using the Merck Molecular Force Field (MMFF) with *Spartan '10* software by Wavefunction, Inc. Irvine, CA, USA.
13. Tanaka, N.; Kasai, T. *Bull. Chem. Soc. Jpn.* **1981**, *54*, 3020-3025.
14. Mallory, F. B.; Mallory, C. W.; Butler, K. E.; Lewis, M. B.; Xia, A. Q.; Luzik, E. D.; Fredenurgh, L. E.; Ramanjulu, M. M.; Van, Q. N.; Francl, M. M.; Freed, D. A.;

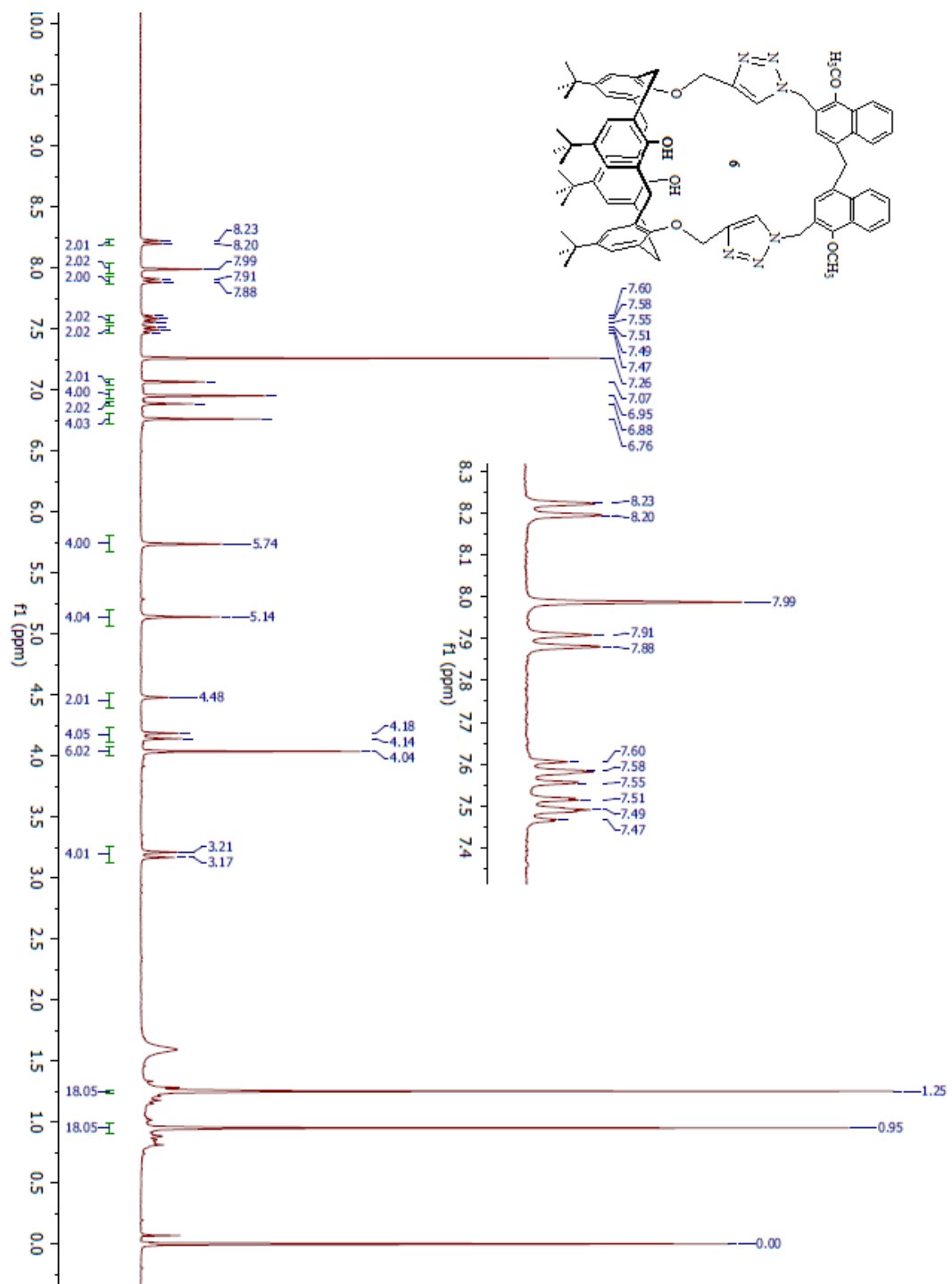
- Wray, C. C.; Hann, C.; Nerz-Stromes, M.; Carroll, P. J.; Chirlan, L. E. *J. Am. Chem. Soc.* **2000**, *122*, 4108-4116.
15. Tesmer, M.; Vahrenkamp, H. *Eur. J. Inorg. Chem.* **2001**, *5*, 1183-1188.
16. Chen, S.; Liu, Z.; Shi, E.; Chen, L.; Wei, W.; Li, H.; Cheng, Y.; Wan, X. *Org. Lett.* **2011**, *13*, 2274-2277.
17. Fieser, L. F.; Fieser, M. *Reagent of Organic Synthesis*, Wiley, New York 1967.
1162-1163.
18. Reetz, M. T.; Steinbach, R. *J. Chem. Soc. Chem. Commun.* **1981**, 237-239.

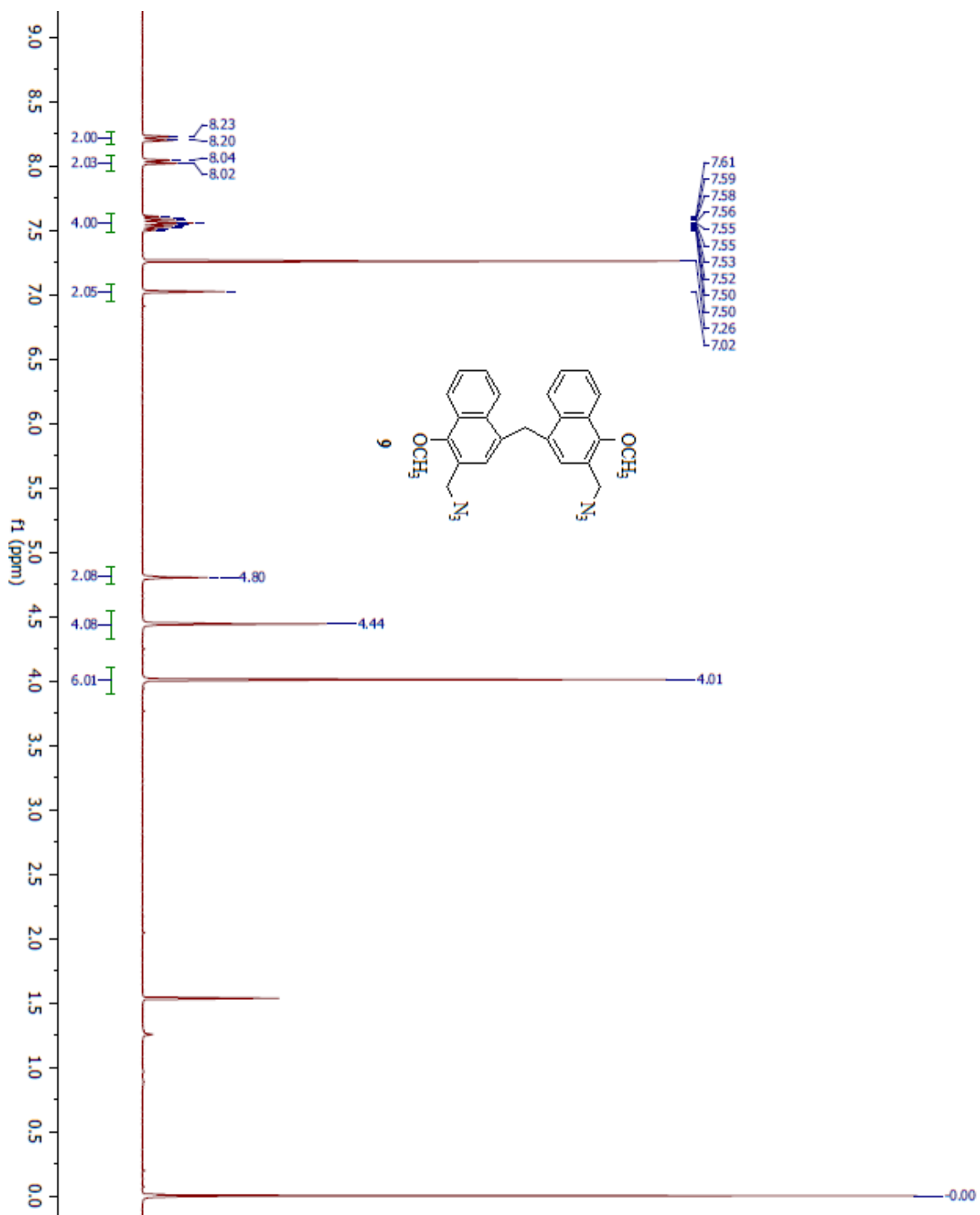
Appendix A

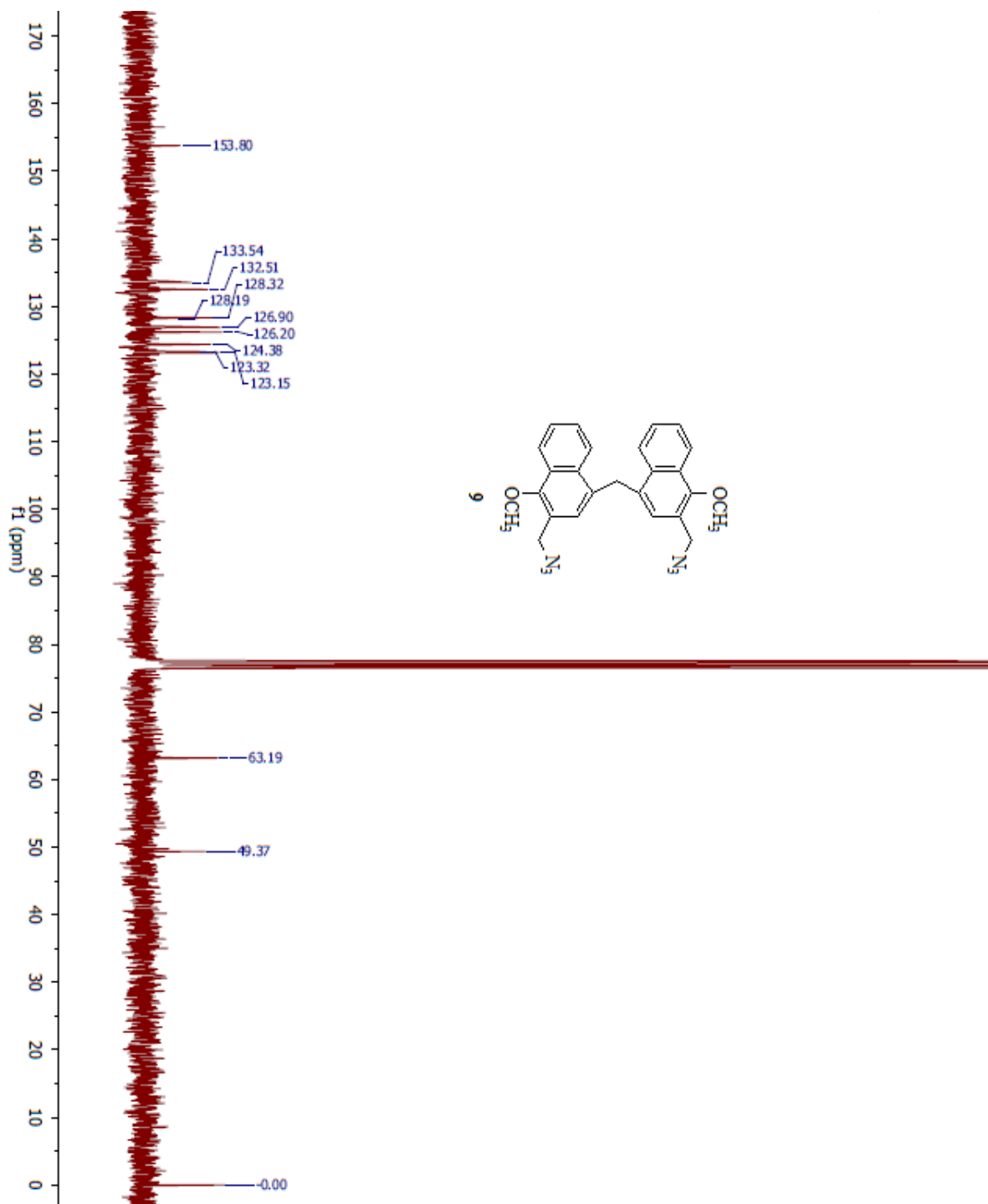
^1H , ^{13}C -NMR spectra for compounds described in Chapter 2









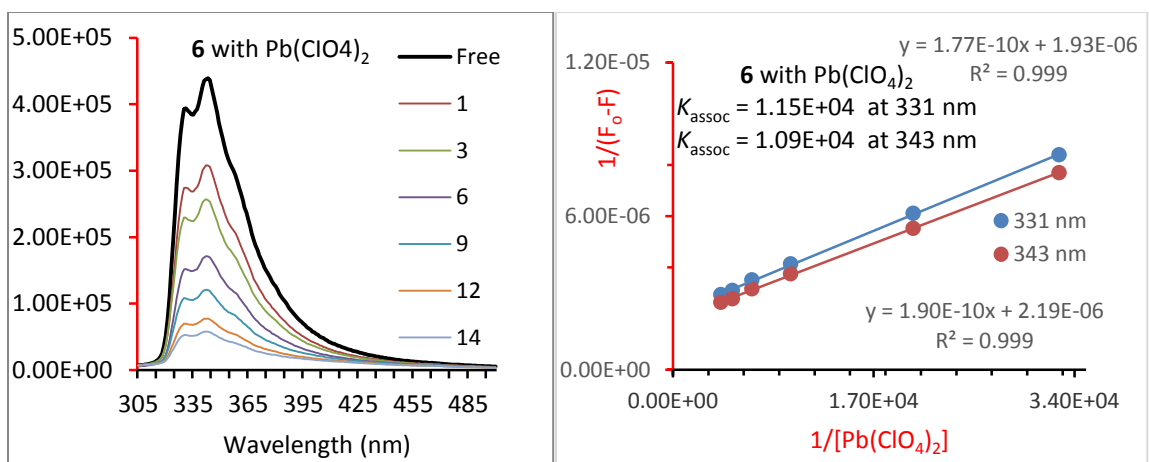


Appendix B

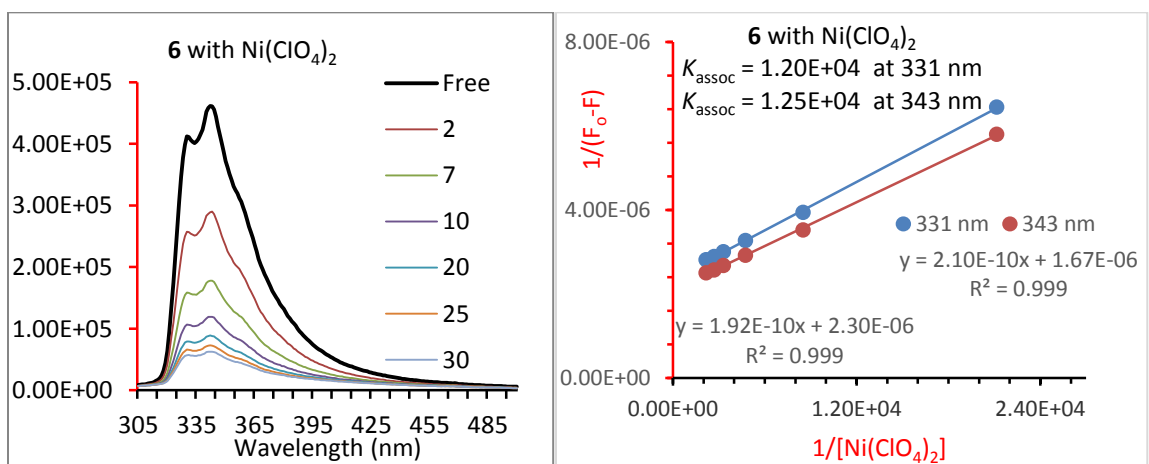
Fluorescence titration experiments of receptors in Chapter 2

Figures 2.27a-n and 2.28a-n show the titration experiments of host **6** and **5** with the metal ions tested. The K_{assoc} values which were calculated for the changes at 331 nm and 343 nm of host **6** while 330 nm and 343 nm of host **5** using the Benesi-Hildebrand plots, are also shown in the figures.

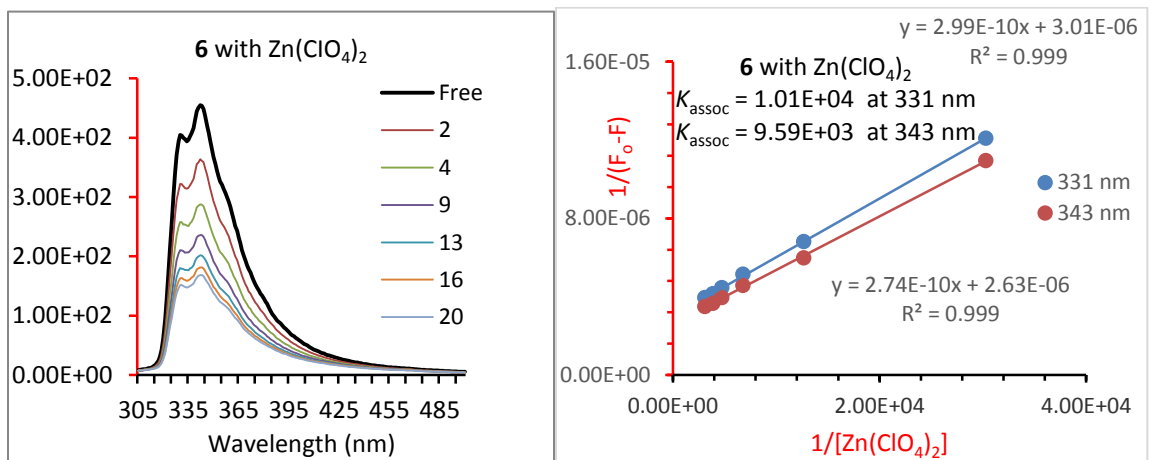
(a)



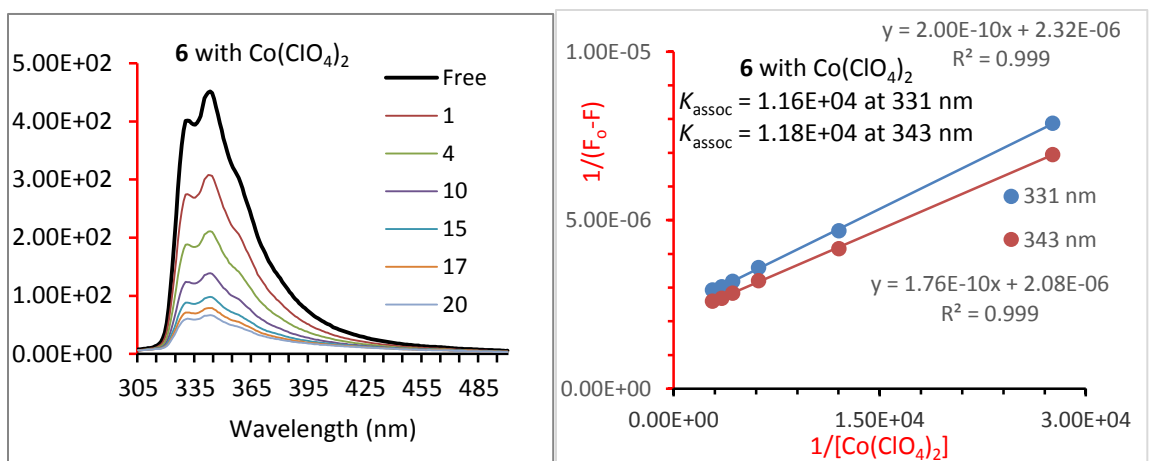
(b)



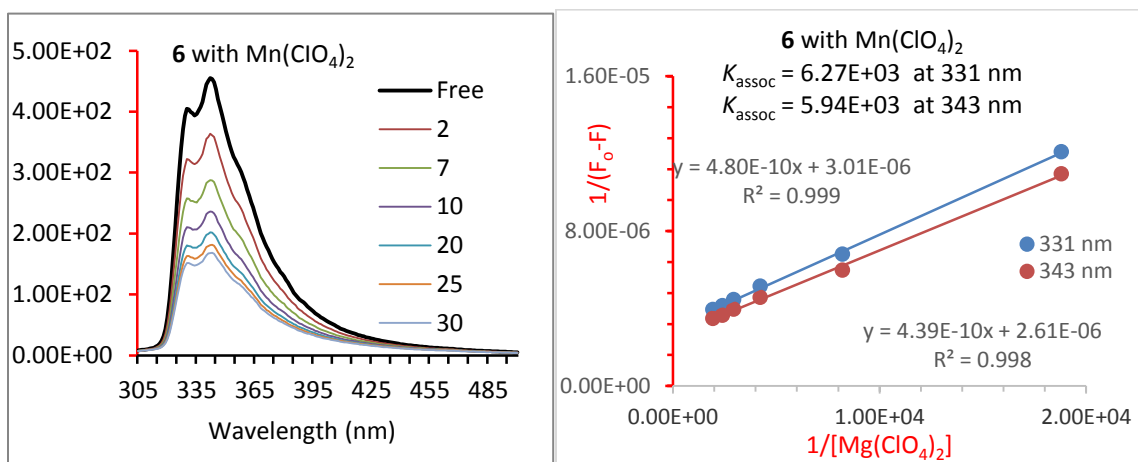
(c)



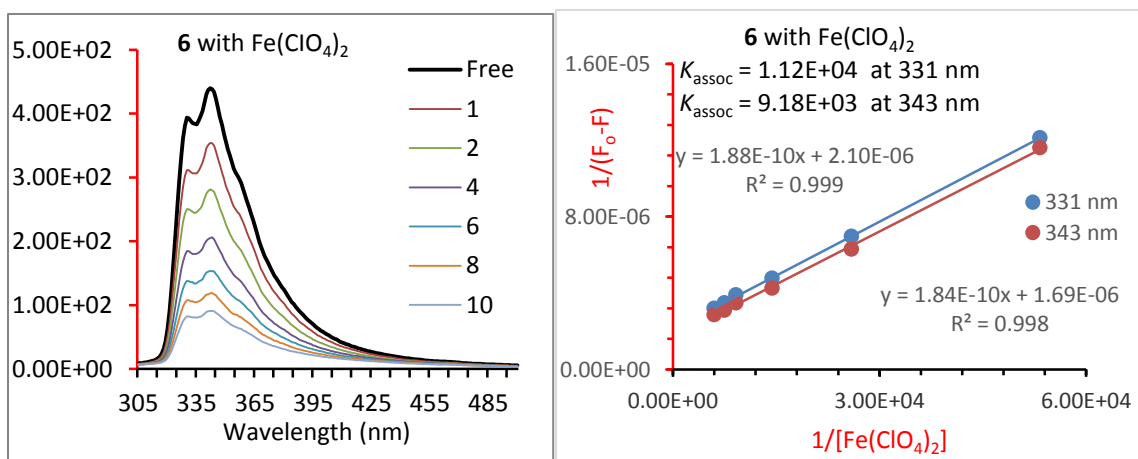
(d)



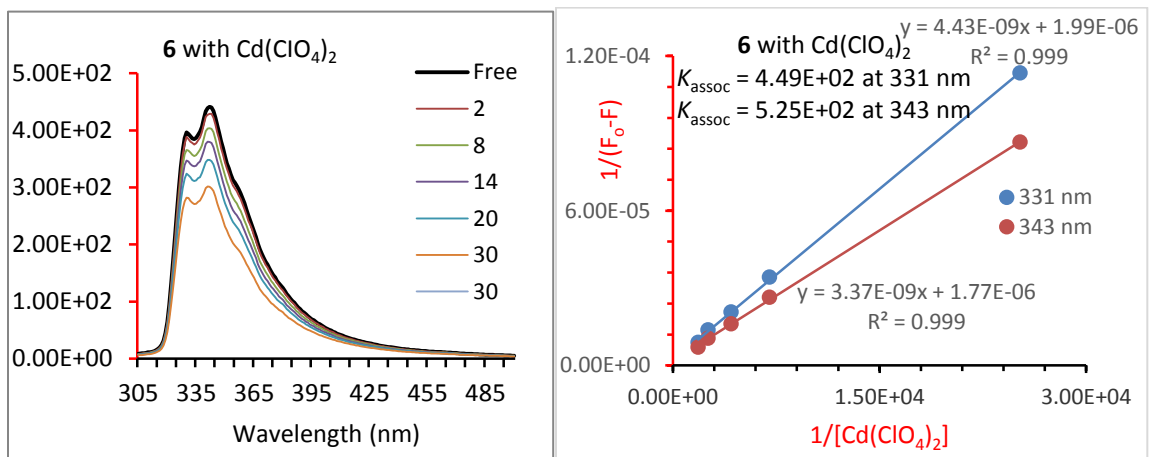
(e)



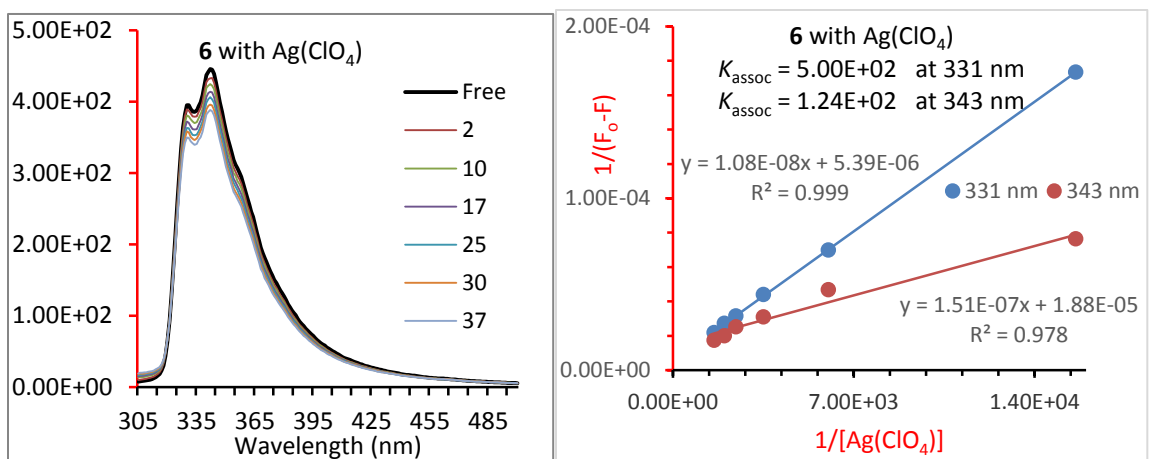
(f)



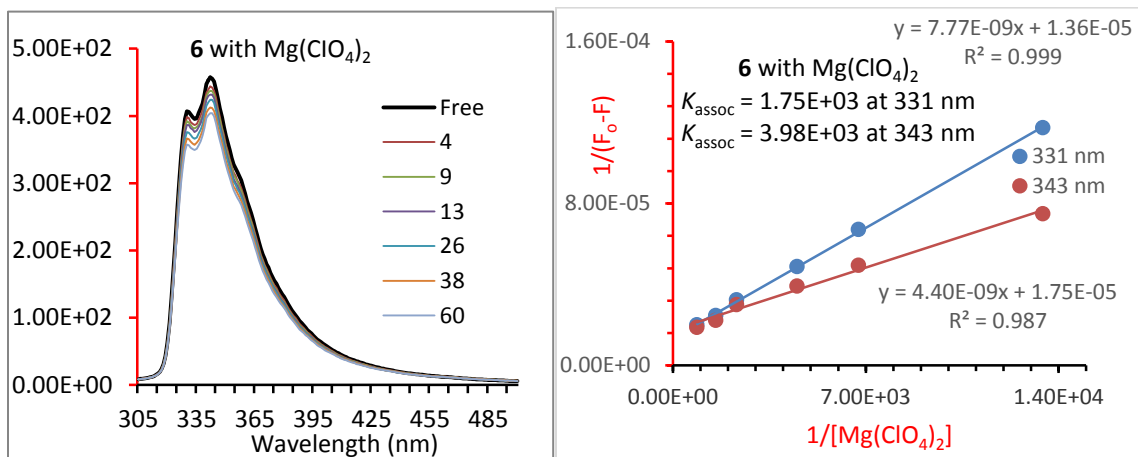
(g)



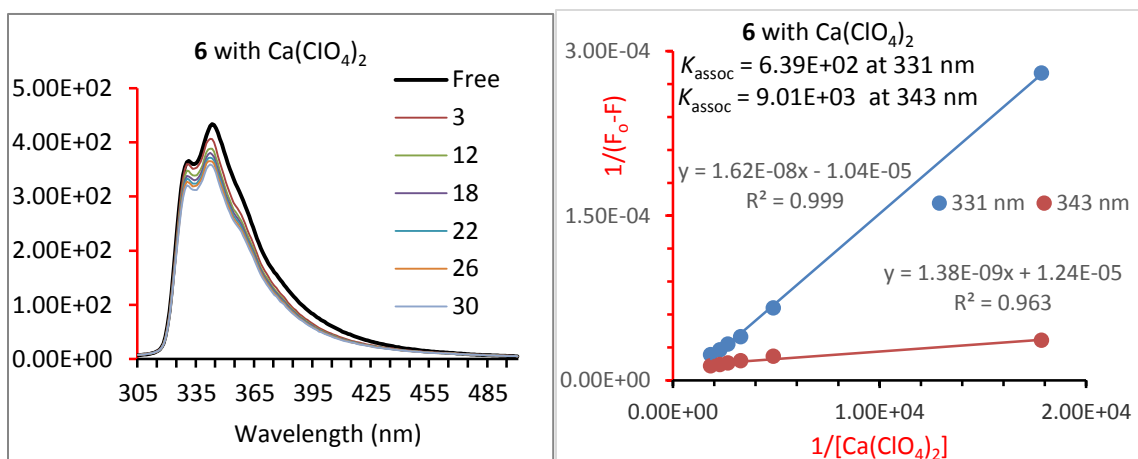
(h)



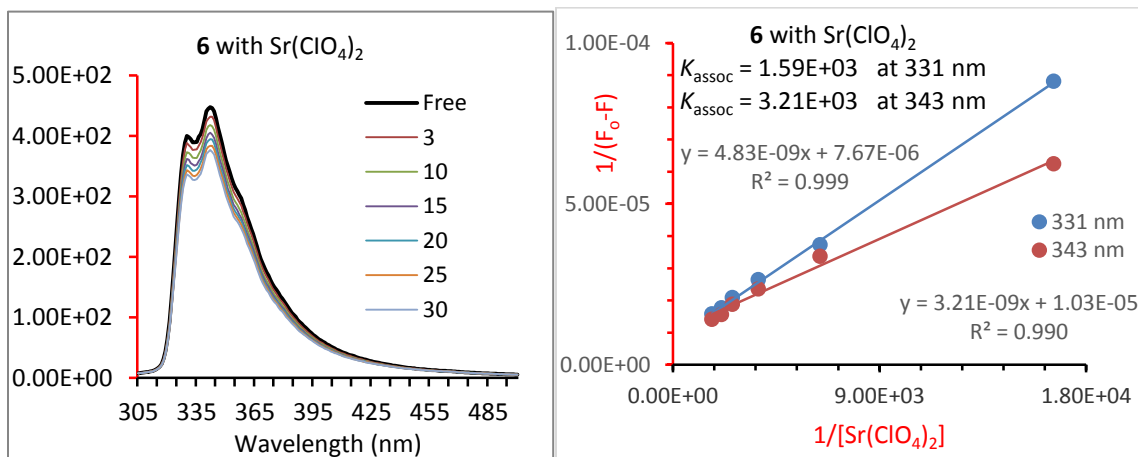
(i)



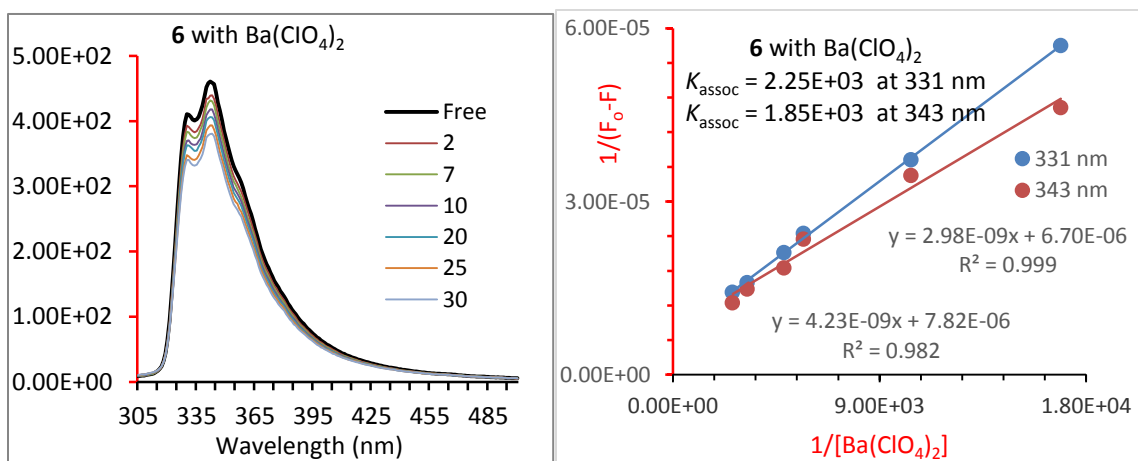
(j)



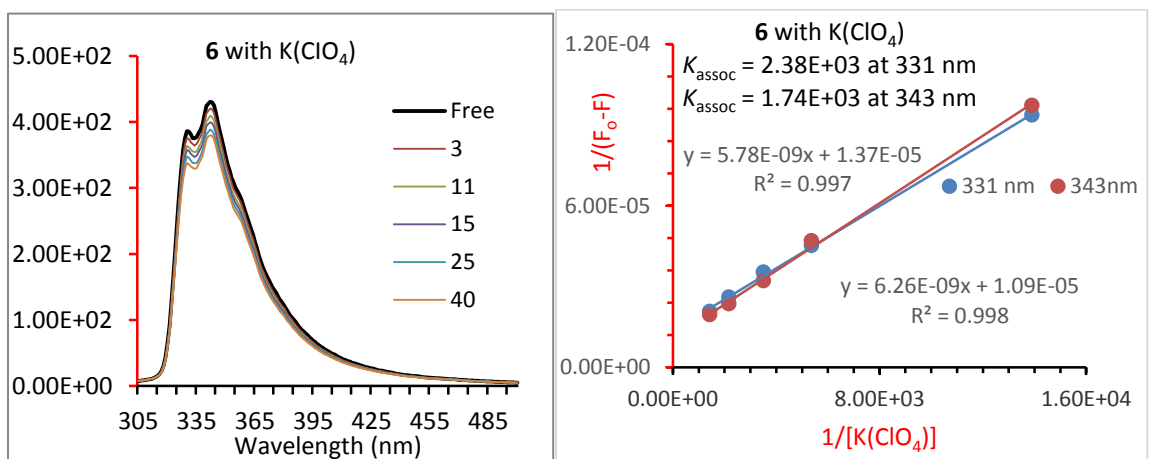
(k)



(l)



(m)



(n)

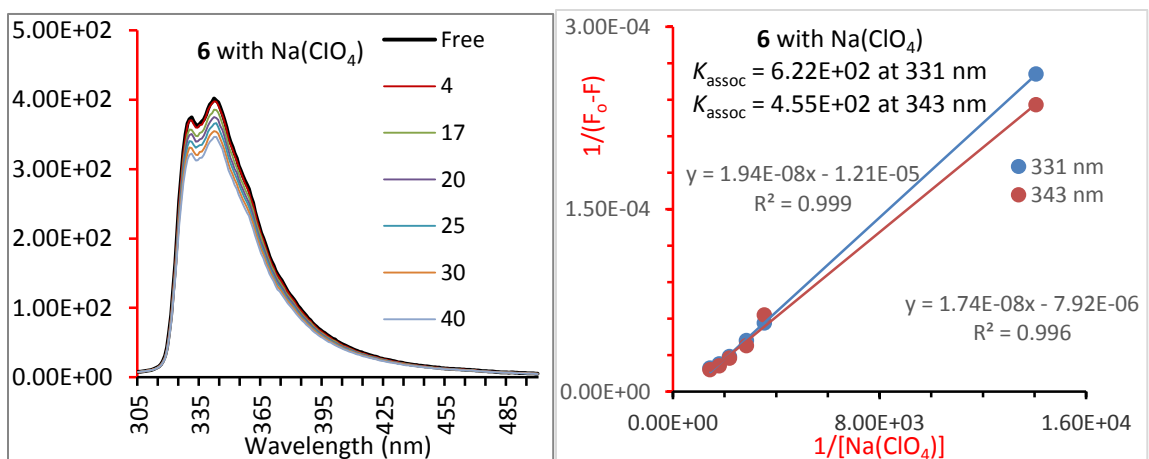
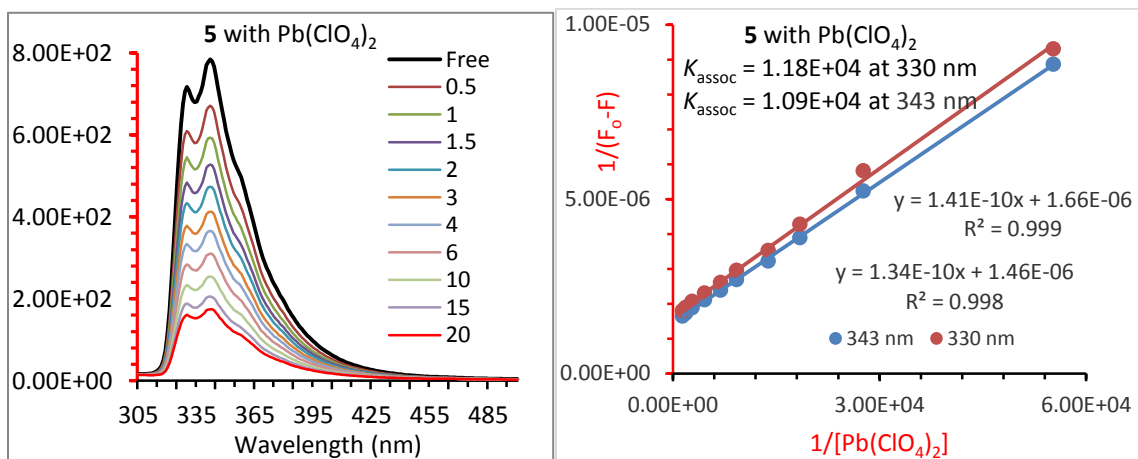
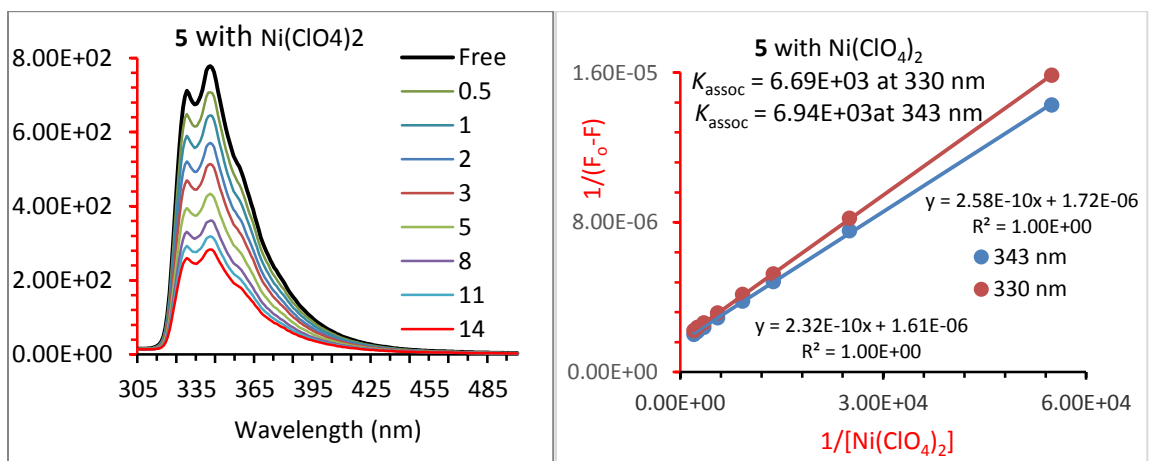


Figure 2.27. Left: Fluorescence spectra of **6** (16.4 μM) upon addition of cationic guests in acetonitrile/ chloroform (v/v= 9:1) solutions. $\lambda_{\text{ex}} = 282$ nm. Right: Benesi-Hildebrand plot of $1/(F_0 - F)$ versus $1/[\text{M}(\text{ClO}_4)]$ for **6** upon titration with metal ions. The linear fit showed a 1:1 complexation between **6** and cationic guests. The association constants were calculated for the changes at the 331 nm and the 343 nm wavelengths.

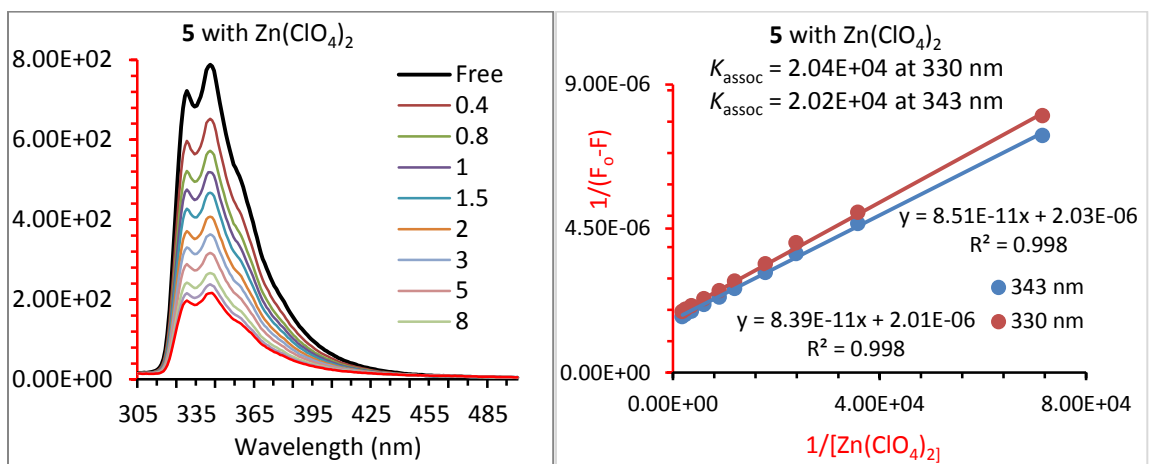
(a)



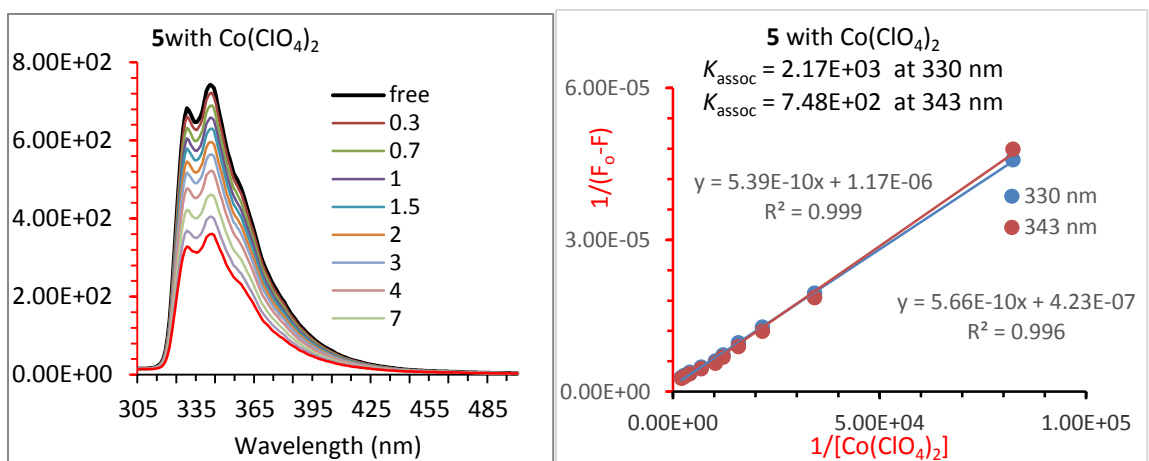
(b)



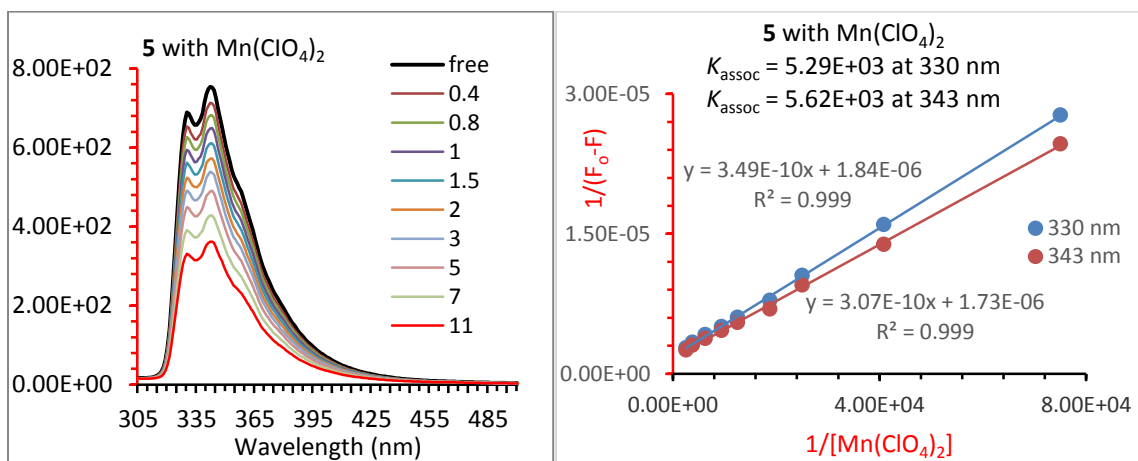
(c)



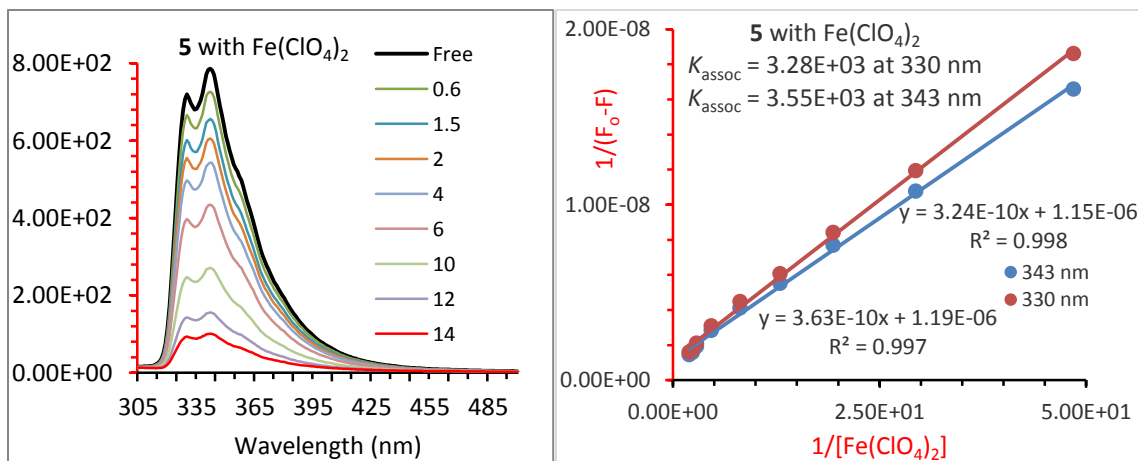
(d)



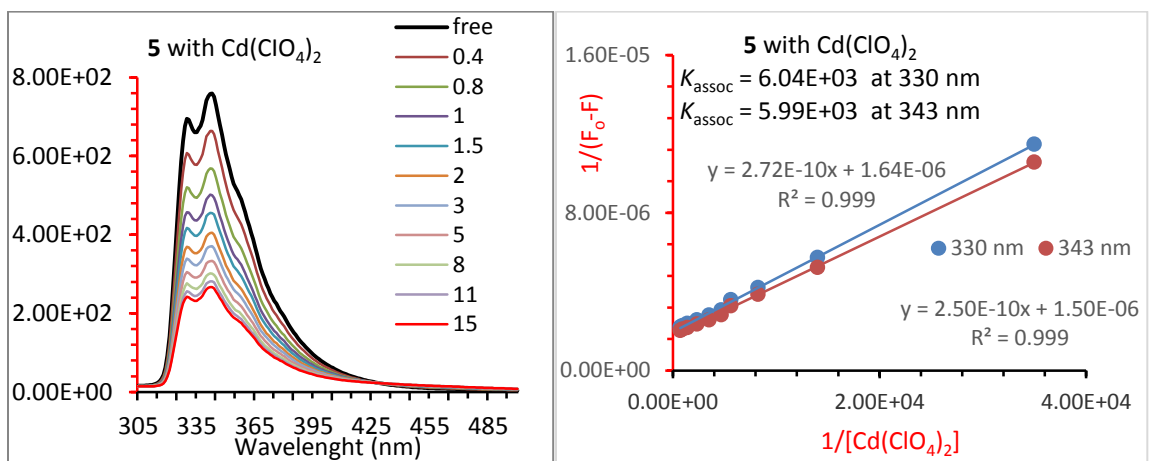
(e)



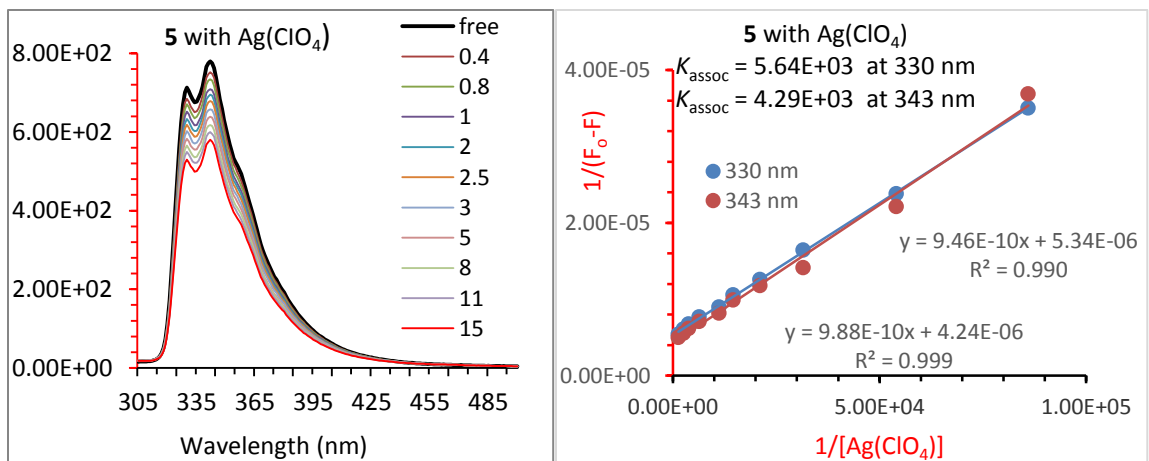
(f)



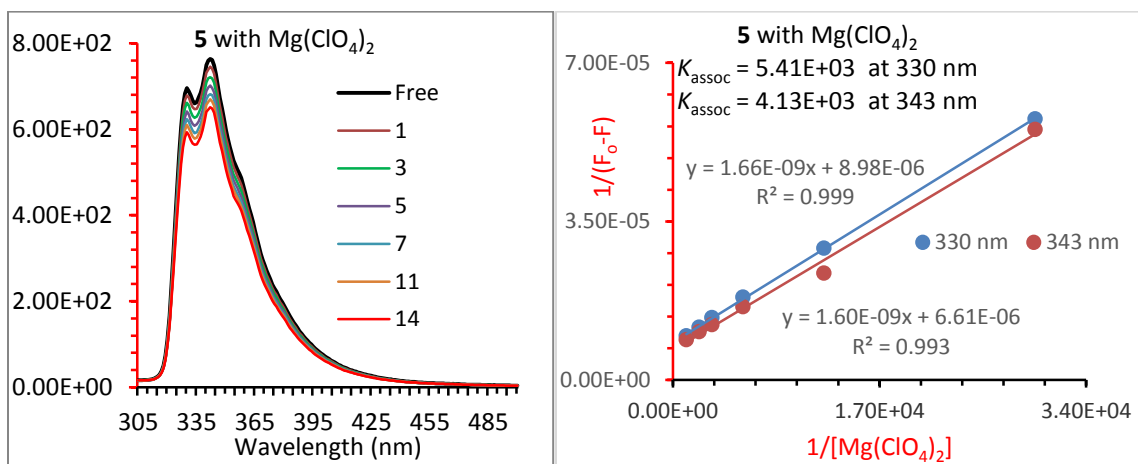
(g)



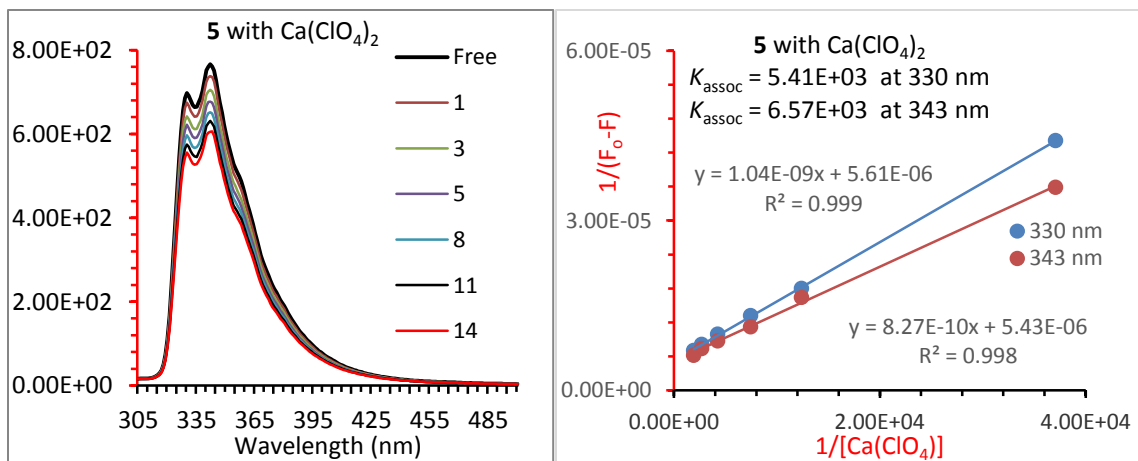
(h)



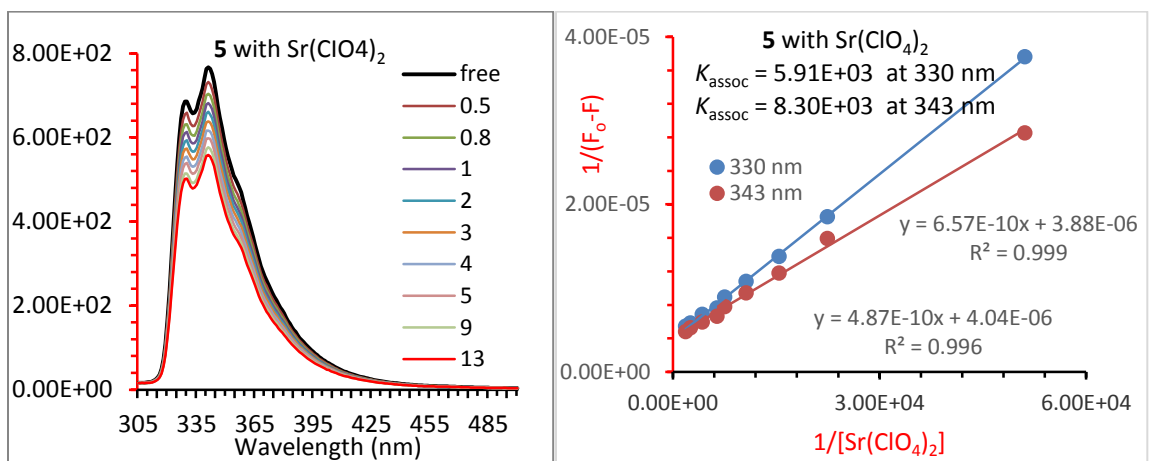
(i)



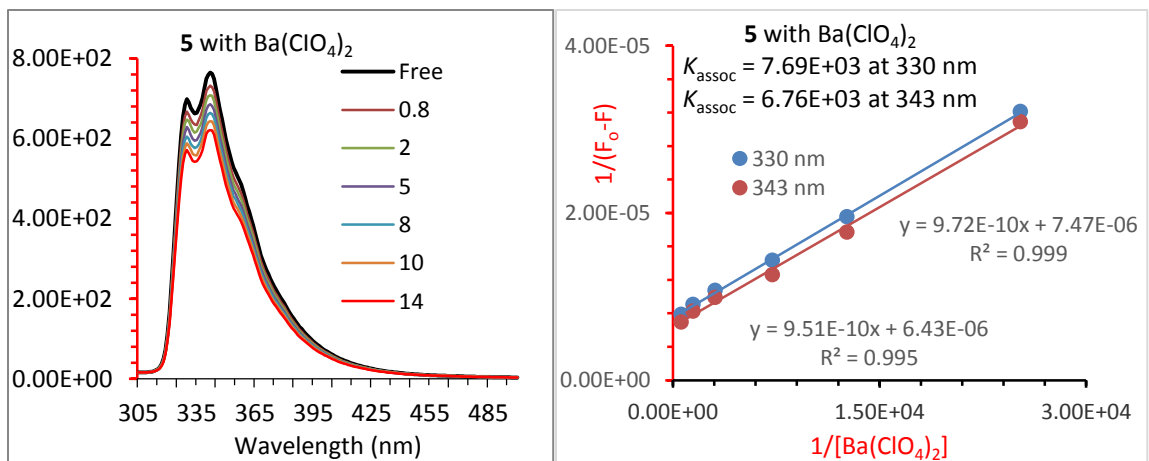
(j)



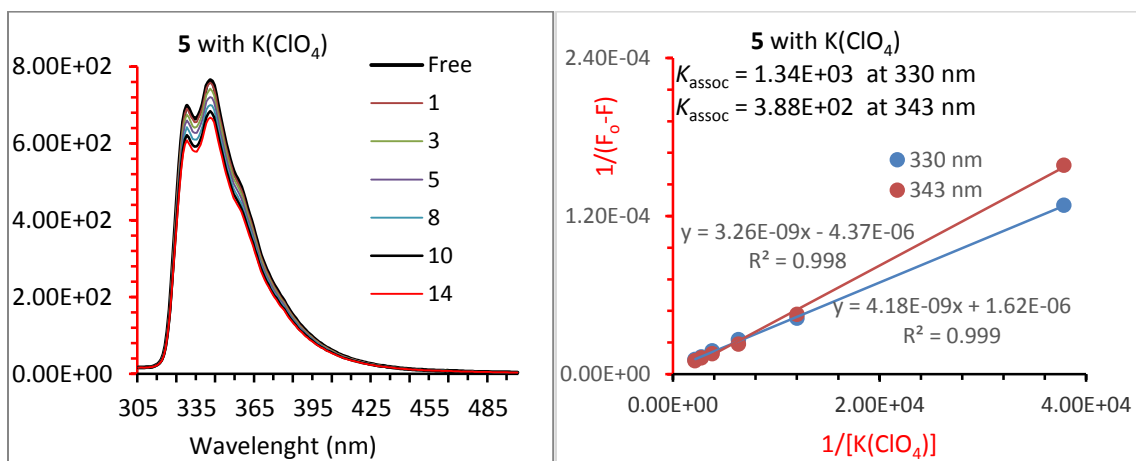
(k)



(l)



(m)



(n)

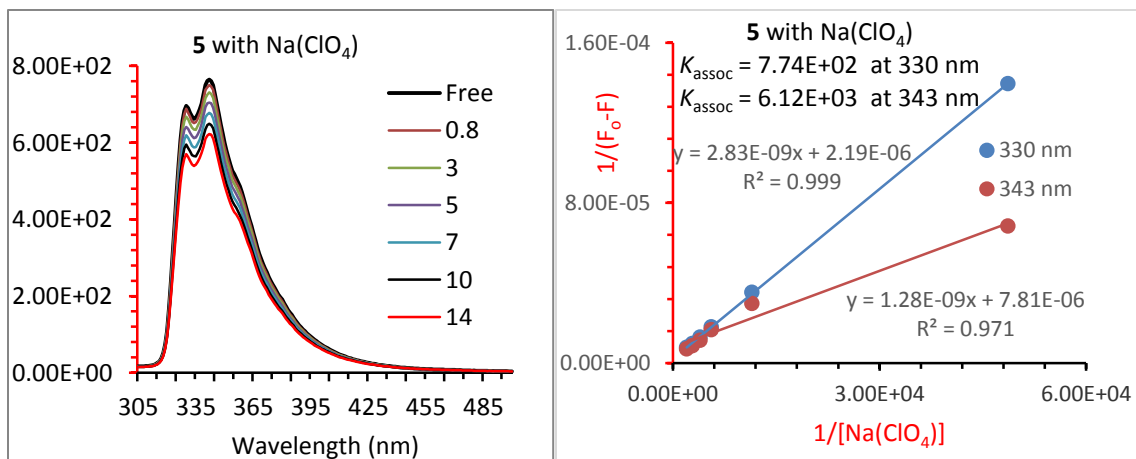
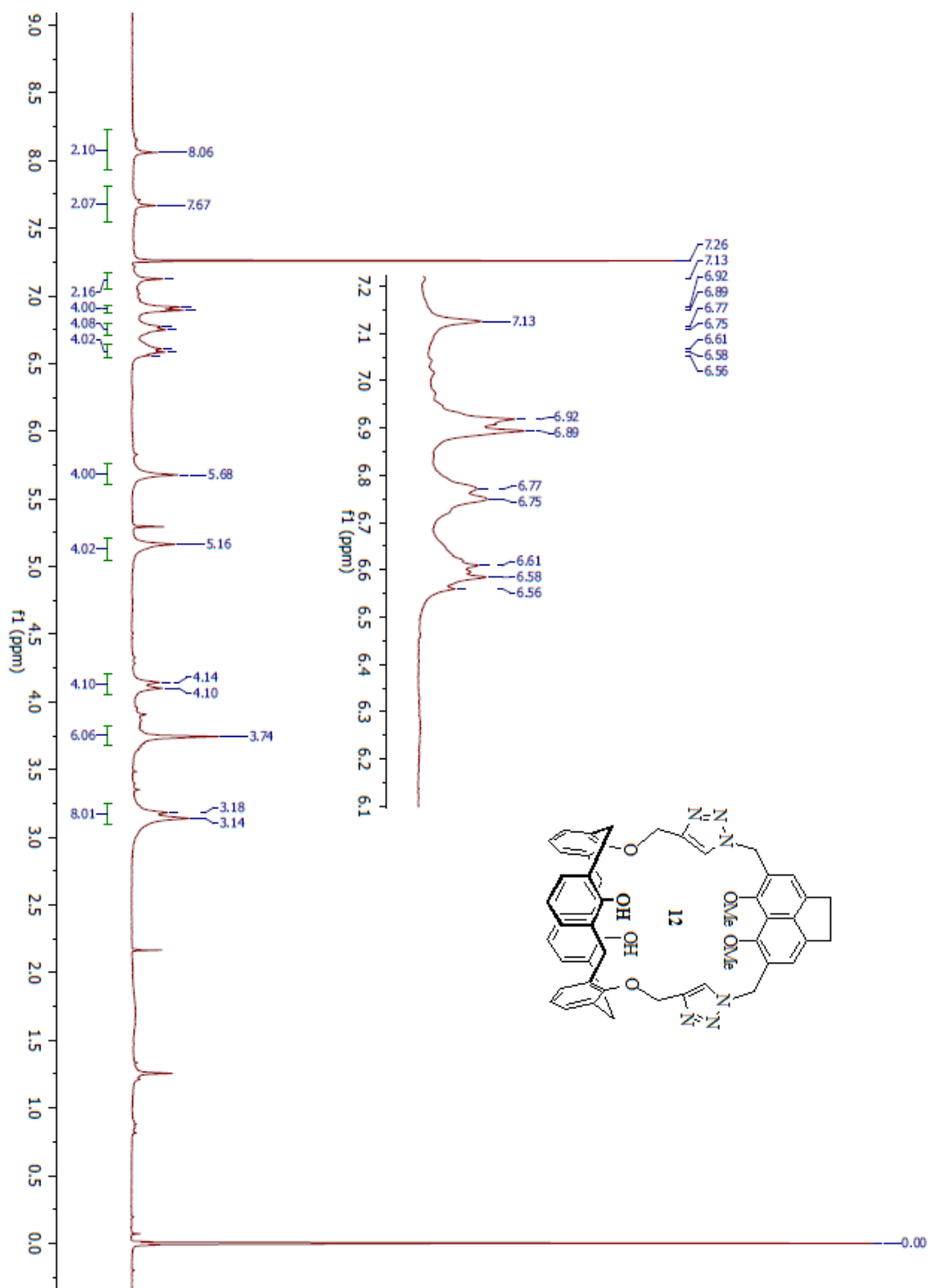
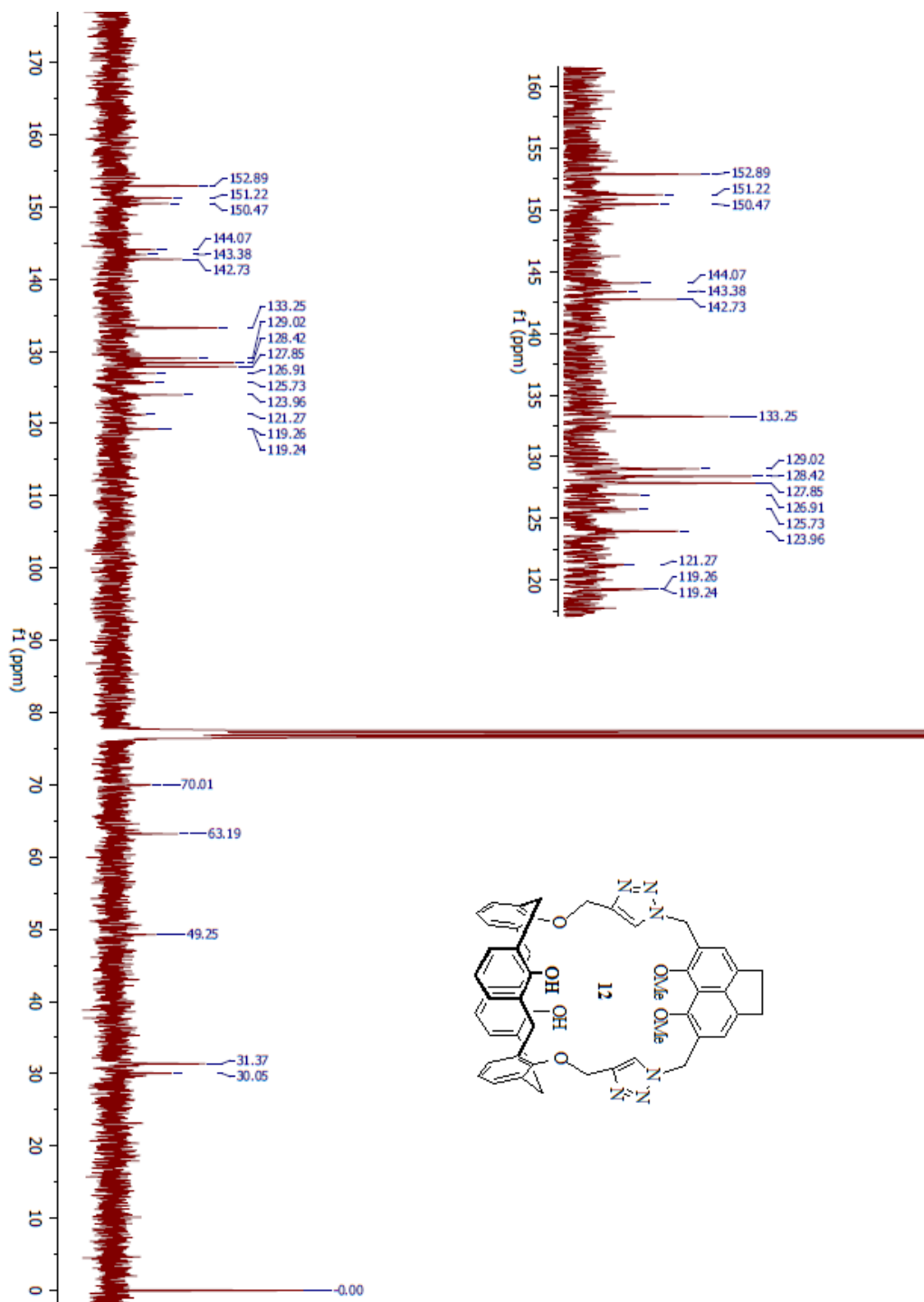


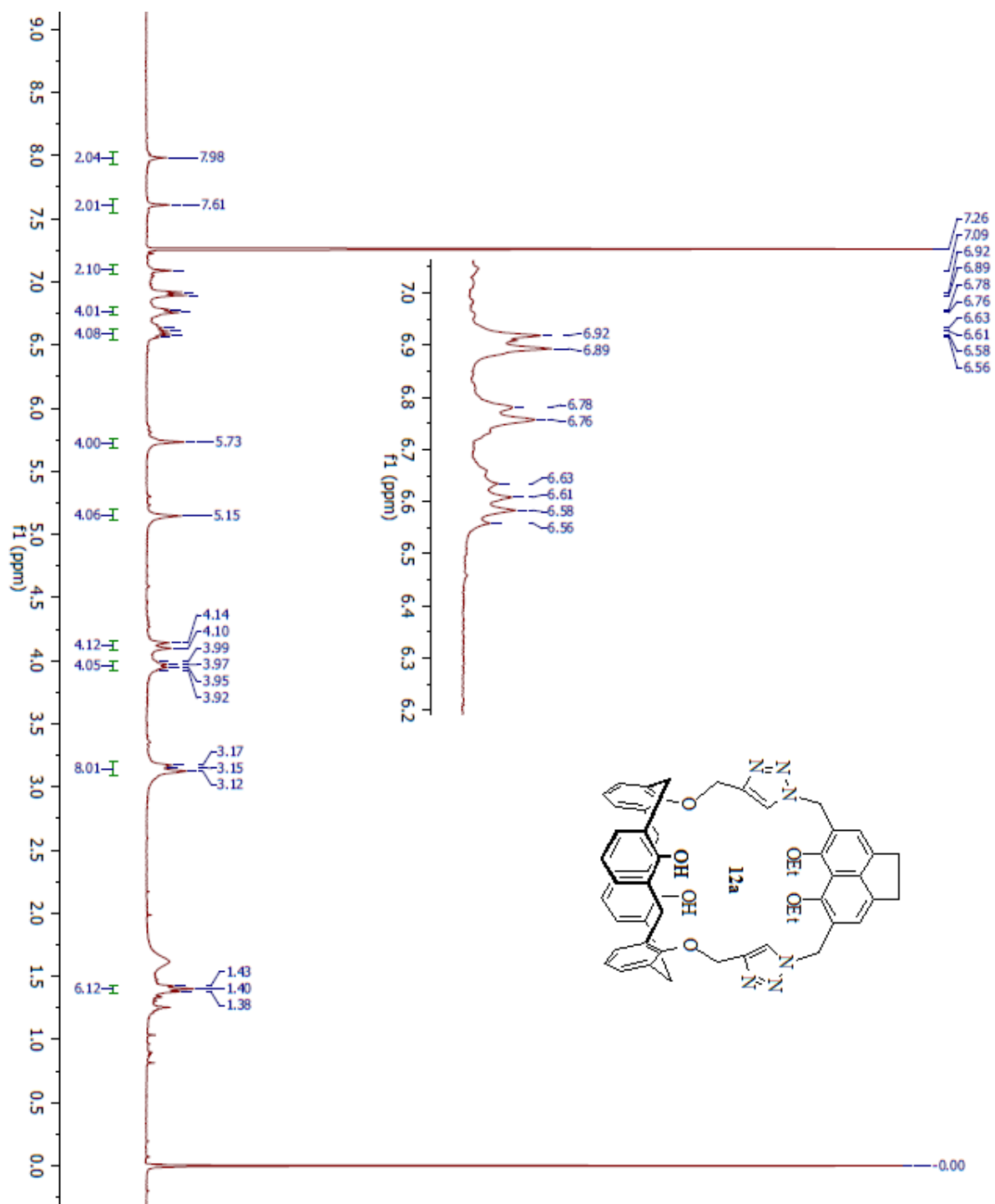
Figure 2.28. *Left:* Fluorescence spectra of **5** (34.6 μ M) upon addition of metal ions in acetonitrile/ chloroform (v/v= 9:1) solutions. $\lambda_{ex} = 284$ nm. *Right:* Benesi-Hildebrand plot of $1/(F_0 - F)$ versus $1/[M(ClO_4)]$ for **5** upon titration with metal ions. The linear fit showed a 1:1 complexation between **5** and metal ions. The association constants were calculated for the changes at the 330 nm and the 343 nm wavelengths.

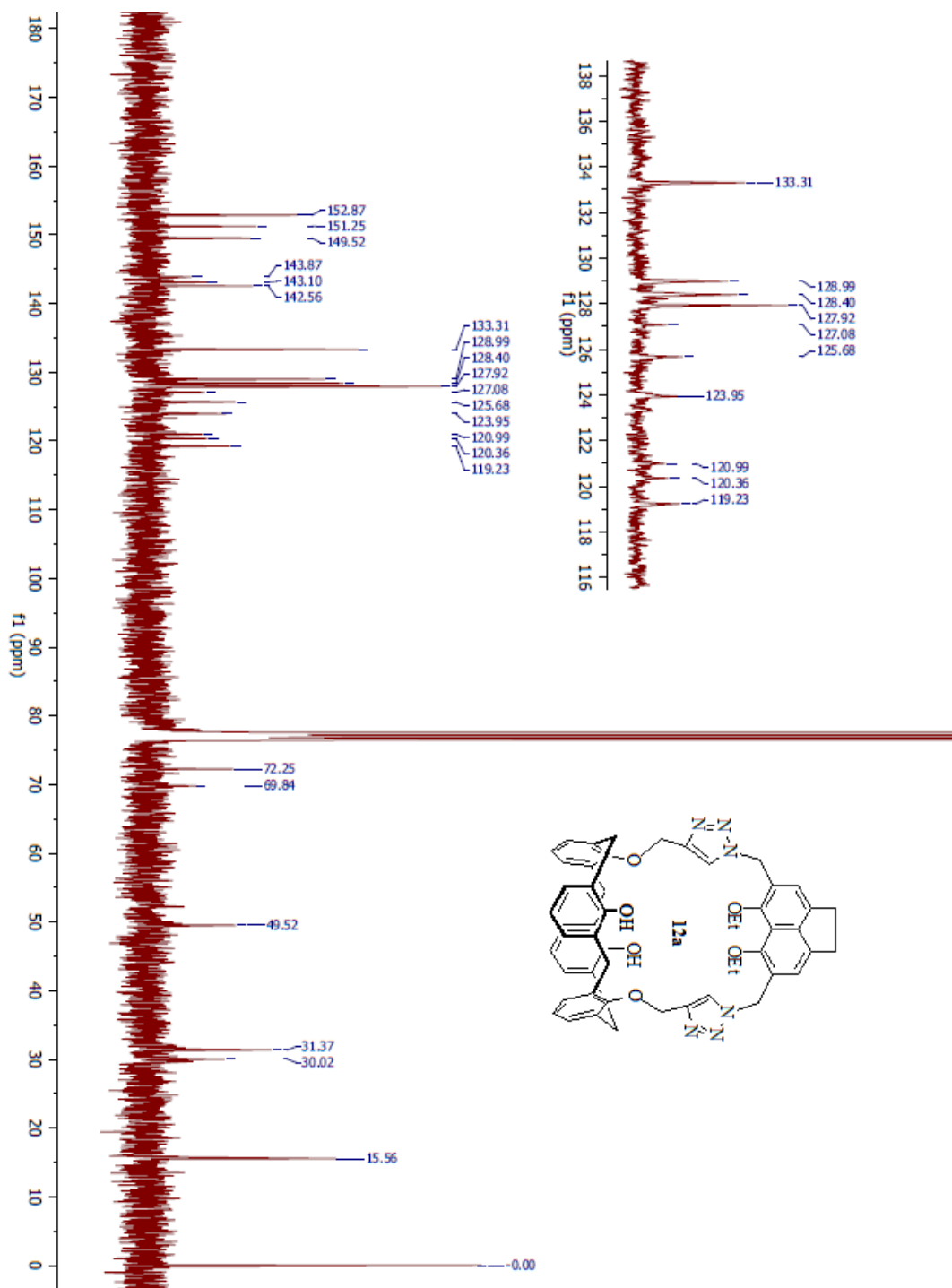
Appendix C

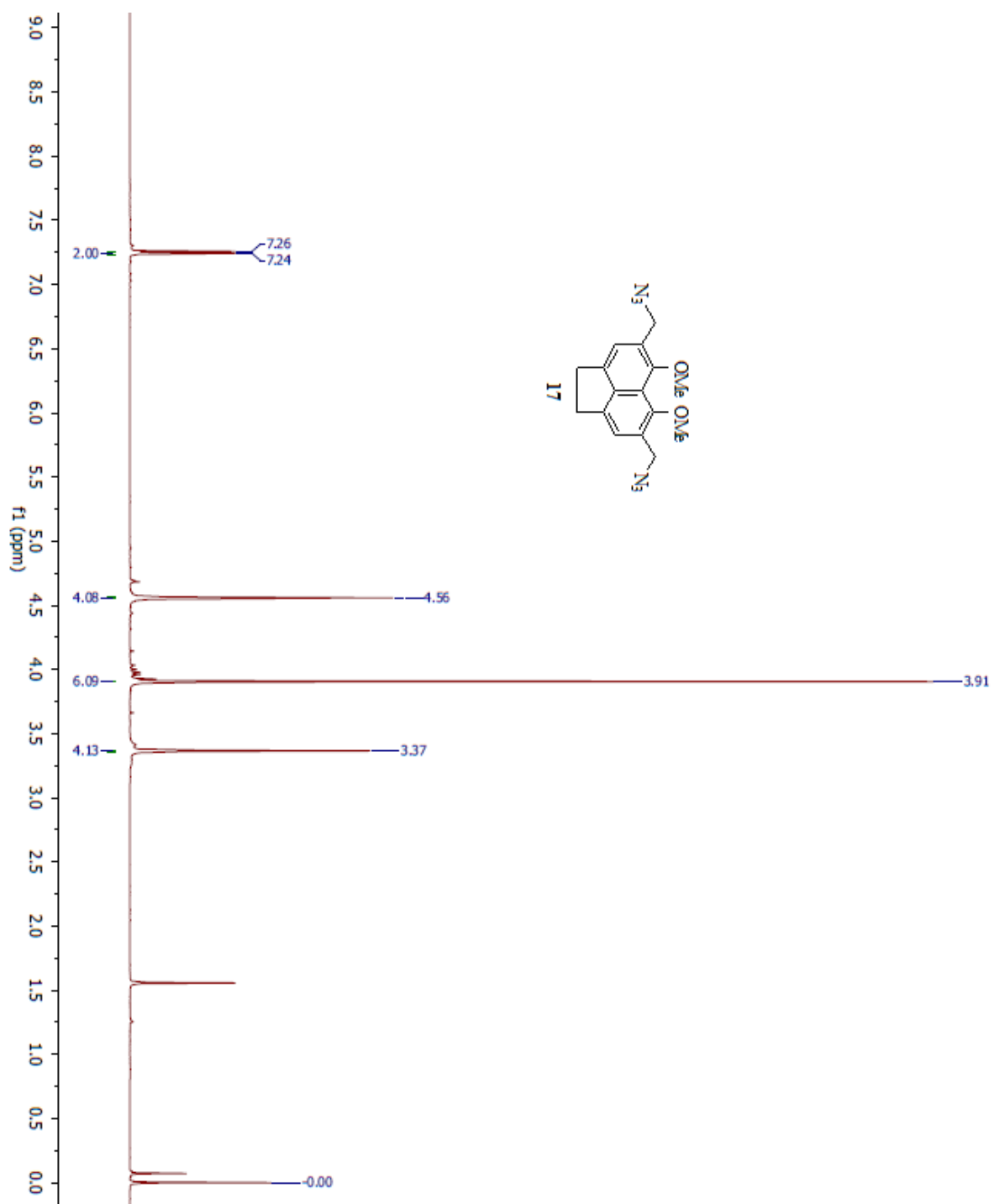
^1H , ^{13}C -NMR spectra for compounds described in Chapter 3

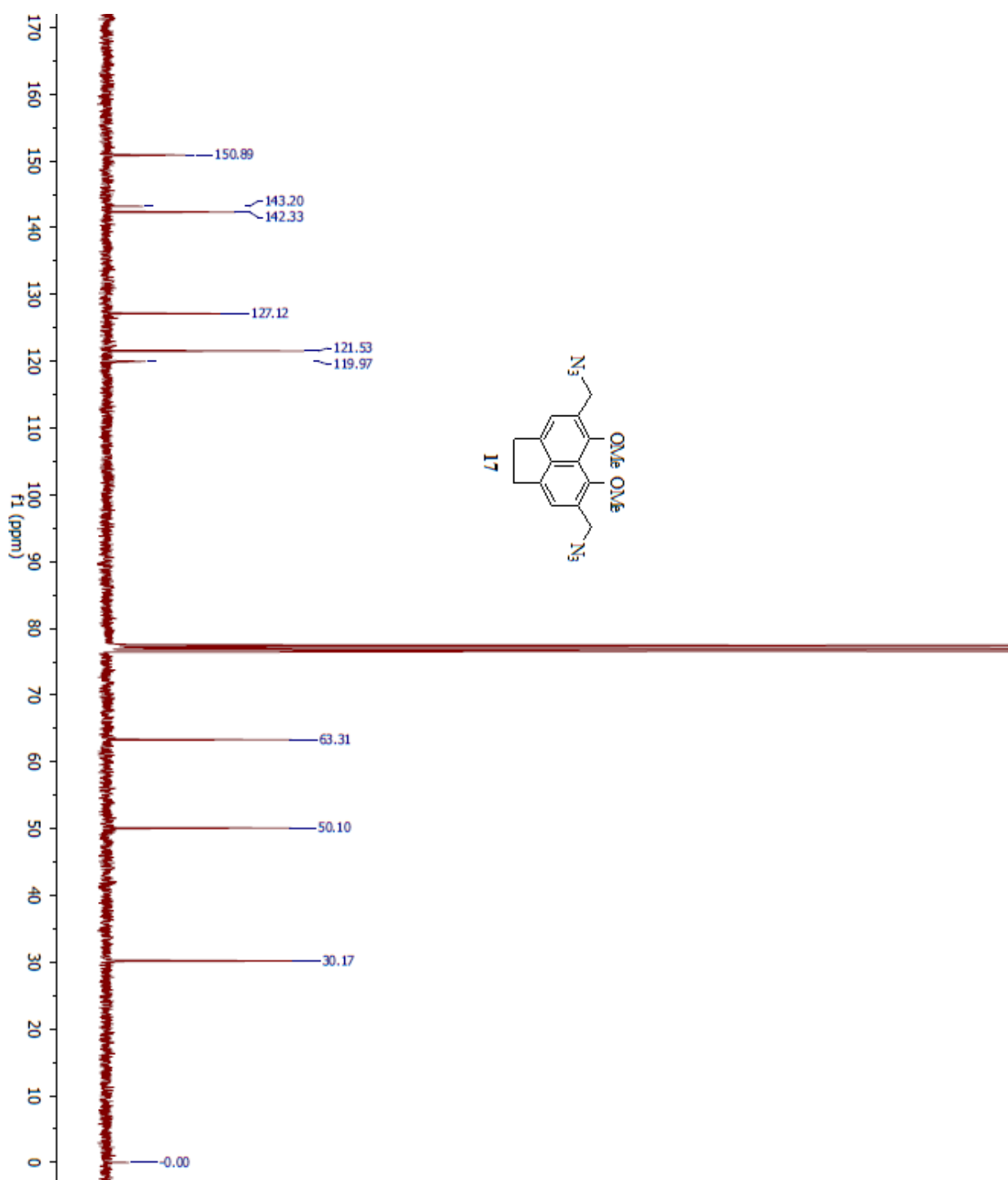


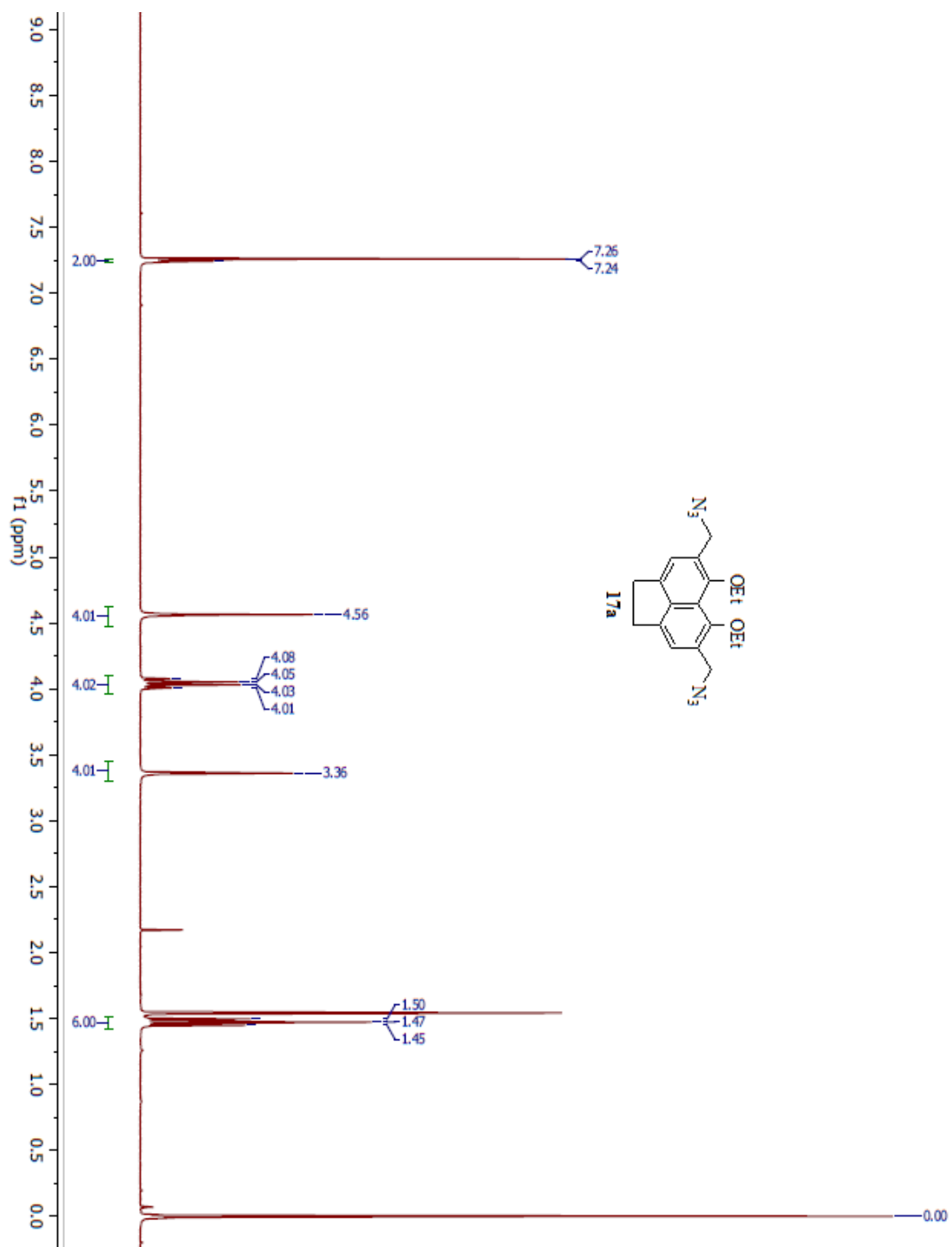


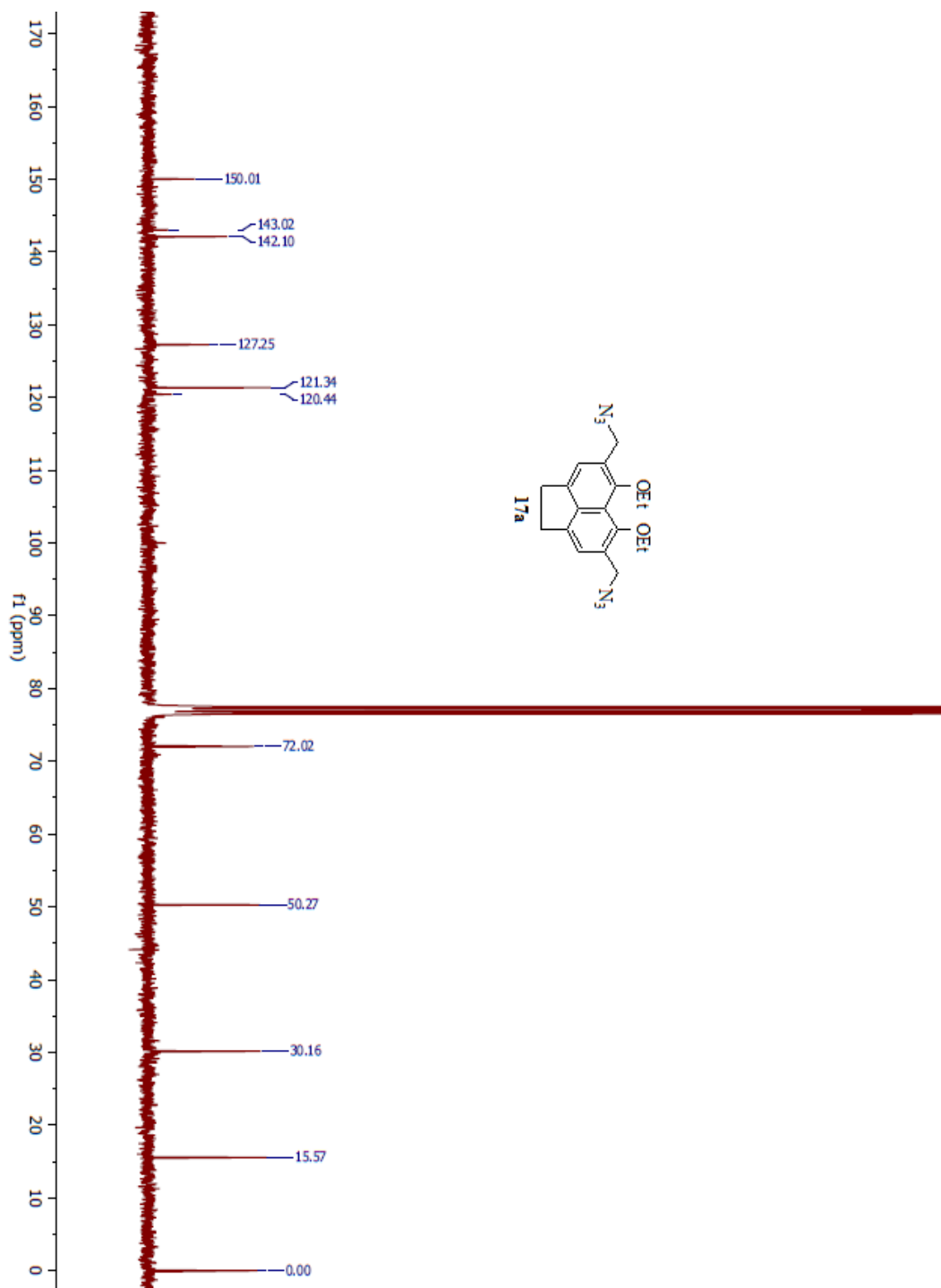


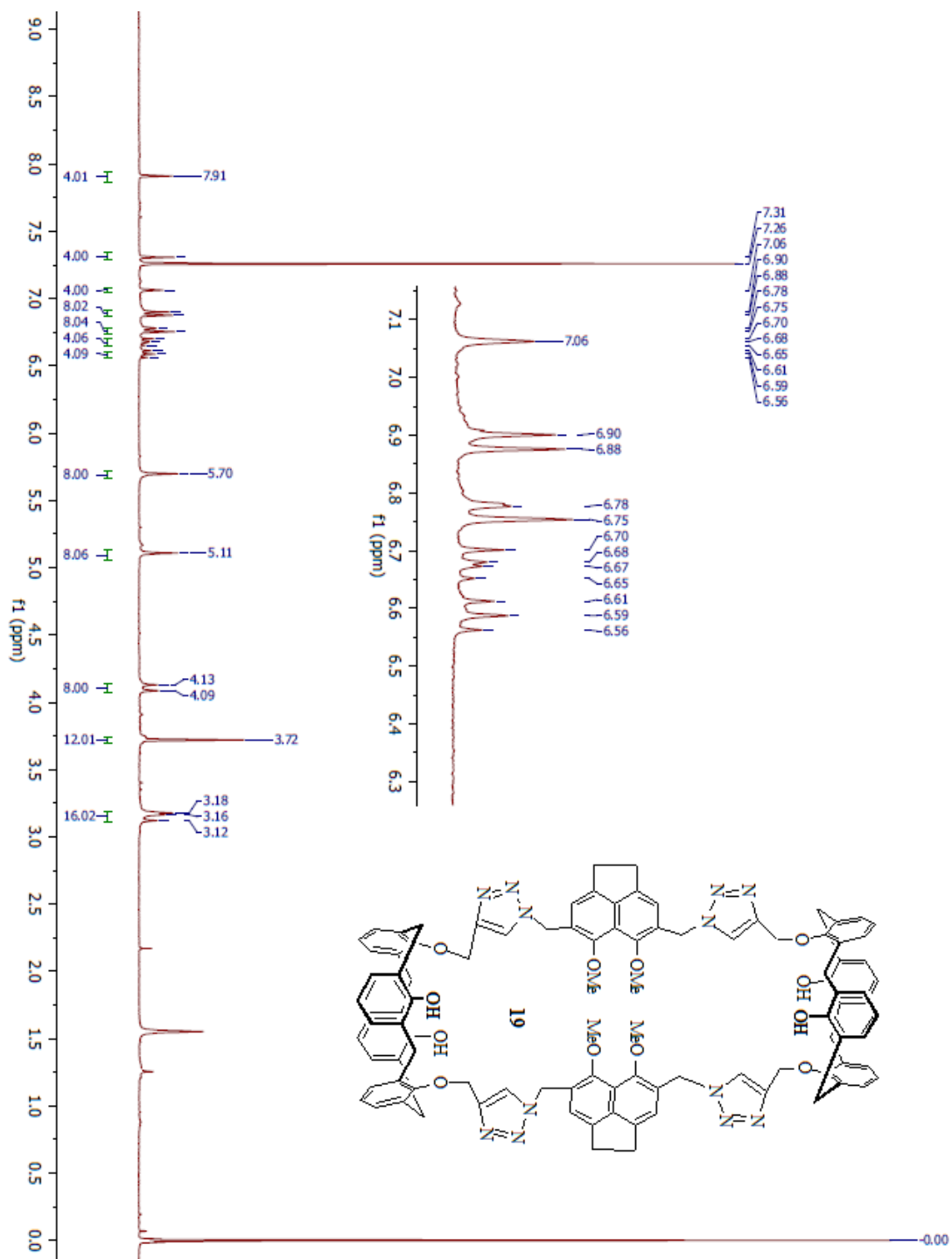


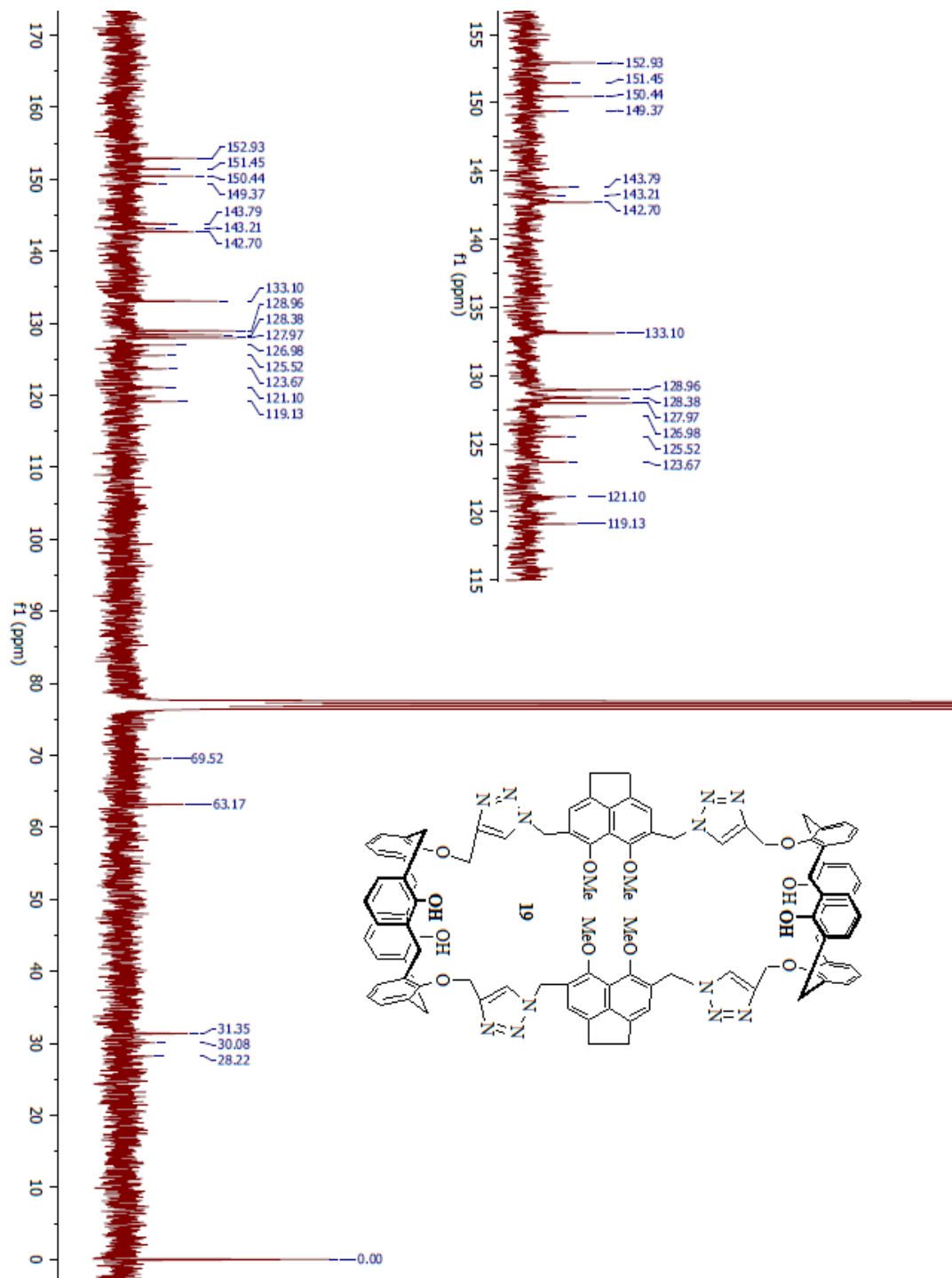


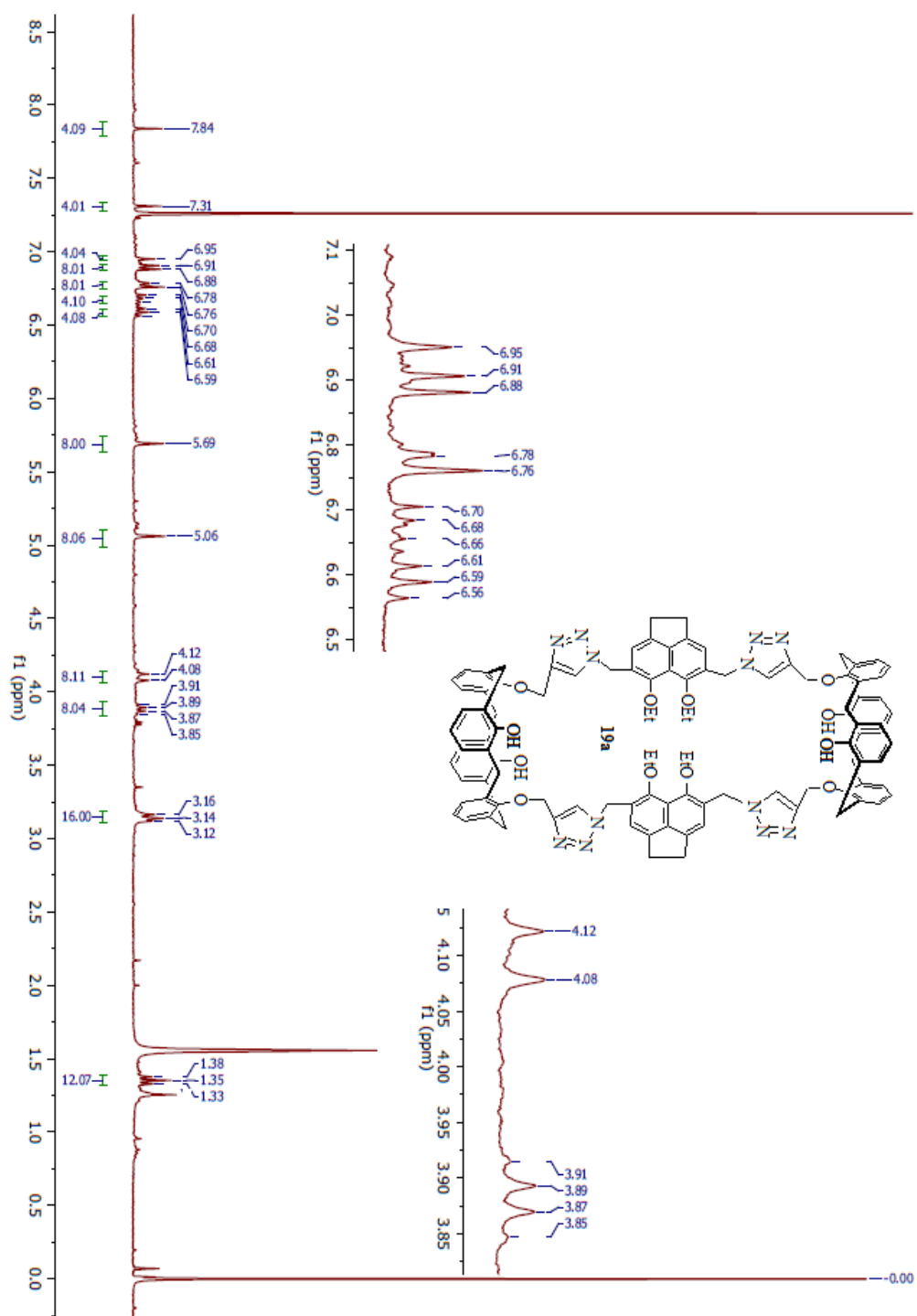


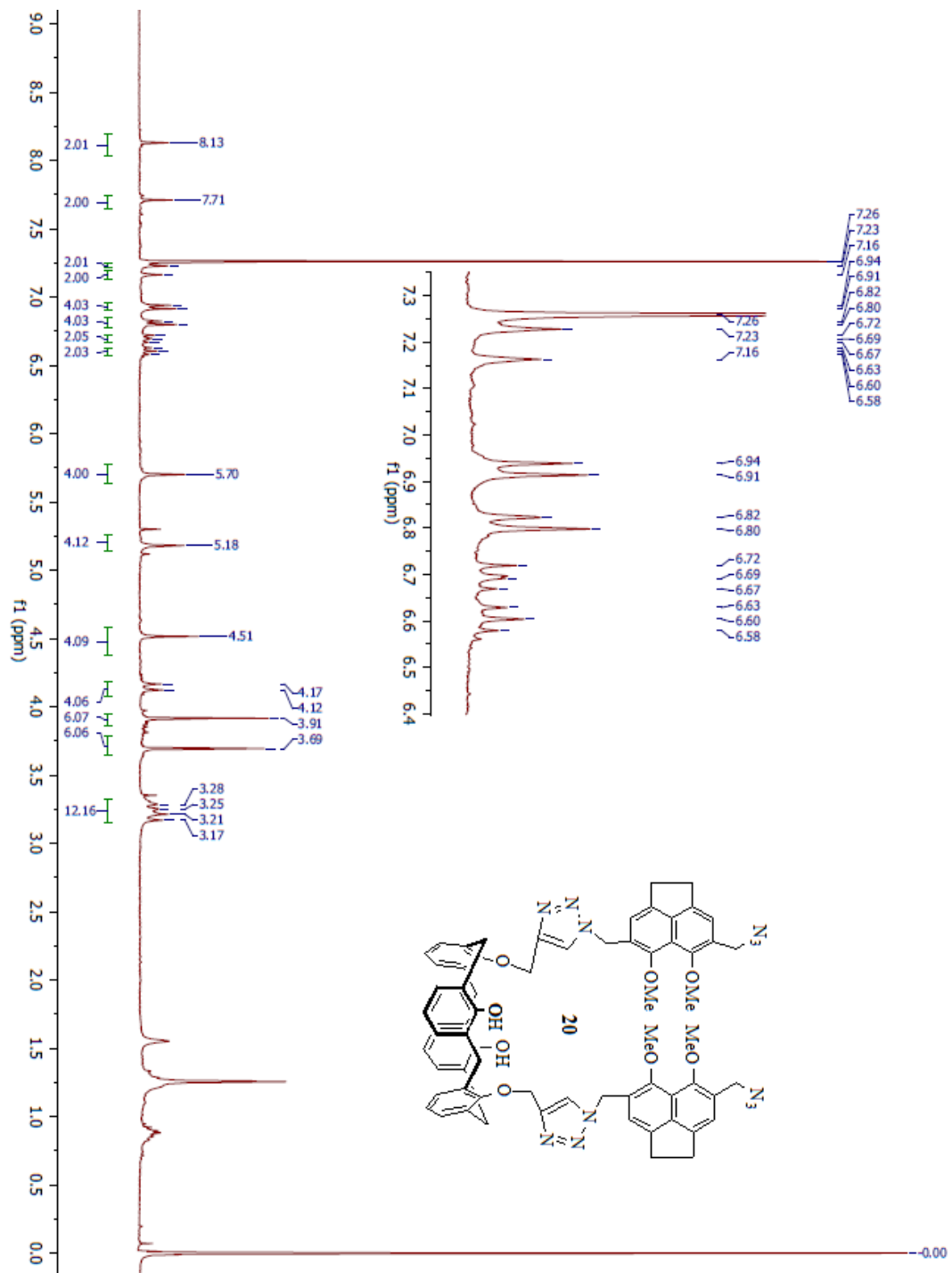


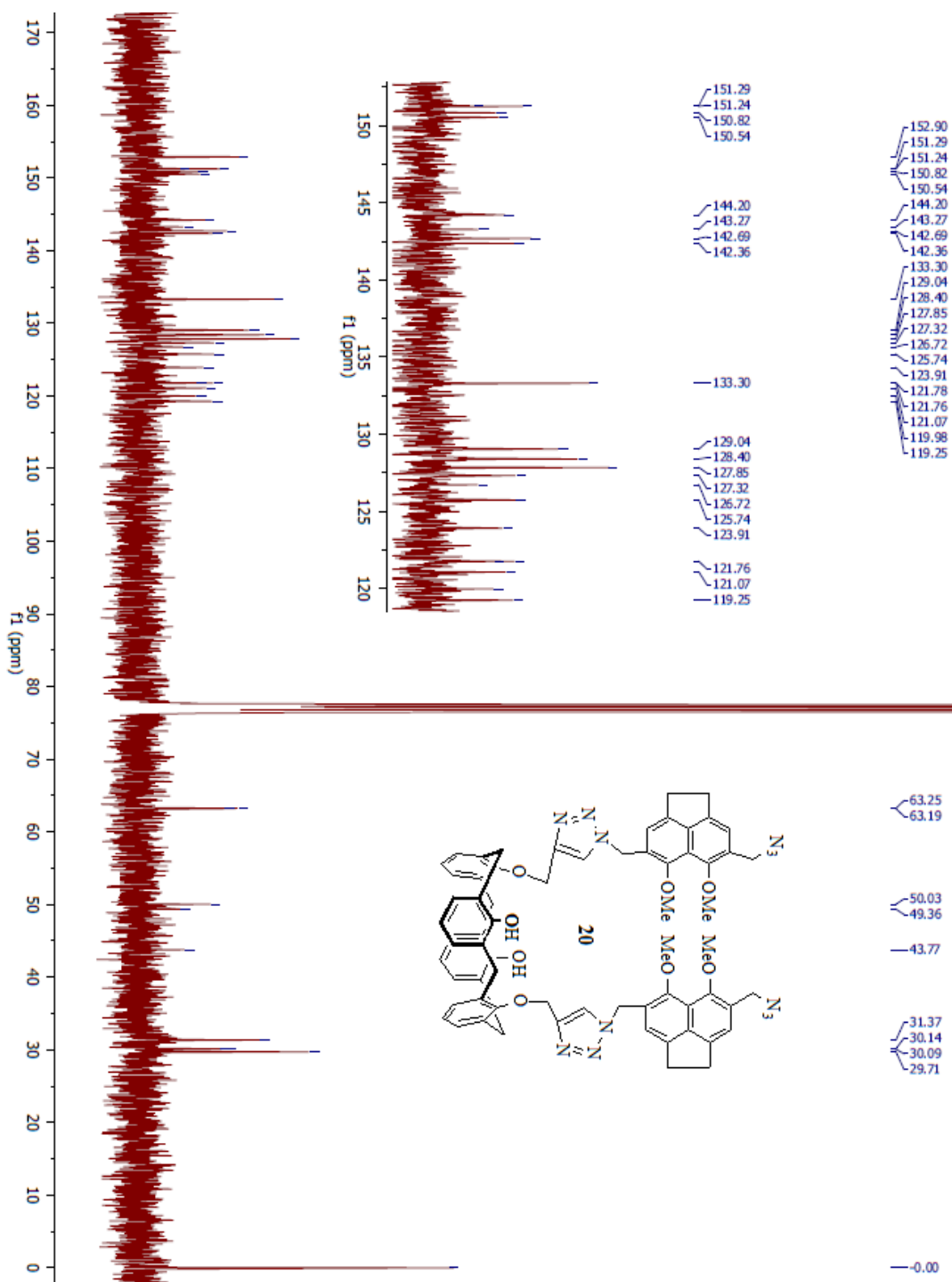










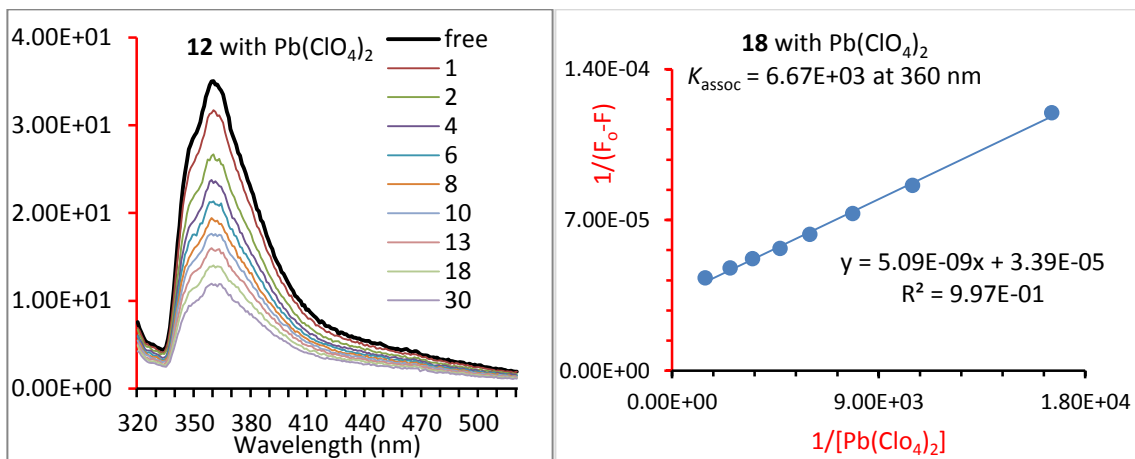


Appendix D

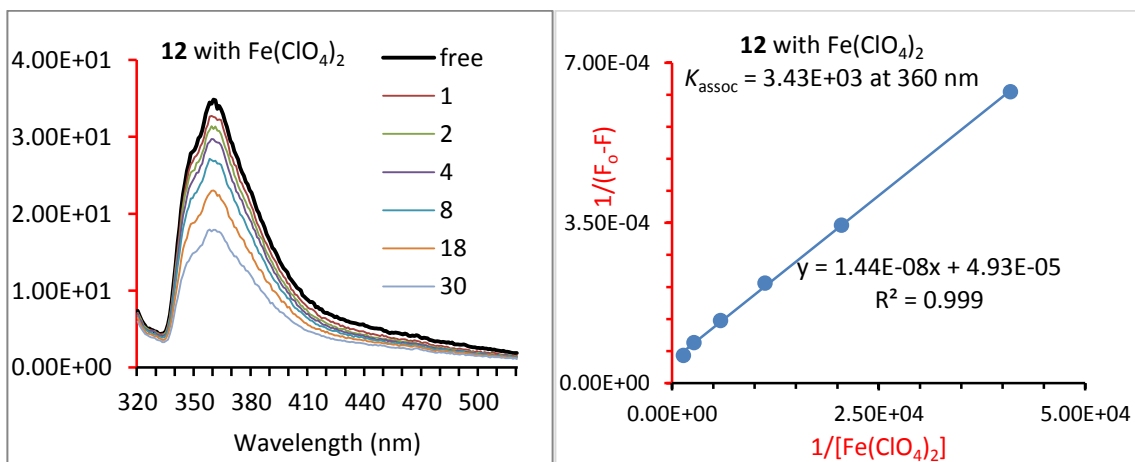
Fluorescence titration experiments of receptors in Chapter 3

Figures 3.21a-h and 3.22a-h show the titration experiments of host **12** and **12a** with the metal ions tested. The K_{assoc} values which were calculated at 360 nm wavelength using the Benesi-Hildebrand plots are also shown in the figures.

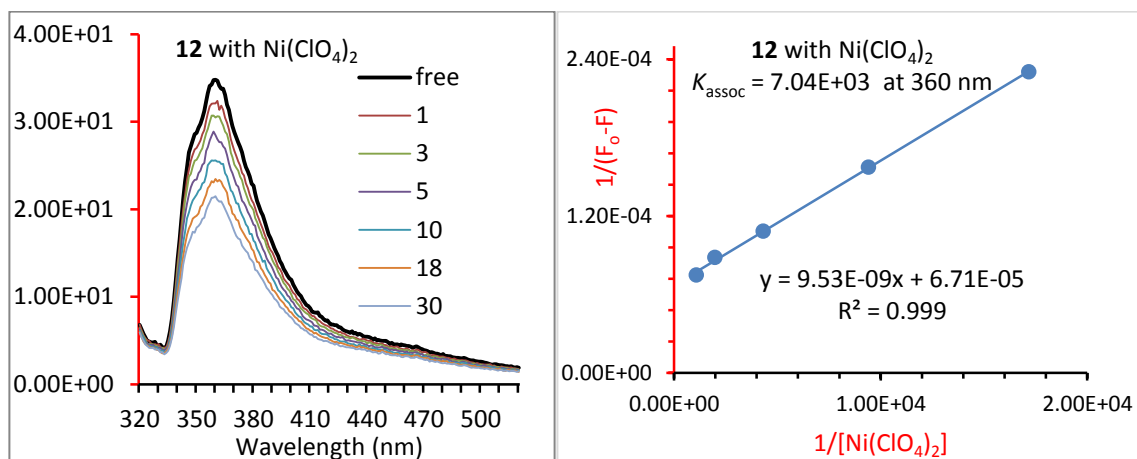
(a)



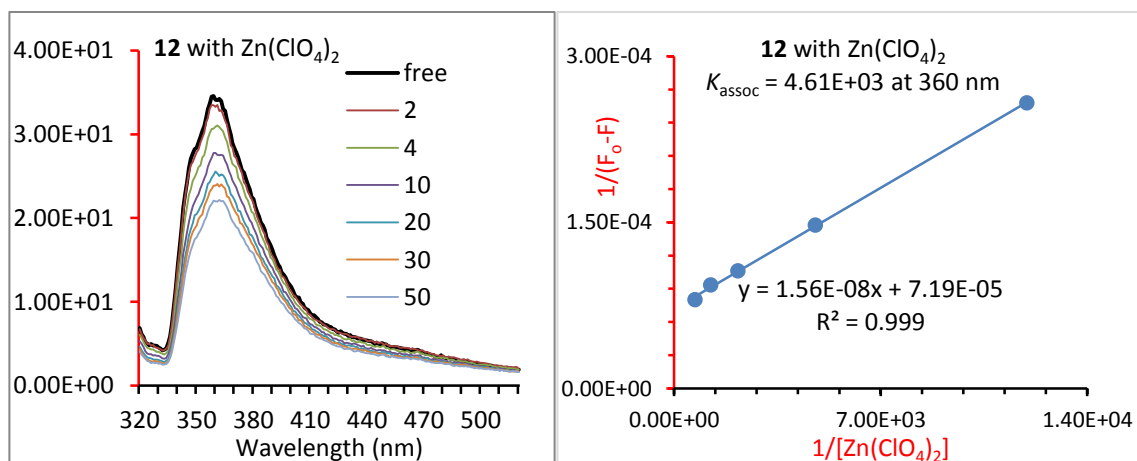
(b)



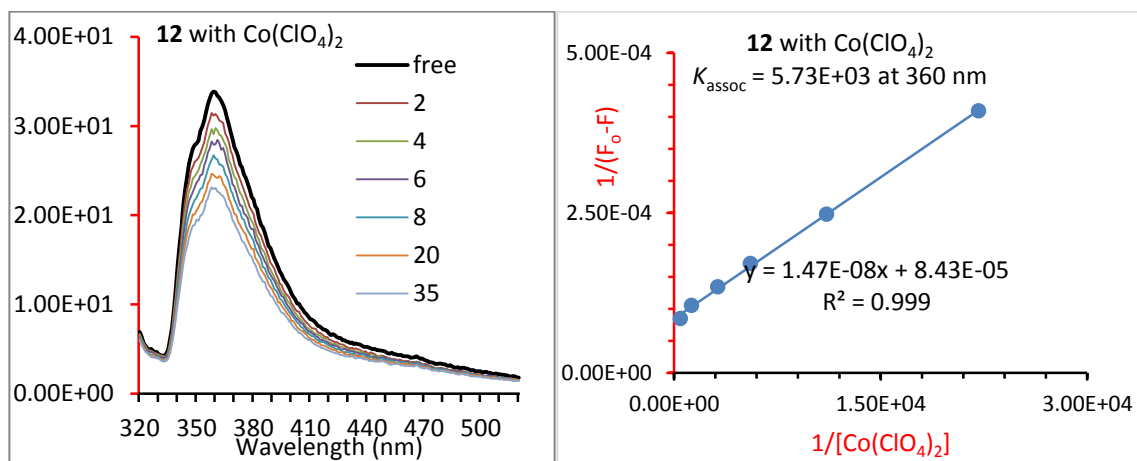
(c)



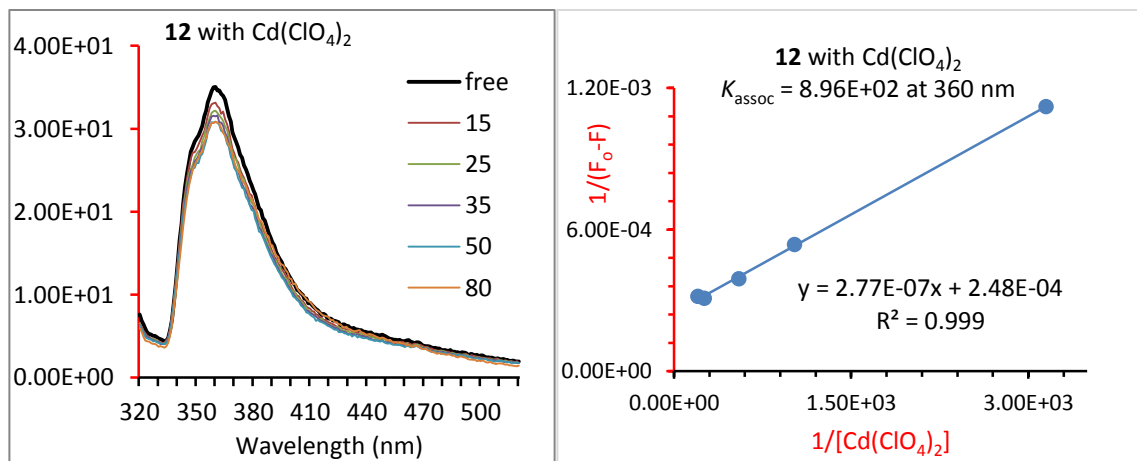
(d)



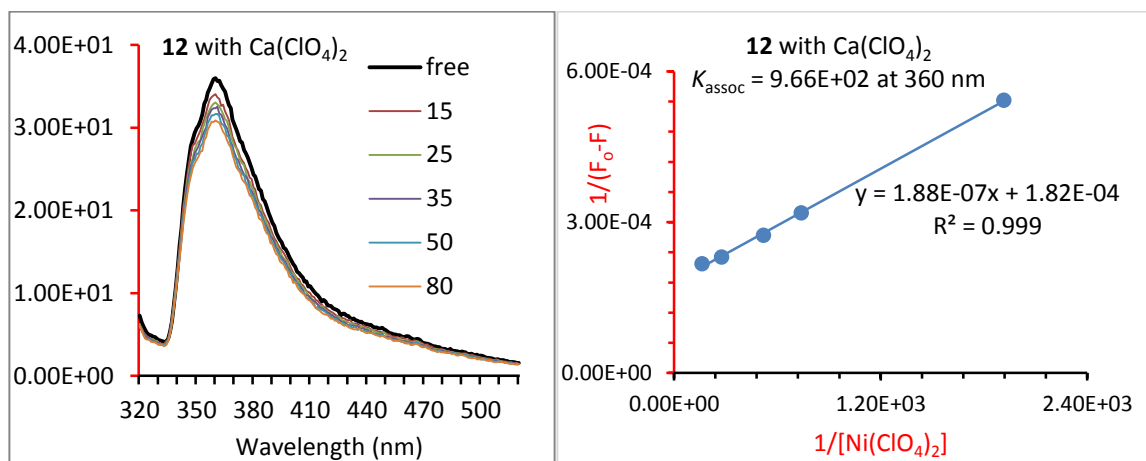
(e)



(f)



(g)



(h)

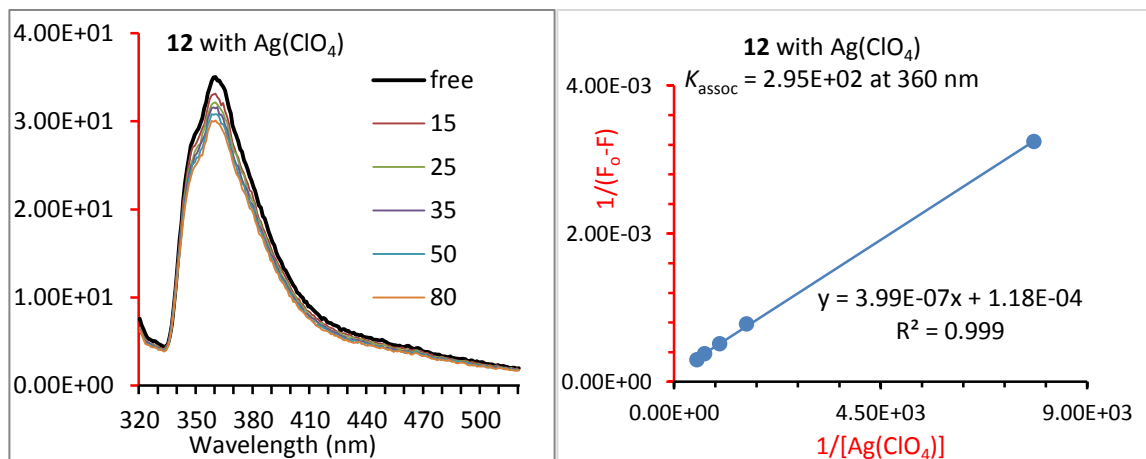
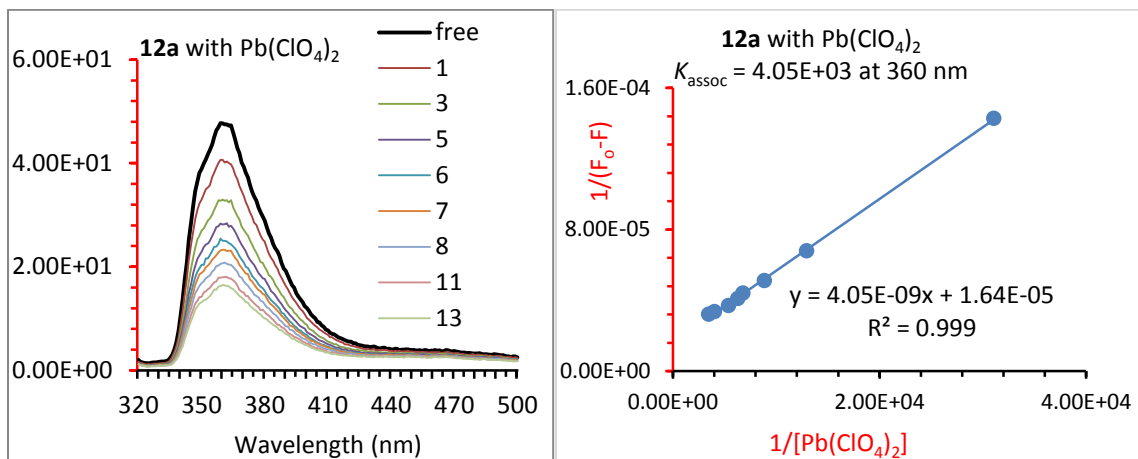
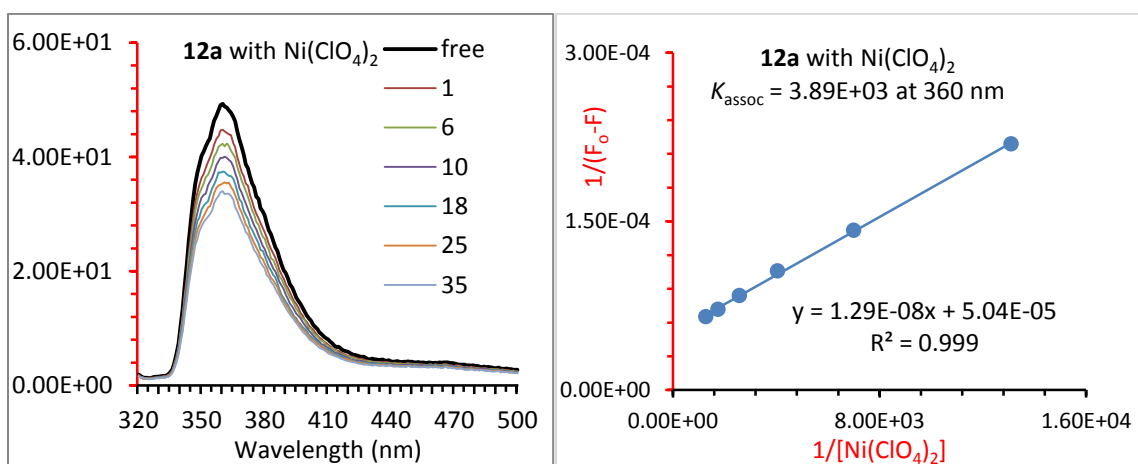


Figure 3.21. *Left:* Fluorescence spectra of **12** (21.1 μM) upon addition of metal ions in acetonitrile/ chloroform (v/v= 9:1) solutions. $\lambda_{\text{ex}} = 309$ nm. *Right:* Benesi-Hildebrand plot of $1/(F_0 - F)$ versus $1/[\text{M}(\text{ClO}_4)]$ for **12** upon titration with metal ions. The linear fit showed a 1:1 complexation of **12** and metal ions. The association constants were calculated for the changes at the 360 nm wavelength.

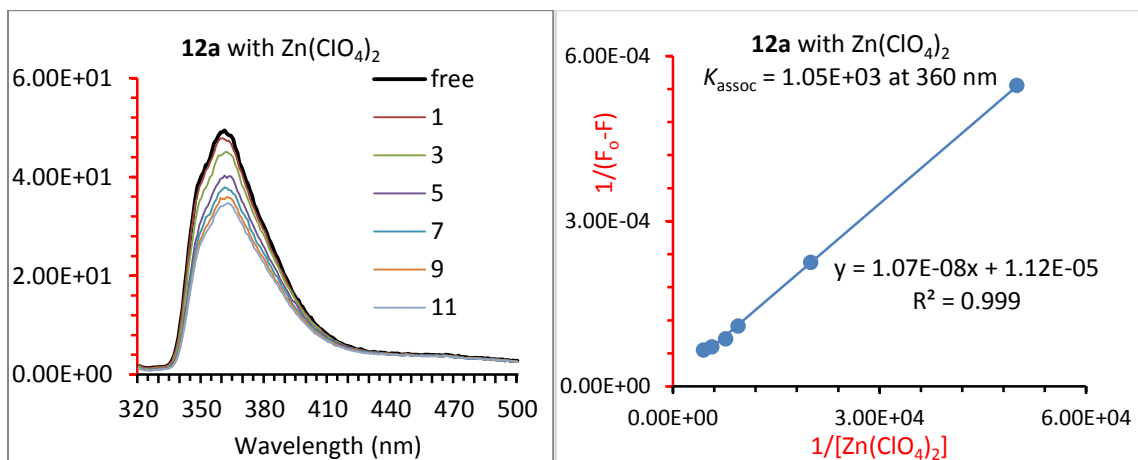
(a)



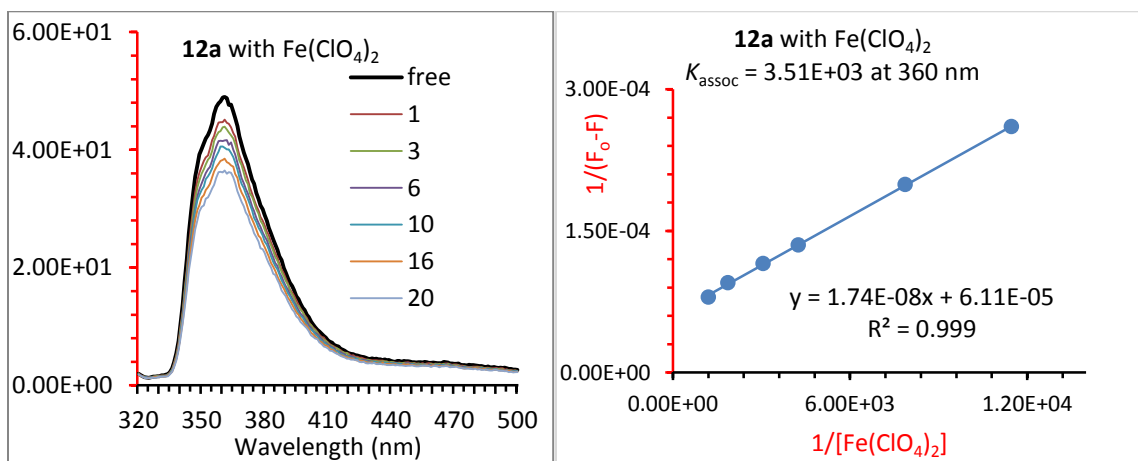
(b)



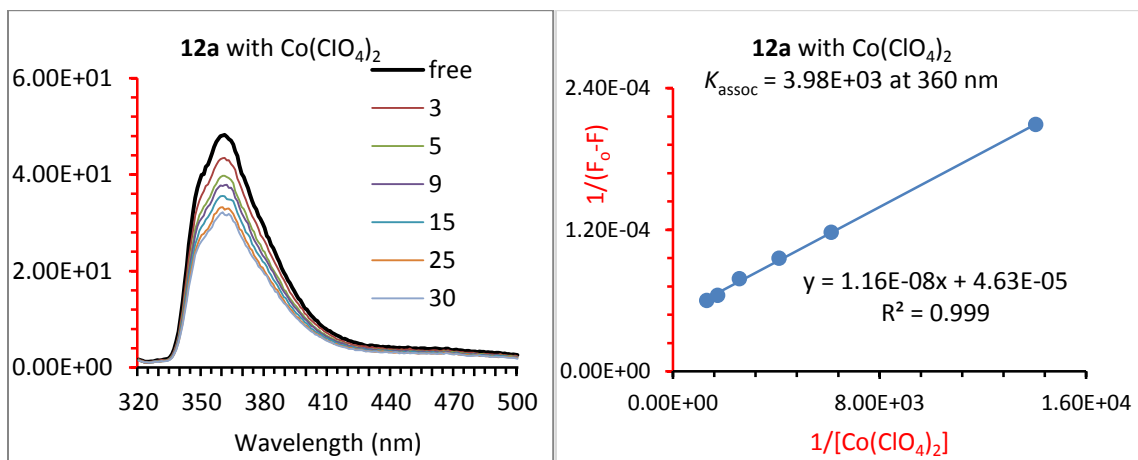
(c)



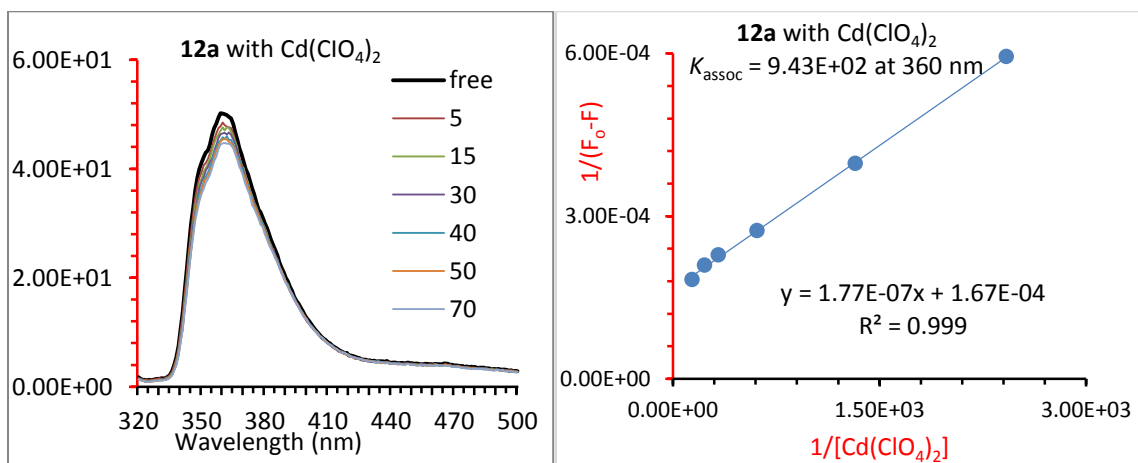
(d)



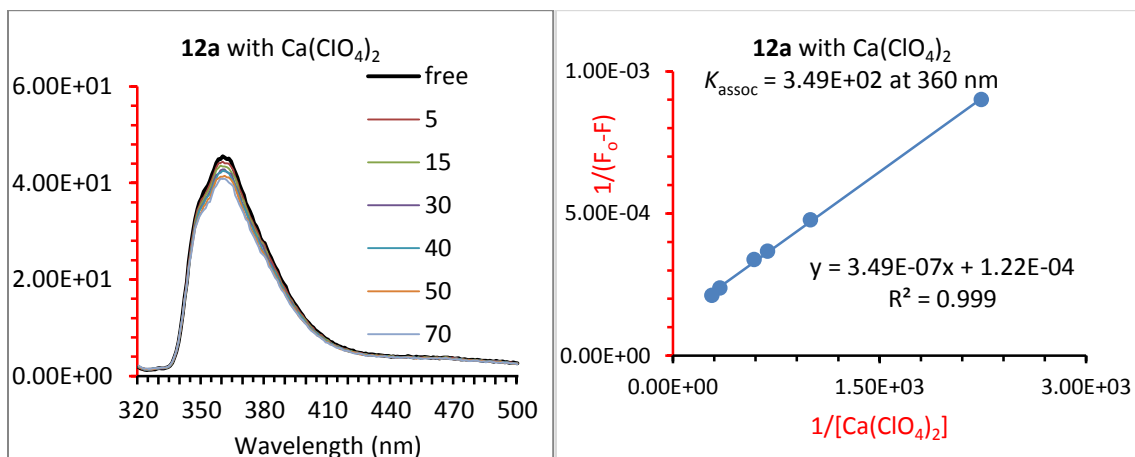
(e)



(f)



(g)



(h)

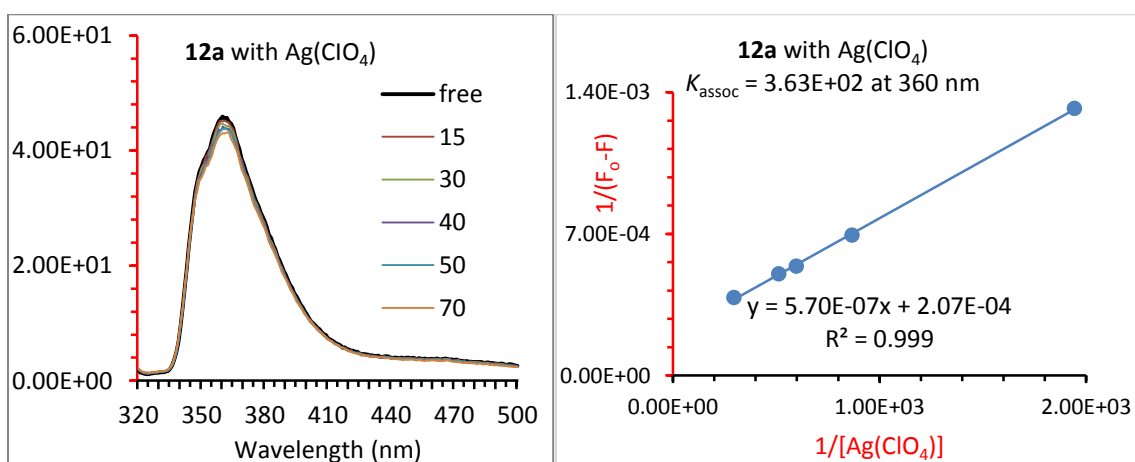


Figure 3.22. *Left:* Fluorescence spectra of **12a** (20.9 μM) upon addition of metal ions in acetonitrile/ chloroform (v/v= 9:1) solutions. $\lambda_{\text{ex}} = 309$ nm. *Right:* Benesi-Hildebrand plot of $1/(F_0 - F)$ versus $1/[\text{M}(\text{ClO}_4)]$ for **12a** upon titration with metal ions. The linear fit showed a 1:1 complexation of **12a** and metal ions. The association constants were calculated for the changes at the 360 nm wavelength.

Appendix E

^1H , ^{13}C -NMR spectra for compound described in Chapter 4

